

LUND UNIVERSITY

Diatom-rich sediment formation in lakes

Zahajská, Petra

2021

Document Version:
Publisher's PDF, also known as Version of record

Link to publication

Citation for published version (APA):
Zahajská, P. (2021). *Diatom-rich sediment formation in lakes*. Lund University (Media-Tryck).

Total number of authors:
1

Creative Commons License:
CC BY

General rights
Unless other specific re-use rights are stated the following general rights apply:
Copyright and moral rights for the publications made accessible in the public portal are retained by the authors and/or other copyright owners and it is a condition of accessing publications that users recognise and abide by the legal requirements associated with these rights.
• Users may download and print one copy of any publication from the public portal for the purpose of private study or research.
• You may not further distribute the material or use it for any profit-making activity or commercial gain
• You may freely distribute the URL identifying the publication in the public portal

Read more about Creative commons licenses: https://creativecommons.org/licenses/

Take down policy
If you believe that this document breaches copyright please contact us providing details, and we will remove access to the work immediately and investigate your claim.

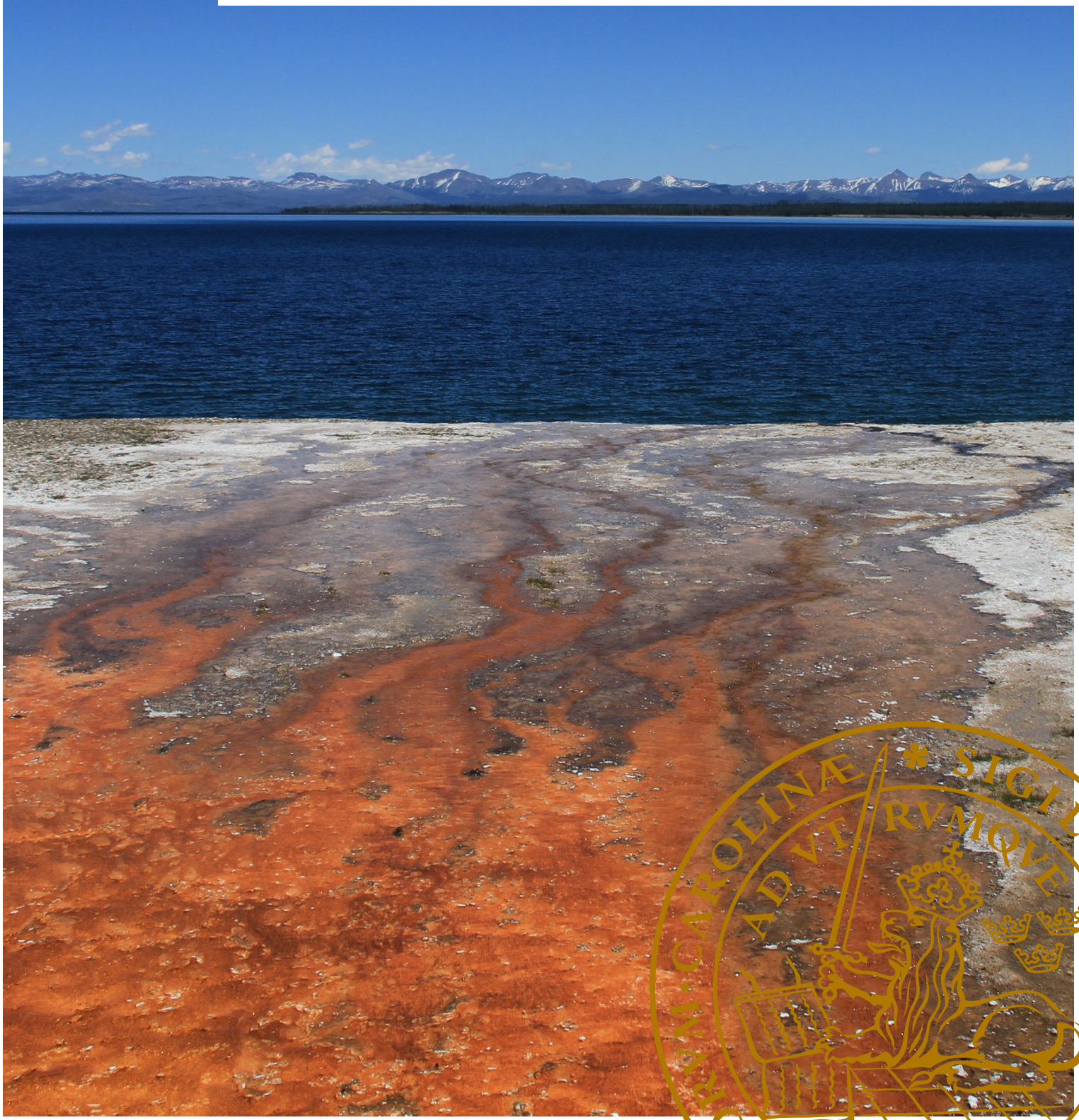
LUND UNIVERSITY

PO Box 117
221 00 Lund
+46 46-222 00 00

LUNDQUA THESIS 91

Diatom-rich sediment formation in lakes

PETRA ZAHAJSKÁ
QUATERNARY SCIENCES | DEPARTMENT OF GEOLOGY | LUND UNIVERSITY 2021





Printed by Media-Tryck, Lund 2021 NORDIC SWAN ECOLABEL 3041 0903

LUND UNIVERSITY

Quaternary Sciences
Department of Geology
Lund University
Sölvegatan 12
SE-223 62 Lund, Sweden
Telephone +46 46 222 78 80

ISSN 0281-3033
ISBN 978-91-87847-56-1

LUNDQUA THESIS 91

Diatom-rich sediment formation in lakes

Petra Zahajská



LUND
UNIVERSITY

Quaternary Sciences
Department of Geology

DOCTORAL DISSERTATION
by due permission of the Faculty of Science, Lund University, Sweden.
To be defended at Pangea, Geocentrum II, Sölvegatan 12 and via Zoom. Date 2021-03-05 at time 13:15.

Faculty opponent
Prof. Anson W. Mackay
University College London

Cover illustration front: Hydrothermal fluids delivery to Yellowstone Lake from West Thumb Geyser Basin in June 2017, Yellowstone National Park, Wyoming, USA. (Credits: Petra Zahajská)

Cover illustration back: View across Isfjorden from Longyearbyen seaside in March 2017, Svalbard, Norway. Photo taken during winter Arctic limnology course. (Credits: Petra Zahajská)

Funding information: The thesis was financially supported by several grants from the Royal Physiographic Society in Lund and by the Swedish Research Council.

© Petra Zahajská 2021

Faculty of Science, Department of Geology

ISBN: 978-91-87847-56-1 (print)
ISBN: 978-91-87847-57-8 (pdf)
ISSN: 0281-3033

Printed in Sweden by Media-Tryck, Lund University, Lund 2021

Media-Tryck is a Nordic Swan Ecolabel certified provider of printed material. Read more about our environmental work at www.mediatryck.lu.se

MADE IN SWEDEN

Organization
LUND UNIVERSITY

Department of Geology
Sölvegatan 12
SE–22362 LUND
Sweden

Author(s)
Petra Zahajská

Document name
DOCTORAL DISSERTATION

Date of disputation
2021-03-05

Sponsoring organization

Title and subtitle
Diatom-rich sediment formation in lakes

Abstract
Unicellular photosynthetic golden-green algae called diatoms are one of the most abundant silicifying organisms. Diatoms take up silicon and build their frustules, in the form of biogenic silica (BSi), which have high preservation potential, and thus are found in sediments. Around 27 % of the annual dissolved silicon (DSi) delivery from the land to the ocean is retained in lakes and reservoirs in the form of BSi. Therefore, diatom production in lakes creates silicon sinks and influences the Si cycle. However, the processes driving and regulating lacustrine diatom-rich sedimentation are poorly constrained.

This dissertation investigates two lakes in very different settings to evaluate the major factors governing diatom-rich sediment accumulation. The first study site is a small subarctic, high-latitude lake, Lake 850 in Northern Sweden, and the other study site is in the hydrothermally active and DSi-rich Yellowstone Lake in Yellowstone National Park, Wyoming, U.S.A.

The study of the recent Si cycle in Lake 850 revealed the importance of groundwater input to the lake's Si budget. Groundwater brings 3 times more DSi compared to the stream inlet and thus is the main source of DSi for diatom production. Low sedimentation rates in the last 150 years are responsible for BSi accumulation as high as 20 dry weight%. The Holocene sedimentary record shows that the lake had low detrital input throughout the last 7400 years, likely due to low-relief geomorphology and a stable environment in the lake's watershed. The stable Si isotopes of fossil diatoms suggest a stable DSi supply for the lake, where only the relative proportion of stream influx and groundwater influx of DSi are driving isotopic changes. The BSi accumulation in the sediment of Lake 850, as high as 46 dry weight% throughout the Holocene, is driven by a combination of sufficient DSi supply from groundwater and the stream inlet, low detrital input and good preservation of diatoms in the sediment.

In Yellowstone Lake the importance of hydrothermal vents bringing DSi into the lake was shown. The impact of hydrothermal DSi supply is observed in the sedimentary record over the last 9800 years as elevated Ge/Si ratios (up to 37 µmol/mol). Holocene hydrothermal input is responsible for a long-term stable lake DSi concentration and its Si isotopic signature, reflected in the fossil diatoms. The high sustained input of DSi masks the effects of the sublacustrine Elliott's Crater hydrothermal explosion ~8500 years ago. The relative proportion of the DSi sources from hydrothermal fluids and stream inlets, diatom production and dissolution are concurrent processes responsible for the variation of the Si isotopic signal. The BSi accumulation is accounted for by low accumulation rates with limited amounts of detrital input and high diatom preservation, which results in BSi concentrations in the sediment of up to 52 dry weight%.

On Holocene timescales, neither lake was DSi limited, which resulted from presence of the additional sources of DSi – groundwater or hydrothermal fluids. The unlimited DSi is partly responsible for BSi accumulation. Additionally, low sediment accumulation rates due to low detrital input, often driven by changes in climate and hydrology, are factors contributing to high BSi concentration. Finally, a fine balance between diatom production and dissolution may influence BSi accumulation. These studies suggest that diatom-rich sediments are likely to accumulate in lakes situated on silicon-rich bedrock and regions influenced by volcanic and hydrothermal activity if accompanied by low clastic sediment inputs. High-latitude lakes, which may have high groundwater input also are candidates for high BSi accumulation. Lakes with low-relief watershed morphology and with limited stream input bringing only fine-grained clastic input have the potential to accumulate BSi.

Key words
Silicon, silica, diatom, biogenic silica, lakes, sediment, stable Si isotopes, Ge/Si, Yellowstone, Northern Sweden

Classification system and/or index terms (if any)

Supplementary bibliographical information

Language
English

ISSN and key title
0281-3033 LUNDQUA thesis

ISBN
978-91-87847-56-1 (print)
978-91-87847-57-8 (pdf)

Recipient's notes

Number of pages
132

Price

Security classification

I, the undersigned, being the copyright owner of the abstract of the above-mentioned dissertation, hereby grant to all reference sources the permission to publish and disseminate the abstract of the above-mentioned dissertation.

Signature  Date 2021-01-27

"In wilderness I sense the miracle of life, and behind it our scientific accomplishments fade to trivia."

Charles Lindbergh

Contents

List of publications . . . 1
Acknowledgements . . . 2
1 Introduction . . . 3
2 Aims of the thesis . . . 3
3 Background . . . 3
3.1 What is diatom-rich sediment? . . . 3
3.2 Silicon behavior . . . 4
3.3 The global Si cycle . . . 4
3.3.1 Terrestrial Si filters . . . 5
3.3.2 Lacustrine continental Si sink . . . 6
3.4 Stable Si isotopes . . . 6
3.5 Si isotope fractionation models . . . 8
3.6 Current state of knowledge of lake Si budgets . . . 9
3.6.1 Groundwater responsible for the high BSi accumulation . . . 11
3.6.2 Hydrothermalism as a driver of high BSi accumulation . . . 12
3.6.3 Using germanium as a trace element . . . 12
4 Methods . . . 14
4.1 Dissolved silicon . . . 14
4.2 Sedimentary biogenic silica . . . 14
4.3 Stable silicon isotopes . . . 14
4.3.1 Sample preparation . . . 14
4.3.2 Silicon isotopic composition determination . . . 15
4.4 Ge/Si ratios determination . . . 17
4.5 Total organic carbon and nitrogen – TOC and TN . . . 18
4.6 ITRAX μX-ray fluorescence – XRF . . . 18
5 Summary of papers . . . 19
Paper I . . . 19
Paper II . . . 20
Paper III . . . 20
Paper IV . . . 21
6 Discussion . . . 22
6.1 Diatomite in society . . . 22
6.2 Constraining the modern Si cycle in lakes . . . 22
6.3 The role of groundwater in lake Si cycles . . . 23
6.4 Is hydrothermalism affecting BSi accumulation? . . . 25

6.5 Factors driving BSi accumulation in pristine lakes 26
6.6 Lake diatom δ^{30}Si proxy interpretation 28
6.7 Future research perspectives 29
7 Conclusions 30
Populärvetenskaplig sammanfattning 31
Popular summary 33
Populárně-vědecký souhrn 35
References 37
Paper I: What is diatomite? 49
Paper II: Modern silicon dynamics of a small high-latitude subarctic lake 57
Paper III: Impact of Holocene changes in climate on silicon cycling in Lake 850, Northern Sweden 81
Paper IV: Impact of Holocene sub-lacustrine hydrothermal activity on the Si cycle and diatom-rich sediment accumulation in Yellowstone Lake 97
LUNDQUA publications 123

List of publications

This thesis is based on the following publications, referred to by their Roman numerals:

I **What is diatomite?**

Zahajská, P., Opfergelt, S., Fritz, S. C., Stadmark, J. and Conley, D. J.
Quaternary Research, vol. 96, pp. 48-52. DOI: 10.1017/qua.2020.14.

II **Modern silicon dynamics of a small high-latitude subarctic lake**

Zahajská, P., Olid, C. G., Stadmark, J., Fritz, S. C., Opfergelt, S. and Conley, D. J.
In review in Biogeosciences. DOI: 10.5194/bg-2020-441.

III **Impact of Holocene changes in climate on silicon cycling in Lake 850, Northern Sweden**

Zahajská, P., Cartier, R., Fritz, S. C., Stadmark, J., Opfergelt, S., Yam, R., Shemesh, A. and Conley, D. J.
Submitted to The Holocene.

IV **Impact of Holocene sub-lacustrine hydrothermal activity on the Si cycle and diatom-rich sediment accumulation in Yellowstone Lake**
Zahajská, P., Frings, P. J., Gaspard, F., Cartier, R., Opfergelt, S., Fritz, S. C., Stadmark, J., and Conley, D. J.
Manuscript.

All papers are reproduced with permission of their respective publishers.

Publications not included in this thesis:

Yellowstone Lake Coring Projects: Research with a History

Spanbauer, T. L., Brown, S.R., Cartier, R., Conley, D. J., Fritz, S. C., Schiller, C. M., Theriot, E. C., Whitlock, C., **Zahajská, P.**
Limnology and Oceanography Bulletin, vol. 27, pp. 6-10. DOI: 10.1002/lob.10229.

Multi-proxy record of Holocene paleoenvironmental conditions from Yellowstone Lake, Wyoming, USA
Brown, S.R., Cartier, R., Schiller, C. M., **Zahajská, P.**, Fritz, S. C., Morgan, L. A., Whitlock, C., Conley, D. J., Lacey, J. H, Leng, M. J. and Shanks III, W. C.
To be submitted to Quaternary Science Reviews.

Acknowledgements

"What I see here is nothing but a shell. What is most important is invisible..." – Antoine de Saint Exupery, The Little Prince

This thesis is just a brief suitcase that wraps my PhD student journey, which was much more than a thesis. My PhD studies were full of diverse joyful and fruitful activities, which brought me to this point. I have learnt a tremendous amount of new things, I've experienced four years of intensive research work as an individual, but also as part of bigger research groups, which I always dreamt of. I've met many passionate, enthusiastic, amiable colleagues, researchers, and people. I was always surrounded by terrific friends, whom all I would like to express my gratitude in a few following lines.

I want to thank all of my supervisors, Daniel, Johanna, Sophie and Sheri, for being here for me, listening and answering my questions, repeating the answers, again and again, discussing new ideas, reading and improving my manuscripts, proposals and supporting me in almost everything that I came with.

Thanks to Magnus Mörth, Christian Bigler, Hans Schöberg for great ideas, help, and connecting with new people. Thanks to my co-authors Carolina and Patrick for discussing and improving the manuscripts, even in short time notice. I also want to thank the HD-YLake group, Sabrina, Chris, Lisa, Pat, Rob and all others for allowing me to be part of a big team of smart people working on Yellowstone. It was an honour for me to meet and work with you all.

Thanks to Honor, my mentor, for being a patient listener, thoughtful mentor, and for still looking after me. Further, I want to thank all of you at the Department of Geology here in Lund, for creating a friendly working environment very opened to international PhD students. I thank Mats, Helena and Mikael for an opportunity to gain some teaching skills. Also, big thanks to Gert for keeping the electronic world well functioning all the time and to whole Kansli for being so great to help anytime.

My thanks go to all my colleagues and friends, who made my days enjoyable. Thanks to all PhD students for coming out for PhD dinners, having PhD fikas and having fun together. I would also like to thank people at the Université Louvain-la-Neuve for being so inviting and open to newcomers, thanks to François, Elisabeth, Arthur, Catherine, Maxime and everybody else. I enjoyed the time in Louvain. I want to thank Chris, Jessica, Jacob and Rosine to going with me to "the grizzly land" in Yellowstone. I couldn't do this without you!

Carla, thanks for being here to talk about anything anytime, for joining the very cold fieldwork and for having all the fun, which we had. Thanks to Zhouling for spreading the good mood and laugh through the department. Thank you, Guillaume and Billy, for answering all my questions about simple things and making Friday beers even more fun. Big thanks go to Bingjie for keeping me in the biomarkers' world updated and for having good times with good food. Thanks to Maria for always having a solution for any situation and patience during our kiteboarding time :-). It was so much fun! Geert, thanks for encouraging me to climb more challenging routes and climb higher than my limits. Laurie, thanks for being such a good listener and having patience with me.

Huge thanks go to Franzi for reading, discussing, suggesting and helping out, because I don't know how this would have ended up if you hadn't come here. I also thank Karola, Tjördis and Ethan for being always a lovely company and for "just chatting" or playing board games with a glass of beverage. Thanks to Yuhao, Isa, Rebecca and Rosine for reading my texts, for bringing new ideas and approaches into the discussions. Thanks to Cindy, Ingrid, Chiara and Sofia for being on the online PhD meetings almost every time and keeping some PhD social life still on even in corona times. This list can go on, so in short, thanks to all of you reading these acknowledgements because if you read them, it means that you've earned my gratitude for something. Thank you all! Tack allihopa!

Since I started my PhD studies here in Lund, many things in my life have changed, but my good old friends were always there for me. Thus, I would like to thank Venca, Fazole, Káťa, Klárka, Péťa, Adél, Adéla, Terka, Anička and many others for being always ready to meet for a cup of tea and cake when I came back to Prague or even online. I also want to thank Sebastian, my good friend, for supplying me with spectacular photos of northern lights and for making me always laugh after reading his messages. Thank you Max, for all the nice days in Lomma! I cannot forget to thank Pällsboll, the cutest cat ever, for keeping a strict, but closed eye on me when writing during the corona times.

I want to thank my esteemed smarties Lukáš, Filip, Míra and Honza who (indirectly) motivated me to try harder, learn more, and they made a creative space for any kind of ideas during our trips. Thank you guys for being still here, even though we are now all over Europe.

Finally, I would like to thank my whole family. Mami, tati děkuji, že jste mě vždy podporovali v mé zvídavosti a že mě stále podporujete v mých bláznivých rozhodnutích dělat vědu a cestovat po světě. Ségra a bráchové, je s vámi sranda a mám vás ráda. Nakonec děkuju šamákovi, že má se mnou trpělivost, učí mě věci dělat lépe a pořádně, že jezdí na dovolenou sbírat vzorky místo válení se na pláži a že mě podporuje v tom pokračovat dál, i když sama dál už nemůžu. Děkuji, že jste!

$$x^2 + (\frac{5y}{4} - \sqrt{|x|})^2 = 1$$

1 Introduction

The Earth's crust is composed of large quantities of silicate minerals, which are chemically weathered once exposed to exogenous processes. Both macro- and micro-nutrients are released during the mineral weathering and distributed to the ecosystem where they are utilized, recycled and buried. Those processes are part of elemental cycling, which is responsible for the Earth's evolution. To understand the distribution of different elements, biogeochemical models are established based on observational data. Here we focus on an essential element for single-cell silicifying algae – *silicon* (Si).

The Si cycle is characterized by two sub-cycles: the continental cycle and the oceanic cycle. These sub-cycles are connected through rivers, which transport the silicon from land to oceans. Diatoms are the most prevalent silicifying organism in aquatic environments (Battarbee et al., 2002; Opfergelt et al., 2011), and marine diatom production accounts for one quarter of the world's entire net primary productivity (Armbrust, 2009; Simpson and Volcani, 1981) and one fifth of world oxygen production. Oceanic diatom production is fully dependent on dissolved silicon delivery from the continental cycle. However, processes in the continental cycle – such as diatom production and accumulation – affect the Si delivery to the oceans as shown by several Si mass-balance studies (Frings et al., 2016, 2014b; Sutton et al., 2018; Tréguer and De La Rocha, 2013). These studies identified knowledge gaps in the Si cycle, particularly the need to better constrain sinks and sources in the continental cycle to better understand Si delivery to the ocean. An example of those sinks or sources is the lacustrine diatom-rich sediments, which can retain silicon on long timescales, but they can also release the silicon if conditions change.

This PhD project aims to investigate the processes governing diatom-rich sediment formation in lakes in order to enhance our understanding of the functioning of continental silicon sinks.

2 Aims of the thesis

The aim of this thesis is to improve current understanding of retention of Si in lakes and factors governing diatom-rich sediment formation during the Holocene. Its main research questions are as follows:

- What nomenclature should be used to name diatom-rich sediment?
- What are the processes responsible for high diatom accumulation in high-latitude lakes?
- How do hydrothermal inputs affect sediment accumulation of diatoms ?
- Do hydrothermal processes during the Holocene affect diatom accumulation in Yellowstone Lake?
- What are the general processes responsible for Holocene diatom-rich sedimentation in lakes?

3 Background

3.1 What is diatom-rich sediment?

Diatom-rich sediment is mainly composed of diatom frustules and accumulates worldwide. *Diatoms* are single-cell golden algae, with an external skeleton made of *biogenic silica (BSi)*, known as a *frustule*. All aquatic environments, such as lakes, rivers, oceans, but also soils, host conditions for diatom growth. Accumulation of diatoms in sediment is known in all aquatic environments including wetlands, lakes, and the oceans

(Clarke, 2003). Furthermore, diatom sensitivity to changes in water temperature, pH, dissolved oxygen, nitrogen, phosphorus, and other nutrients make diatoms often used as a proxy in paleoenvironmental reconstructions (Battarbee et al., 2002). *Dissolved silicon (DSi)* concentrations in the environment are essential for diatoms to grow, as diatoms take up DSi to build their frustules. Therefore, to investigate factors driving freshwater diatom production and then accumulation, we need to understand what is driving changes in DSi concentrations. Essential understanding of silicon behavior, coupled with constraining the processes affecting DSi concentration in the environment, is part of global Si cycle studies.

3.2 Silicon behavior

In natural waters, only small amounts of silicon are found in the form of *orthosilicic acid* (H_4SiO_4), which acts as a weak acid. Orthosilicic acid does not dissociate below pH 9, and Si is soluble at basic pH ranges (Oelze, 2015). Silica solubility in hydrous fluids and soils increases with pH and temperature (Albarède, 2009). The highest silica solubility occurs under alkaline conditions at a pH higher than 9 (Oelze, 2015). Additionally, formation of silicate complexes with Fe and Al hydroxides decreases solubility of silicates in sediment and decreases silicate solubility in waters at pH $>$ 7 (Wetzel, 1975). Thus, the presence of clay minerals rich in Al and Fe can influence silica solubility.

3.3 The global Si cycle

The biogeochemical cycle of Si occurs in both terrestrial and aquatic environments. A simplified model of the Si cycle shows how DSi released by weathering directly enters the fluvial system via surficial run-off or groundwater (Figure 1). The DSi delivered by rivers into the ocean accounts for 80 % of the total annual DSi delivery to the ocean (Frings et al., 2016; Sutton et al., 2018). Therefore, processes in the watershed are studied to understand the DSi fluxes. Several sinks and sources of DSi, such as soils, lakes and reservoirs (e.g., damming), were identified as important in regulating DSi delivery (Frings et al., 2016).

Dissolved silicon is delivered from weathered bedrock. The Earth's crust is composed primarily of Si, Al and O in the form of aluminosilicates. Silicon occurs as 1. a crystalline form of *lithogenic silica* in soils, minerals and rocks (LSi), 2. poorly ordered crystalline *amorphous silica* (ASi), which includes *biogenic silica* (BSi) produced by organisms, and 3. *dissolved silicon* (DSi) available in waters (McKeague and Cline, 1963). Quartz, feldspar and chalcedony are the predominant forms of crystalline lithogenic silica that are weathered and supply the system with DSi (McKeague and Cline, 1963).

The silicon release to the environment by chemical weathering of igneous silicate rocks and minerals is accompanied by CO_2 consumption (Sommer et al., 2006):

$$\begin{aligned} &CaAl_2Si_2O_8 + 2\,CO_2 + 8\,H_2O \longrightarrow \\ &Ca^{2+} + 2\,Al(OH)_3 + 2\,H_4SiO_4 + 2\,HCO_3^- \end{aligned} \quad (1)$$

Silicate weathering produces *orthosilicic acid* (H_4SiO_4), also reported as *dissolved silicon (DSi)*, which is transported by rivers to the ocean. The global mean of DSi concentration in natural waters is 9.5 mg SiO_2 l^{-1} (~160 µM) (Dürr et al., 2011). The highest DSi concentrations (up to 125 mg SiO_2 l^{-1}) occur in groundwaters and hydrothermal fluids (580 mg SiO_2 l^{-1}) that are in contact with volcanic rock (Fowler et al., 2019b; Georg et al., 2009; Schopka and Derry, 2012; Wetzel, 1975). Intermediate concentrations are associated with plutonic rocks, sediments containing feldspar, and volcanic rock fragments. Carbonates and marine sandstones are generally associated with a lower amount of DSi (Wetzel,

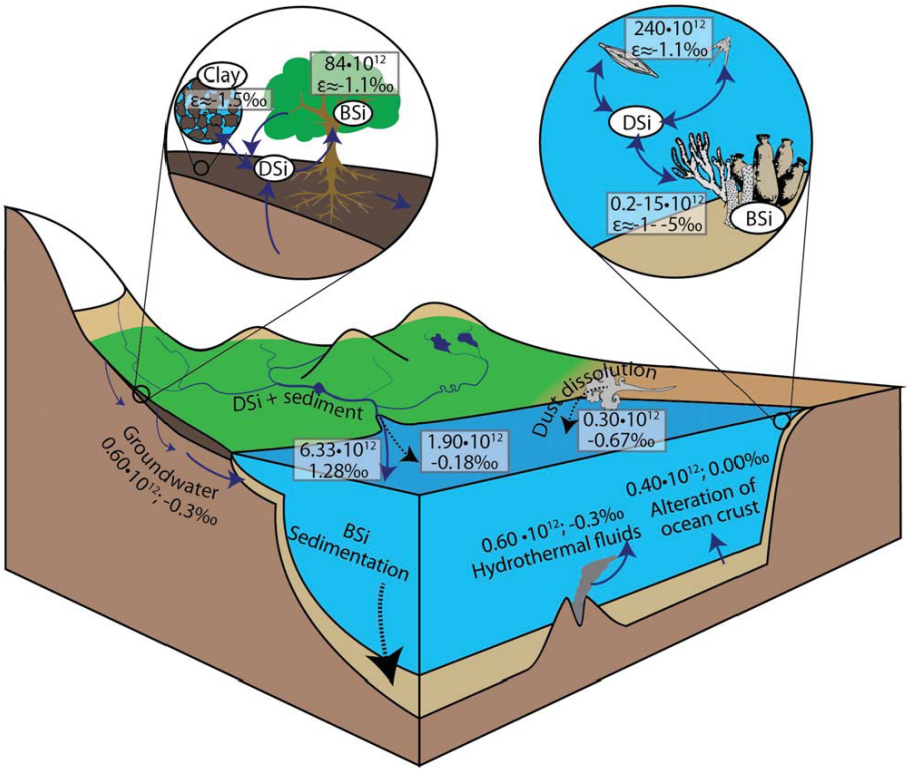


Figure 1: Schematic figure of the modern day global Si cycle by Frings et al. (2016). Values shows the magnitudes of the fluxes (in mol yr^{-1}) and also δ^{30}Si values (in ‰). The values of fractionation (ε, ‰) showed in the inset panels are associated with BSi production and clay minerals.

1975). On its pathway to the ocean, DSi cycles through continental filters, such as soils, lakes and reservoirs, which can efficiently remove DSi from the water and retain it for a long time (Frings et al., 2014b).

3.3.1 Terrestrial Si filters

Most of the DSi passes through a terrestrial filter before it is exported into river systems (Derry et al., 2005; Struyf et al., 2009). In many terrestrial ecosystems the soil-plant ASi pool stores more Si than the DSi released annually by weathering; therefore, the soil-plant system acts as a filter (Clymans et al., 2011; Frings et al., 2016; Struyf et al., 2010). Soils can retain DSi as it is taken up by vascular plants to build supportive siliceous structures – *phytoliths* (Piperno, 2001). Those silica bodies are precipitated in roots, stems, branches, leaves or needles as biogenic silica (BSi) and can be recycled in litterfall after the plant dies.

The phytolith BSi can be structurally or chemically altered by dissolution and precipitation processes in soils (Barão et al., 2014; Cornelis et al., 2011; Sommer et al., 2006), forming pedogenic silica. Due to loss of water during dissolution and precipitation processes, the pedogenic silica can gain more structural order, and thus its solubility and reactivity decreases compared to the original BSi and ASi (Saccone et al., 2007). Under acidic conditions in soils, the ASi and pedogenic silica are lost slowly, because they are insoluble (McKeague and Cline, 1963). Hence, soils can store large Si stocks, but they are particularly susceptible to human perturbation connected to changes in pH (Clymans et al., 2011).

3.3.2 Lacustrine continental Si sink

Not only soils, but also lakes and reservoirs (damming) can store silicon. Lakes are considered to store 21–27 % of the annual global DSi delivery to the ocean in lake sediments (Frings et al., 2014b). Diatoms act as a silicon sink, as they grow in all aquatic environments and take up DSi to build their frustules, which are deposited in the sediment in the form of biogenic silica (BSi) after their death. The BSi accumulation depends on several factors:

1. Favorable conditions for diatoms to grow, such as light and nutrients. Diatoms are limited by the DSi concentration in the environment. Therefore, continuous DSi supply or Si recycling in the water column are crucial for sustaining diatom production and thus BSi accumulation (Ragueneau et al., 2006).
2. The DSi supply must be higher than the DSi removal by an outlet in order to accumulate BSi. An excessive supply of DSi or fast sedimentation rates prevent diatom dissolution in the water column and diatom-rich sediments are formed.
3. Lakes with low detrital input (Conger, 1942) have the potential to accumulate BSi in the sediment.
4. Volcanic and hydrothermal lakes enriched in DSi may accumulate BSi (Conley, 1998).

A conceptual model was created to illustrate all the above mentioned factors influencing diatom-rich sediment formation in volcanic and non-volcanic settings, which were both studied for their silicon cycle (Figure 2).

3.4 Stable Si isotopes

Stable silicon isotopes have previously been used as a tool to constrain different biological and chemical processes influencing DSi concentrations in the global Si cycle. Silicon has three stable isotopes, which have different relative abundances in nature: ^{28}Si (92.18 %), ^{29}Si (4.71 %), and ^{30}Si (3.12 %) (Reynolds, 1953). Due to different masses of the

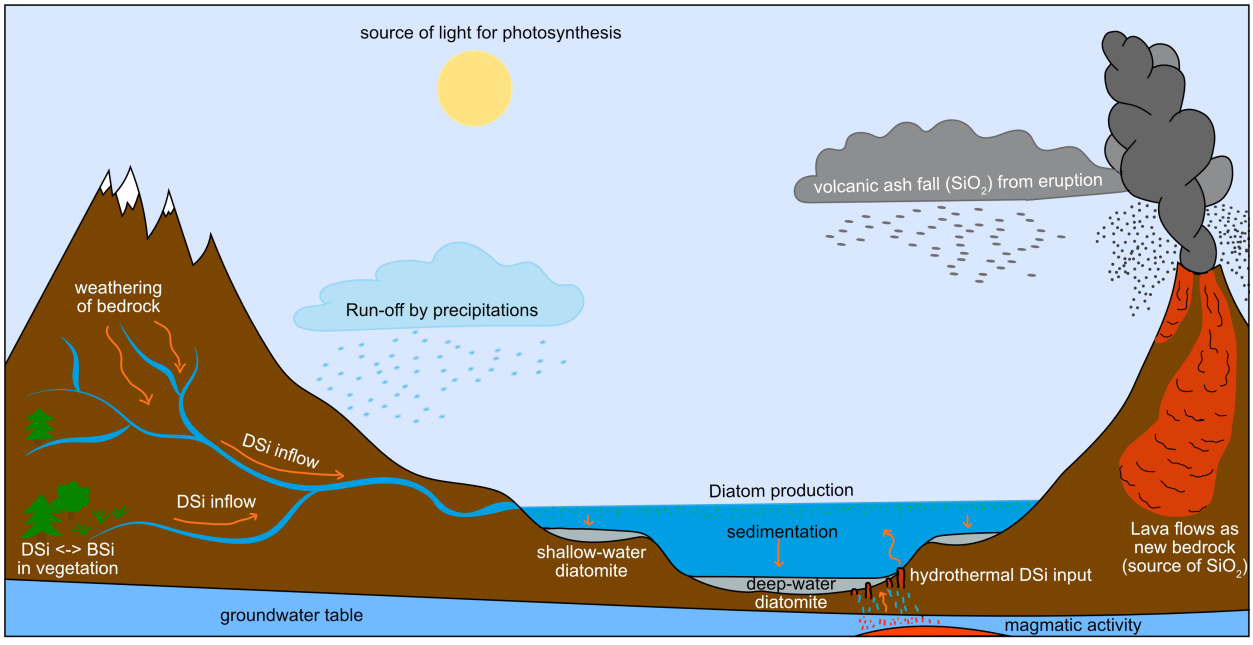


Figure 2: A conceptual model of diatom-rich sediment formation.

isotopes – ^{28}Si (27.976927), ^{29}Si (28.976495), ^{30}Si (29.973770) – there is mass-dependent fractionation, which occurs during physical, chemical, and biological processes. Two main isotopic fractionation types are distinguished: 1. kinetic fractionation, and 2. equilibrium fractionation. Kinetic fractionation occurs during an irreversible chemical reaction of physical processes and preferentially enriches the product in lighter isotopes. One example of kinetic fractionation is the uptake and incorporation of Si by diatoms or plants. Equilibrium fractionation is associated with reversible chemical reactions and physical processes (when the chemical reaction is in equilibrium) (Opfergelt et al., 2011; Wiederhold, 2015).

Because mass spectrometric methods allow the difference in isotopic ratio of two stable isotopes to be measured much more precisely than their absolute abundance (Poitrasson, 2017), the isotopic composition is expressed as a ratio of two isotopes. Additionally, to compare the isotopic composition of different materials, the measured isotopic ratios in the materials are normalized by comparing them with an international reference standard.

The Si isotopic fractionation between the sample and the standard is then expressed in ‰ as:

$$\delta^{30}\mathrm{Si}(‰) = \left(\frac{\left(\frac{^{30}\mathrm{Si}}{^{28}\mathrm{Si}}\right)_{\text{sample}}}{\left(\frac{^{30}\mathrm{Si}}{^{28}\mathrm{Si}}\right)_{\text{standard}}} - 1 \right) \cdot 1000. \quad (2)$$

Different reference materials are used as standards, most often NBS-28, now registered as RM-8546, a reference for silicate solid samples or secondary standard diatomite (Reynolds et al., 2007). To describe the degree of isotopic fractionation between two materials, e.g., A and B, we use the *fractionation factor* α_{A-B}:

$$\alpha_{A-B} = \frac{\left(\frac{^{30}\mathrm{Si}}{^{28}\mathrm{Si}}\right)_A}{\left(\frac{^{30}\mathrm{Si}}{^{28}\mathrm{Si}}\right)_B}. \quad (3)$$

In natural environments, α_{A-B} is very close to 1; hence, the discrimination between two materials A and B is presented in permille as

$$^{30}\varepsilon_{A-B} = (\alpha_{A-B} - 1) \cdot 1000. \quad (4)$$

Because of a small Si isotope fractionation, the discrimination between two materials A and B can be expressed as $\Delta^{30}\mathrm{Si}_{A-B}$, which gives us a good approximation for the fractionation ($^{30}\varepsilon$):

$$^{30}\varepsilon_{A-B} \approx 10^3 \ln(\alpha_{A-B}) \approx \Delta^{30}\mathrm{Si}_{A-B}, \quad (5)$$

$$^{30}\varepsilon_{A-B} = \delta^{30}\mathrm{Si}_A - \delta^{30}\mathrm{Si}_B. \quad (6)$$

In general, Si isotopes have a tendency to fractionate in association with the formation of a solid form from a solution and preferentially incorporate the lighter isotopes into the newly formed solid.

Fractionation results in the residual solution being enriched in the heavier isotopes (De La Rocha et al., 2000, 1997; Opfergelt and Delmelle, 2012; Ziegler et al., 2005). There are three main processes observed in the Si cycle that fractionate the Si isotopes: rock forming processes, water-rock interaction processes, and biological processes (Figure 3).

Rock forming processes happen on longer geological timescales and thus are not in the scope of this thesis. The water-rock interaction processes are of two types: firstly, the formation of secondary minerals and soils, and secondly, the hydrothermal fluids and deposits. In all cases the light isotopes are preferentially incorporated into the clay, hydrothermal fluid or deposit, and the residual water DSi carries a heavier isotopic signature (Figure 3).

Finally, biological processes are represented by silicifying organisms, which come from different phylogenetic branches, such as the stramenopiles (e.g., diatoms), rhizarians (e.g., radiolarians), opisthokonts (e.g., sponges), land plants, and cyanobacteria. They all take up DSi and deposit it in the form of biogenic silica (Marron et al., 2016). The BSi formed by diatoms, sponges, radiolarians and plants will show a lighter isotopic signature

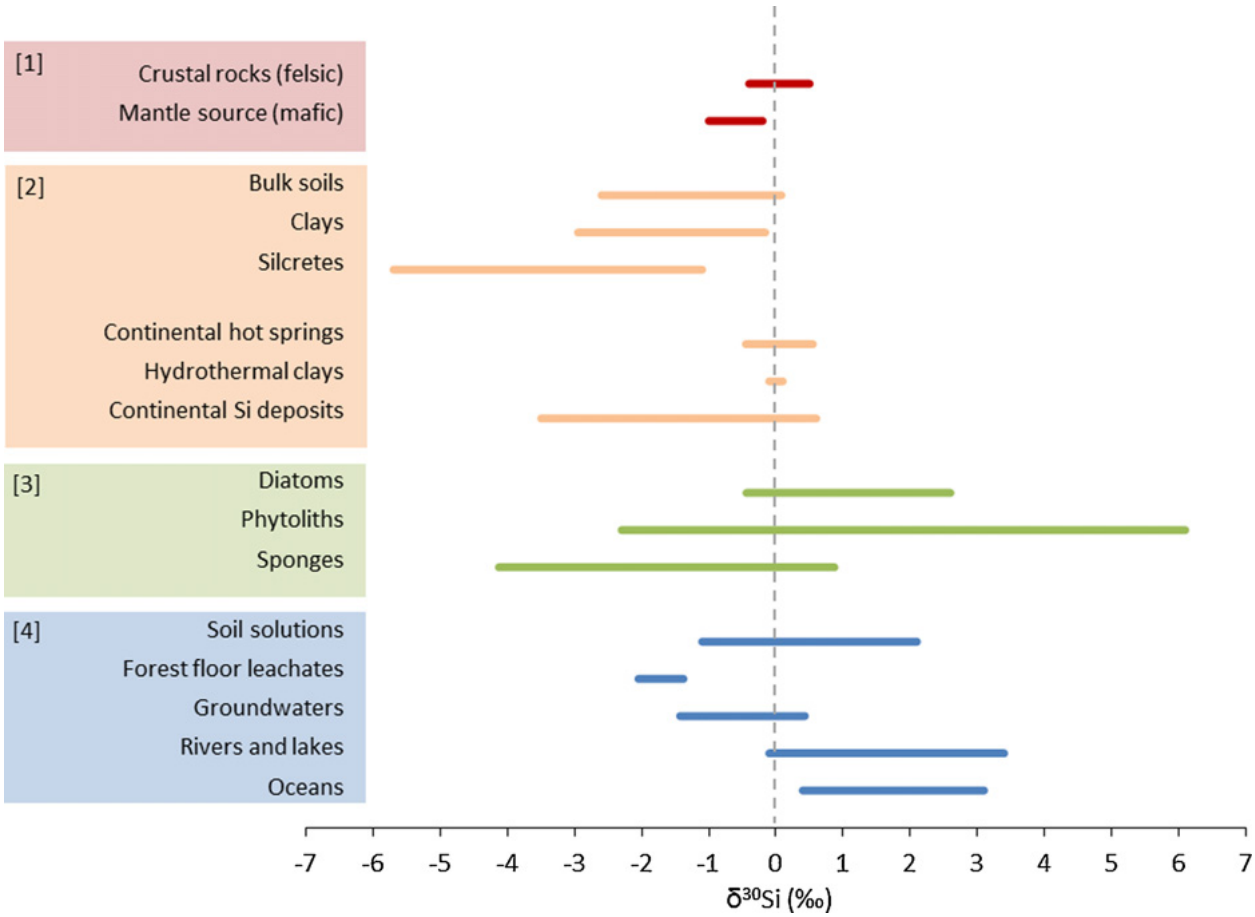


Figure 3: Variation of δ^{30}Si in the different materials. [1] are rock forming processes, [2] water-rock interactions, [3] biological processes, [4] water reservoir by Opfergelt and Delmelle (2012).

than the DSi source, and fractionates differently (Figure 3).

3.5 Si isotope fractionation models

The effect of the discrimination of the heavier Si isotopes during DSi utilization by diatoms is described in *isotopic fractionation models*. Such models follow one of two approaches.

The first approach uses the Rayleigh model of isotope distillation and predicts the Si isotopes behavior in a closed system (see Box 1 and Figure 4). This model assumes a finite silicon reservoir without any external sources (De La Rocha et al., 1997). It is often used in systems with a limited DSi source, such as well stratified lakes and oceans, where the evolution of the Si isotopic signature reflects DSi utilization. The more DSi is consumed, the smaller the fractionation ε (Figure 4, black lines). The second approach is a steady-state model describing an open system where a continuous supply of DSi from the same external source is assumed (Varela et al., 2004) (see Box 1, Figure 4).

Lakes with high DSi concentrations and large BSi accumulation are considered to have an infinite pool, and hence the open system model is used. As the isotopic signature of BSi does not reflect the DSi utilization in open DSi-unlimited systems, the interpretation of stable Si isotopes in these cases includes more variables, such as DSi sources and in-lake processes. Therefore, knowledge of

current lake DSi and BSi concentrations is an important starting point for defining all variables potentially driving BSi accumulation and Si isotopic signatures.

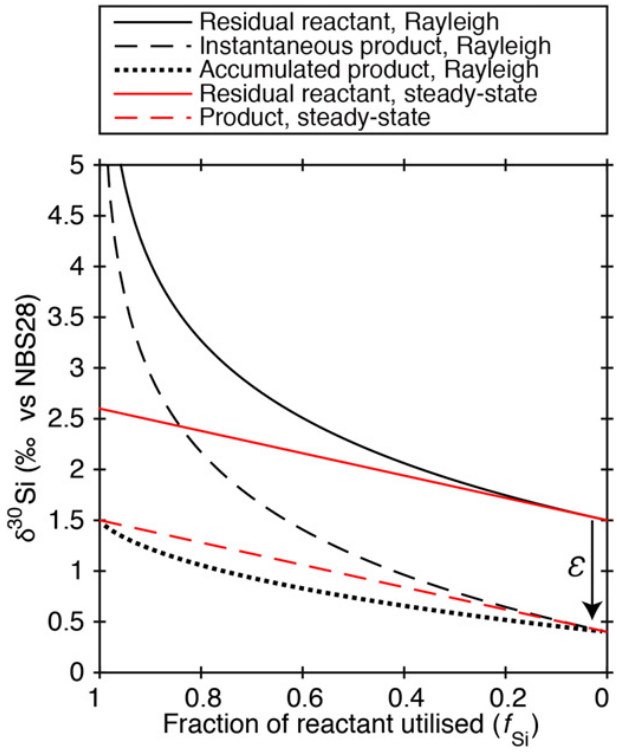


Figure 4: Two fractionation models showing the evolution of the Si isotopic signature during the formation of BSi from DSi by organisms by Frings et al. (2016). On the *x*-axis is the fraction of DSi used from 1 to 0, where 1 represents the situation when no DSi is left in the system.The open system model is shown by red lines, whereas the Rayleigh closed system is in black. The *y*-axis shows the Si isotopic composition. The dashed lines represent the δ^{30}Si BSi product, solid lines show the δ^{30}Si of the residual DSi and the dotted line represents the accumulated product of the closed system model. The fractionation factor (ε) is the difference between the dashed and solid lines.

3.6 Current state of knowledge of lake Si budgets

Some lake sediments have a BSi concentration as high as 60 weight percent (wt%) of SiO_2 (Frings et al., 2014b; Rosén et al., 2010), but no mechanism or pattern has been proposed for such high values. Frings et al. (2014b) demonstrated that surface sediment BSi concentration in lakes shows no correlation with pH, DSi concentration, lake size and depth, latitude, altitude, vegetation type or lithology. Nevertheless, high BSi accumulations tend to be found in high latitudes, low-nutrient lake systems (Rosén et al., 2010), which would require sufficient DSi concentration, low detrital input (Conger, 1942) and additionally limited dissolution and low competition by other organisms (Egge and Aksnes, 1992; Panizzo et al., 2016; Swann et al., 2010).

Stable Si isotopes have been used to constrain DSi utilization by diatoms and identification of DSi sources; however, only a limited number of studies on Si mass balances and/or stable Si isotopes in lakes have been published. Studies on Si mass balance have been done on Lake Superior and Lake Michigan in the USA (Johnson and Eisenreich, 1979; Schelske, 1985), Lake Tanganyika in the East African Rift (Alleman et al., 2005), Lake Kasumigaura in Japan (Arai and Fukushima, 2012), Lake Myvatten in Iceland (Opfergelt et al., 2011), and Lake Baikal in Russia (Panizzo et al., 2017). In addition, estimated mass balance of 34 lakes and reservoirs has been done on datasets from Frings et al. (2014b). However, from all of the studies mentioned above, only few include stable Si isotope balance.

Isotopic signature from fossil diatoms has been used as a proxy in oceanic and continental systems for changes in climate (De La Rocha et al., 1998; Hendry and Brzezinski, 2014; Opfergelt and Delmelle, 2012), changes in vegetation (Frings et al., 2016, 2014a; Leng et al., 2009; Sun et al.,

Box 1: Silicon fractionation models

The Rayleigh model

The Rayleigh model for closed systems describes the post-production DSi ($\delta^{30}Si_{postDSi}$) as:

$$\delta^{30}Si_{postDSi} = {}^{30}\varepsilon_{DSi-BSi} \cdot \ln(f_{Si}), \quad (7)$$

where ${}^{30}\varepsilon_{DSi-BSi}$ is the fractionation factor between the solid and the aqueous DSi isotopic signature and f_{Si} is the fraction of utilized DSi.

Furthermore, the accumulated BSi signature is modeled as (De La Rocha et al., 1997; Frings et al., 2016; Opfergelt and Delmelle, 2012):

$$\delta^{30}Si_{BSi} = \delta^{30}Si_{in} - \left(\frac{f_{Si}}{1 - f_{Si}}\right) \cdot {}^{30}\varepsilon_{DSi-BSi} \cdot \ln(f_{Si}), \quad (8)$$

where $\delta^{30}Si_{in}$ is the Si isotopic signature of the initial DSi before uptake (Mariotti et al., 1981).

Steady-state model

The open system model is used for systems with constant supply of DSi and the expected post-production $\delta^{30}Si_{postDSi}$ is modeled as (Frings et al., 2016; Varela et al., 2004):

$$\delta^{30}Si_{postDSi} = {}^{30}\varepsilon_{DSi-BSi} \cdot (1 - f_{Si}), \quad (9)$$

and the expected BSi signature $\delta^{30}Si_{BSi}$ is calculated as:

$$\delta^{30}Si_{BSi} = \delta^{30}Si_{in} + {}^{30}\varepsilon_{DSi-BSi} \cdot f_{Si}, \quad (10)$$

where $\delta^{30}Si_{in}$ is the isotopic signature of the initial DSi source, and ${}^{30}\varepsilon_{DSi-BSi}$ is the fractionation factor. For marine diatoms, ${}^{30}\varepsilon_{DSi-BSi} = 1.1‰ \pm 0.41‰$ (De La Rocha et al., 1997), whereas for freshwater diatoms, ${}^{30}\varepsilon_{DSi-BSi} = 1.61‰$ (Panizzo et al., 2016). Most paleoenvironmental studies use the fractionation factor of marine diatoms since there are few data for the fractionation factor by freshwater diatoms. Moreover, the species-specific fractionation is still discussed in the Si isotope community.

2011), and changes in DSi sources (Nantke et al., 2019; Vandevenne et al., 2015). Nevertheless, in lacustrine sediments the $\delta^{30}Si_{BSi}$ method is still not widely used, with only a few published studies. These studies have shown that $\delta^{30}Si_{BSi}$ in lake environments is related to processes in the watershed and to regional climate systems, e.g., Lake Victoria and Lake Edward in East Africa (Cockerton et al., 2015). Moreover, in-lake biogeochemical processes, such as diatom production and dissolution, were shown to drive the $\delta^{30}Si_{BSi}$ in Lake Rutundu (Street-Perrott et al., 2008) and Lake Huguangyan (Chen et al., 2012). In ultra-oligotrophic Lake El'gygytgyn, $\delta^{30}Si_{BSi}$ reflects changes in nutrient supply directly linked to diatom DSi utilization (Swann et al., 2010).

Additionally, in the dammed river Changjiang, changes in $\delta^{30}Si_{BSi}$ are related to the co-occurrence of clay mineral formation and seasonal diatom DSi uptake (Zhang et al., 2020). The complexity of long-term changes in the isotopic composition

and several simultaneous processes is also demonstrated in Lake Baikal (Panizzo et al., 2016).

Based on current knowledge of lake Si cycling, I investigate two lakes in this thesis for the key controlling factors, such as sedimentation rates, detrital input, continuous DSi sources, including groundwater and hydrothermalism that influence lake Si cycles in order to better constrain BSi accumulation.

3.6.1 Groundwater responsible for the high BSi accumulation

Groundwater is one of the poorly understood parts of lake systems, as measurements of groundwater discharges and chemistry are very complex. Submarine groundwater discharge is an important component in the ocean nutrient budget (Johannes, 1980; Moore, 2010; Null et al., 2012). High DSi concentrations have been identified in groundwaters worldwide (Georg et al., 2006a, 2009; Hurley et al., 1985; Luijendijk et al., 2020; Maavara et al., 2018). However, only a few studies on groundwater influences on lake and river Si cycle have been carried out, even though it has been shown that the contribution of groundwater input is substantial, especially into alpine and mountain lakes (Clow et al., 2003; Hood et al., 2006; Huth et al., 2004; Liu et al., 2004). The distinctive characteristic of the influx of groundwater DSi into lakes compared to surface waters is the low amount of detrital material carried. Therefore, groundwaters can contribute to BSi accumulation by keeping the sedimentation undiluted by clastics.

The first task is to identify the presence of substantial groundwater into to the lake. For this purpose, several methods can be used. Water mass-balance calculations have been used (Box 3), where all influxes and outfluxes were well constrained (Hood et al., 2006). A method of hydrograph separation using stable oxygen isotopes to identify the contribution of different end-members' inflowing water into a lake has been used in several mountain lakes (Huth et al., 2004; Liu et al., 2004). Additionally, silicon concentrations have been used to identify how much snow meltwater has been delivered through subsurface paths (Huth et al., 2004).

Another approach to track and quantify groundwater is to use ^{222}Rn balance (Paper II) (Dimova et al., 2013). Radon is released from radium-bearing minerals present in bedrock, soils, and sediments. Released radon is the product of radioactive decay of ^{226}Ra. Therefore, radon is more concentrated in subsurface waters compared to surface waters. A quantification of groundwater

Box 2: Groundwater quantification

Radon fluxes

Radon concentration measurements are used in Paper II for the construction of a radon mass balance and calculation of groundwater fluxes into the lake (Dimova and Burnett, 2011; Dimova et al., 2013). Radon (^{222}Rn) is produced during the radioactive decay of ^{226}Ra, which is present in rocks, soils, and sediments. Radon released from radium (Ra) bearing minerals enters the groundwater and is transported through aquifers. Groundwaters usually contain Rn concentrations orders of magnitude higher than surface waters. Thus, groundwater discharging into lakes can be detected by measuring the Rn in the lake water and end-members from sediment (the groundwater). Further, by using the steady-state ^{222}Rn, mass balance the Rn enrichment of the lake water is quantified, as well as the groundwater flux (Burnett and Dulaiova, 2003; Dimova and Burnett, 2011; Dimova et al., 2013).

influx is then calculated by radon mass balance knowing all radon sources and sinks (Box 2; Dimova and Burnett, 2011).

3.6.2 Hydrothermalism as a driver of high BSi accumulation

One of the study sites is the silicon-rich volcanic Yellowstone Lake, partly situated in the Yellowstone Caldera, which was formed by the last cataclysmic eruption 640 000 years ago (Christiansen, 2001). The Yellowstone Plateau Volcanic Field is still active mainly with on-land hydrothermalism (Hurwitz and Lowenstern, 2014).

However, two types of sublacustrine hydrothermal vents have been found within Yellowstone Lake (Balistrieri et al., 2007; Fowler et al., 2019b; Gemery-Hill et al., 2007; Morgan et al., 2003; Shanks et al., 2007). One of the vent systems in the west of Yellowstone Lake is of neutral to alkaline chemistry, and those vents bring high DSi concentration (~200 mg SiO_2 l^{-1}) water into the lake (Fowler et al., 2019b). The other venting system in the northern part of the lake is of acidic, steam-heated character, and does not contribute much to the lake Si budget (Fowler et al., 2019a).

Steam vents have a fluid chemistry close to the lake chemistry, which suggests that the steam heats up groundwater or pore water in the sediment, and those fluids are percolating upwards through the sediment and subsequently mix with the lake bottom waters. Those vents bring fluids with a DSi concentration of around 15 mg SiO_2 l^{-1} (Fowler et al., 2019a).

A result of the combination of on-land hydrothermal vents feeding lake tributaries with the sublacustrine hydrothermalism and the weathering of the silica-rich bedrock in the watershed is that the DSi concentration of Yellowstone Lake is high, around 12 mg SiO_2 l^{-1} (Balistrieri et al., 2007; Gemery-Hill et al., 2007), which is above the world's river mean (Frings et al., 2016). Those increased DSi concentrations are responsible for unlimited diatom growth and limited dissolution of diatom valves, which together create favorable conditions for massive BSi accumulation. The Yellowstone Lake system demonstrates the importance of hydrothermalism for diatom-rich sedimentation. However, studies on sublacustrine hydrothermalism and its impact on Si budgets are very sparse. To untangle the sources of DSi in Yellowstone Lake, a trace element, germanium, is used together with silicon to identify the relative importance of processes, such as hydrothermalism or weathering of bedrock in the watershed.

3.6.3 Using germanium as a trace element

Germanium (Ge) is a trace element, which mimics the behavior of Si in natural processes. Due to the very similar atom ionic sizes, covalent Si-O and Ge-O bond lengths, and identical outer electronic structures, Ge behaves like stable Si isotopes (Froelich et al., 1992). Similarly to DSi, dissolved Ge (DGe) originates ultimately from silicate rock weathering (Froelich et al., 1989). Ge/Si ratios are used as a tracer of sources and silicon behavior in exogenic processes, such as chemical weathering, biological uptake or secondary mineral formation (Froelich et al., 1992; Kurtz et al., 2002, 2011; Murnane and Stallard, 1990). The Ge/Si ratios characteristic for bedrock range between 1.5 and 6.8 µmol/mol (Mortlock and Frohlich, 1987; Tribovillard, 2013), the riverine Ge/Si ratios are within a range of 0.1 to 1.3 µmol/mol, and hydrothermal fluids have Ge/Si ratios ranging from 2 to 1000 µmol/mol (Arnórsson, 1984; Evans and Derry, 2002; Mortlock et al., 1993).

Because of the large difference between riverine and hydrothermal Ge/Si ratios, Ge/Si ratios have a high potential to trace hydrothermal inputs. However, to distinguish processes driving changes in Ge/Si ratios, where both hydrothermalism and

Box 3: Balance models

The effect of lakes on the Si cycle can be quantified through BSi accumulation, where mass balance is used to quantify all Si fluxes and BSi sinks. DSi is brought by rivers and tributaries, as well as by groundwater. Diatoms form BSi, which is partly preserved in the sediment. The flux of BSi into the sediment is a sign of higher DSi influxes relative to outfluxes. To constrain DSi fluxes, the water balance must be constructed prior to the Si mass balance. When the lake water balance is in steady-state, the Si mass balance can be calculated. The lake water (eq. 11) or DSi mass balance (eq. 12) is calculated using balance equations:

$$\Delta V = Q_{\text{in}} + Q_{\text{GWin}} + P - Q_{\text{out}} - Q_{\text{GWout}} - E, \tag{11}$$

where ΔV is the change in lake water volume, Q_{in} is stream inflow, Q_{GWin} is groundwater inflow, P is precipitation, Q_{out} is stream outflow, Q_{GWout} is out-flowing groundwater, and E is evaporation. Groundwater can be replaced or complemented with hydrothermal fluid discharges.

The DSi flux is calculated as $F = Q \cdot c$, where Q is discharge and c is DSi concentration. The DSi balance is then calculated as:

$$\Delta DSi = F_{\text{in}} + F_{\text{GW in}} - F_{\text{out}} - F_{\text{GW out}} - F_{\text{BSi}}, \tag{12}$$

where ΔDSi is the change of lake DSi, F_{in} is the stream DSi influx, F_{out} is the stream DSi outflux, $F_{\text{GW in}}$ is the incoming groundwater DSi flux, and finally $F_{\text{GW out}}$ is the DSi outflux via groundwater. Groundwater fluxes can be replaced or complemented with hydrothermal fluid fluxes. F_{BSi} is flux of BSi into the sediment calculated as:

$$F_{\text{BSi}} = SR \cdot \rho_{\text{dry}} \cdot BSi\ wt\%, \tag{13}$$

where SR is sedimentation rate, ρ_{dry} is dry bulk sediment density, and $BSi\ wt\%$ is the BSi concentration in sediment.

A positive Si mass balance is defined as $F_{BSi} > 0$, which occurs in condition where $F_{in} > F_{out}$. Hence, if steady-state is reached, $\Delta DSi = 0$.

Based on the water and Si mass-balance models, stable Si isotope balance models (Section 3.5) can be used to calculate the DSi utilization, the DSi source isotopic composition or the BSi isotopic composition, depending on known variables.

clay mineral formation show enrichment in Ge, stable Si isotopes are used. The stable Si isotopes are typically isotopically lighter in hydrothermal fluids compared to the remaining DSi after clay mineral formation; therefore, the processes responsible for the Ge/Si ratio and δ^{30}Si signature can be identified. A combination of these two proxies is a useful tool for studying the influence of hydrothermal inputs into Yellowstone Lake. Additionally, δ^{30}Si combined with Ge/Si in diatom frustules has the potential to identify the relative proportion of the effects of diatom production

versus hydrothermal inputs on the diatom isotopic signature.

4 Methods

4.1 Dissolved silicon

Silicon dissolved in water is present as orthosilicic acid (H_4SiO_4), with an assumption that most of the DSi is a monomer. Polymerization occurs only at extreme pH and temperatures (Dietzel, 2000; Wonisch et al., 2008) and in the presence of a high concentration of organics (Coradin and Livage, 2001). Therefore, natural samples from organic-rich environments or hydrothermal fluid samples with extreme pH, both high and low, and extreme temperatures need to be treated cautiously in order to deliver accurate DSi concentrations. Water samples measured in this thesis originate from oligotrophic lakes and streams, therefore, the risk of polymerization is low. Hydrothermal vent fluid were sampled by a specialized sampling system developed by Wu et al. (2011) and diluted to lower DSi concentrations (described in Fowler et al. (2019a,b) to prevent effects of fractionation during the sampling process.

All river and lake water samples were filtered directly in the field through a 0.45 µm cellulose Sterivex™-HV Durapore filter and acidified with HCl to pH 2 in the laboratory before the analysis of DSi concentrations. An automated molybdate-blue method (Grasshoff, 1999; Hansen and Grasshoff, 1983) was used for DSi measurements with a Smartchem 200 (AMS System) discrete analyzer with an instrumental error of ±3.7 %. The molybdate-blue method is based on the reaction of monomeric silicic acid with ammonium molybdate forming a yellow molybdosilicic acid complex. This complex is reduced from Mo(IV) to Mo(V) by ascorbic acid to heteropoly-molybdenum, which is measured spectrophotometrically at 660 nm.

4.2 Sedimentary biogenic silica

The quantification of BSi is done through a conversion of BSi into DSi via weak-alkaline extraction (Conley and Schelske, 2001; DeMaster, 1981). This method is based on slower dissolution rates of minerals compared to the dissolution rates of BSi in a weak alkaline reagent. Thus, the extraction is done by digesting 30 mg of freeze-dried homogenized sediment in 0.1M Na_2CO_3 for 5 hours with sub-sampling of 0.1 ml after 3, 4, and 5 hours.

A limited number of samples (~5 %) was tested for dissolution of SiO_2 by prolonged digestion over 24 hours with sub-sampling after 3, 4, 5, 9, 10, 11, 20, 22, and 24 hours of the digestion. Based on those samples, no distinguishable minerogenic SiO_2 dissolution occurred during the digestion. Therefore, weight percentages of biogenic SiO_2 were calculated as the mean value of extracted SiO_2 during the first five hours. DSi concentrations were measured as described in Section 4.1.

4.3 Stable silicon isotopes

4.3.1 Sample preparation

Stable silicon isotope analyses are done on pure diatoms, opaline silica materials, or waters. To gain clean diatoms, secondary minerals, organic matter, and carbonates have to be removed from the sample by a combination of chemical, physical, and mechanical separations. Organic matter and carbonates are removed using 33 % H_2O_2 and 5 % to 30 % HCl, respectively (Morley et al., 2004). The mineral fraction is separated by using density differences between the mineral fraction (2.6 g cm^{-3}) and the biogenic silica (2.0 g cm^{-3}). The method of heavy liquid separation using sodium polytungstate at densities of 2.05 to

2.1 g cm^{-3} is used to separate the floating opaline silica from the settled mineral fraction. Clusters of secondary minerals often have similar densities as biogenic silica. Therefore, 0.05 M sodium pyrophosphate ($Na_4P_2O_7$) is used to disintegrate fine grain-size clay clusters, and the sample is then sieved at 53 and/or 25 µm for the final removal of clay particles (grain size <53 µm). The sample purity is always confirmed by using first light microscopy and further by using a scanning electron microscope (SEM) (Figure 5) with the possible extension of energy-dispersive X-ray spectroscopy (EDS) to map possible contaminants.

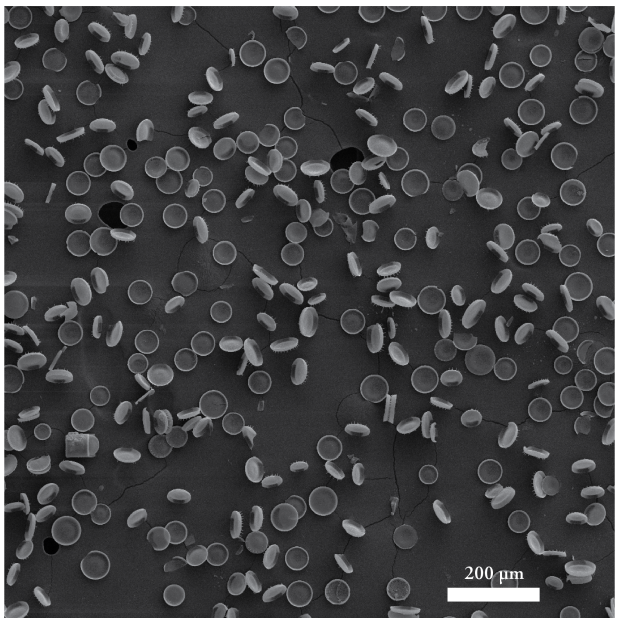


Figure 5: An example of cleaned diatoms from Yellowstone Lake

Cleaned opaline material – diatoms – is transformed into solution by dissolution in 0.5 to 1 ml of 0.4 M NaOH (analytical purity) at 50 °C for at least 48 hours. After 48 hours of dissolution, samples are diluted with Milli-Q® water to prevent amorphous silica precipitation and artificially caused fractionation. The samples are further neutralized by 0.5 to 1 ml of 0.4 M suprapur® HCl. The DSi concentration of the produced solutions is analyzed (Section 4.1) to obtain Si recovery, which must be between 90 and 100 %.

Water samples are usually filtered directly in the field and later acidified to prevent any processes causing fractionation. For most of the water samples no additional cleaning is needed. Only samples with excessive concentrations of sulfates or chlorides must be additionally pre-cleaned by using anion-chromatographic separation (Gaspard et al., 2020) or overcome by doping with H_2SO_4 before isotope measurements (Chen et al., 2020; Hughes et al., 2011; Oelze et al., 2016).

Sample solutions are further purified before silicon analysis by a cation-chromatographic separation, which removes any contaminants left and results in a solution of pure Si (Georg et al., 2006b). The international Si standard NIST reference material RM-8546 (former NBS-28) and the laboratory standard Diatomite are both cleaned along the sample purification to constrain the cleaning process, and full chemical column blanks are also included.

4.3.2 Silicon isotopic composition determination

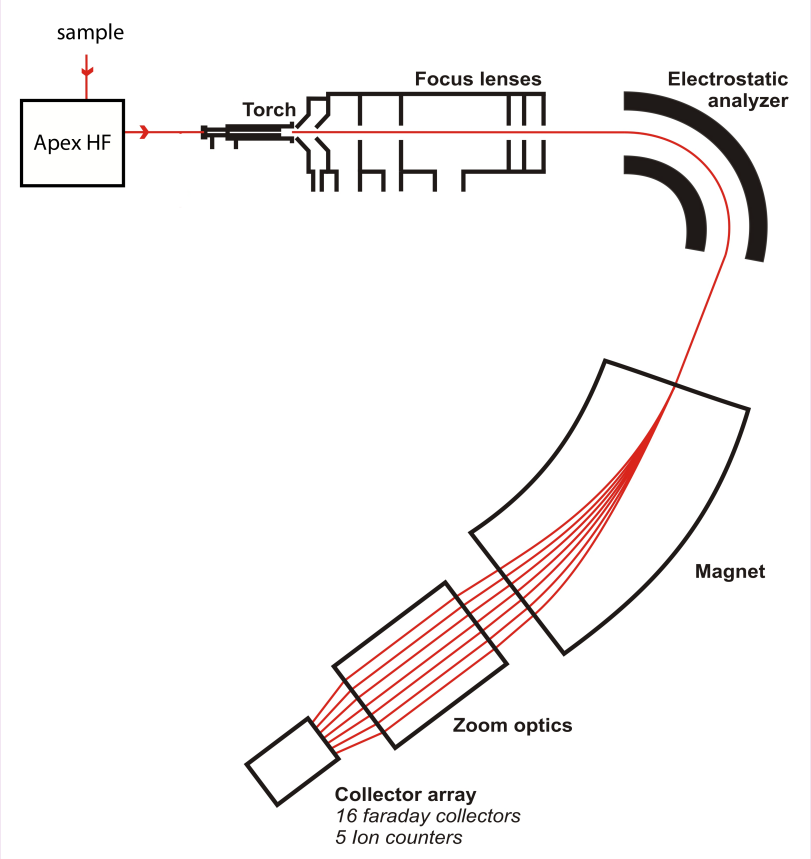
Stable Si isotopes are commonly measured by multi-collector inductively coupled plasma mass-spectrometers (MC-IPC-MS, Box 4). Our measurements were performed on a NuPlasma (II) HR MC-ICP-MS (Nu Instruments™) in dry plasma mode using an Apex HF desolvation nebulizer at the Vegacenter, Swedish Museum of Natural History, Stockholm.

All samples were spiked with Li to match the standard matrix (see Box 5). The instrumental mass bias is constrained by using the sample–standard bracketing technique. The ^{28}Si signal of full procedural blanks is always determined in order to identify possible sample contamination.

Silicon isotopes data are reported as deviations of $\frac{^{30}Si}{^{28}Si}$ and $\frac{^{29}Si}{^{28}Si}$ from the RM-8546 in ‰, denoted $\delta^{30}Si$ as shown in equation 2. Full chemical sample

Box 4: MC-ICP-MS

Multi-collector inductively-coupled plasma mass-spectrometers are nowadays commonly used for Si isotope measurements. The principal mechanisms behind the measurements are that a solution is introduced, in our case through Apex HF, into an inductively-coupled plasma created by a torch, where electrons are removed and positively charged ions are formed. These ions are accelerated across an electrical potential gradient up to 10 kV, focused into a beam using a series of slits and focus lenses, and passed through an energy filter (electrostatic analyzer). A consistent energy spectrum is created by the energy filter and further passes through a magnetic field, which separates ions based on their mass-to-charge ratio. Finally, the beams of sorted ions are collected by multiple collectors simultaneously, where the ions are converted to voltage. The isotope ratios are then calculated by comparing voltages from different collectors.



A simplified scheme of MC-ICP-MS NuPlasma instrument in Vegacenter, Swedish Museum of Natural History, Stockholm. Modified from the original Vegacenter scheme (Vegacenter, 2020).

replicates are measured in order to determine the natural variability of the sample, whereas analytical replicates are used to quantify the measurement deviation.

Box 5: Standard preparation

The sample isotopic ratio is always normalized to a standard material. Therefore, the international Si standard NIST reference material RM-8546 (former NBS-28), as well as laboratory standards are prepared via NaOH fusion (Georg et al., 2006b).

Another way of standard preparation is used in the Vegacenter facilities, where Si isotopes were measured. The laboratory standards IRMM-018, Big-Batch, Diatomite, and the international Si standard RM-8546 were prepared by fusion with $LiBO_2$ (Sun et al., 2010), and thus the standard matrix contains Li.

Therefore, our alkaline NaOH fused RM-8546 and Diatomite standards, cleaned along with the sample purification, were matrix matched to contain 3 mg l^{-1} Li IPC-MS standard. Similarly, all purified samples were diluted to a concentration of 3 mg l^{-1} of Si in a 0.12 M Seastar™ HCl matrix and doped with Li to contain 3 mg l^{-1} of Li to match the Vegacenter standard matrix.

A three-isotope plot δ^{30}Si vs δ^{29}Si is used to ensure that there are no polyatomic interferences present during mass spectrometry measurements. All measured samples should fall on the expected mass-dependent fractionation line with a slope of 0.5092 (Figure 6, Reynolds et al., 2007).

The secondary reference materials Diatomite, Big-Batch, and IRMM-018 are measured throughout all measuring sessions. Our measuring sessions (over 3 years) resulted in means of $\delta^{30}\text{Si} = 1.26 \pm 0.19$ ‰ ($2\text{SD}_{\text{repeated}}$, $n = 219$) for Diatomite, $\delta^{30}\text{Si} = -10.64 \pm 0.18$ ‰ ($2\text{SD}_{\text{repeated}}$, $n = 77$) for Big-Batch, and $\delta^{30}\text{Si} = -1.77 \pm 0.18$ ‰ ($2\text{SD}_{\text{repeated}}$, $n = 100$) for IRMM-018. All secondary reference material values are in good agreement with values from previous inter-laboratory comparisons (Reynolds et al., 2007). The reproducibility and repeatability of all samples is 0.2 ‰. In the Vegacenter laboratory long-term precision was determined to be 0.15 ‰ (expressed as 2SD).

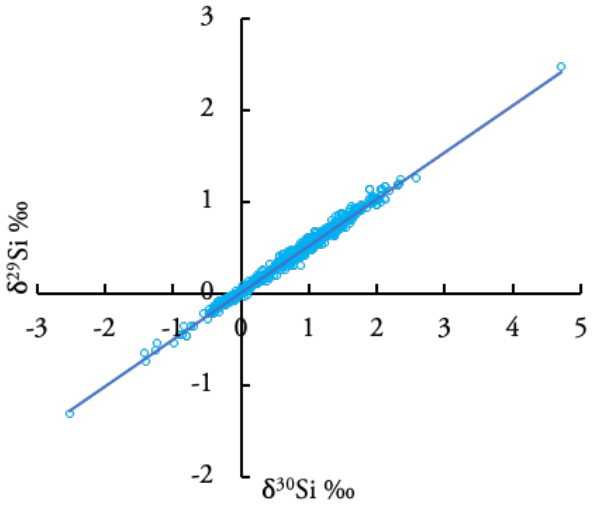


Figure 6: Three-isotopes plot of all Si isotope measurements in this thesis. Data plotted without error bars, however, all data follow the expected mass-dependent fractionation line with slope 0.5092 (blue line) (Reynolds et al., 2007), $\delta^{29}\text{Si} = 0.51 \cdot \delta^{30}\text{Si}$, $R^2 = 0.99$, $n = 986$.

4.4 Ge/Si ratios determination

Ge/Si mole ratios can be determined using several techniques, but in general, concentrations of DGe and DSi are measured, and the Ge/Si ratios are calculated from those values. To measure Si concentrations, the molybdate-blue method can be used, as well as inductively-coupled plasma-optical emission spectrometry (ICP-OES) or inductively-coupled plasma mass spectrometry (ICP-MS). Due to its low natural abundance, germanium needs to be measured by an ICP-MS through measuring the most abundant ^{74}Ge isotope (35.9 %). In case of measuring both DSi and DGe concentrations on an ICP-MS, the two

isotopes ^{74}Ge and ^{29}Si are monitored. Polyatomic interferences (e.g., ^{36}Ar, ^{38}Ar on ^{74}Ge) are removed by a collision cell with He as reaction gas. Then, the Ge/Si ratios are calculated directly from the ratio of beam intensities.

4.5 Total organic carbon and nitrogen – TOC and TN

Total organic carbon (TOC) and total nitrogen (TN) analyses are used to better constrain the sediment composition by quantification of organic matter (Papers II, III, and IV). To measure TOC and TN, a COSTECH ECS4010 elemental analyzer was used. Samples of dried homogenized sediment are packed in tin capsules and introduced into an ignition chamber, where the capsules are combusted. During this combustion, nitrogen and carbon gasses are released and carried by a carrier gas (He) to a pre-packed reaction column. The pre-packed column contains copper wires to remove any oxygen which was not consumed during the initial combustion and converts any oxides of nitrogen into N_2 gas. Further, the de-oxidized gasses pass through a gas-chromatographic (GC) column placed in an oven and heated up; thus the carbon and nitrogen are separated. After the separation, the C and N are quantified by a thermal conductivity detector. TOC and TN are measured simultaneously and the C/N ratio is calculated to identify the organic matter source (Meyers, 2003).

If a sediment contains calcium carbonate, the TOC measurements would be biased. Therefore, samples are tested for carbonate ($CaCO_3$) content by comparing bulk sediment TOC with the de-calcified replicate. The de-calcification is done before the TOC measurements by adding HCl and heating to 60 °C in silver capsules (Brodie et al., 2011). Both replicates are measured, and the carbonate content is calculated as the difference in TOC between the de-calcified sample and the bulk sample.

4.6 ITRAX µX-ray fluorescence – XRF

All long cores (Papers III and IV) were scanned by ITRAX µXRF analyzer using the X-Ray Fluorescence principle. The technique of X-Ray Fluorescence is used to determine the elemental composition of sediment. The principle of this method is to expose the sediment to X-rays, which causes ionization of the atoms, excitation of electrons from the atomic inner orbit. When an electron is excited, the atom becomes unstable, and electrons from higher orbitals must stabilize the atom by filling the gap left by the excited electron. As these electrons are moving from higher energy orbitals to lower ones, the excessive energy is released in the form of photons. The energy released is equal to the energy difference between two orbitals, which is element-specific, and thus, the element is identified. The ITRAX is an automated multi-function core-scanning instrument recording elemental variations in the sediment cores with a resolution of up to 100 µm. We have used data from X-ray-fluorescence analysis and from the integrated magnetic susceptibility sensor to constrain the detrital input through the elements Ti and Fe or through magnetic susceptibility (Davies et al., 2015). Ti and Fe are elements released during bedrock weathering and are part of the minerals brought by rivers or run-off into the sedimentary basins. Further, elements such as Cl and As, which are characteristic for some hydrothermal fluids in Yellowstone Lake (Balistrieri et al., 2007; Gemery-Hill et al., 2007; Shanks et al., 2007), were used for detection of past hydrothermal activity.

5 Summary of papers

Paper I

Zahajská, P., Opfergelt, S., Fritz, S. C., Stadmark, J., & Conley, D. J. (2020). What is diatomite? Quaternary Research, Vol. 96, pp. 48–52. doi:10.1017/qua.2020.14

Widespread inconsistencies in the use of the word "diatomite" in the literature were the motivation for bringing clarity into diatom-rich sediment nomenclature. In order to stimulate scientific discussion and communicate our research efficiently, a clear definition of diatom-rich sediment was proposed.

Paper I is a literature review on sediment nomenclature and suggests unification of variability in the naming of diatom-rich sediment. We defined the principal name diatomite to be used for a siliceous/opaline consolidated sediment composed of more than 50 % of diatom biogenic silica, with a porosity higher than 70 % and formed in temperatures below 50 °C and at burial depths of 0 to 600 m. The stand-alone word *diatomite* is used

Table 1: Authors' contribution to the papers

	Paper I	**Paper II**	**Paper III**	**Paper IV**
Planning and study desgin	P. Zahajská, D. J. Conley	P. Zahajská	P. Zahajská	P. Zahajská, D. J. Conley
Literature review	P. Zahajská	n/a	n/a	n/a
Fieldwork and data collection	n/a	P. Zahajská, C. G. Olid	P. Zahajská	P. Zahajská, R. Cartier, D. J. Conley, S. Fritz, HD-YLake team*
Labwork, sample preparation	n/a	P. Zahajská, C. G. Olid	P. Zahajská	P. Zahajská, R. Cartier
Analysis	n/a	P. Zahajská, C. G. Olid	P. Zahajská	P. Zahajská, F. Gaspard, P. Frings
Figures	P. Zahajská	P. Zahajská	P. Zahajská	P. Zahajská, R. Cartier, L. Morgan*
Data interpretation and discussion	All authors	All authors	All authors	All authors
Lead author(s)	P. Zahajská	P. Zahajská, C. G. Olid	P. Zahajská	P. Zahajská
Comments and editing of manuscript	All authors	All authors	All authors	All authors

* *contributors who are not co-authors*

specifically for sediment composed of more than 80 % of diatom biogenic silica.

Unconsolidated sediments with a content higher than 50 % of diatom biogenic silica are called *diatomaceous ooze*. Consolidated sediments with a content of diatom biogenic silica from 10 to 50 % are called *diatomaceous sediment* combined with the prevailing sediment name. Burial depth, low temperatures and diatom content are three main classifiers in the naming of diatom-rich sediment.

Paper I aims to bring awareness about the inconsistencies in terminology used for diatom-rich sediment and proposes a solid classification system.

Paper II

Zahajská, P., Olid, C. G., Stadmark, J., Fritz, S. C., Opfergelt, S., & Conley, D. J. (2020). Modern silicon dynamics of a small high-latitude subarctic lake. Biogeosciences Discuss., in review. doi:10.5194/bg-2020-441

Several lakes in northern Sweden have high BSi concentrations, up to 60 wt% (Frings et al., 2014b; Rosén et al., 2010). Paper II focuses on finding the sources of the silica and conditions leading to diatom-rich sedimentation in a small, high-latitude subarctic lake. Factors responsible for the high BSi concentration in the sediment (up to 46 wt% of SiO_2) of Lake 850 are explored using water, Si, and stable Si isotope mass-balance models.

The water balance revealed the importance of groundwater supply, which was quantified by using a ^{222}Rn mass-balance model. Strong seasonality in the stream inlets and outlet was observed. The water balance models showed lake-level changes of $\pm$ 0.95 m annually due to the seasonality of inputs, despite the presence of groundwater supply. Additionally, the water and Si mass-balance models suggest that groundwater brings three times more water and DSi into the lake than the ephemeral stream inlets. The Si and stable Si isotope mass balances revealed groundwater input to be a potential Si source for diatom production.

Furthermore, sedimentation rates of 0.08 cm yr^{-1} and high diatom preservation suggest low residence time of diatoms in the water column, which results in high BSi accumulation. When including all sources and the total BSi burden into the mass- and Si isotopic model, diatom production consumes up to 79 % of the lake DSi. The stable Si isotopic signature of sediment diatoms reflects the DSi sources and diatom production. Groundwater supply and mass accumulation rates justify the good preservation of diatoms in the sediment. BSi accumulation during the last 150 years is driven by sufficient DSi supply with relatively light isotopic signature and by accumulation rates, which are responsible for good diatom preservation.

Paper III

Zahajská, P., Cartier, R., Fritz, S. C., Stadmark, J., Opfergelt, S., Yam, R., Shemesh, A. & Conley, D. J. Impact of Holocene changes in climate on silicon cycling in Lake 850, Northern Sweden. Submitted to The Holocene, 2021.

Although the continental silicon cycle has been intensively studied during the last 20 years, the diatom δ^{30}Si records from lake sediments are still sparse. Moreover, the interpretation of those data is usually complex and site specific. The individual factors driving changes in lake DSi concentrations are often poorly understood. The study in Paper III contributes to the understanding of the functioning of continental silicon cycle sinks on long-term scales.

Diatoms have a high preservation potential and their frustules carry an isotopic signature of the source DSi. Climate, diatom productivity, DSi availability, detrital input, and weathering rates are potential factors influencing the variability in

diatom BSi deposits.

In Paper III the Holocene variability in BSi deposits and their stable Si isotopes in Lake 850 are studied to identify factors driving diatom-rich sediment formation. Stable silicon isotopes were used as a tracer of changes in DSi sources and processes in the last 9400 cal. yr BP. Changes in sedimentation due to allochthonous detrital input were identified through sediment elemental composition.

Paper III suggests that the lake was mainly influenced by changes in summer temperatures and by hydrological fluctuations during the last 9400 cal. yr BP. The diatom δ^{30}Si in Lake 850 suggests the presence of a sufficient, isotopically light DSi source, such as groundwater or freshly weathered primary minerals. Moreover, the δ^{30}Si shows a linkage to changes in regional climate, where lighter isotopic values coincide with continental climate during the mid-Holocene, and a heavier Si isotopic signature shows a connection to the oceanic climate in the early and late Holocene. The BSi accumulation ranges between 0.28 and 1.50 mg cm^2 yr^{-1} of SiO_2 during the Holocene. Good preservation, where sedimentary diatoms show no sign of dissolution, combined with low sedimentation rates induced by low detrital input leads to a BSi concentration as high as 42 wt% of SiO_2. However, correlations of proxies showed that both the BSi concentrations and the δ^{30}Si values result from several concurrent processes.

Paper IV

Zahajská, P., Frings, P., Gaspard, F., Cartier, R., Opfergelt, S., Fritz, S. C., Stadmark, J., & Conley, D. J. Impact of Holocene sub-lacustrine hydrothermal activity on the Si cycle and diatom-rich sediment accumulation in Yellowstone Lake. Manuscript.

Yellowstone Caldera is one of the largest active silicic volcanoes in the world (Mason et al., 2004). Yellowstone Lake is situated within the Yellowstone Caldera, which results in lake water enriched in DSi compared to other freshwater environments. The elevated DSi concentrations are driving diatom production, which results in sedimentary BSi.

Sub-lacustrine hydrothermal activity has previously been identified in Yellowstone Lake, and Paper IV is focusing on the impact of hydrothermal events on the lake Si cycle and diatom BSi accumulation. Stable silicon isotopes (δ^{30}Si) together with Ge/Si ratios are used to study a single fossil diatom species *Stephanodiscus yellowstonensis*, as well as recent water DSi sources. Recent lake water, tributaries, and hydrothermal vent fluids samples were studied to better constrain the impact of Holocene hydrothermal events on the sedimentary BSi record.

An undisturbed deep basin sedimentary record and a hydrothermally affected record were both studied for their elemental composition, BSi concentration, δ^{30}Si, and Ge/Si ratios. A series of hydrothermal explosions and the Mazama ash layer originating from the Mazama volcano explosion (~7700 cal. yr BP) were present in both studied cores, and, together with lithological units (Tiller, 1995), those were used for correlation between the two cores.

The hydrothermal explosions showed no identifiable impact on BSi accumulation, δ^{30}Si signature, and thus on the lake DSi budget. Both cores show several similarities, which suggest a stable and homogeneous DSi source within the entire lake. Additionally, the ranges of δ^{30}Si and Ge/Si values of the diatom *Stephanodiscus yellowstonensis* suggest that the productive layer of the lake where the diatoms live was well mixed and biogeochemically very stable, with a large hydrothermal background, which limits the impact of most of the disturbances during the last 9800 cal. yr BP. BSi, stable Si isotopes, Ge/Si ratios, the elemental composition of the sediment and lithology data

all suggest that Yellowstone Lake is a stable, well-buffered system on long timescales.

The variation of BSi is partly connected to changes in production reflected in the δ^{30}Si fossil diatom record. However, the variation in the δ^{30}Si likely shows changes in the relative proportion of DSi sources (hydrothermal to rivers) combined with effects of production and potentially dissolution. All those processes occur concurrently.

A shift of 0.6 ‰ toward heavier δ^{30}Si throughout both cores reflects changes in diatom production associated with changes in Holocene climate, specifically summer temperatures and lake water column mixing. An alternative explanation of this systematic isotopic shift toward heavier δ^{30}Si is a gradual shift in the relative proportion of hydrothermal DSi input and riverine DSi supply. Relatively larger contribution of heavier δ^{30}Si brought by increased run-off from watershed could explain the trend in δ^{30}Si. Likely both explanations are plausible.

These results illustrate that hydrothermal activity has a significant impact on the lake Si cycle and on BSi accumulation. However, hydrothermal explosions are masked by the high long-term hydrothermal background inputs to the lake. Long-term stability of large lake systems, such as Yellowstone Lake, results in a significant sink of Si in the Si cycle; however, quantification of those sinks is still needed for improved understanding of the global Si cycle.

6 Discussion

6.1 Diatomite in society

Diatomite is a widely used word, as well as a material used in everyday production. Due to its high porosity, large surface area, high permeability, and chemical inertness, diatomite is used for filtering inorganic and organic chemicals, pharmaceuticals, but also beer, wine, whiskey, and fruit and vegetable juices (Inglethorpe, 1993). Diatomite filtering removes fine-grained particles from fluids. There are many other industrial applications of diatomite, such as fillers, insulators, abrasives, fertilizers or absorbent powders with potential use for heavy metals and oil water contamination removal (Bakr, 2010). Thus, diatomite is of great importance for society. But what is diatomite actually? Materials used in those industrial processes are sediments with more than 80 % of diatoms.

When investigating diatom-rich sediment formation, a clear definition of the sedimentary content of diatom SiO_2 is needed. In order to draw general conclusions about what factors are crucial for diatom-rich sediment formation, the comparison of several sedimentary records is essential. Inconsistencies in the present use of the term diatomite and diatomaceous sediment throughout literature were the motivation to clarify nomenclature.

Paper I describes the inconsistency of usage of the word diatomite in the scientific literature and suggest a classification of consolidated and unconsolidated diatom-rich sediments.

6.2 Constraining the modern Si cycle in lakes

Estimates of the global Si fluxes usually require simplification or assumptions due to the lack of data on lakes and rivers, which introduces high uncertainties into models of Si dynamics. Stable Si isotopes can be used to constrain the DSi utilization by processes within the lake and the watershed. Building a detailed Si or Si isotope mass-balance model requires monitoring data on discharge, DSi concentration, and δ^{30}Si from all inlets and outlets, as well as lake water. Moreover, other elements, such as sulfur, chloride or sodium are important to monitor, as those elements can

modify the δ^{30}Si if they are not removed from the matrix (Hughes et al., 2011). An important part of Si and Si isotope mass-balance models is to test the presence of additional DSi sources, such as groundwater, hydrothermal input or dissolution of secondary minerals. Groundwater and hydrothermal vents were investigated in our studies on Lake 850 (Paper II) and Yellowstone Lake (unpublished data, Figure 8).

Additionally, knowledge about BSi production and accumulation is also essential for building a mass balance. Finally, processes, such as clay mineral formation or dissolution, can also play an important roles in the Si budget. Information about the bathymetry and annual lake volume dynamics is needed in order to quantify water and DSi residence times. With all these data, a very detailed model describing the lake system and its functioning can be constructed and forecasting of BSi accumulation or release can be calculated. In the case of missing data, they can be modeled, which brings uncertainties into the mass balances. In this thesis, I have constrained most of the factors and processes influencing the DSi and BSi variation, and I modeled missing data, as suggested above.

Previous Si mass balances have been constructed on Lake Michigan and Lake Superior (Schelske, 1985), the African Great Lakes (Hecky et al., 1996), Williams Lake (LaBaugh et al., 1995), Lake Kasumigaura (Arai and Fukushima, 2012), and many more (Frings et al., 2014b); however, only some of those studies constrained all the influxes and outfluxes, as we did in our study (Paper II). Based on our results, the mass balances need to be conducted cautiously, as all DSi sources need to be constrained to evaluate whether the lake acts as Si sink or source.

Studies on Si isotope mass balances are more sparse and have been conducted on Lake Baikal (Panizzo et al., 2017), Lake Tanganyika (Alleman et al., 2005), and lakes of the Taupo Volcanic Zone (Pearson et al., 2016). In Lake Baikal it was shown that one-fourth of the inflowing DSi during the last century is stored in the sediment as BSi (Panizzo et al., 2017). The δ^{30}Si long-term trend indicated the complexity of the Lake Baikal system, where several co-occurring processes affect the isotopic composition. A similar phenomenon is observed in Yellowstone Lake (Paper IV). In Lake Tanganyika the mass balance resulted in a non-steady state Si cycle in the lake, where the DSi concentration has been increasing in the last 30 years, and diatom production has decreased as a response to the lowering of N and P supply (Alleman et al., 2005). In contrast, our models assume steady-state in order to quantify missing DSi sources and further interpret the sedimentary data. One of the potential DSi sources was demonstrated in several Taupo Volcanic lakes, where an Si efflux from the sediment to the lake water is present even at high lake DSi concentrations often due to hydrothermal input (Pearson et al., 2016). Thus, similar processes are expected in Yellowstone Lake, however, no data for identification of Si efflux had yet been measured.

All those studies together indicate that the Si cycle in lakes reflects local processes and that it is site specific. Therefore, to understand and later quantify the importance of continental DSi filters and BSi sinks in lakes and reservoirs, more complex models that include lake balance data must be used, including the potential effects of bedrock, groundwater, hydrothermal inputs and weathering rates.

6.3 The role of groundwater in lake Si cycles

Lakes, reservoirs, and processes in the watersheds of rivers regulate the DSi concentration and stable Si signature exported into the ocean (Cockerton et al., 2015; Phillips and Cowling, 2019). Groundwater has been identified to be an important

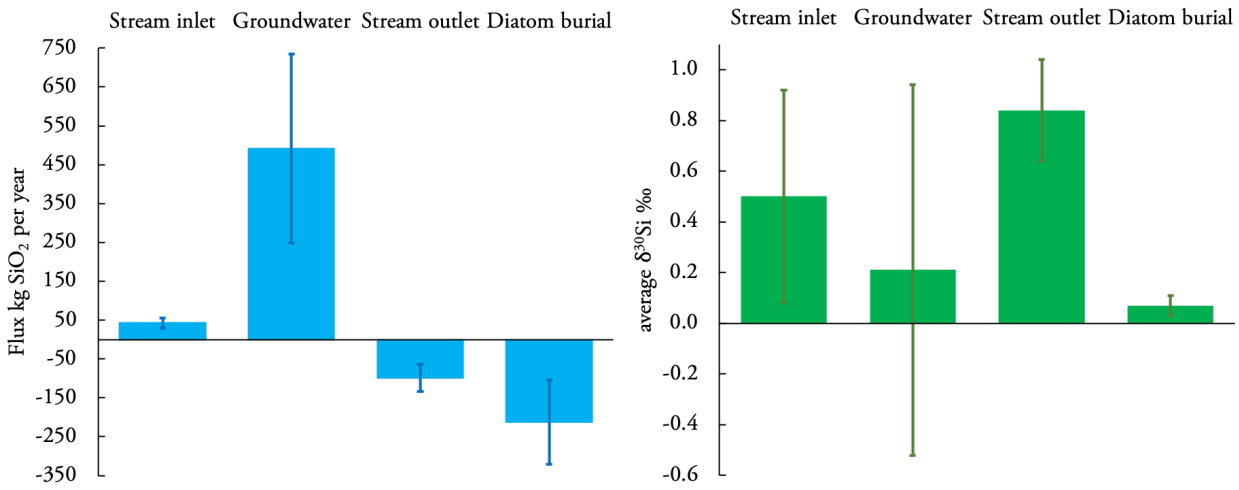


Figure 7: Mean annual Si and stable Si mass balance of Lake 850 (based on data from Paper II).

water source in mountain lakes (Clow et al., 2003; Hood et al., 2006; Huth et al., 2004; Liu et al., 2004). Groundwaters are not only a water source, they also provide the lakes and rivers with DSi (Paper II) (Hurley et al., 1985; Maavara et al., 2018; Opfergelt and Delmelle, 2012). However, mass balances conducted for the global Si cycle have not accounted for this additional source of DSi into lakes, which contributes to BSi accumulation, and therefore the BSi retention in the continental cycle is likely underestimated.

Papers II and III show an example of the impact of groundwater on BSi accumulation in an oligotrophic mountain and high-latitude lake in northern Sweden. Lake 850 is situated above the treeline and is not in steep terrain. No substantive impact on the DSi budget is likely caused by vegetation, as no developed soils are acting as a DSi pool; only bare bedrock with mosses, lichens and grasses are found in the lake watershed. Additionally, low sedimentation rates and DSi brought into the lake by groundwater are contributing to high BSi accumulation (Papers II and III). The groundwater brings 3 times more DSi into the lake than the ephemeral streams during the ice-free period. If a simplified mass balance using only the stream inlet DSi flux and the outlet DSi flux were made, this lake would act as a DSi source (Figure 7). However, if the BSi accumulation rate and groundwater are accounted for in the mass-balance model, the lake becomes a DSi sink, which is in agreement with observations in sediment cores (Figure 9).

Paper II used a short gravity core to quantify the BSi accumulation, which resulted in a slightly lower BSi concentration (mean 18.8 wt%) than we found in a long piston core (mean 32.3 wt%) presented in Paper III. Additionally, the uppermost 6 cm of the sediment from Lake 850 sampled in 1999 (Bigler and Hall, 2003) showed BSi as high as 40 wt% of diatom SiO_2 (Frings et al., 2014b; Rosén et al., 2010). Therefore, despite the small sedimentation area of the lake basin (7300 m^2) a great heterogeneity of sediment composition is observed. This brings us to the conclusion that more than one core should be used to study lake sediments in order to constrain lake sedimentation as suggested by Anderson (1990). As observed here, the heterogeneity of sediment and BSi accumulation can greatly increase the uncertainties in the model.

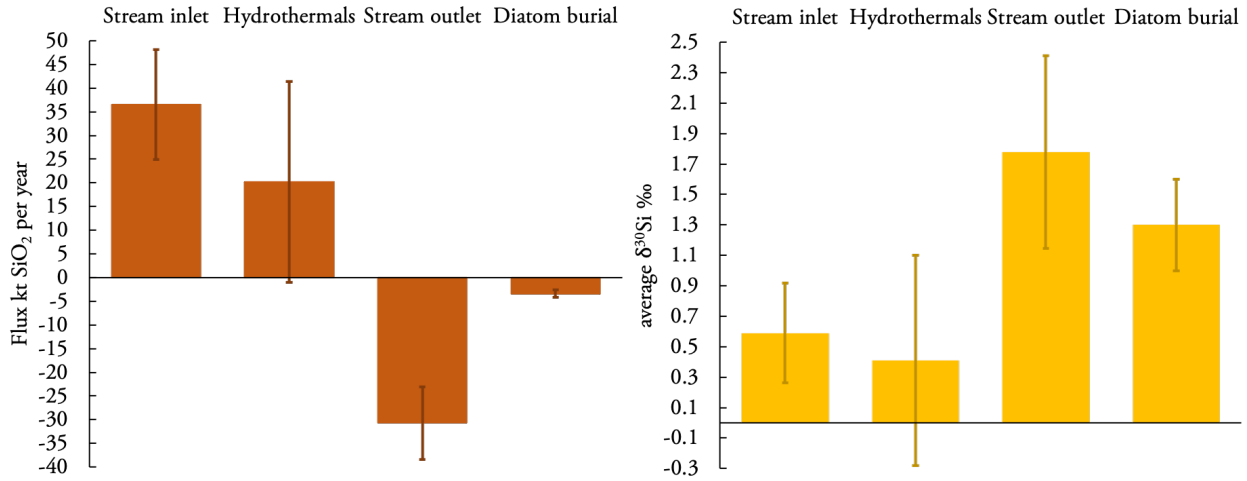


Figure 8: A schematic Si and Si isotope mass balance of Yellowstone Lake (preliminary unpublished data).

6.4 Is hydrothermalism affecting BSi accumulation?

An example of an environment with a high potential for BSi accumulation is Yellowstone Lake. The lake and Yellowstone River outlet DSi concentrations are higher than the world river mean, and the lake diatom production does not show DSi depletion. The rhyolitic bedrock surrounding Yellowstone Lake in combination with hydrothermal vents is suggested to contribute greatly to the lake DSi budget. Further, the oligotrophic conditions in Yellowstone Lake along with deep mixing make the lake ideal for diatom growth without being out-competed by other organisms. If the hydrothermal input into the lake was not included in a Si budget, the lake would act as DSi source rather than DSi sink. However, the Si mass balance (preliminary data, Figure 8) and the lake sediment BSi accumulation (Paper IV) both indicate that the lake is acting as a DSi sink.

Hydrothermalism in Yellowstone Lake was previously quantified to contribute with around 1 % of the lake water inflow (Balistrieri et al., 2007), but the DSi concentration in those hydrothermal fluids can be 10 times higher compared to the inlets. A preliminary Yellowstone Lake annual Si and Si isotope mass balance based on 6 and 2 years of data, respectively (Figure 8) reveals the importance of hydrothermal vent fluids, which were likely underestimated in the previous balance model (Balistrieri et al., 2007). However, great uncertainties of those mass-balance models arose from the lack of monitoring data to constrain the budget. Therefore, a simplification of the annual water fluxes, DSi concentration and δ^{30}Si fluxes is needed to account for variability in the two seasons defined by the rivers' flow regime: high flow inputs in the spring, and low flow during the late summer. These results bring initial insights into the Yellowstone Lake δ^{30}Si mass balance. To improve the preliminary δ^{30}Si model, samples of living diatoms, sediment pore water samples, and annual monitoring of the lake diatom production and dissolution in the water column are prospects for future studies.

Another approach to investigate the importance of hydrothermalism is to focus on the sediment δ^{30}Si (Paper IV). In volcanic systems, such as Yellowstone, a continuous, long-term hydrothermal influence is demonstrated in the thermal features on land, such as hot springs or geysers (Hurwitz and Lowenstern, 2014). However, Yellowstone Lake is a large water body situated on the Yellowstone

Caldera rim, remote ~10 km to 50 km from the main hydrothermalism. The main Yellowstone Lake water input is the Yellowstone River with its watershed outside the Yellowstone Caldera. All these factors suggest that hydrothermal input into the lake will be rather local. Nevertheless, diatom Ge/Si ratios in the sediment showed that the lake has a high hydrothermal background input during the last 9800 years. This background is large enough that it masks the hydrothermal explosion of Elliott's Crater (Paper IV), which created a 1 m thick hydrothermal deposits within the lake.

The results of these analyses suggest the answer to the question whether hydrothermalism is responsible for BSi accumulation is likely yes. Even though we do not see the direct impact of the hydrothermal explosion in the sedimentary BSi and δ^{30}Si (Paper IV), the long-term hydrothermal input shows long-term biogeochemical lake stability. Additionally, the fossil diatom δ^{30}Si is likely influenced by relative changes in DSi sources. Thus, a combination of our preliminary mass-balance models together with the fossil diatom record (Paper IV) highlighted the importance of including an additional source of DSi, e.g., hydrothermal inputs, for mass-balance models.

6.5 Factors driving BSi accumulation in pristine lakes

To understand which lakes have the potential to accumulate large amounts of BSi, several factors must be taken into account. The DSi source, which is often connected to the bedrock type and further depends on the presence of vegetation and soils, influences the DSi budget of a lake. Areas with exposed igneous bedrock combined with a lack of vegetation and developed soils have large potential to deliver high DSi concentrations originating from bedrock weathering into a lake (Paper II). Further, the importance of groundwater can be often neglected, even though it can play a crucial role in some lakes (Paper II, Figure 7). We have studied mass balances of a small high-latitude lake in northern Sweden (Paper II) and of one of the largest high-altitude lakes in the USA, Yellowstone Lake. Groundwater or hydrothermal fluids (Figures 7 and 8) are distinct sources of DSi into Lake 850 and Yellowstone Lake, respectively, which are not traditionally measured.

By comparing our two study sites some similarities are found. The DSi concentration of the outlets in both models (not shown, Paper II) is lower than the concentration in the inlets. The first explanation for this observation is diatom production and DSi uptake. Using only these two variables for the mass balance suggests that the lakes act as sinks. However, when comparing the DSi fluxes (Figures 7 and 8), both lakes rather act as sources of DSi. When adding BSi flux to the sediment into the mass balance, the inlet is not sufficient to feed both the outlet DSi flux and the BSi accumulation. Therefore, if a mass balance needs to be simplified, the BSi accumulation to the sediment is a more robust characterization of mass balance than the DSi concentrations of the stream inlets and outlets in determining whether the lake acts as a source or a sink in the Si cycle.

Both lakes show relatively light isotopic values of the inlets (Figures 7 and 8), which are likely connected to the transport of DSi originating from freshly weathered bedrock. Both transport over a short distance (Lake 850) and the oligotrophic status of high-altitude rivers (Yellowstone tributaries) can account for the relatively light δ^{30}Si of DSi observed in inlets. Another similarity observed is the additional DSi sources, the groundwater and the hydrothermal fluids, that both bring lighter δ^{30}Si and a substantial DSi flux compared to the inlets. The difference in the δ^{30}Si of the DSi in the outlet waters of both lakes is caused by great differences in lake size. In Yellowstone Lake several concurrent processes, such as diatom production and dissolution, amorphous silica precipitation or

clay mineral formation may influence the lake δ^{30}Si, whereas in Lake 850, the lake δ^{30}Si is mostly affected by DSi sources and diatom production.

The mass accumulation rates and BSi fluxes to the sediment studied here (Papers II, III, IV) differ considerably. Yellowstone Lake has about five times larger BSi accumulation rates compared to Lake 850, but both lakes show BSi concentrations over 30 wt% of diatom SiO_2 in the sediment. Therefore, low or high sediment mass accumulation rates stand-alone do not guarantee high or low BSi accumulation, respectively, which is consistent with the great variability of mass accumulation rates and BSi concentrations demonstrated in this thesis and in other lakes (Arai and Fukushima, 2012; Conley, 1988; Kaplan et al., 2002; McKay

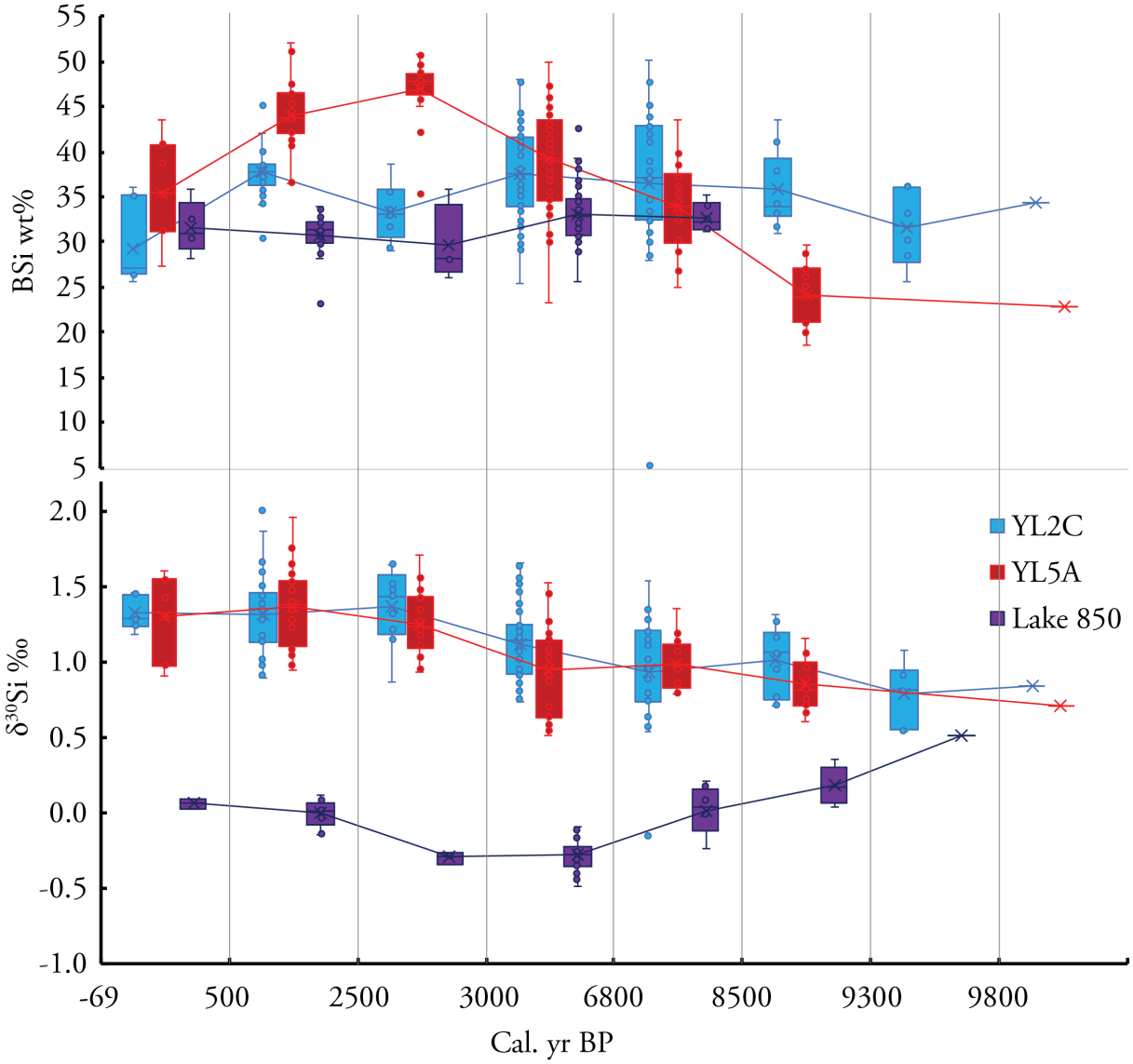


Figure 9: Box-plot showing BSi concentration and $\delta^{30}Si_{BSi}$ variability in all three sedimentary cores from Papers III and IV aligned by ages. YL2C is a core from Yellowstone Lake deep sedimentary basin, YL5A is a core from Yellowstone Lake in the distal part of Elliott's crater, and Lake 850 is a core from Lake 850 in northern Sweden.

et al., 2008; Newberry and Schelske, 1986; Opfergelt et al., 2011; Schelske et al., 1987). BSi accumulation always depends on a combination of factors, such as higher diatom production than diatom dissolution, higher DSi influx than DSi outflux, and low detrital flux.

As demonstrated by two lakes in very different settings, multiple factors act simultaneously and drive BSi accumulation. The results support previous suggestions that high-latitude, low-nutrient lakes tend to accumulate a large amount of BSi in the sediment (Frings et al., 2014b). Further, the data support the generalization that high BSi accumulation is dependent on low detrital input (Conger, 1942).

I have also confirmed that sedimentation rates play a role in the BSi accumulation (Panizzo et al., 2016; Ryves et al., 2003), but are dependent on other factors, such as detrital input and DSi concentration in the water column influencing BSi preservation. Indirectly, we have shown that watershed vegetation and length of transport of weathered DSi is affecting the DSi isotopic composition. Additionally, places with silicic volcanism or hydrothermalism are good candidates for high BSi accumulation.

6.6 Lake diatom δ^{30}Si proxy interpretation

Only a limited number of studies on freshwater diatom Si isotopic records have been published (Chen et al., 2012; Cockerton et al., 2015; Panizzo et al., 2016; Street-Perrott et al., 2008; Swann et al., 2010; Zhang et al., 2020). Our results in Papers III and IV add data sets of lakes where the diatom δ^{30}Si is affected by several simultaneous processes, such as changes in DSi sources, DSi utilization, and diatom dissolution. The sedimentary diatom δ^{30}Si of Yellowstone Lake is comparable to values from Lake El'gygytgyn (Swann et al., 2010), Lake Baikal (Panizzo et al., 2016) and Lake Edward (Cockerton et al., 2015), whereas sedimentary diatom δ^{30}Si from Lake 850 is relatively lighter compared to the world mean of 0.63 ‰ for diatoms buried in sediments (Frings et al., 2016; Sutton et al., 2018).

With a combination of the BSi concentration and stable Si isotopes, the variation in DSi supply and changes in DSi sources can be tracked. In Lake 850 the BSi concentration is pretty stable throughout the core (Figure 9), and the δ^{30}Si shows lighter values in the period from ca 9400 until ca 3000 cal. yr BP. As BSi is stable, an explanation of the Si isotopic behavior is that the relative proportion of DSi sources has changed towards isotopically lighter sources. In the last 3000 years another change in the relative proportion of DSi sources (larger surficial stream contribution), groundwater residence time or increased DSi utilization by diatom production is recorded in the δ^{30}Si, this time towards heavier sources.

In Yellowstone Lake the data record several co-occurring processes (changes in DSi sources, DSi utilization, diatom dissolution) driving the δ^{30}Si. Moreover, the Yellowstone cores vary in BSi concentrations at a given time (Figure 9), which indicates a DSi-unlimited system, where shifts in relative proportion of several processes, such as production, dissolution and detrital input, result in variation of BSi in the sediment. Additionally, a considerable heterogeneity of the sediment composition within one lake is demonstrated.

The δ^{30}Si in both Yellowstone Lake cores show similar trends (Figure 9), which suggest that the lake DSi sources is homogeneous. The systematic shift towards heavier δ^{30}Si through time is likely connected to production as influenced by Holocene climate development (Brown, 2019), relative changes in the proportions of DSi sources and diatom dissolution in the water column. Disentangling of those processes would require additional data on recent functioning and other proxies,

such as Ge/Si ratios or other trace elements when building mass-balance models and reconstructing Si cycling through the past. Ge/Si ratios can be used as a tracer for weathering rates (Filippelli et al., 2000; Froelich et al., 1992; Kurtz et al., 2002; Lugolobi et al., 2010; Shemesh et al., 1989), as well as for hydrothermal input when studying fossil diatoms and thus bring another perspective into data interpretation. Our δ^{30}Si and Ge/Si data demonstrate the impact of local DSi sources on δ^{30}Si, which indicates that knowledge of the lake or river watershed is crucial for estimating BSi accumulation, as well as DSi export into the ocean.

The comparison of the diatom δ^{30}Si of Yellowstone Lake and Lake 850 (Figure 9) shows a dependency of the δ^{30}Si on the signature of the source DSi. The δ^{30}Si in Yellowstone Lake is rather related in to in-lake processes, whereas diatom δ^{30}Si of Lake 850 reflects the lighter DSi sources. Likely, the water and Si residence time plays a role in the diatom δ^{30}Si. Yellowstone Lake with longer water and Si residence times has higher potential for Si recycling compared to Lake 850.

6.7 Future research perspectives

The global stable Si isotope cycle is built on available data, which for some continental systems, especially lakes, are still sparse (Frings et al., 2016; Sutton et al., 2018). The processes in watersheds of rivers and lakes drive Si fluxes. The rates of these processes contribute to the size of pools, which act as sources and sinks of silicon. However, these watershed processes are still understudied (Frings et al., 2014b; Phillips, 2020). By studying more individual lake Si cycles, Si flux estimates can be specified in more detail by taking into account different site-specific factors. Moreover, by studying processes that influence the DSi concentration in lakes and rivers, we will get a better understanding of the Si cycle, which can then be better constrained on longer timescales.

The coupling of silicon and carbon cycles has previously been shown to be important for the CO_2 drawdown on a geological timescale through weathering (Street-Perrott et al., 2008). Moreover, chemical weathering determines the nutrient supply to rivers, lakes, and the ocean. Weathering processes are connected to climate and vegetation changes and influence ecosystems development. Therefore, tracing chemical weathering by using different elemental and isotopic proxies can help us better understand past changes in ecosystems. Germanium and silicon, but also aluminum, zinc or lithium (Sutton et al., 2018) are elements that can be used individually or coupled to trace chemical weathering and the processes in global elemental cycles (Kurtz et al., 2002; Mortlock and Frohlich, 1987; Murnane and Stallard, 1990).

7 Conclusions

- A diatom-rich sediment nomenclature has been proposed for more clarity. Diatom-rich sediments should be evaluated based on BSi concentration. Diatomite was defined as consolidated sediment with more than 50 wt% of diatom SiO_2 accompanied with the name of the remainder of the sediment. The stand-alone word "diatomite" is composed of more than 80 wt% of diatom SiO_2. Unconsolidated sediment with diatom content above 50 wt% is called "diatomaceous ooze", with similar rules as for diatomite applied.
- Diatom-rich sediment tends to accumulate in lakes situated on silicon rich bedrock, volcanic and hydrothermal areas. Further, diatom-rich sediment can accumulate in high-latitude lakes with significant groundwater input. Moreover, lakes with low-relief watershed morphology and with low stream inlet resulting in low and fine-grained clastic input are potential places for high BSi concentration in the sediment. All those water bodies with potentially high BSi accumulation are acting as sinks of Si in the global silicon cycle.
- The groundwater supplying Lake 850 with DSi was shown to be an important factor for high BSi concentration in this high-latitude subarctic lake. Generally, groundwater can be an important source of DSi in lakes and should not be overlooked in mass-balance models and when building global elemental cycles.
- The δ^{30}Si in Lake 850 reflects the isotopically light DSi sources – weathered bedrock and groundwater. Both sources experience very few processes that fractionate Si, likely due to poor soil development and sparse vegetation.
- The variations in fossil diatom δ^{30}Si in Lake 850 indicate changes in the relative proportion of DSi sources. The DSi sources are influenced by Holocene summer temperature and precipitation changes.
- Continuous Holocene hydrothermal input supplies Yellowstone Lake with high DSi and DGe concentrations that is reflected in the high BSi concentrations and high Ge/Si ratios in a single fossil species, the diatom *Stephanodiscus yellowstonensis*.
- The δ^{30}Si of *Stephanodiscus yellowstonensis* shows a gradual shift of $+0.6$ ‰ throughout the Holocene, which is either connected with the Holocene summer temperature increase driving diatom production, or to changes in the relative proportion of DSi sources. Increased stream input brings isotopically heavier DSi from the watershed compared to the hydrothermal input. Alternatively, an increase of hydrothermal source could supply the lake with even more DSi, which would fertilize the diatom production. Increased production would lead to an increase of the δ^{30}Si.
- The understanding whether a lake acts as a source or a sink of Si requires constraint of BSi accumulation, which depends on sufficient DSi concentrations for diatom production and further on diatom dissolution and detrital input. Using inlet and outlet DSi fluxes to estimate the BSi accumulation in a lake is not sufficient as other substantial DSi sources, such as groundwater or hydrothermalism, can be present.

Populärvetenskaplig sammanfattning

Kiselalgsrika sediment är vanligtvis en blandning av mineraler och encelliga fotosyntetiserande alger, där de största är ca 0.0025 mm och de minsta är mindre än 0.0005 mm. Dessa alger har ett ytterskal av kiseldioxid (SiO_2), vilket gör att de är helt beroende av att det finns löst kisel (Si) i deras miljö, eftersom kisel behövs för att bygga deras skal. Kiselalgerna lever i alla vattenmiljöer så som sjöar, floder och hav, men även i jord. Om det finns en stor mängd löst kisel och tillräckligt med näring i vattnet och låg konkurrens från andra organismer, kan kiselalger växa i stora mängder och när de dör bildas kiselrika sediment som kiselgur.

Kiselgur består till största del av kiseldioxid och är ett material med många olika användningsområden i samhället. Det används exempelvis för att filtrera oorganiska och organiska kemikalier och läkemedel, eller som filter vid framställning av öl, vin, whisky och frukt- och grönsaksjuicer. Många av oss har faktiskt stött på produkter som innehåller kiselgur då det t.ex. används som milt slipmedel i tandkräm. Kiselgur undersöks även som ett möjligt och relativt billigt sätt att absorbera tungmetaller och oljespill i vatten. Användningsområdena är alltså många, men det är inte helt klarlagt hur det kiselrika sedimentet bildas och vilka förhållanden och faktorer som leder till de massiva ansamlingarna av kiselalger.

Även om kisel är det näst vanligaste grundämnet i jordskorpan är det mesta bundet i bergarter, i en form som organismer inte kan använda. De flesta organismer kan endast ta upp ämnen i flytande- eller gasform och därför måste kisel först frigöras från bergarterna, vilket kan ske genom så kallad kemisk vittring. Kemisk vittring är en process där koldioxid och vatten reagerar med bergarten och löser upp den. Det tidigare bundna kislet är nu löst i vatten och kan transporteras via floder till haven. På vägen från det vittrade berget till havet kan dock jord, växter eller sjöar fungera som filter och fånga upp och lagra det lösta kislet och därmed minska mängden löst kisel i vattnet nedströms, vilket i sin tur begränsar kiselalgstillväxten.

I denna avhandling har olika kiselrika sediment definierats genom andelen kiselalger i sedimentet. För att utforska vilka faktorer som möjliggör ansamlingar av kiselalger har två sjöar med kiselrika sediment har studerats. Den ena sjön är en liten sjö (Lake 850) i ett fjällområde som ligger ovanför polcirkeln, nära Abisko nationalpark i norra Sverige. Den andra sjön är Yellowstone Lake, den största fjällsjön i USA, belägen i Yellowstone National Park, som är känd för sin vulkaniska och hydrotermiska aktivitet. Båda sjöarna är istäckta under vintern och på grund av det sker större delen av kiselinbindningen i alger under en mycket kort växtsäsong på sommaren.

För att identifiera vilka faktorer som leder till stora mängder kiselalger i vattnet och som ansamling i sedimenten, undersöktes först hur förhållandena i sjöarna varit de senaste åren. Detta gjordes genom att studera vattenflöden och analysera mängden löst kisel i vattendragen som leder till och från sjöarna, och mängden kisel i själva sjövattnet. Sedimentet i sjöarna undersöktes också och från det har vi kunnat beräkna hur stor del av sedimentets vikt som utgjordes av kiseldioxid bundet i kiselalger. För att uppskatta hur gammalt sedimentet var på olika djup och för att avgöra hur mycket kiselalgs-kisel som varje år fastlagts i sjöbotten har två dateringsmetoder (kol-14 och bly-210) använts. Tillsammans har alla dessa mätningar och beräkningar visat att det saknas någon kiselkälla för att halten kisel med de kända flödena ska gå ihop i de i de båda sjöarna.

För att identifiera varifrån det ”förlorade” lösta kislet kommer från användes en metod där stabila kiselisotoper analyseras. Metoden baseras på det faktum att kiselatomen kan ha olika antal

neutroner i sin kärna. Den vanligaste och mest utbredda kiselisotopen (92 procent) är ^{28}Si som har 14 neutroner och 14 protoner och således en atomvikt på 28. Det finns ytterligare två isotoper, ^{29}Si (5 procent) och ^{30}Si (3 procent), som har 15 respektive 16 neutroner och som på grund av deras högre atomvikt inte används lika frekvent i kemiska, fysiska och biologiska processer. Med andra ord föredras den lätta isotopen, ^{28}Si, av kiselalger, och det är också den isotopen som främst släpps ut vid vittring av berg och mineraler. På grund av dessa olika egenskaper kan de stabila kiselisotoperna därför berätta var det lösta kislet kommer ifrån, om det funnits någon kiselalgs- eller växtproduktion på dess väg eller hur stor mängd kisel som var tillgänglig i vattnet när kiselalgerna växte.

Med alla dessa verktyg har vi upptäckt att det i Lake 850 finns en stor mängd grundvatten som bidrar med löst kisel till sjön och dess kiselalgsproduktion. Vi har också sett att sjöförhållandena har varit stabila under de senaste 9400 åren och att växtsäsongens längd och förändringar i fördelningen av tillförseln från grundvatten och vattendrag påverkat ansamlingen av kiselalger. Undersökningarna tyder på att det var mindre tillförsel av mineraler från vattendrag som rinner in i sjön i tider då klimatet var varmare och torrare. Eftersom det var en mindre mängd mineraler som spädde ut sedimentet under de varmare klimatförhållandena bestod sedimentet då till 40 procent av kiselalger. Vi fick också reda på att det mesta av det lösta kisel som togs upp av kiselalger under den varmare perioden kom från grundvattnet eller från nyligen vittrad kisel.

På samma sätt observerade vi att den extra källan till löst kisel i Yellowstone Lake är hydrotermiska utflöden från botten av sjön. Dessa utflöden har bidragit med löst kisel till sjön under de senaste 9800 åren och det är anledningen till att sjön har ett väldigt högt kiselinnehåll. Mängden löst kisel i sjön är så hög att hela 50 procent av sedimentet består av kiselalger. Dessutom observerade vi att en hydrotermisk explosion inträffade för omkring 8000 år sedan, men som inte påverkade sedimentationen av kiselalger. Denna observation leder oss till slutsatsen att Yellowstone Lake har varit ett mycket stabilt sjösystem de senaste 9800 åren.

I den här avhandlingen visar jag att både grundvatten och hydrotermiska utflöden är viktiga källor till löst kisel i sjöar som bidrar till bildningen av kiselalgsrika sediment. Våra studier tyder på att kiselalgsrika sediment kommer att bildas i sjöar belägna på kiselrik berggrund, i vulkaniska och hydrotermiska områden samt i sjöar på höga breddgrader som tenderar att ha ett påtagligt grundvatteninflöde. Vattendrag i relativt platta områden med ett lågt vattenflöde kan leda till en låg tillförsel av lera och sand till sjöar och därför bidra till sediment med en hög andel kiselalger. Alla dessa vattensystem som ansamlar stora mängder kisel bundet i kiselalger, fungerar som kiselsänkor i den globala kiselomsättningen.

Popular summary

Diatom-rich sediment is an accumulation of a single-cell photosynthetic algae of size from 0.005 mm to less than 0.0005 mm usually mixed with minerals. These microscopic organisms with an external skeleton of silica, known as a frustule, live in all aquatic environments, such as lakes, rivers, oceans, but also in soils. They account for one fourth of the world's entire net primary productivity and one fifth of world oxygen production. However, diatoms are fully dependent on the presence of dissolved silicon in the environment, because it is an essential element for building their frustules. If there is a great amount of dissolved silicon in the water and favorable conditions (high nutrients and low competition) are met, diatoms can grow in large abundance and then diatom-rich sediments can be formed and composed of more than 80 % of diatoms.

Diatomite is a material with wide socio-economical utilization. It is used for filtering inorganic and organic chemicals, pharmaceuticals, beer, wine, whiskey, and fruit and vegetable juices. Many of us might have come across products containing diatomite regularly, such as a mild abrasive in toothpaste. Diatomite is further used in construction as insulators, metal polish, fillers, absorbents or as concrete additive abrasives. Diatomaceous silica is also used to improve plastic properties, as well as a stabilizing agent in explosives. Last but not least, diatomites are used as economically affordable absorbent powders for heavy metals and oil water contamination removal. To be able to use diatomite for all those purposes, first we need to know how the diatom-rich sediment is formed and what are the conditions and factors leading to the massive diatom-rich accumulation.

Even though silicon is the second most abundant element in the Earth's crust, most of it is bound in rocks, which is a form unavailable for organisms to use. Most organisms can use only elements in liquid or gaseous form; therefore, silicon must be released from rocks via chemical weathering. During this process, CO_2 and water react with the source rock and dissolve it. The silicon is dissolved in water and transported through rivers to the ocean. In rivers, lakes and in the ocean, the dissolved silicon can be taken up by diatoms, which after their death sink down to the bottom and accumulate. However, on the way from the weathered rock to the ocean there are other filters, such as in soils or though plant uptake, which catch and store dissolved silicon and thus, decrease the dissolved silicon in the waters, which limits diatom growth.

This thesis starts by defining different diatom-rich sediments by the relative contribution of diatom silica. Then, two lakes with diatom-rich sediment were studied to explore factors responsible for diatom accumulation. Two different lake systems were investigated; one is a small lake (Lake 850) in a mountainous area situated above the polar circle in Northern Sweden close to Abisko National Park. The other lake is Yellowstone Lake, the biggest mountain lake in the United States, situated in Yellowstone National Park, which is well known for its volcanic and hydrothermal activity. Both lakes are ice-covered during winter, and thus most of the diatom production happens during a very short growing season in summer.

To identify factors responsible for diatom production and accumulation, the functioning of lakes during recent years was examined first. I measured water fluxes and the amount of dissolved silicon in rivers and streams entering and leaving the lakes, as well as the amount of dissolved silicon in the lake water and calculated how much silicon contained in diatoms is retained in the lakes. Furthermore, I looked into the deposits from the bottom of the lakes and measured the percent of diatom silica. Dating methods (^{14}C and ^{210}Pb) were used to estimate the ages of those deposits, and I calculated how much diatom silica

is deposited into the lake bottom for one year. From all those measurements, I could see that I have not accounted for an important dissolved silicon source in both lakes.

Therefore, I used stable silicon isotopes to identify sources of dissolved silicon to reveal what is the missing source. The measurement of stable silicon isotopes is a method based on the different number of neutrons in the atomic nucleus. Due to one or two additional neutrons in the atomic core, the whole atom differs in weight. The most common and widespread silicon isotope (comprising 92 %, of all Si) is ^{28}Si, which has 14 neutrons and 14 protons, and has an atomic weight of 28. There are two more isotopes, ^{29}Si (5 %) and ^{30}Si (3 %), which have 15 and 16 neutrons, respectively, and due to their increased atomic weight, they are discriminated against during chemical, physical, and biological processes. In other words, the light isotope ^{28}Si is preferred by diatoms and it is preferentially released during rock and mineral weathering. Therefore, the stable silicon isotopes can tell us where the dissolved silicon comes from, or if there was some diatom or plant production on its pathway, or the amount of available silicon in water when the diatoms were growing.

Using all those tools, I found that in Lake 850 there is substantial groundwater input bringing a lot of dissolved silicon into the lake and supplying diatom production. I also observed that lake conditions were relatively stable over the last 9400 years, and that the length of the growing season and changes in the relative proportion of groundwater input and river input influenced diatom accumulation. The data suggest that in times when the climate was warmer and drier, there was less stream input, which is also bringing minerals. Therefore, more diatoms (40 %) were found in the sediment, because there was a reduced input of minerals diluting the sediment during warmer climate conditions. I also found that during this warmer period, most of the dissolved silicon taken up by diatoms was brought by groundwater or from freshly released dissolved silicon from the rocks.

Similarly, in Yellowstone Lake, it was observed that the additional source of dissolved silicon is hydrothermal vents situated on the lake bottom. Those vents have contributed dissolved silicon into the lake for the last 9800 years, and this is the reason for the really high content of silicon in the lake. The amount of dissolved silicon in the lake is so high that 50 % of the sediment is composed of diatoms. Additionally, it was observed that a hydrothermal explosion that happened around 8000 years ago did not affect diatom sedimentation, which brings us to a conclusion that Yellowstone Lake has been a stable lake system for the last 9800 years.

In this thesis it have been shown that groundwater and hydrothermal vents are both important sources of dissolved silicon in lakes and are partly responsible for diatom-rich sediment formation. Three listed studies suggest that diatom-rich sediments are likely to form in lakes situated on silicon rich bedrock, volcanic and hydrothermal areas, as well as in lakes at high latitudes with pronounced groundwater input. Furthermore, lakes with low-relief watershed morphology and with low stream inflow resulting in low and fine-grained clastic input, such as mud and sand, are potential places for diatom-rich sediment formation. All those water bodies with potentially high BSi accumulation are acting as sinks of Si in the global silicon cycle.

Populárně-vědecký souhrn

Sediment s vysokým obsahem rozsivek je usazenina složená z jednobuněčných fotosyntetických řas – rozsivek – o velikosti 0.005 až 0.0005 mm a minerálů. Rozsivky si tvoří křemičitou schránku, která se nazývá frustula, a žijí ve všech vodních prostředích, jako jsou jezera, řeky, moře a oceány, ale také v půdě. Představují čtvrtinu celé primární produkce v oceánech a pětinu světové produkce kyslíku. Nicméně rozsivky jsou plně závislé na přítomnosti rozpuštěného křemíku v prostředí, jelikož ten je základním prvkem pro budování jejich schránek. Za příznivých podmínek (dostatek živin a nízká konkurence), a pokud je ve vodě velké množství rozpuštěného křemíku, mohou rozsivky růst v hojném počtu. Za těchto podmínek mohou vznikat sedimenty bohaté na rozsivky jako je křemelina, v níž se vyskytuje více než 80 % rozsivek.

Křemelina je materiál s širokým socioekonomickým využitím. Používá se pro filtraci anorganických a organických chemických látek nebo léčiv. Mnozí z nás se již setkali s výrobky, které obsahují křemelinu s funkcí jemného brusiva například v zubních pastách. Křemelina se dále používá během výroby piva, vína, whisky či ovocných a zeleninových šťáv jako filtr. Dále se používá ve stavebnictví jako izolant, při leštění kovů, jako plnivo, absorbent nebo jako aditivum do betonu. Křemelina se také používá ke zlepšení vlastností plastů a jako stabilizační činidlo ve výbušninách. V neposlední řadě je křemelina používána v cenově dostupných sypkých sorbentech pro odstraňování kontaminace těžkými kovy a při úniku ropy. Abychom mohli používat křemelinu pro všechny tyto účely, nejprve potřebujeme vědět, jak a za jakých podmínek vzniká.

Přestože je křemík druhým nejhojnějším prvkem zemské kůry, většina je vázána v horninách a minerálech, což je forma, kterou organismy nedokáží využít. Většina organismů je schopna využívat pouze prvky rozpuštěné v kapalině nebo prvky v plynné formě; proto musí být křemík uvolněn z hornin a minerálů chemickým zvětráváním. Během chemického zvětrávání dochází k reakci oxidu uhličitého a vody s horninou, jež je takto rozpouštěna. Křemík rozpuštěný tímto způsobem je dále odnášen vodními toky až do oceánu. V řekách, jezerech a v oceánech je rozpuštěný křemík spotřebováván rozsivkami, které po svém úhynu klesnou na dno, kde se hromadí. Nicméně na cestě od zvětrávání hornin a minerálů až do oceánu se nacházejí místa, která mohou zadržovat rozpuštěný křemík a tím snižovat koncentraci a dostupnost rozpuštěného křemíku ve vodách, což omezuje růst rozsivek. Těmito filtry jsou například půdy, rostliny nebo jezera.

V této dizertaci se nejprve podíváme na systém určování jmen rozsivkových sedimentů, založený na procentuálním podílu rozsivek. Následně prezentujeme studie dvou jezer, které disponují vysokým obsahem rozsivek v sedimentu. V těchto studiích zkoumáme faktory vedoucí k akumulaci rozsivek. Podíváme se do dvou různých jezerních systémů. Prvním z nich je malé jezero (Lake 850) za polárním kruhem v severním Švédsku v blízkosti národního parku Abisko. Druhým jezerem je Yellowstonské jezero, jež je největší horské jezero ve Spojených státech amerických nacházející se v Yellowstonském národním parku, dobře známým pro svou sopečnou a hydrotermální aktivitu. Obě jezera jsou v zimě pokryta ledem, a proto většina rozsivek roste jen během velmi krátkého vegetačního období v létě.

Abychom našli faktory odpovědné za tvorbu a akumulaci rozsivek, nejprve musíme znát současné fungování jezer. Proto jsme změřili množství rozpuštěného křemíku v řekách a potocích, které vtékají a vytékají z jezera, stejně jako množství křemíku v jezeře. Z usazenin ze dna jezera jsme změřili, kolik procent rozsivek je v usazeninách. Poté jsme použili metody datování usazenin (metoda radioaktivního uhlíku ^{14}C a pomocí olova ^{210}Pb),

abychom odhadli stáří usazenin a vypočítali tak, kolik křemíku sedimentuje na dno jezera za jeden rok. Ze všech těchto měření jsme zjistili, že nám chybí nějaký dodatečný zdroj křemíku v obou jezerech.

Proto jsme použili analýzu izotopů křemíku, která umožnuje identifikovat zdroje rozpuštěného křemíku a odhalit původ chybějícího zdroje. Měření stabilních izotopů křemíku je metoda založená na rozdílných atomových hmotnostech křemíku. Izotopy křemíku jsou atomy křemíku lišící se počtem neutronů v atomovém jádře, a tedy i atomovou hmotností. Nejběžnější a nejrozšířenější izotop křemíku (92 %), ^{28}Si, má 14 neutronů a 14 protonů, a tedy jeho atomová hmotnost je 28. Existují další dva izotopy, ^{29}Si (5 %) a ^{30}Si (3 %), které mají 15 a 16 neutronů. Vzhledem k jejich zvýšené atomové hmotnosti jsou během chemických, fyzikálních a biologických procesů diskriminovány. Jinými slovy, lehký izotop ^{28}Si je upřenostňován rozsivkami, ale zároveň je přednostně uvolňován během zvětrávání. Proto nám stabilní izotopy křemíku mohou poskytnout informaci o původu rozpuštěného křemíku a o procesech, které mohou křemík odebírat během jeho transportu do oceánu, jako jsou například růst rozsivek či rostlin. Zároveň lze v některých případech rekonstruovat množství dostupného křemíku ve vodě v době růstu rozsivek.

Za použití všech těchto nástrojů jsme zjistili, že v jezeře Lake 850 je velké množství podzemní vody, která přináší do jezera spoustu rozpuštěného křemíku a podporuje růst rozsivek. Také jsme zjistili, že podmínky v jezeře byly stabilní v posledních 9400 letech. Délka vegetačního období, změny v relativním podílu podzemní vody a přítoku pramene do jezera ovlivnily akumulaci rozsivek. Naše data naznačují, že v době, kdy bylo klima teplejší a sušší, přitékalo méně vody skrze povrchové toky, které by jinak přinášely písek a jíl, což by naředilo usazování rozsivek. Proto jsme našli více rozsivek (40 %) v usazenině během teplejších klimatických podmínek. Také jsme zjistili, že v tomto teplejším období byla většina rozpuštěného křemíku, který byl spotřebován rozsivkami, přinesena podzemní vodou.

Podobně jsme zjistili, že hydrotermální prameny umístěné na dně Yellowstonského jezera jsou dodatečným zdrojem rozpuštěného křemíku. Za posledních 9800 let tyto prameny přinášely dostatek rozpuštěného křemíku, a z toho důvodu má jezerní usazenina opravdu vysoký obsah rozsivek. Množství rozpuštěného křemíku v jezeře je tak vysoké, že umožňuje nalézt usazeniny tvořené až z 50 % rozsivkami. Kromě toho jsme zjistili, že hydrotermální exploze, ke které došlo asi před 8000 lety, neovlivnila usazování rozsivek, což nás přivádí k závěru, že Yellowstonské jezero je velmi stabilní jezerní systém v posledních 9800 letech.

V této studii jsme ukázali, že podzemní voda a hydrotermální prameny jsou důležitým zdrojem rozpuštěného křemíku v jezerech a jsou částečně zodpovědné za tvorbu rozsivkových usazenin. Naše studie naznačují, že rozsivkové usazeniny se pravděpodobně vytvoří v jezerech vzniklých na křemičitých horninách, či ve vulkanických a hydrotermálních oblastech. Podobně jezera ve vysokých zeměpisných šířkách, která mají přítok podzemních vod, ukládají rozsivkové usazeniny. Jezera situovaná v mírném reliéfu bez strmých svahů v povodí a s nízkým přítokem jsou potenciální místa pro tvorbu roszivkových usazenin. Všechny tyto vodní plochy s vysokým potenciálem akumulovat rozsivky působí jako uložiště křemíku v globálním křemíkovém cyklu.

8 References

Albarède, F. (2009) *Geochemistry: An introduction*. Cambridge University Press, second edn. doi:10.1017/cbo9780511807435.

Alleman, L.Y., Cardinal, D., Cocquyt, C., Plisnier, P.D., Descy, J.P., Kimirei, I., Sinyinza, D., and André, L. (2005) Silicon isotopic fractionation in Lake Tanganyika and its main tributaries. *Journal of Great Lakes Research* 31(4), 509 – 519. doi:10.1016/S0380-1330(05)70280-X.

Anderson, N. (1990) Variability of diatom concentrations and accumulation rates in sediments of a small lake basin. *Limnology and Oceanography* 35(2), 497–508. doi:10.4319/lo.1990.35.2.0497.

Arai, H. and Fukushima, T. (2012) Silicon budget of eutrophic Lake Kasumigaura, Japan. *Journal of Soils and Sediments* 12(10), 1501–1507. doi:10.1007/s11368-012-0603-0.

Armbrust, E.V. (2009) The life of diatoms in the world's oceans. *Nature* 459(7244), 185–192. doi:10.1038/nature08057.

Arnórsson, S. (1984) Germanium in Icelandic geothermal systems. *Geochimica et Cosmochimica Acta* 48(12), 2489–2502. doi:10.1016/0016-7037(84)90300-4.

Bakr, H. (2010) Diatomite: its characterization, modifications and applications. *Asian journal of materials science* 2(3), 121–136. doi:10.3923/ajmskr.2010.121.136.

Balistrieri, L.S., Shanks, W.C., Cuhel, R.L., Aguilar, C., and Klump, J.V. (2007) The influence of sublacustrine hydrothermal vent fluids on the geochemistry of Yellowstone Lake. *Publications of the US Geological Survey* (66), 1–30. URL `https://digitalcommons.unl.edu/usgspubs/66`.

Barão, L., Clymans, W., Vandevenne, F., Meire, P., Conley, D., and Struyf, E. (2014) Pedogenic and biogenic alkaline-extracted silicon distributions along a temperate land-use gradient. *European journal of soil science* 65(5), 693–705. doi:10.1111/ejss.12161.

Battarbee, R.W., Jones, V.J., Flower, R.J., Cameron, N.G., Bennion, H., Carvalho, L., and Juggins, S. (2002) Diatoms. In J.P. Smol, H.J.B. Birks, W.M. Last, R.S. Bradley, and K. Alverson (eds.), *Tracking environmental change using lake sediments*, 155–202. Springer. doi:10.1007/0-306-47668-1_8.

Bigler, C. and Hall, R.I. (2003) Diatoms as quantitative indicators of July temperature: a validation attempt at century-scale with meteorological data from northern Sweden. *Palaeogeography, Palaeoclimatology, Palaeoecology* 189(3), 147–160. doi:10.1016/s0031-0182(02)00638-7.

Brodie, C.R., Casford, J.S., Lloyd, J.M., Leng, M.J., Heaton, T.H., Kendrick, C.P., and Yongqiang, Z. (2011) Evidence for bias in C/N, δ^{13}C and δ^{15}N values of bulk organic matter, and on environmental interpretation, from a lake sedimentary sequence by pre-analysis acid treatment methods. *Quaternary Science Reviews* 30(21-22), 3076–3087. doi:10.1016/j.quascirev.2011.07.003.

Brown, S. (2019) *Diatom-inferred records of paleolimnological variability and continental hydrothermal activity in Yellowstone National Park, USA*. PhD thesis. URL `https://digitalcommons.unl.edu/geoscidiss/122`.

Burnett, W.C. and Dulaiova, H. (2003) Estimating the dynamics of groundwater input into the coastal zone via continuous radon-222 measurements. *Journal of environmental radioactivity* 69(1-2), 21–35. doi:10.1016/s0265-931x(03)00084-5.

Chen, J., Li, J., Tian, S., Kalugin, I., Darin, A., and Xu, S. (2012) Silicon isotope composition of diatoms as a paleoenvironmental proxy in Lake Huguangyan, South China. *Journal of Asian Earth Sciences* 45, 268–274. doi:10.1016/j.jseaes.2011.11.010.

Chen, X.Y., Chafetz, H.S., and Lapen, T.J. (2020) Silicon isotope variations in hydrothermal systems at Yellowstone National Park, Wyoming, USA. *Geochimica et Cosmochimica Acta* 283, 184–200. doi:10.1016/j.gca.2020.06.004.

Christiansen, R.L. (2001) The Quaternary and Pliocene Yellowstone plateau volcanic field of Wyoming, Idaho, and Montana. Tech. rep. URL `https://pubs.er.usgs.gov/publication/pp729G`.

Clarke, J. (2003) The occurrence and significance of biogenic opal in the regolith. *Earth-Science Reviews* 60(3), 175–194. doi:10.1016/s0012-8252(02)00092-2.

Clow, D., Schrott, L., Webb, R., Campbell, D., Torizzo, A., and Dornblaser, M. (2003) Ground water occurrence and contributions to streamflow in an alpine catchment, Colorado Front Range. *Groundwater* 41(7), 937–950. doi:10.1111/j.1745-6584.2003.tb02436.x.

Clymans, W., Struyf, E., Govers, G., Vandevenne, F., and Conley, D.J. (2011) Anthropogenic impact on amorphous silica pools in temperate soils. *Biogeosciences* 8(8), 2281–2293. doi:10.5194/bg-8-2281-2011.

Cockerton, H.E., Street-Perrott, F.A., Barker, P.A., Leng, M.J., Sloane, H.J., and Ficken, K.J. (2015) Orbital forcing of glacial/interglacial variations in chemical weathering and silicon cycling within the upper White Nile basin, East Africa: stable-isotope and biomarker evidence from Lakes Victoria and Edward. *Quaternary science reviews* 130, 57–71. doi:10.1016/j.quascirev.2015.07.028.

Conger, P.S. (1942) Accumulation of diatomaceous deposits. *Journal of Sedimentary Research* 12(2), 55–66. doi:10.1306/d4269143-2b26-11d7-8648000102c1865d.

Conley, D.J. (1988) Biogenic silica as an estimate of siliceous microfossil abundance in Great Lakes sediments. *Biogeochemistry* 6(3), 161–179. doi:10.1007/bf02182994.

Conley, D.J. (1998) An interlaboratory comparison for the measurement of biogenic silica in sediments. *Marine chemistry* 63(1-2), 39–48. doi:10.1016/s0304-4203(98)00049-8.

Conley, J.D. and Schelske, C. (2001) Biogenic Silica. In *Tracking environmental change using lake sediments*, vol. 3, chap. 14, 281–293. Springer Netherlands, Dordrecht. doi:10.1007/0-306-47668-1_14.

Coradin, T. and Livage, J. (2001) Effect of some amino acids and peptides on silicic acid polymerization. *Colloids and Surfaces B: Biointerfaces* 21(4), 329–336. doi:10.1016/s0927-7765(01)00143-6.

Cornelis, J.T., Delvaux, B., Georg, R., Lucas, Y., Ranger, J., and Opfergelt, S. (2011) Tracing the origin of dissolved silicon transferred from various soil-plant systems towards rivers: a review. *Biogeosciences* 8(1), 89–112. doi:10.5194/bg-8-89-2011.

Davies, S.J., Lamb, H.F., and Roberts, S.J. (2015) *Micro-XRF Studies of Sediment Cores*, vol. 17, chap. Micro-XRF Core Scanning in Paleolimnology: Recent Developments, 189–226. Springer. ISBN 978-94-017-9848-8. doi:10.1007/978-94-017-9849-5.

De La Rocha, C., Brzezinski, M.A., DeNiro, M., and Shemesh, A. (1998) Silicon-isotope composition of diatoms as an indicator of past oceanic change. *Nature* 395(6703), 680–683. doi:10.1038/27174.

De La Rocha, C., Brzezinski, M.A., and DeNiro, M.J. (2000) A first look at the distribution of the stable isotopes of silicon in natural waters. *Geochimica et Cosmochimica Acta* 64(14), 2467–2477. doi:10.1016/s0016-7037(00)00373-2.

De La Rocha, C.L., Brzezinski, M.A., and Deniro, M.J. (1997) Fractionation of silicon isotopes by marine diatoms during biogenic silica formation. *Geochimica et Cosmochimica Acta* 61(23), 5051–5056. doi:10.1016/s0016-7037(97)00300-1.

DeMaster, D.J. (1981) The supply and accumulation of silica in the mariene environment. *Geochimica et Cosmochimica Acta* 45, 1715–1732. doi:10.1016/0016-7037(81)90006-5.

Derry, L.A., Kurtz, A.C., Ziegler, K., and Chadwick, O.A. (2005) Biological control of terrestrial silica cycling and export fluxes to watersheds. *Nature* 433(7027), 728. doi:10.1038/nature03299.

Dietzel, M. (2000) Dissolution of silicates and the stability of polysilicic acid. *Geochimica et Cosmochimica Acta* 64(19), 3275–3281. doi:10.1016/s0016-7037(00)00426-9.

Dimova, N.T. and Burnett, W.C. (2011) Evaluation of groundwater discharge into small lakes based on the temporal distribution of radon-222. *Limnology and Oceanography* 56(2), 486–494. doi:10.4319/lo.2011.56.2.0486.

Dimova, N.T., Burnett, W.C., Chanton, J.P., and Corbett, J.E. (2013) Application of radon-222 to investigate groundwater discharge into small shallow lakes. *Journal of Hydrology* 486, 112–122. doi:10.1016/j.jhydrol.2013.01.043.

Dürr, H., Meybeck, M., Hartmann, J., Laruelle, G.G., and Roubeix, V. (2011) Global spatial distribution of natural riverine silica inputs to the coastal zone. *Biogeosciences* 8(3), 597–620. doi:10.5194/bg-8-597-2011.

Egge, J. and Aksnes, D. (1992) Silicate as regulating nutrient in phytoplankton competition. *Marine ecology progress series. Oldendorf* 83(2), 281–289. doi:10.3354/meps083281.

Evans, M.J. and Derry, L.A. (2002) Quartz control of high germanium/silicon ratios in geothermal waters. *Geology* 30(11), 1019–1022. doi:10.1130/0091-7613(2002)030<1019:qcohgs>2.0.co;2.

Filippelli, G.M., Carnahan, J.W., Derry, L.A., and Kurtz, A. (2000) Terrestrial paleorecords of Ge/Si cycling derived from lake diatoms. *Chemical Geology* 168(1-2), 9–26. doi:10.1016/s0009-2541(00)00185-6.

Fowler, A.P., Tan, C., Cino, C., Scheuermann, P., Volk, M.W., Shanks, W.P., and Seyfried, W.E. (2019a) Vapor-driven sublacustrine vents in Yellowstone Lake, Wyoming, USA. *Geology* 47(3), 223–226. doi:10.1130/g45577.1.

Fowler, A.P., Tan, C., Luttrell, K., Tudor, A., Scheuermann, P., Shanks III, W.P., and Seyfried Jr., W.E. (2019b) Geochemical heterogeneity of sublacustrine hydrothermal vents in Yellowstone Lake, Wyoming. *Journal of Volcanology and Geothermal Research* 386, 106677. doi:10.1016/j.jvolgeores.2019.106677.

Frings, P.J., Claymans, W., Fontorbe, G., Rocha, C.L.D.L., and Conley, D.J. (2016) The continental Si cycle and its impact on the ocean Si isotope budget. *Chemical Geology* 425, 12–36. doi:10.1016/j.chemgeo.2016.01.020.

Frings, P.J., Clymans, W., and Conley, D.J. (2014a) Amoprhous silica transport int he Ganges basin: Implications for Si delivery to the oceans. *Procedia Earth and Planetary Science* 10, 271–274. doi:10.1016/j.proeps.2014.08.059.

Frings, P.J., Clymans, W., Jeppesen, E., Lauridsen, T.L., Struyf, E., and Conley, D.J. (2014b)

Lack of steady-state in the global biogeochemical Si cycle: emerging evidence from lake Si sequestration. *Biogeochemistry* 117(2), 255–277. doi:10.1007/s10533-013-9944-z.

Froelich, P., Blanc, V., Mortlock, R., Chillrud, S., Dunstan, W., Udomkit, A., and Peng, T.H. (1992) River fluxes of dissolved silica to the ocean were higher during glacials: Ge/Si in diatoms, rivers, and oceans. *Paleoceanography* 7(6), 739–767. doi:10.1029/92pa02090.

Froelich, P., Mortlock, R., and Shemesh, A. (1989) Inorganic germanium and silica in the Indian ocean: biological fractionation during (Ge/Si) opal formation. *Global biogeochemical cycles* 3(1), 79–88. doi:10.1029/gb003i001p00079.

Gaspard, F., Opfergelt, S., Dessert, C., Robert, V., Ameijeras-Marino, Y., and Demelle, P. (2020) Imprint of chemical weathering and hydrothermal on the Ge/Si ratio and Si isotopic composition of rivers in a volcatinc tropical island, Basse-Terre, Guadeloupe (French West Indies). *Chemical Geology* Submitted.

Gemery-Hill, P.A., Shanks, W.C., Balistrieri, L.S., and Lee, G.K. (2007) Geochemical data for selected rivers, lake waters, hydrothermal vents, and subaerial geysers in Yellowstone National Park, Wyoming and vicinity, 1996–2004. *Publications of the US Geological Survey* (71). URL `https://digitalcommons.unl.edu/usgspubs/71`.

Georg, R., Reynolds, B., Frank, M., and Halliday, A. (2006a) Mechanisms controlling the silicon isotopic compositions of river waters. *Earth and Planetary Science Letters* 249(3), 290–306. doi:10.1016/j.epsl.2006.07.006.

Georg, R., Reynolds, B., Frank, M., and Halliday, A. (2006b) New sample preparation techniques for the determination of Si isotopic compositions using MC-ICPMS. *Chemical Geology* 235(1), 95 – 104. doi:10.1016/j.chemgeo.2006.06.006.

Georg, R.B., Zhu, C., Reynolds, B.C., and Halliday, A.N. (2009) Stable silicon isotopes of groundwater, feldspars, and clay coatings in the Navajo Sandstone aquifer, Black Mesa, Arizona, USA. *Geochimica et Cosmochimica Acta* 73(8), 2229–2241. doi:10.1016/j.gca.2009.02.005.

Grasshoff, K. (1999) *Methods of seawater analysis*. Wiley-VCH, Weinheim ;, 3. ed. edn. ISBN 3-527-29589-5.

Hansen, H. and Grasshoff, K. (1983) Automated chemical analysis. In G. K. (ed.), *Methods of seawater analysis*, 347–379. Verlag Chemie Weinheim.

Hecky, R., Bootsma, H., Mugidde, R., and Bugenyi, F. (1996) *Phosphorus pumps, nitrogen sinks, and silicon drains: plumbing nutrients in the African Great Lakes*. 1st edn. ISBN 9780203748978. doi:10.1201/9780203748978-11.

Hendry, K.R. and Brzezinski, M.A. (2014) Using silicon isotopes to understand the role of the Southern Ocean in modern and ancient biogeochemistry and climate. *Quaternary Science Reviews* 89, 13–26. doi:10.1016/j.quascirev.2014.01.019.

Hood, J.L., Roy, J.W., and Hayashi, M. (2006) Importance of groundwater in the water balance of an alpine headwater lake. *Geophysical Research Letters* 33(13). doi:10.1029/2006gl026611.

Hughes, H.J., Delvigne, C., Korntheuer, M., De Jong, J., André, L., and Cardinal, D. (2011) Controlling the mass bias introduced by anionic and organic matrices in silicon isotopic measurements by MC-ICP-MS. *Journal of Analytical Atomic Spectrometry* 26(9), 1892–1896. doi:10.1039/C1JA10110B.

Hurley, J.P., Armstrong, D.E., Kenoyer, G.J., and Bowser, C.J. (1985) Ground water as a silica source for diatom production in a precipitation-dominated lake. *Science* 227(4694), 1576–1578. doi:10.1126/science.227.4694.1576.

Hurwitz, S. and Lowenstern, J.B. (2014) Dynamics of the Yellowstone hydrothermal system. *Reviews of Geophysics* 52, 375–411. doi:10.1002/2014rg000452.

Huth, A., Leydecker, A., Sickman, J., and Bales, R. (2004) A two-component hydrograph separation for three high-elevation catchments in the Sierra Nevada, California. *Hydrological Processes* 18(9), 1721–1733. doi:10.1002/hyp.1414.

Inglethorpe, S.D.J. (1993) Industrial minerals laboratory manual: Diatomite. Tech. rep., British Geological Survey. URL `www.bgs.ac.uk/research/international/dfid-kar/WG92039_col.pdf`.

Johannes, R. (1980) The ecological significance of the submarine discharge of groundwater. *Marine Ecology Progress Series* 365–373. doi:10.3354/meps003365.

Johnson, T.C. and Eisenreich, S.J. (1979) Silica in Lake Superior: mass balance considerations and a model for dynamic response to eutrophication. *Geochimica et Cosmochimica Acta* 43(1), 77–92. doi:10.1016/0016-7037(79)90048-6.

Kaplan, M.R., Wolfe, A.P., and Miller, G.H. (2002) Holocene environmental variability in southern Greenland inferred from lake sediments. *Quaternary Research* 58(2), 149–159. doi:10.1006/qres.2002.2352.

Kurtz, A.C., Derry, L.A., and Chadwick, O.A. (2002) Germanium-silicon fractionation in the weathering environment. *Geochimica et Cosmochimica Acta* 66(9), 1525–1537. doi:10.1016/s0016-7037(01)00869-9.

Kurtz, A.C., Lugolobi, F., and Salvucci, G. (2011) Germanium-silicon as a flow path tracer: Application to the Rio Icacos watershed. *Water Resources Research* 47(6), W06516. doi:10.1029/2010wr009853.

LaBaugh, J.W., Rosenberry, D.O., and Winter, T.C. (1995) Groundwater contribution to the water and chemical budgets of Williams Lake, Minnesota, 1980–1991. *Canadian Journal of Fisheries and Aquatic Sciences* 52(4), 754–767. doi:10.1139/f95-075.

Leng, M.J., Swann, G.E., Hodson, M.J., Tyler, J.J., Patwardhan, S.V., and Sloane, H.J. (2009) The potential use of silicon isotope composition of biogenic silica as a proxy for environmental change. *Silicon* 1(2), 65–77. doi:10.1007/s12633-009-9014-2.

Liu, F., Williams, M.W., and Caine, N. (2004) Source waters and flow paths in an alpine catchment, Colorado Front Range, United States. *Water Resources Research* 40(9). doi:10.1029/2004wr003076.

Lugolobi, F., Kurtz, A.C., and Derry, L.A. (2010) Germanium–silicon fractionation in a tropical, granitic weathering environment. *Geochimica et Cosmochimica Acta* 74(4), 1294–1308. doi:10.1016/j.gca.2009.11.027.

Luijendijk, E., Gleeson, T., and Moosdorf, N. (2020) Fresh groundwater discharge insignificant for the world's oceans but important for coastal ecosystems. *Nature communications* 11(1), 1–12. doi:10.1038/s41467-020-15064-8.

Maavara, T., Slowinski, S., Rezanezhad, F., Van Meter, K., and Van Cappellen, P. (2018) The role of groundwater discharge fluxes on Si: P ratios in a major tributary to Lake Erie. *Science of the Total Environment* 622, 814–824. doi:10.1016/j.scitotenv.2017.12.024.

Mariotti, A., Germon, J., Hubert, P., Kaiser, P., Letolle, R., Tardieux, A., and Tardieux, P. (1981) Experimental determination of nitrogen kinetic isotope fractionation: some principles; illustration for the denitrification and nitrification processes. *Plant and soil* 62(3), 413–430. doi:doi.org/10.1007/BF02374138.

Marron, A.O., Ratcliffe, S., Wheeler, G.L., Goldstein, R.E., King, N., Not, F., De Vargas, C., and Richter, D.J. (2016) The evolution of silicon transport in eukaryotes. *Molecular biology and evolution* 33(12), 3226–3248. doi:10.1093/molbev/msw209.

Mason, B.G., Pyle, D.M., and Oppenheimer, C. (2004) The size and frequency of the largest explosive eruptions on Earth. *Bulletin of Volcanology* 66(8), 735–748. doi:10.1007/s00445-004-0355-9.

McKay, N.P., Kaufman, D.S., and Michelutti, N. (2008) Biogenic silica concentration as a high-resolution, quantitative temperature proxy at Hallet Lake, south-central Alaska. *Geophysical Research Letters* 35(5). doi:10.1029/2007gl032876.

McKeague, J. and Cline, M. (1963) Silica in soils. *Advances in Agronomy* 15, 339 – 396. doi:10.1016/S0065-2113(08)60403-4. Joint contribution as No. 71 of the Soil Research Institute, Canada Department of Agriculture, Ottawa, and as Agronomy paper No. 602, Cornell University, Ithaca, New York.

Meyers, P.A. (2003) Applications of organic geochemistry to paleolimnological reconstructions: a summary of examples from the Laurentian Great Lakes. *Organic geochemistry* 34(2), 261–289. doi:10.1016/s0146-6380(02)00168-7.

Moore, W.S. (2010) The effect of submarine groundwater discharge on the ocean. *Annual review of marine science* 2, 59–88. doi:10.1146/annurev-marine-120308-081019.

Morgan, L., Shanks, W.C., Lovalvo, D., Johnson, S., Stephenson, W., Pierce, K., Harlan, S., Finn, C., Lee, G., Webring, M. et al. (2003) Exploration and discovery in Yellowstone Lake: results from high-resolution sonar imaging, seismic reflection profiling, and submersible studies. *Journal of Volcanology and Geothermal Research* 122(3), 221–242. doi:10.1016/s0377-0273(02)00503-6.

Morley, D.W., Leng, M.J., Mackay, A.W., Sloane, H.J., Rioual, P., and Battarbee, R.W. (2004) Cleaning of lake sediment samples for diatom oxygen isotope analysis. *Journal of Paleolimnology* 31, 391–401. doi:10.1023/B:JOPL.0000021854.70714.6b.

Mortlock, R.A., Froelich, P.N., Feely, R.A., Massoth, G.J., Butterfield, D.A., and Lupton, J.E. (1993) Silica and germanium in Pacific Ocean hydrothermal vents and plumes. *Earth and Planetary Science Letters* 119(3), 365–378. doi:10.1016/0012-821x(93)90144-x.

Mortlock, R.A. and Frohlich, P.N. (1987) Continental weathering of germanium: Ge/Si in the global river discharge. *Geochimica et Cosmochimica Acta* 51(8), 2075–2082. doi:10.1016/0016-7037(87)90257-2.

Murnane, R.J. and Stallard, R.F. (1990) Germanium and silicon in rivers of the Orinoco drainage basin. *Nature* 344(6268), 749–752. doi:10.1038/344749a0.

Nantke, C.K., Frings, P.J., Stadmark, J., Czymzik, M., and Conley, D.J. (2019) Si cycling in transition zones: a study of Si isotopes and biogenic silica accumulation in the Chesapeake Bay through the Holocene. *Biogeochemistry* 146(2), 145–170. doi:10.1007/s10533-019-00618-w.

Newberry, T.L. and Schelske, C.L. (1986) Biogenic silica record in the sediments of Little Round Lake, Ontario. *Hydrobiologia* 143(1), 293–300. doi:10.1007/978-94-009-4047-5_37.

Null, K.A., Dimova, N.T., Knee, K.L., Esser, B.K., Swarzenski, P.W., Singleton, M.J., Stacey, M., and Paytan, A. (2012) Submarine groundwater discharge-derived nutrient loads to San Francisco Bay: Implications to future ecosystem changes. *Estuaries and coasts* 35(5), 1299–1315. doi:10.1007/s12237-012-9526-7.

Oelze, M. (2015) *Silicon isotope fractionation at low temperatures in the presence of Aluminum: An experimental approach and application to different weathering regimes*. PhD thesis, Freie Univ. Berlin. URL `https://gfzpublic.gfz-potsdam.de/rest/items/item_1375006_4/component/file_1375005/content`.

Oelze, M., Schuessler, J.A., and Blanckenburg, F.V. (2016) Mass bias stabilization by Mg doping for Si stable isotope analysis by MC-ICP-MS. *Journal of Analytical Atomic Spectrometry* 31, 2094–2100. doi:10.1039/C6JA00218H.

Opfergelt, S. and Delmelle, P. (2012) Silicon isotopes and continental weathering processes: Assessing controls on Si transfer to the ocean. *Comptes Rendus Geoscience* 344, 723–738. doi:10.1016/j.crte.2012.09.006.

Opfergelt, S., Eiriksdottir, E.S., Burton, K.W., Einarsson, A., Siebert, C., Gislason, S.R., and Halliday, A.N. (2011) Quantifying the impact of freshwater diatom productivity on silicon isotopes and silicon fluxes: Lake Myvatn, Iceland. *Earth and Planetary Science Letters* 305(1-2), 73–82. doi:10.1016/j.epsl.2011.02.043.

Panizzo, V.N., Swann, G.E.A., Mackay, A.W., Vologina, E., Alleman, L., André, L., Pashley, V.H., and Horstwood, M.S.A. (2017) Constraining modern-day silicon cycling in Lake Baikal. *AGU Publications* 556–574. doi:10.1002/2016gb005518.

Panizzo, V.N., Swann, G.E.A., Mackay, A.W., Vologina, E., Sturm, M., Pashley, V., and Horstwood, M.S.A. (2016) Insights into the transfer of silicon isotopes into the sediment record. *Biogeosciences* 13, 147–157. doi:10.5194/bg-13-147-2016.

Pearson, L.K., Hendy, C.H., and Hamilton, D.P. (2016) Dynamics of silicon in lakes of the Taupo Volcanic Zone, New Zealand, and implications for diatom growth. *Inland Waters* 6(2), 185–198. doi:10.5268/iw-6.2.813.

Phillips, A. (2020) *Modelling riverine dissolved silica on different spatial and temporal scales using statistical and machine learning methods*. PhD thesis. URL `https://tspace.library.utoronto.ca/bitstream/1807/101210/1/Phillips_Anna_202006_PhD_thesis.pdf`.

Phillips, A.K. and Cowling, S.A. (2019) Biotic and abiotic controls on watershed Si cycling and river Si yield in western Canada. *Biogeochemistry* 143(2), 221–237. doi:10.1007/s10533-019-00557-6.

Piperno, D.R. (2001) *Phytoliths*, 235–251. Springer Netherlands, Dordrecht. ISBN 978-0-306-47668-6. doi:10.1007/0-306-47668-1_11.

Poitrasson, F. (2017) Silicon isotope geochemistry. *Reviewa in Mineralogy & Geochemistry* 82, 289–344. doi:10.2138/rmg.2017.82.8.

Ragueneau, O., Schultes, S., Bidle, K., Claquin, P., and Moriceau, B. (2006) Si and C interactions in the world ocean: Importance of ecological processes and implications for the role of diatoms in the biological pump.

Global Biogeochemical Cycles 20(4). doi:10.1029/2006gb002688. GB4S02.

Reynolds, B.C., Aggarwal, J., Andre, L., Baxter, D., Beucher, C., Brzezinski, M.A., Engstrom, E., Georg, R.B., Land, M., Leng, M.J., Opfergelt, S., Rodushkin, I., Sloane, H.J., van den Boorn, S.H.J.M., Vroon, P.Z., and Cardinal, D. (2007) An inter-laboratory comparison of Si isotope reference materials. *Journal of Analytical Atomic Spectrometry* 22, 561–568. doi:10.1039/b616755a.

Reynolds, J.H. (1953) The isotopic constitution of silicon, germanium, and hafnium. *Physical Review* 90(6), 1047. doi:10.1103/physrev.90.1047.

Rosén, P., Vogel, H., Cunningham, L., Reuss, N., Conley, D.J., and Persson, P. (2010) Fourier transform infrared spectroscopy, a new method for rapid determination of total organic and inorganic carbon and biogenic silica concentration in lake sediments. *Journal of Paleolimnology* 43(2), 247–259. doi:10.1007/s10933-009-9329-4.

Ryves, D.B., Jewson, D.H., Sturm, M., Battarbee, R.W., Flower, R.J., Mackay, A.W., and Granin, N.G. (2003) Quantitative and qualitative relationships between planktonic diatom communities and diatom assemblages in sedimenting material and surface sediments in Lake Baikal, Siberia. *Limnology and Oceanography* 48(4), 1643–1661. doi:10.4319/lo.2003.48.4.1643.

Saccone, L., Conley, D., Koning, E., Sauer, D., Sommer, M., Kaczorek, D., Blecker, S., and Kelly, E. (2007) Assessing the extraction and quantification of amorphous silica in soils of forest and grassland ecosystems. *European Journal of Soil Science* 58(6), 1446–1459. doi:10.1111/j.1365-2389.2007.00949.x.

Schelske, C.L. (1985) Biogeochemical silica mass balances in Lake Michigan and Lake Superior. *Biogeochemistry* 1(3), 197–218. doi:10.1007/bf02187199.

Schelske, C.L., Conley, D.J., Stoermer, E.F., Newberry, T.L., and Campbell, C. (1987) *Biogenic silica and phosphorus accumulation in sediments as indices of eutrophication in the Laurentian Great Lakes*, vol. 37, 79–86. Springer, developments in hydrobiology edn. ISBN 978-94-010-8296-9. doi:10.1007/978-94-009-4047-5_12.

Schopka, H.H. and Derry, L.A. (2012) Chemical weathering fluxes from volcanic islands and the importance of groundwater: The Hawaiian example. *Earth and Planetary Science Letters* 339, 67–78. doi:10.1016/j.epsl.2012.05.028.

Shanks, W.C., Alt, J.C., and Morgan, L.A. (2007) Geochemistry of sublacustrine hydrothermal deposits in Yellowstone Lake - Hydrothermal reactions, stable-isotope systematics, sinter deposition, and spire formation. *Publications of the US Geological Survey* (85). URL `https://digitalcommons.unl.edu/usgspubs/85`.

Shemesh, A., Mortlock, R., and Froelich, P. (1989) Late Cenozoic Ge/Si record of marine biogenic opal: Implications for variations of riverine fluxes to the ocean. *Paleoceanography* 4(3), 221–234. doi:10.1029/pa004i003p00221.

Simpson, T.L. and Volcani, B.E. (1981) *Silicon and siliceous structures in biological systems*, chap. Silicon in the Cellular Metabolism of Diatoms, 16–42. Springer-Verlag New York. doi:10.1007/978-1-4612-5944-2.

Sommer, M., Kaczorek, D., Kuzyakov, Y., and Breuer, J. (2006) Silicon pools and fluxes in soils and landscapes – a review. *Journal of Plant Nutrition and Soil Science* 169(3), 310–329. doi:10.1002/jpln.200521981.

Street-Perrott, F.A., Barker, P.A., Leng, M.J., Sloane, H.J., Wooller, M.J., Ficken, K.J., and

Swain, D.L. (2008) Towards an understanding of late Quaternary variations in the continental biogeochemical cycle of silicon: multi-isotope and sediment-flux data for Lake Rutundu, Mt Kenya, East Africa, since 38 ka BP. *Journal of Quaternary Science: Published for the Quaternary Research Association* 23(4), 375–387. doi:10.1002/jqs.1187.

Struyf, E., Mörth, C.M., Humborg, C., and Conley, D.J. (2010) An enormous amorphous silica stock in boreal wetlands. *Journal of Geophysical Research: Biogeosciences* 115(G4), G04008. doi:10.1029/2010jg001324.

Struyf, E., Smis, A., Van Damme, S., Meire, P., and Conley, D.J. (2009) The global biogeochemical silicon cycle. *Silicon* 1(4), 207–213. doi:10.1007/s12633-010-9035-x.

Sun, X., Andersson, P., Humborg, C., Gustafsson, B., Conley, D.J., Crill, P., and Mörth, C.M. (2011) Climate dependent diatom production is preserved in biogenic Si isotope signatures. *Biogeosciences* 8(11), 3491–3499. doi:10.5194/bg-8-3491-2011.

Sun, X., Andersson, P., Land, M., Humborg, C., and Mörth, C.M. (2010) Stable silicon isotope analysis on nanomole quantities using MC-ICP-MS with a hexapole gas-collision cell. *Journal of Analytical Atomic Spectrometry* 25(2), 156–162. doi:10.1039/B911113A.

Sutton, J.N., André, L., Cardinal, D., Conley, D.J., De Souza, G.F., Dean, J., Dodd, J., Ehlert, C., Ellwood, M.J., Frings, P.J. et al. (2018) A review of the stable isotope bio-geochemistry of the global silicon cycle and its associated trace elements. *Frontiers in Earth Science* 5(112). doi:10.3389/feart.2017.00112.

Swann, G.E., Leng, M.J., Juschus, O., Melles, M., Brigham-Grette, J., and Sloane, H.J. (2010) A combined oxygen and silicon diatom isotope record of Late Quaternary change in Lake El'gygytgyn, North East Siberia. *Quaternary Science Reviews* 29(5-6), 774–786. doi:10.1016/j.quascirev.2009.11.024.

Tiller, C.C. (1995) *Postglacial sediment stratigraphy of large lakes in Greater Yellowstone: Scenarios of tectonic and climatic forcing*. Master's thesis, University of Minnesota.

Tréguer, P.J. and De La Rocha, C.L. (2013) The world ocean silica cycle. *Annual Review of Marine Science* 5, 477–501. doi:10.1146/annurev-marine-121211-172346.

Tribovillard, N. (2013) The Ge/Si ratio as a tool to recognize biogenic silica in chert. *Comptes Rendus Geoscience* 345(3), 160–165. doi:10.1016/j.crte.2013.02.005.

Vandevenne, F., Barão, L., Ronchi, B., Govers, G., Meire, P., Kelly, E., and Struyf, E. (2015) Silicon pools in human impacted soils of temperate zones. *Global Biogeochemical Cycles* 29(9), 1439–1450. doi:10.1002/2014gb005049.

Varela, D.E., Pride, C.J., and Brzezinski, M.A. (2004) Biological fractionation of silicon isotopes in Southern Ocean surface waters. *Global biogeochemical cycles* 18(1), GB1047. doi:10.1029/2003gb002140.

Vegacenter (2020) Inductively Coupled Plasma Mass Spectrometry (ICP-MS) scheme. URL `https://www.nrm.se/english/researchandcollections/geosciences/vegacenter/instrumentation.9000161.html`.

Wetzel, R.G. (1975) *Limnology*. W. B. Saunders Company. ISBN 0-7216-9240-0.

Wiederhold, J.G. (2015) Metal stable isotope signatures as tracers in environmental geochemistry. *Environmental science & technology* 49(5), 2606–2624. doi:10.1021/es504683e.

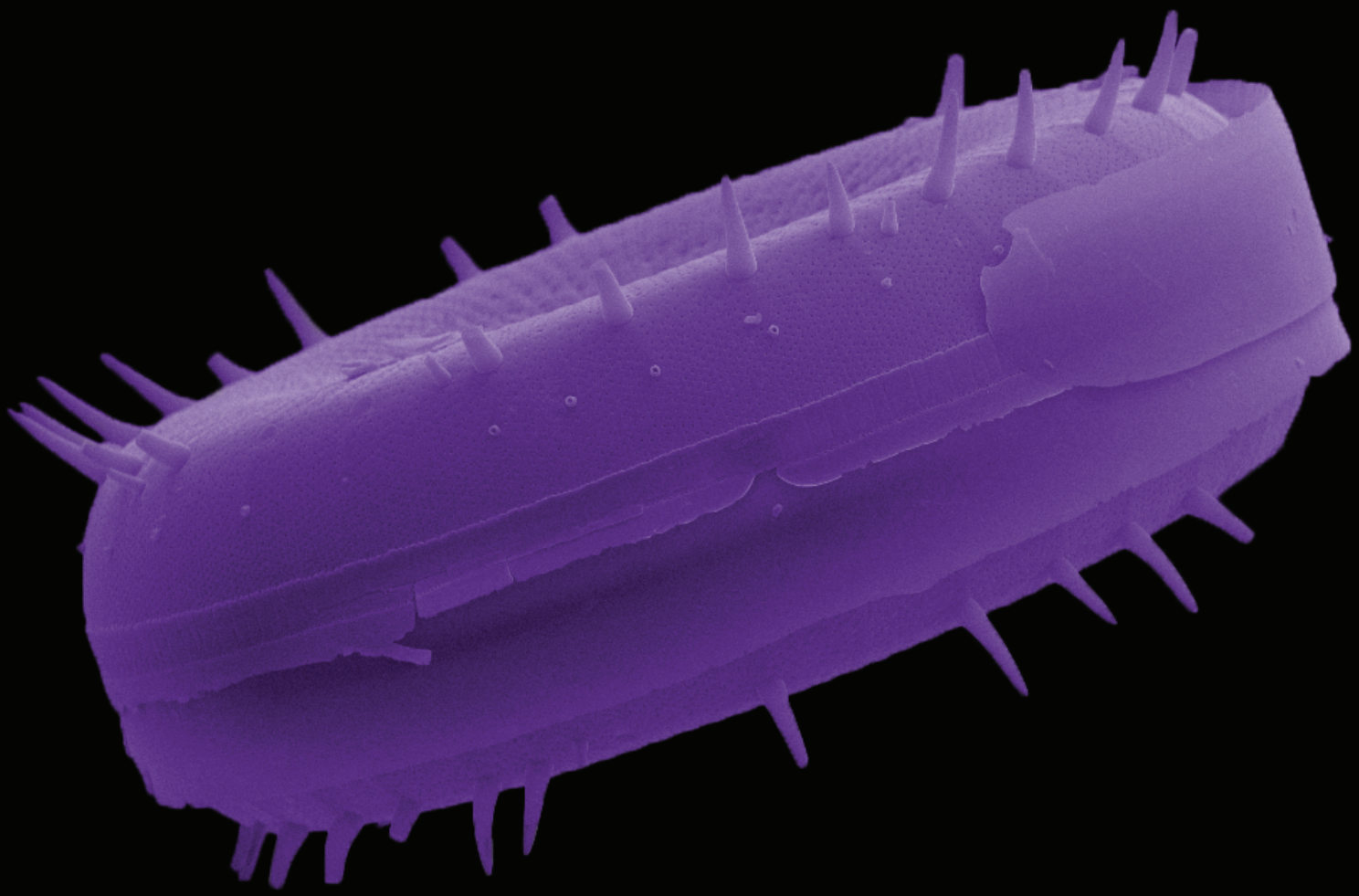
Wonisch, H., Gérard, F., Dietzel, M., Jaffrain, J., Nestroy, O., and Boudot, J.P. (2008) Occurrence of polymerized silicic acid and aluminum species in two forest soil solutions with different acidity. *Geoderma* 144(3-4), 435–445. doi:10.1016/j.geoderma.2007.11.022.

Wu, S., Yang, C., Pester, N.J., and Chen, Y. (2011) A new hydraulically actuated titanium sampling valve for deep-sea hydrothermal fluid samplers. *Journal of Oceanic Engineering* 36(3), 462–469. doi:10.1109/JOE.2011.2140410.

Zhang, A., Zhang, J., and Liu, S. (2020) Spatial and temporal variations of dissolved silicon isotope compositions in a large dammed river system. *Chemical Geology* 119645. doi:10.1016/j.chemgeo.2020.119645.

Ziegler, K., Chadwick, O.A., Brzezinski, M.A., and Kelly, E.F. (2005) Natural variations of δ^{30}Si ratios during progressive basalt weathering, Hawaiian Islands. *Geochimica et Cosmochimica Acta* 69(19), 4597–4610. doi:10.1016/j.gca.2005.05.008.

Paper I



20 µm

"The characteristic of scientific progress is our knowing that we did not know."

Gaston Bachelard

Cover photo: SEM photo of *Stephanodiscus yellowstonensis*

Picture credits: Petra Zahajská & Rosine Cartier

Quaternary Research
Copyright © University of Washington. Published by Cambridge University Press, 2020. This is an Open Access article, distributed under the terms of the Creative Commons Attribution licence (http://creativecommons.org/licenses/by/4.0/), which permits unrestricted re-use, distribution, and reproduction in any medium, provided the original work is properly cited.
doi:10.1017/qua.2020.14

CONTRIBUTIONS TO THE QR FORUM

What is diatomite?

Petra Zahajská[a,b]*, Sophie Opfergelt[c], Sherilyn C. Fritz[d], Johanna Stadmark[a], Daniel J. Conley[a]

[a]Department of Geology, Lund University, Sölvegatan 12, 22362 Lund, Sweden
[b]Institution of Palaeontology and Geology, Charles University, Albertov 6, 12832 Prague, Czechia
[c]Earth and Life Institute, Université catholique de Louvain, 1348 Louvain-la-Neuve, Belgium
[d]Department of Earth and Atmospheric Sciences, School of Biological Sciences, University of Nebraska, Lincoln, Nebraska 68588-0340 USA
*Corresponding author at: Department of Geology, Lund University, Sölvegatan 12, 22362 Lund, Sweden. E-mail address: petra.zahajska@geol.lu.se (P. Zahajská).

(Received August 19, 2019; Accepted February 15, 2020)

Abstract

Different types of biogenic remains, ranging from siliceous algae to carbonate precipitates, accumulate in the sediments of lakes and other aquatic ecosystems. Unicellular algae called diatoms, which form a siliceous test or frustule, are an ecologically and biogeochemically important group of organisms in aquatic environments and are often preserved in lake or marine sediments. When diatoms accumulate in large numbers in sediments, the fossilized remains can form diatomite. In sedimentological literature, "diatomite" is defined as a friable, light-coloured, sedimentary rock with a diatom content of at least 50%, however, in the Quaternary science literature diatomite is commonly used as a description of a sediment type that contains a "large" quantity of diatom frustules without a precise description of diatom abundance. Here we pose the question: What is diatomite? What quantity of diatoms define a sediment as diatomite? Is it an uncompacted sediment or a compacted sediment? We provide a short overview of prior practices and suggest that sediment with more than 50% of sediment weight comprised of diatom SiO_2 and having high (>70%) porosity is diatomaceous ooze if unconsolidated and diatomite if consolidated. Greater burial depth and higher temperatures result in porosity loss and recrystallization into porcelanite, chert, and pure quartz.

Keywords: Diatomite; Sediment classification; Biogenic sediment; Diatomaceous sediment; Diatomaceous ooze

In many lakes worldwide, as well as in marine environments, diatoms are an important component of phytoplankton populations. Accumulations of diatoms are known from all aquatic environments including wetlands, lakes, and the marine environment (Clarke, 2003). In marine environments, accumulations of diatom-rich sediments extend back to the Late Cretaceous (Harwood et al., 2007), whereas the oldest diatom-rich lake sediments are from the Eocene (Flower et al., 2013), with large deposits found in the Miocene (Bradbury and Krebs, 1995). Massive accumulations of fossil diatom frustules have been observed in multiple lakes situated in silica-rich environments, especially in volcanic and hydrothermally active areas, such as Yellowstone Lake, US (Theriot et al., 2006), Lake Myvatn, Iceland (Opfergelt et al., 2011), or Lake Challa, Tanzania/Kenya (Barker et al., 2013). In these settings, the high dissolved silicon concentrations promote the growth of diatoms (Wallace, 2003). However, high diatom concentrations in sediment also have been observed in lakes with no volcanic or hydrothermal influence, for example in lakes of Northern Sweden (Frings et al., 2014) or Lough Neagh, Ireland (Plunkett et al., 2004). In the oceanic environment, high biogenic silica accumulations occur in the equatorial Pacific Ocean, where diatoms grow in zones fed by continental siliceous dust and nutrients brought by upwelling. Similarly, cold-water regions, such as the productive Antarctic convergence zone, have sufficient nutrient and dissolved silicon supply that diatom-rich sediments are formed (Flower et al., 2013).

Cite this article: Zahajská, P., Opfergelt, S., Fritz, S. C., Stadmark, J., Conley, D. J. 2020. What is diatomite? *Quaternary Research* 1–5. https://doi.org/10.1017/qua.2020.14

Downloaded from https://www.cambridge.org/core. Lund University Libraries, on 29 Apr 2020 at 15:34:15, subject to the Cambridge Core terms of use, available at https://www.cambridge.org/core/terms. https://doi.org/10.1017/qua.2020.14

Conger (1942) hypothesized that the requirements for diatomaceous accumulation are to have (1) conditions favourable for diatom growth, and (2) a reduced accumulation of other sedimentary constituents that would dilute the concentration of the siliceous tests of diatoms. Diatom growth is dependent on many environmental factors, such as dissolved silicon availability, phosphorus and nitrogen availability, pH, salinity, and light (Battarbee et al., 2002). Diatom test preservation is sensitive to temperature and pH; biogenic silica dissolves faster with increasing pH (>8) and temperature (Alexander et al., 1954). Although diatom-rich sediments are found worldwide in various environments, of various ages and various settings, the terminology for classifying high accumulations of diatom frustules in sediment is not consistent in the literature, particularly in the Quaternary literature.

Sediments can be classified based on the sedimentary environment, sedimentary structures and processes, and sediment texture and composition, including sorting, shape of grains, grain size, and the ratio of matrix to grains. Grain size, for example, is used in various classification systems (e.g., Wentworth, 1922 or see summary in Pettijohn [1949]). This is appropriate for minerogenic sediments, but biogenic sediments contain more than just mineral grains. Biogenic sediments (also called bioclastic or organic) are composed of skeletal remains, shells, or tests from organisms composed of biogenic silica or calcium carbonate, or remains of soft organic material, mainly organic carbon. The classification of calcium carbonate sediments based on texture and the ratio of matrix to the abundance of grains is well described by Dunham (1962), and an effective general classification of lacustrine sediments was proposed by Schnurrenberger (2003), but it has not been widely used.

The first usage of the word diatomite dates to the nineteenth century from deep-sea deposits that were called diatom ooze, collected during the voyage of the HMS Challenger (Murray and Renard, 1891). Later, Conger (1942) described pure diatomaceous earth as material that reached a purity of 95 to 98% of diatom silica. According to Terzaghi et al. (1996), diatomaceous ooze should be used for loose unconsolidated sediment containing mainly diatoms. In colloquial nonscientific literature, diatomaceous earth is used as a name for both milled diatomite and for diatomaceous ooze, which creates ambiguity in the usage of diatomaceous earth as a definition. For this reason, we exclude diatomaceous earth from our proposed classification, which is intended for use in scientific literature rather than in the public domain.

Inglethorpe (1993) described the characteristics of diatomite as a unique combination of physical and chemical properties (high porosity, high permeability, small particle size, large surface area, low thermal conductivity, and chemical inertness) that make diatomite suitable for a wide range of industrial applications. Diatomite was defined as a "pale coloured, soft, light-weight rock composed principally of the silica microfossils" (Inglethorpe, 1993, p. 1). A diatomite of high SiO_2 purity (ranging from 80 to 99 wt% of biogenic SiO_2) is now commonly used in scientific research as a reference material in isotope geochemistry for the measurement of stable silicon isotopes. One widely used standard (Reynolds et al, 2007) originates from the Lompoc quarry in California, more precisely from the Miocene strata of the Monterey Formation, which is well known for numerous lithological stages of siliceous deposits—diatomite, diatomaceous shales, diatomaceous mudstones, porcelanite, and cherts (Bramlette, 1946). The Lompoc area is well described by Bramlette (1946), including a description of the purity of diatomaceous deposits.

Various generalized classification systems for lacustrine and marine sediments have been proposed by Dean (1985), Mazzullo et al. (1988), Owen (2002), and Schnurrenberger (2003). Dean (1985) and Mazzullo et al. (1988) proposed that biogenic sediment be defined as sediment that contains at least 50% of biogenic material. In this approach, biogenic content is estimated visually or by point-counting on smear slides, which has been an efficient method for calcareous nanoplankton sediment classification. For siliceous nanoplankton (diatoms, radiolarians, and chrysophyte cysts), which are comparatively big and porous, the point-counting method can both overestimate (Dean et al., 1985) and underestimate (Conley, 1988) the percentage of biogenic silica. An alternative approach is to use the wt% biogenic silica relative to the dry sediment to classify unconsolidated biogenic silica-rich sediment using the methods of DeMaster (1981), Morlock and Froelich (1989), or Conley and Schelske (2001). However, the weak base extractions dissolve only biogenic silica that is classified as opal-A, and sediments that are more diagenetically altered containing highly ordered opal-CT require a much stronger base.

A detailed classification based on diatom SiO_2 content by Owen (2002) does not consider the stage of lithification caused by diagenetic processes. Diagenetic processes decrease the sediment porosity and alter the crystalline structure of SiO_2. For example, non-crystalline opal-A (such as the SiO_2 found in live siliceous organisms and their biogenic remains) is transformed into the disordered silica polymorph opal-CT (Rice et al., 1995) with some of the stacking disorder removed (Murata and Randall, 1975). Temperature and burial depth play an important role in the extent of diagenesis. Therefore, the interpretation of diatomite raises an important second question of whether an unconsolidated sediment can be called diatomite. We suggest here that diatomite, a term widely used for diatom-rich sediments, be used only for consolidated sediments.

We are using a variety of previous studies as a guide, including Murray and Renard (1891), Conger (1942), Bramlette (1946), Murata and Larson (1975), Isaacs (1981c), Pedersen (1981), Kadey (1983), Dean et al. (1985), Mazzullo et al. (1988), Minoura et al. (1996), Inglethorpe (1993), Lemons (1996), Akin et al. (2000), Owen (2002), Moyle (2003), and Schnurrenberger (2003). We adopt the recommendation from Mazzulo et al. (1988), in which any sediment material that is present in the sediment with more than 10% of the composition is considered as a modifier and, therefore, it should be stated in the name. The following definitions of

Downloaded from https://www.cambridge.org/core. Lund University Libraries, on 29 Apr 2020 at 15:34:15, subject to the Cambridge Core terms of use, available at https://www.cambridge.org/core/terms. https://doi.org/10.1017/qua.2020.14

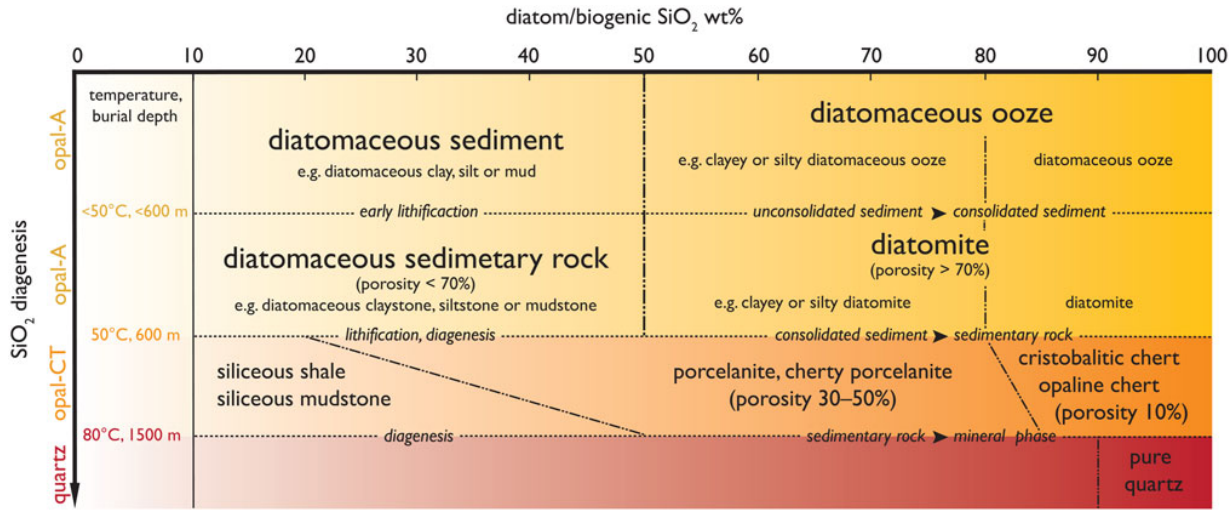


Figure 1. Proposed classification of sediment containing diatoms. The weight percentage (wt%) of diatom/biogenic SiO_2 contained in sediments is on the *x*-axis and their transformations as a function of burial depth appears on the *y*-axis.

diatomaceous ooze and diatomite are proposed in Figure 1 and we suggest nomenclature for defining related materials rich in diatom silica.

The principal name describing unconsolidated sediment containing diatom frustules with more than 50% of sediment weight is *diatomaceous ooze*. Oozes have a content of 50 to 80 wt% of diatom SiO_2 together with another major sediment component, such as clay or silt. This major sediment modifier should be stated in the name, e.g., *clayey* or *silty diatomaceous ooze*. The stand-alone principal name *diatomaceous ooze* is used for ooze composed of more than 80 wt% of diatoms without any major sediment modifier. Unconsolidated sediment with diatom frustules less than 50% of sediment weight should be called *diatomaceous sediment* using supporting sediment terminology, such as *diatomaceous clay*, *diatomaceous silt*, or *diatomaceous mud*, to describe the matrix. Sediments with less than 10 wt% of diatom SiO_2 are named based on the clastic sediment classification without reference to diatoms.

Diatomite is defined as a siliceous/opaline consolidated sediment with a diatom SiO_2 content higher than 50% of sediment weight and porosity higher than 70%. As diatomites are often composed of 50–80% by weight of diatom SiO_2, the major sediment modifier material must be named with the adjectives describing the sediment matrix components, such as clay or silt, for example *clayey* or *silty diatomite*. Further, we suggest that the stand-alone principal name *diatomite* is used strictly for consolidated sediment with more than 80% of sediment weight comprised of diatom SiO_2. Chrysophyte cysts, radiolarians, and sponge spicules can be a minor part of the sediment (Bramlette, 1946). Consolidated sediments containing less than 50% sediment weight of diatom SiO_2 are then named based on the prevalent sediment component, e.g., *diatomaceous claystone*, *siltstone,* or *mudstone*. The porosity of these consolidated sediments should be lower than 70%. Diatomite and diatomaceous sediments are formed at low temperatures and pressures (<50°C and burial depth <600m). Significant recrystallization occurs at higher temperature and burial depths.

The boundary at 50% by weight of diatom/biogenic SiO_2, e.g., between diatomaceous sediment and diatomaceous ooze (unconsolidated sediment) or between diatomaceous sedimentary rock and diatomite (consolidated sediment), as shown in Figure 1, is consistent with the widely used Ocean Drilling Program marine sediment classification system (Mazzullo et al., 1988), as well as the commonly used sedimentological nomenclature practices described by e.g., Schnurrenberger et al. (2003). The boundary at 80% by weight of diatom/biogenic SiO_2, e.g., between clayey or silty diatomaceous ooze and diatomaceous ooze (unconsolidated sediment) or between clayey or silty diatomite and diatomite (consolidated sediment), is based on the industrial and commercially used diatomite, which has a diatom content higher than 80% by weight.

At burial depths between 600 to 1500 m and temperatures ranging from 50 to 80°C, as found for example in the Monterey Formation, diatomite is transformed into opaline chert with a low porosity of around 10% (Isaacs, 1981b, 1981c). *Chert* is then defined as sedimentary rock with more than 80% of sediment weight originating from biogenic SiO_2 (predominantly diatom SiO_2). Diagenetic processes transform the biogenic SiO_2 (chrysophyte cysts, diatoms, radiolarians, and sponge spicules), and the original source of SiO_2 is difficult to determine, although fossils can be found in cherts (Pessagno and Newport, 1972). For this reason, we use biogenic SiO_2 in our definition of chert instead of the wt% of diatom SiO_2. Diatomites and diatomaceous sediments containing, for example, clay or silt in combination with between 20 and 85 wt% biogenic SiO_2, exposed to deeper burial depths and higher temperatures are altered to porcelanite or cherty porcelanite, with a final porosity between 30 and 50%, depending on the clay/silt content (Bramlette, 1946; Isaacs, 1981a; MacKinnon, 1989).

Downloaded from https://www.cambridge.org/core. Lund University Libraries, on 29 Apr 2020 at 15:34:15, subject to the Cambridge Core terms of use, available at https://www.cambridge.org/core/terms. https://doi.org/10.1017/qua.2020.14

Sediments that contain less than 20 to 50 wt% biogenic SiO_2 under these conditions form shales, siliceous shales or siliceous mudstones, depending on the mineral content (Isaacs, 1981a).

With increasing temperatures and burial depth, the final stage of alteration is reached at depths between 1500 to 2000 m and temperatures above 80°C; these conditions result in recrystallization of opal-CT into quartz (Murata and Larson, 1975; Isaacs, 1980). The boundaries based on biogenic SiO_2 content between cherts, and especially between porcelanites and shales, are not sharp (Fig. 1). This is because the definitions of these siliceous sedimentary rocks take into account not only porosity and content of biogenic SiO_2 but also hardness, fracturing patterns, and other petrological criteria (Isaacs, 1981a), as diagenesis changes the properties of the sedimentary rock. We summarize our suggested classification of diatomaceous sediments and sedimentary rocks based on diatom/biogenic SiO_2 wt% in Figure 1.

In summary, there are inconsistencies in the present use of the term diatomite and diatomaceous sediment throughout the literature. Based on our definition, unconsolidated lake or marine sediments that have not undergone any diagenesis (burial depth and temperature, as defined above), such as those of Holocene age, should not be referred to as diatomite, but instead should be called diatomaceous ooze. We encourage scientists working with diatomaceous sediments and sedimentary rocks to apply the definitions used here to ensure consistent use of terminology and hence comparability among studies. For sediment types that do not fit within the parameters that we have defined (Fig. 1), we suggest that all sediment components (mineralogy, texture, and porosity) be described in detail. We believe that proper naming will bring clarity to future studies focused on diatomaceous sediments and diatomite.

ACKNOWLEDGMENTS

This work was supported by The Royal Physiographic Society in Lund, by the Center for Geosphere Dynamics (UNCE/SCI/006) and by the Charles University project (GA UK 40217) to PZ, the Swedish Research Council to DJC, and NSF EAR-1514814 to SCF.

REFERENCES

Akin, S., Schembre, J.M., Bhat, S.K., Kovscek, A.R., 2000. Spontaneous imbibition characteristics of diatomite. *Journal of Petroleum Science and Engineering* 25, 149–165.

Alexander, G.B., Heston, W., Iler, R.K., 1954. The solubility of amorphous silica in water. *The Journal of Physical Chemistry* 58, 453–455.

Battarbee, R.W., Jones, V.J., Flower, R.J., Cameron, N.G., Bennion, H., Carvalho, L., Juggins, S., 2002. Diatoms. In: Smol, J. P., Birks, H. J. B., Last, W. M., Bradley, R. S., and Alverson, K. (Eds.), *Tracking Environmental Change Using Lake Sediments Volume 3: Terrestrial, Algal, and Siliceous Indicators*. Springer, Dordrecht, pp. 155–202.

Barker, P.A., Hurrell, E.R., Leng, M.J., Plessen, B., Wolff, C., Conley, D.J., Keppens, E., Milne, I., Cumming, B.F., Laird, K.R., Kendrick, C.P., Wynn, P.M., Verschuren, D., 2013. Carbon cycling within an East African lake revealed by the carbon isotope composition of diatom silica: a 25-ka record from Lake Challa, Mt. Kilimanjaro. *Quaternary Science Reviews* 66, 55–63.

Bradbury, J.P., Krebs, W.N., 1995. Fossil continental diatoms: paleolimnology, evolution, and biochronology. In: *Siliceous Microfossils* (Short Courses in Paleontology 8). 1995. The Paleontological Society, Knoxville, Tennessee, pp. 119–138.

Bramlette, M., 1946. The Monterey Formation of California and the Origin of its Siliceous Rocks. Professional Paper 212. U.S. Geological Survey, Washington.

Clarke, J., 2003. The occurrence and significance of biogenic opal in the regolith. *Earth-Science Reviews* 60, 175–194.

Conger, P.S., 1942. Accumulation of diatomaceous deposits. *Journal of Sedimentary Research* 12, 55–66.

Conley, D., Schelske, C., 2001. Biogenic silica. In: Smol, J., Birks, H.J., Last, W., Bradley, R., and Alverson, K. (Eds.), *Tracking Environmental Change Using Lake Sediments, Volume 3: Terrestrial, Algal, and Siliceous Indicators*, Developments in Paleoenvironmental Research. Springer, Dordrecht, pp. 281–293.

Conley, D.J., 1988. Biogenic silica as an estimate of siliceous microfossil abundance in Great Lakes sediments. *Biogeochemistry* 6, 161–179.

Dean, W. E., Leinen, M., Stow, D. A. (1985). Classification of deep-sea, fine-grained sediments. *Journal of Sedimentary Petrology* 55(2), 250–256.

DeMaster, D.J., 1981. The supply and accumulation of silica in the marine environment. *Geochimica et Cosmochimica Acta* 45, 1715–1732

Dunham, R.J., 1962. Classification of Carbonate Rocks According to Depositional Texture. In: Ham, W.E. (Ed.), *Classification of Carbonate Rocks*, AAPG, Tulsa, pp. 108–121.

Flower, R.J., 2013. Diatom Methods| Diatomites: Their Formation, Distribution, and Uses. In: Elias S.A. and Mork, C.J. (Eds.), *Encyclopedia of Quaternary Science*, Elsevier, Amsterdam, pp. 501–506.

Frings, P.J., Clymans, W., Jeppesen, E., Lauridsen, T.L., Struyf, E., Conley, D.J., 2014. Lack of steady-state in the global biogeochemical Si cycle: emerging evidence from lake Si sequestration. *Biogeochemistry* 117, 255–277.

Harwood, D.M., Nikolaev, V.A., Winter, D.M., 2007. Cretaceous records of diatom evolution, radiation, and expansion. *The Paleontological Society Papers* 13, 33–59.

Inglethorpe, S.D.J., 1993. Industrial minerals laboratory manual: Diatomite. Technical report, British Geological Survey, Nottingham.

Isaacs, C.M., 1980. *Diagenesis in the Monterey Formation examined laterally along the coast near Santa Barbara, California* (Vol. 80, No. 606). Department of Geology, Stanford University.

Isaacs, C.M., 1981a. Field characterization of rocks in the Monterey Formation along the coast near Santa Barbara, California. In: Isaacs, C.M. (Ed.), *Guide to the Monterey Formation in the California coastal areas, Ventura to San Luis Obispo*. Pacific Section AAPG Spec. Publ., 52, pp. 39–53

Isaacs, C.M., 1981b. Outline of diagenesis in the Monterey Formation examined laterally along the Santa Barbara coast, California. In: Isaacs, C.M. (Ed.), *Guide to the Monterey Formation in the California coastal areas, Ventura to San Luis Obispo*. Pacific Section AAPG Spec. Publ., 52, pp. 25–38.

Isaacs, C.M., 1981c. Porosity reduction during diagenesis of the Monterey Formation, Santa Barbara coastal area, California. In: Garrison, R.E., Douglas R.G., Pisciotto K.E., Isaacs, C.M. and Ingle J.C. (Eds.), *The Monterey Formation and Related Siliceous*

Downloaded from https://www.cambridge.org/core. Lund University Libraries, on 29 Apr 2020 at 15:34:15, subject to the Cambridge Core terms of use, available at https://www.cambridge.org/core/terms. https://doi.org/10.1017/qua.2020.14

Rocks of California. Pacific Section SEPM Spec. Publ., 15, pp. 257–272.

Kadey, F.L., Jr, 1983. Diatomite. *Industrial Rocks and Minerals* 1, 677–708.

Lemons, J.F.J., 1996. Diatomite. Minerals Yearbook - Metals and Minerals. United States Geological Survey, Reston, available online: https://www.usgs.gov/centers/nmic/diatomite-statistics-and-information.

MacKinnon, T.C., 1989. Origin of the Miocene Monterey Formation in California. In: MacKinnon, T.C., Randall, J.W. and Garrison, R.E. (Eds.), *Coal and Hydrocarbon Resources of North America*; Volume 1, Oil in the California Monterey Formation, Field Trips for the 28th International Geological Congress, Washington, DC, Am. Geophys. Union, T311, pp. 1–10.

Mazzullo, J.M., Meyer, A., Kidd, R.B., 1988. New sediment classification scheme for the Ocean Drilling Program. In: Mazzullo, J.M., Graham, A.G. (Eds.), *Handbook for shipboard sedimentologists*. Texas A&M University, ODP, Technical Note, 8, pp. 45–67.

Minoura, K., Susaki, T., Horiuchi, K., 1996. Lithification of biogenic siliceous sediments: Evidence from Neogene diatomaceous sequences of northeast Japan. *Sedimentary Geology* 107, 45–59.

Mortlock, R.A., Froelich, P.N., 1989. A simple method for the rapid determination of biogenic opal in pelagic marine sediments. Deep Sea Research Part A. *Oceanographic Research Papers* 36, 1415–1426.

Moyle R.P., Dolley P.T., 2003. Chapter D: With or without Salt—A comparison of marine and continental-lacustrine diatomite deposits. In: Bliss J.D., Moyle, P.R, Long, K.R. (Eds.), *Contributions to Industrial-Minerals Reserch*. Bulletin 2209–D. US Geological Survey. https://doi.org/10.2172/820335

Murata, K.J, Larson, R.R., 1975. Diagenesis of Miocene siliceous shales, Temblor Range, California. *Journal of Research of the U.S. Geological Survey* 3, 553–566.

Murata, K. J., & Randall, R. G. (1975). Silica mineralogy and structure of the Monterey shale, Temblor Range, California. *Journal of Research of the U.S. Geological Survey*, 3, 567–572.

Murray, J., Renard, A.F., 1891. *Report on Deep-sea Deposits based on the Specimens collected during the Voyage of H.M.S. Challenger in the years 1872 to 1876*. HM Stationery Office, Edinburgh.

Opfergelt, S., Eiriksdottir, E.S., Burton, K.W., Einarsson, A., Siebert, C., Gislason, S.R., Halliday, A.N., 2011. Quantifying the impact of freshwater diatom productivity on silicon isotopes and silicon fluxes: Lake Myvatn, Iceland. *Earth and Planetary Science Letters* 305, 73–82.

Owen, R.B., 2002. Sedimentological characteristics and origins of diatomaceous deposits in the East African Rift System. *SEPM Special Publication* 73, 233–246.

Pedersen, G.K., 1981. Anoxic events during sedimentation of a Palaeogene diatomite in Denmark. *Sedimentology* 28, 487–504.

Pessagno, E.A., Jr., Newport, R.L., 1972. A technique for extracting radiolaria from radiolarian cherts. *Micropaleontology* 18, 231–234.

Pettijohn, F., 1949. *Sedimentary Rocks*. 2nd ed. Harper and Row, New York.

Plunkett, G.M., Whitehouse, N.J., Hall, V.A., Brown, D.M., Baillie, M.G.L., 2004. A precisely-dated lake-level rise marked by diatomite formation in northeastern Ireland. *Journal of Quaternary Science* 19, 3–7.

Reynolds B.C., Aggarwal J., André L., Baxter D., Beucher C., Brzezinski M.A., Engström E., *et al*.., 2007. An inter-laboratory comparison of Si isotope reference materials. *Journal of Analytical Atomic Spectrometry* 22, 561–568

Rice, S.B., Freund, H., Huang, W.L., Clouse, J.A., Isaacs, C.M., 1995. Application of Fourier transform infrared spectroscopy to silica diagenesis: The opal-A to opal-CT transformation. *Journal of Sedimentary Research* 65, 639–647.

Schnurrenberger, D., Russell, J., Kelts, K., 2003. Classification of lacustrine sediments based on sedimentary components. *Journal of Paleolimnology* 29, 141–154.

Terzaghi, K., Peck, R.B., Mesri, G., 1996. *Soil Mechanics in Engineering Practice*. 3rd ed. John Wiley and Sons, New York.

Theriot, E.C., Fritz, S.C., Whitlock, C., Conley, D.J., 2006. Late Quaternary rapid morphological evolution of an endemic diatom in Yellowstone Lake, Wyoming. *Paleobiology* 32, 38–54.

Wallace, A. R. (2003). Regional geologic setting of Late Cenozoic lacustrine diatomite deposits, Great Basin and surrounding region: overview and plans for investigation. US Department of the Interior, US Geological Survey.

Wentworth, C.K., 1922. A scale of grade and class terms for clastic sediments. *The Journal of Geology* 30, 377–392.

Downloaded from https://www.cambridge.org/core. Lund University Libraries, on 29 Apr 2020 at 15:34:15, subject to the Cambridge Core terms of use, available at https://www.cambridge.org/core/terms. https://doi.org/10.1017/qua.2020.14



Paper II

"If we knew what it was we were doing, it would not be called research, would it?"

Albert Einstein

Cover photo: Lake 850 in August 2019

Picture credits: Petra Zahajská

Modern silicon dynamics of a small high-latitude subarctic lake

Petra Zahajská[1,5], Carolina Olid[2], Johanna Stadmark[1], Sherilyn C. Fritz[3], Sophie Opfergelt[4], and Daniel J. Conley[1]

[1]Department of Geology, Lund University, Lund, Sweden
[2]Department of Ecology and Environmental Science, Umeå University, Umeå, Sweden
[3]Department of Earth and Atmospheric Sciences and School of Biological Sciences, University of Nebraska–Lincoln, Lincoln, Nebraska, USA
[4]Earth and Life Institute, Université catholique de Louvain, Louvain-la-Neuve, Belgium
[5]Institute of Geology and Palaeontology, Faculty of Science, Charles University, Prague, Czech Republic

Correspondence: Petra Zahajská (petra.zahajska@geol.lu.se)

Abstract. High biogenic silica (BSi) concentrations occur sporadically in lake sediments throughout the world, however, the processes leading to high BSi concentrations vary. While BSi formation and preservation is expected to occur in silica-rich environments with high dissolved silicon (DSi) concentrations such as volcanic and hydrothermal inputs, the factors and mechanisms explaining high DSi and BSi concentrations in lakes remain unclear. We explored the factors responsible for the high BSi concentration in sediments of a small, high-latitude subarctic lake (Lake 850). To do this, we combined measurements of variations in stream discharge, DSi concentrations and stable Si isotopes in both lake and stream water with measurements of BSi content in lake sediments. Water, radon, and Si mass balances revealed the importance of groundwater discharge as a main source of DSi to the lake, with groundwater-derived DSi inputs 3 times higher than those from ephemeral stream inlets. After including all external DSi sources (i.e., inlets and groundwater discharge) and estimating the total BSi accumulation in the sediment, we show that diatom production consumes up to 79% of total DSi input. Additionally, low sediment accumulation rates were observed based on the dated gravity core. Our findings thus demonstrate that groundwater discharge and low mass accumulation rate can account for the high BSi accumulation during the last 150 cal. yr BP. Globally, lakes have been estimated to retain one fifth of the annual DSi delivery into the ocean. Well constrained lake mass balances, such as presented here, bring clarity to those estimates of the terrestrial Si cycle sinks.

1 Introduction

Diatoms – unicellular golden-brown algae – are found worldwide in all aquatic environments, wetlands, and soils (Battarbee et al., 2002; Clarke, 2003). Diatoms take up dissolved silicic acid, H_4SiO_4, expressed here as dissolved silicon (DSi), and build their shells in the form of amorphous silica, also known as biogenic silica (BSi). Diatom production is thus a crucial component in the global Si cycle (Tréguer and De La Rocha, 2013). Massive accumulations of fossil diatom frustules in sediments have been observed in multiple lakes situated in silicon-rich environments, especially on volcanic bedrock, such as Lake Challa, Tanzania/Kenya (Barker et al., 2013), or in hydrothermally active areas, such as Yellowstone Lake, US (Theriot et al., 2006) or Lake Myvatn, Iceland (Opfergelt et al., 2011). However, lakes without volcanism can also accumulate high concentrations of BSi in the sediment (Frings et al., 2014). One example is high-elevation and high-latitude lakes, where BSi concentrations as high as 60 weight percent of SiO_2 have been found (Frings et al., 2014; Rosén et al., 2010). In addition, high BSi concentrations in sediment have been observed in Lough Neagh, Northern Ireland (Plunkett et al., 2004), Lake Baikal (Swann and Mackay, 2006), Lake Edward (Russell and Johnson, 2005), and Lake Malawi (Johnson et al., 2011). The processes responsible for the diatom-rich sediment formation in these non-volcanic settings, however, are poorly understood.

High BSi accumulation in sediment has been hypothesized to require sufficient DSi concentration in the water column for diatoms to grow and low detrital input to minimize dilution of autochthonous BSi (Conger, 1942). DSi originates ultimately from weathering of bedrock, and it is transported

by rivers through the environment where it can be removed by biological or physico-chemical processes, such as secondary clay mineral formation or amorphous silica precipitation (Jenny, 1941). DSi concentrations in the environment are influenced by factors, such as vegetation type (Jenny, 1941; Leng et al., 2009; Struyf et al., 2010), bedrock type (Jenny, 1941; Opfergelt and Delmelle, 2012), indirectly by climate forcing (Fortin and Gajewski, 2009; Jenny, 1941), or watershed geomorphology (Jenny, 1941). In particular, attention has been paid to the relative importance of groundwater discharge as a main source of DSi for a few lakes, such as Lake O'Hara, British Columbia (Hood et al., 2006), Lake Myvatn, Iceland (Opfergelt et al., 2011), Crystal Lake, Wisconsin (Kenoyer and Anderson, 1989; Hurley et al., 1985), at the mouth of the Changjiang river system, China (Zhang et al., 2020), and in Canadian and Siberian rivers (Maavara et al., 2018; Pokrovsky et al., 2013). However, the significance of groundwater discharge is still often overlooked in studies about Si dynamics in lakes.

The contribution of groundwater to lake Si cycle can be evaluated using Si isotopes. Stable Si isotopes are used to trace variation in DSi sources or diatom production and discern processes affecting BSi accumulation in lake sediments. Among the three stable isotopes (^{28}Si, ^{29}Si and ^{29}Si) diatoms preferentially take up the lighter ^{28}Si (De La Rocha et al., 1997). Diatoms tend to fractionate the Si isotopes with a fractionation factor of -1.1 ‰ (De La Rocha et al., 1997), which means that the diatom BSi will have an isotopically lighter ratio compared to the source DSi. Riverine DSi usually shows isotopically heavier ratios compared to groundwater, as there are more processes that fractionate Si isotopes during river transport (Frings et al., 2016; Opfergelt and Delmelle, 2012; Sutton et al., 2018). Therefore, stable Si isotopes provide an ideal tracer for the contribution of groundwater.

Here, we investigate the mechanisms responsible for the diatom-rich sediment formation in high-latitude lake from a non-volcanic setting. Lake 850, northernmost Sweden, is an ideal case study with a high content of BSi in the sediment ca. 40 weight percent (wt%) (Rosén et al., 2010). Oxygen isotopes from diatoms suggested that the lake's isotopic ratio is mostly influenced by summer precipitation and variations in the ephemeral inlet streams (Shemesh et al., 2001). Unlike previous studies in this lake, we hypothesize that groundwater discharge is an important mechanism controlling lake DSi concentrations. To test this hypothesis, we estimate groundwater flows discharging into the lake using a water and a radon (^{222}Rn) mass balance. DSi concentration and stable Si isotope mass balances were used to determine Si sources for diatom-rich sediment in recent decades.

2 Study area

Lake 850 (68°15′ N, 19°7′ E) is located $14\,\mathrm{km}$ southeast from Abisko Research Station (388 m a.s.l.), northern Sweden. From 1913 to 2019, the mean annual surface atmospheric temperature was $-0.4\,^{\circ}\mathrm{C}$, whereas during the study years (2018-2019) the mean annual temperature was $0.03\,^{\circ}\mathrm{C}$. Further, the mean surface atmospheric temperature during the aquatic growing season in 2018-2019 (June to August) was $-10.1\,^{\circ}\mathrm{C}$ (1SD = $2.8\,^{\circ}\mathrm{C}$), and the long-term (1913-2019) mean summer temperature of $9.8\,^{\circ}\mathrm{C}$ (1SD = $3.6\,^{\circ}\mathrm{C}$) (ANS, 2020a). Lake 850 lies above the tree-limit (600 m a.s.l) at 850 m a.s.l. The lake surface area is $0.02\,\mathrm{km}^2$, with a maximum depth of $8\,\mathrm{m}$ and a catchment area of $0.35\,\mathrm{km}^2$ (Rubensdotter and Rosqvist, 2003). Lake deep basin represents 48% of the lake surface area. The underlying bedrock is composed of granites and syenites and is overlain by a thin layer of till. The catchment vegetation is comprised of Arctic species of mosses, grasses, and shrubs (Shemesh et al., 2001). There are two ephemeral inlets (max $6\,\mathrm{cm}$ deep) in the eastern part of the lake and one outlet ($10\,\mathrm{cm}$ deep) in the western part (Figure 1, Table S1). Besides streams, additional sources of water to rivers and lakes can be snow patches or inputs of groundwater (Pienitz et al., 2008). From mid-October until late May–early June, the lake is ice-covered. The catchment is snow-covered from mid-September to mid-June. In August, the lake is well-mixed, with no thermal stratification. The lake is classified as oligotrophic and has a pH of 6.8 and a dissolved organic carbon concentration of $2.3\,\mathrm{mg\,l^{-1}}$ (Shemesh et al., 2001).

3 Numerical analyses – mass balance models

Mass balances for water and radon were constructed to estimate the potential contribution of groundwater discharge to Lake 850. A Si mass balance was used to constrain DSi inputs (inlets, groundwater) and DSi outputs (outlet DSi, sediment BSi accumulation).

3.1 Radon mass balance

Radon (^{222}Rn, hereafter Rn) is produced from the radioactive decay of ^{226}Ra (Ra hereafter) present in rocks, soils, and sediments. Radon emanates from Ra bearing minerals, enters the groundwater, and is transported through the aquifer. Groundwaters usually contain Rn concentrations orders of magnitude higher than surface waters, and groundwater discharging into surface waters can thus be easily detected by a Rn enrichment with respect to surface waters (Burnett and Dulaiova, 2003).

Groundwater discharge into the Lake 850 was quantified using a Rn mass balance approach and assuming steady-state (Dimova and Burnett, 2011; Dimova et al., 2013). In the study lake, the sources of Rn are the main inlet streams ($\mathrm{n} = 2$), Rn production by dissolved Ra in the water col-

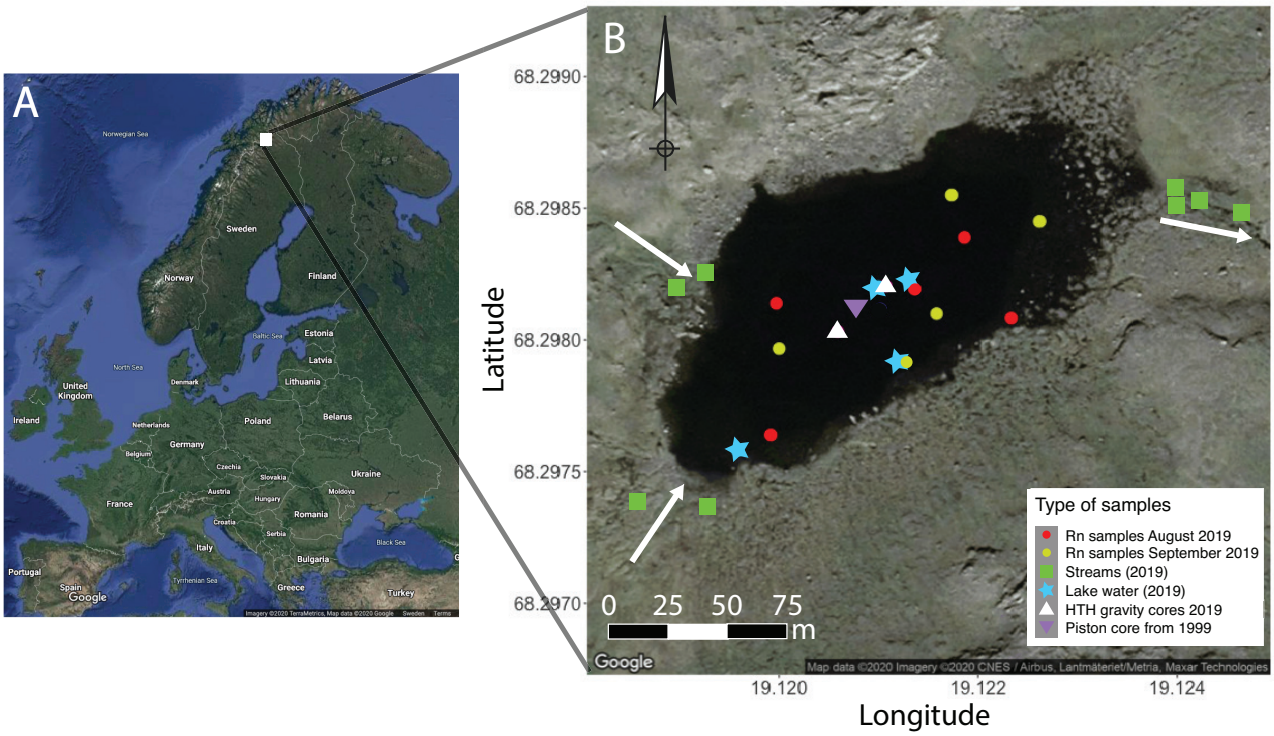


Figure 1. Sampling sites of Lake 850 (northern Sweden). Inlets and outlet streams are signified by white arrows. Plotted in R using package ggmaps (Kahle and Wickham, 2013) and modified.

umn, Rn diffusion from underlying sediments, and groundwater discharge. Radon losses include radioactive decay, atmospheric evasion, and losses through the outlet streams ($n = 1$). Losses by recharge into underlying aquifers are considered minor, because the concentration of Rn seeping into sediments is usually much lower that seeping into the lake (Dimova and Burnett, 2011). By evaluating all Rn source and loss terms, the groundwater flow discharging into the lake can be determined using the following equation:

$$Q_{gw}Rn_{gw} + F_{sed}A + \lambda Ra_{lake}V + Q_{in}Rn_{in} = F_{atm}A + \lambda Rn_{lake}V + Q_{out}Rn_{out} \quad (1)$$

where Q_{gw} is the unknown groundwater discharge [$m^3\,d^{-1}$]; Q_{in} and Q_{out} are the discharge from inlet and outlet streams [$m^3\,d^{-1}$], respectively; Rn_{lake} and Rn_{gw} are the concentrations of Rn [$Bq\,m^{-3}$] in lake water and groundwater, respectively; Rn_{in} and Rn_{out} are the concentrations of Rn [$Bq\,m^{-3}$] in the main inlet and outlet streams, respectively; Ra_{lake} is the concentration of Ra in lake water column [$Bq\,m^{-3}$]; F_{sed} is the net diffusive flux of Rn per unit area from lake sediments [$Bq\,m^{-2}\,d^{-1}$]; F_{atm} is the loss of Rn to the atmosphere [$Bq\,m^{-2}\,d^{-1}$]; λ is the radioactive decay constant of Rn [d^{-1}]; and A [m^2] and V [m^3] are the area and volume of the lake, respectively.

The calculation of Rn loss to the atmosphere was based on the empirical equation by MacIntyre et al. (1995):

$$F_{atm} = k(Rn_{lake} - \alpha Rn_{air}) \quad (2)$$

where k is the gas transfer coefficient [$m\,d^{-1}$] based on an empirical relationship that relates k with wind speed and lake area (Vachon and Prairie, 2013), and α is the air-water partitioning of Rn corrected for salinity and temperature (Schubert et al., 2012).

Groundwater discharges (Q_{gw}) were estimated for August and September 2019. For the remainder months, we interpolated the estimated values by assuming two different scenarios of i) constant or ii) variable groundwater inflows over the year (see Appendix A1) for variable groundwater inflows scenario).

3.2 Water balance

The lake water balance was calculated from the volumetric water balance equation:

$$\Delta V = Q_{in} + P + Q_{gw} - Q_{out} - E \quad (3)$$

where ΔV is the change in lake water volume, Q_{in} and Q_{out} are the stream inflow and outflow, respectively, Q_{gw} is the groundwater inflow, P is precipitation, E is evaporation. Monthly summer precipitation of 48 mm (ANS, 2020a)

has been considered to be included in the stream inflow term. Evaporation and precipitation have been shown to only have a small contribution to the lake water balance, and thus they are considered negligible here (Shemesh et al., 2001).

3.3 Silicon mass balance

The DSi flux into and from the lake is calculated as $\phi = \mathrm{Q} \cdot \mathrm{c}$, where Q is discharge [$\mathrm{l s^{-1}}$] and c is DSi concentration [$\mathrm{mg\ SiO_2\ l^{-1}}$]. The DSi balance is then calculated as:

$$\Delta\mathrm{DSi} = \phi_{\mathrm{in}} + \phi_{\mathrm{gw}} - \phi_{\mathrm{out}} - \phi_{\mathrm{BSi}} \quad (4)$$

where ΔDSi is the change of lake DSi [$\mathrm{mg\ SiO_2\ yr^{-1}}$], and ϕ_{in}, ϕ_{out} and ϕ_{gw} are the DSi fluxes of the inlet, outlet, and groundwater discharge [$\mathrm{mg\,yr^{-1}}$], respectively. Finally, ϕ_{BSi} represents the flux of BSi into the sediment [$\mathrm{mg\ SiO_2\ yr^{-1}}$], and it was calculated as:

$$\phi_{\mathrm{BSi}} = (\mathrm{SAR} \cdot \rho_{\mathrm{dry}} \cdot \mathrm{BSiwt\%} \cdot \mathrm{A_{sed}}) \cdot 1000, \quad (5)$$

where SAR is sediment accumulation rate [$\mathrm{cm\,yr^{-1}}$] calculated from the age-depth model (see Methods section 4.1.2), ρ_{dry} is dry bulk sediment density [$\mathrm{g\,cm^{-3}}$], BSiwt% is the mean of BSi content in sediments, $\mathrm{A_{sed}}$ is the area of sedimentary basin of the lake [$\mathrm{cm^2}$] and 1000 is unit conversion from g to mg.

Assuming that the lake is in steady-state, which means that sum of input DSi fluxes equals to sum of output Si fluxes, thus $\Delta\mathrm{DSi} = 0$, DSi concentration in groundwater was then calculated by dividing ϕ_{gw} from Equation 4 by $\mathrm{Q_{gw}}$. The groundwater DSi flux in ice-free period is dependent on inlet (ϕ_{in}), outlet DSi flux (ϕ_{out}) and BSi flux to sediment (ϕ_{BSi}). However, during ice-covered period, the ϕ_{gw} is dependent only on ϕ_{BSi}, if there is some (scenario 1, Appendix B) and on differences of lake volume and DSi concentration. Thus, in order to solve Equation 4, ϕ_{BSi} and lake DSi concentration changes in ice-covered period are required. The ϕ_{gw} during ice covered period is calculated by a mixing model (see Appendix A2).

To constrain DSi concentrations in groundwater, we have examined 3 different scenarios considering different BSi fluxes (ϕ_{BSi}) to the sediment driven by the length of diatom production. Two scenarios with maximal and minimal monthly BSi flux appear in the Appendix B aiming to describe maximal and minimal diatom production period and thus groundwater DSi concentrations. The scenario better describing recent diatom production considers that the diatom growing season and, thus, the BSi flux occurs in 4 months, from June until August, in a year (Shemesh et al., 2001), and that scenario is presented here.

3.4 Silicon isotope mass balance

The variability of the isotopic Si ratio of the lake water is likely to be biologically driven and, therefore, was described using a Si isotopic fractionation model. We hypothesize that the lake has sufficient inlet and groundwater supply to allow for DSi concentrations to remain high and that DSi is unlimited for diatom growth, thus, an open system model was used. The open system model (Varela et al., 2004) describes the expected diatom $\delta^{30}\mathrm{Si_{BSi}}$, as well as the post-uptake ratio of the lake water $\delta^{30}\mathrm{Si_{postuptake}}$.

$$\delta^{30}\mathrm{Si_{BSi}} = \delta^{30}\mathrm{Si_{initial}} + \varepsilon \cdot \mathrm{f} \quad (6)$$

$$\delta^{30}\mathrm{Si_{postuptake}} = \delta^{30}\mathrm{Si_{initial}} - \varepsilon \cdot (1 - \mathrm{f}) \quad (7)$$

where $\delta^{30}\mathrm{Si_{initial}}$ is the isotopic ratio of the initial DSi source, ε is the fractionation factor of freshwater diatoms $\breve{}1.1 \pm 0.41$ ‰ (De La Rocha et al., 1997), and f is the fraction of remaining DSi calculated as $\mathrm{f} = \frac{\mathrm{c_{out}}}{\mathrm{c_{initial}}}$, where $\mathrm{c_{initial}}$ and $\mathrm{c_{out}}$ are DSi concentrations before and after diatom production uptake. Thus, $(1 - \mathrm{f})$ is the DSi utilization by diatom production. The initial DSi concentration is calculated through mixing model with knowledge of the discharges ($\mathrm{Q_{in}}$ and $\mathrm{Q_{gw}}$) and DSi concentrations ($\mathrm{c_{in}}$ and $\mathrm{c_{gw}}$) of the endmembers .

The initial isotopic ratio of lake DSi before diatom uptake is back calculated from $\delta^{30}\mathrm{Si_{postuptake}}$ (Appendix A3). The known variables are the $(1 - \mathrm{f})$ and the $\delta^{30}\mathrm{Si_{postuptake}}$ represented either in the lake isotopic composition or in the lake outlet $\delta^{30}\mathrm{Si_{out}}$, if $\delta^{30}\mathrm{Si_{lake}} = \delta^{30}\mathrm{Si_{out}}$. Further, the groundwater isotopic composition can be calculated from the initial isotopic Si mixture before diatom uptake and fractionation through isotope mixing model (see Appendix A3).

Similar to the Si mass balance, the isotope Si mass balance was examined through three scenarios that differ in BSi flux to the sediment representing different length of diatom production (Appendix B). As differences in BSi fluxes alter groundwater DSi concentrations, the isotopic composition is also changing. However, the scenario describing the recent lake functioning is used for the model presented here. Results of this model were compared with measured data of $\delta^{30}\mathrm{Si_{BSi}}$ and $\delta^{30}\mathrm{Si_{postuptake}}$ (which equals to $\delta^{30}\mathrm{Si_{lake}}$). For validation, the groundwater $\delta^{30}\mathrm{Si_{gw}}$ for monthly steady-state was calculated and compared with data in the literature.

4 Materials and Methods

4.1 Sample collection, chemical analyses and chronology

4.1.1 Water sampling

For DSi analyses, water samples from the ephemeral inlets and outlet streams, and lake waters were collected monthly from June to September 2019 (Figure 1, Table S1). Additionally, samples of two profiles of lake water from the deepest and a shallower part of the lake were collected in August and September 2019. All water samples were filtered

directly in the field through a $0.45\,\mu\mathrm{m}$ cellulose Sterivex™-HV Durapore filter and acidified with HCl to pH 2 in the laboratory. DSi concentrations were analyzed by the automated molybdate-blue method (Strickland and Parsons, 1972) with a Smartchem 200, AMS System™ discrete analyzer at Lund University with an instrumental error of $\pm 3.7\%$.

For Rn analyses, surface water samples (maximum of $1.5\,\mathrm{m}$ depth from the surface or $0.5\,\mathrm{m}$ depth at the shallow depths) were collected from 5 different stations (Figure 1, Table S1). A deeper water sample ($4\,\mathrm{m}$ depth) was collected from the central deeper point of the lake to evaluate the potential stratification of Rn concentrations. Samples of water from the main inlet and the outlet stream were also collected. Water samples were collected in $1.5\,\mathrm{l}$ polyethylene terephthalate (PET) bottles with no headspace using a peristaltic pump. Water was pumped directly into the bottle and left overflowing to replenish the volume at least three times to ensure minimal contact with air. Shortly after collection, Rn concentrations were determined using a Rn-in-air alpha spectrometer RAD7 (Durridge Inc.) coupled to the Big Bottle RAD H_2O accessory (Durridge Inc.). All Rn concentrations were decay corrected for the time of collection.

Discharges from the inlet and outlet streams were determined by measuring the water velocity at 60% of the sampling point depth using the six-tenths-depth method (Turnipseed and Sauer, 2010) and creating a cross section through the tributary.

4.1.2 Sediment sampling

Two short ($\sim 15\,\mathrm{cm}$) sediment gravity cores were sampled with a HTH gravity corer in March and August 2019 (Table S1). Both cores showed an undisturbed water-sediment interface. One of the cores was sliced directly in the field in $1\,\mathrm{cm}$ sections. Each section was weighed before and after freeze drying to determine water content, porosity, and wet and dry bulk densities. Total organic carbon (TOC) and total nitrogen (TN) analyses were carried out on all freeze dried samples, after packing 5 to $10\,\mathrm{mg}$ of dry sediment into tin capsules. Five samples throughout the core were tested for carbonate content by acidifying with HCl and heating to $60\,^{\circ}\mathrm{C}$ before the TOC measurements (Brodie et al., 2011). The measurements were done on a COSTECH ECS4010 elemental analyzer at the Department of Geology, Lund University, with the mean analytical uncertainty for TOC of 0.3 wt% based on duplicate analysis ($n = 14$). The carbonate content calculated as a difference in TOC between de-calcified and bulk sample was below 0.5 wt%, thus considered negligible.

Biogenic SiO_2 content in the sediment was analyzed by sequential alkaline extraction (Conley and Schelske, 2001). Freeze dried and homogenized samples were digested in $0.1\,\mathrm{M}\,Na_2CO_3$ (sample reagent ratio $0.03/40\,\mathrm{g/ml}$) in a shaking bath at $85\,^{\circ}\mathrm{C}$ for 5 hours. Subsamples of $100\,\mu\mathrm{l}$ were taken at 3, 4, and 5 hours and neutralized in $9.9\,\mathrm{ml}$ of HCl to examine for the dissolution of minerals. The extracted DSi was measured using the automated molybdate-blue method (Strickland and Parsons, 1972) with a Smartchem 200, AMS System™ discrete analyzer at Lund University with an instrumental error of $\pm 3.7\%$. As there were no changes in the amount of total Si extracted during the time course of dissolution ($n = 3$, slope ≈ 0), the mean BSi concentration from all the values was used to estimate BSi concentration with no Si-containing minerals correction applied (Conley, 1998).

All sediment samples were analyzed for radionuclide concentrations (^{210}Pb, ^{226}Ra, and ^{137}Cs) at Lund University. ^{210}Pb, ^{226}Ra, and ^{137}Cs were determined by direct γ-counting using a high-purity germanium detector ORTEC (Model GEM FX8530P4-RB). Freeze-dried and ground samples were sealed for at least 3 weeks before counting to ensure secular equilibrium of ^{226}Ra daughters. ^{210}Pb was determined through the $46\,\mathrm{keV}$ γ-emission and ^{226}Ra through the 351 and $609\,\mathrm{keV}$ γ-emission of its daughter nuclide ^{214}Pb and ^{214}Bi, respectively. ^{137}Cs was measured by its emission at $662\,\mathrm{keV}$. Self-absorption was measured directly, and the detector efficiency was determined by counting a National Institute of Standards and Technology sediment standard.

Sediment core chronologies were obtained by applying the Bayesian statistics approach with software package Plum (Aquino-López et al., 2018). The Plum package was applied using the default settings for the thickness of Bacon sections ($1\,\mathrm{cm}$). Plum used the individual ^{226}Ra measurements as an estimate of the supported ^{210}Pb concentration. The unsupported ^{210}Pb was found in upper most $7\,\mathrm{cm}$, and the software package Plum (Aquino-López et al., 2018) extrapolated the ages for the remaining $7\,\mathrm{cm}$ based on measured data.

To constrain the Rn mass balance, the second sediment gravity core was used for equilibration experiments in order to determine Rn diffusion from underlying sediments and the Rn concentration representative of the groundwater discharging into the lake. Briefly, diffusive flux experiments were carried out in the laboratory by incubating $\sim 200\,\mathrm{g}$ of dry sediment placed into $500\,\mathrm{ml}$ PET bottles with Milli-Q® water, as described in Chanyotha et al. (2014). Using the RAD7 coupled to the Big Bottle RAD H_2O accessory (Durridge Inc.), Rn concentrations were monitored for 14 hours. The rate of Rn diffusion from the sediment (F_{diff}) was derived from the exponential ingrowth of Rn concentrations with time. The bottles containing grab sediments were then stored for more than a month and periodically shaken. After this time, the Rn concentration in water was measured using the RAD7 and converted into groundwater endmember activities using porosity and bulk density as described in Chanyotha et al. (2014).

4.2 Stable Si isotopes analyses

Stable Si isotope analyses were performed on diatoms recovered from sediment, lake, and stream water samples. Cleaned diatom material from a previous study (Shemesh et al., 2001) was processed for stable Si isotopes. Briefly,

Table 1. Summary of discharge from the inlets (Q_{in}), the outlet (Q_{out}) stream, groundwater discharge (Q_{gw}), dissolved Si concentration as $mgSiO_2\,l^{-1}$ in the inlets (c_{in}), the outlet (c_{out}), and the lake water (c_{lake}), stable Si isotopic signal of the inlet ($\delta^{30}Si_{in}$), outlet ($\delta^{30}Si_{out}$), and the lake ($\delta^{30}Si_{lake}$).

		March	June	July	August	September
Q_{in}	$l\,s^{-1}$		2.9	1.5	0.5	dry
Q_{out}	$l\,s^{-1}$		21.5	9.9	4.5	1.6
Q_{gw}	$l\,s^{-1}$	not sampled	not sampled	not sampled	3.57 ± 1.24	3.88 ± 1.06
c_{in}	$mg\,SiO_2\,l^{-1}$		2.34 ± 0.05	4.79 ± 0.05	5.05 ± 0.12	dry
c_{out}	$mg\,SiO_2\,l^{-1}$		1.19 ± 0.02	0.94 ± 0.01	1.12 ± 0.03	1.37 ± 0.01
c_{lake}	$mg\,SiO_2\,l^{-1}$	2.51 ± 0.35	1.24 ± 0.02	not sampled	0.96 ± 0.06	1.37 ± 0.04
$\delta^{30}Si_{in}$	‰		0.02 ± 0.10	0.72 ± 0.10	0.78 ± 0.15	dry
$\delta^{30}Si_{out}$	‰		0.89 ± 0.10	0.61 ± 0.10	0.79 ± 0.12	1.09 ± 0.20
$\delta^{30}Si_{lake}$	‰	1.27 ± 0.15	0.73 ± 0.10	not sampled	0.77 ± 0.32	1.02 ± 0.24

pure diatom samples ($\sim 0.8\,mg$) were digested with 0.5 to $1\,ml$ of $0.4\,M$ NaOH (analytical purity) at $50\,°C$ for at least 48 hours. When all diatoms were dissolved, samples were diluted with Milli-Q® water to prevent precipitation and fractionation of amorphous silica, then neutralized by 0.5 to $1\,ml$ of $0.4\,M$ suprapur® HCl. The solutions were measured for their DSi concentration to obtain the Si recovery, which was between 90 and 100%. Sample solutions were purified for Si isotope analysis by cation-chromatographic separation using $1.5\,ml$ cation-exchange DOWEX® 50W-X8 (200-400 mesh) resin following the method of Georg et al. (2006). Silicon from filtered water samples was purified using the same cation-exchange method (Georg et al., 2006). The international Si standard NIST reference material RM-8546 (former NBS-28) and laboratory standard Diatomite were prepared by alkaline NaOH fusion and purified following protocol by Georg et al. (2006).

The reference material RM-8546 (former NBS-28) and laboratory standards IRMM-018, Big-Batch, and Diatomite used in the VegaCenter were prepared by another type of fusion with $LiBO_2$ (Sun et al., 2010). Thus, our alkaline NaOH fused NBS-28 and Diatomite standards (Georg et al., 2006), purified in identical way as the samples, were matrix matched to contain $3\,mg\,l^{-1}$ Li IPC-MS standard. Similarly, all purified samples were diluted to a concentration of $3\,mg\,l^{-1}$ of Si in $0.12\,M$ SeaStar™ HCl matrix and doped with Li to contain $3\,mg\,l^{-1}$ Li to match the standard matrix.

The stable isotope measurements were carried out on a NuPlasma (II) HR multi-collector inductively conducted plasma mass spectrometry (MC-ICP-MS, Nu Instruments™) with an Apex HF desolvation nebulizer at the Vegacenter, Swedish Museum of Natural History, Stockholm. The ^{28}Si signal intensity of full procedural blanks was determined to be less than 0.35% of the total signal intensity, thus no sample contamination was observed. Silicon isotope data are reported as deviations of $\frac{^{30}Si}{^{28}Si}$ and $\frac{^{29}Si}{^{28}Si}$ from the NBS-28 reference solution in ‰, denoted $\delta^{30}Si$ and $\delta^{29}Si$ as follows:

$$\delta^{30}Si = \left(\frac{\frac{^{30}Si}{^{28}Si\,sample}}{\frac{^{30}Si}{^{28}Si\,NBS28}} - 1 \right) \cdot 1000. \quad (8)$$

Each sample was measured three times, bracketed by NBS-28 in between, and full chemical replicates for all samples ($n = 25$, total measurements $= 180$) were measured. Secondary reference materials Diatomite, Big-Batch, and IRMM-018 were measured throughout all measuring sessions in a period of 3 years, with means of $\delta^{30}Si = 1.26 \pm 0.19$ ‰ ($2SD_{repeated}$, $n = 219$) for Diatomite, $\delta^{30}Si = -10.64 \pm 0.18$‰ ($2SD_{repeated}$, $n = 77$) for Big-Batch, and $\delta^{30}Si = -1.77 \pm 0.18$‰ ($2SD_{repeated}$, $n = 100$) for IRMM-018 for quality control purposes. All secondary reference material values were in good agreement with values from a previous interlaboratory comparison (Reynolds et al., 2007). The reproducibility of all samples was < 0.2 ‰. At the Vegacenter laboratory, the long-term precision for $\delta^{30}Si$ is 0.15‰ (2SD).

5 Results

5.1 Lake water chemical and isotopic properties

Lake 850 is a subarctic lake in a region with strong seasonality. The discharge from inlets and the outlet streams show a decreasing trend throughout the ice-free period from June through September (Table 1). The highest water flow rates are observed during the snowmelt period (June and July). Inflow from the stream inlet to the lake in August is low, and both inlets are dry in September.

During the ice-free period direct surface precipitation contribution from the watershed, was estimated from the mean precipitation of $48\,mm\,month^{-1}$ (ANS, 2020a). With the watershed area of $0.35\,km^2$ (Rubensdotter and Rosqvist, 2003), precipitation results in $0.65\,l\,s^{-1}$, which represents only 1.4% of the lake volume. Similar or higher discharges are observed in the stream inlets from July to August. Therefore, the influence of precipitation on the water mass bal-

ance is limited. The calculated lake water residence time during the high-flow regime in June, defined as lake volume ($1.2 \cdot 10^5 \mathrm{m}^3$) divided by the lake outlet discharge (Table 1), is 55 days. During the rest of the year, the lake water residence time is more than 1 year.

Lake DSi concentration varies seasonally (Table 1), with the highest values during the ice-covered period in March, reaching $2.51 \pm 0.35\,\mathrm{mg\,SiO_2\,l^{-1}}$. With snowmelt, the lake DSi decreases to $1.24 \pm 0.02\,\mathrm{mg\,SiO_2\,l^{-1}}$ in June and to its minimum value of $0.96 \pm 0.06\,\mathrm{mg\,SiO_2\,l^{-1}}$ in August. With the first snow in September, lake DSi concentration rebounds, having values of $1.37 \pm 0.04\,\mathrm{mg\,SiO_2\,l^{-1}}$. Data of DSi for the inlets and the outlet streams show two different patterns during the year (Table 1). A lower inlet DSi concentration of $2.34 \pm 0.05\,\mathrm{mg\,SiO_2\,l^{-1}}$ is observed during snow melt in June compared to July and August, when the inlet DSi concentrations increase to $4.79 \pm 0.05\,\mathrm{mg\,SiO_2\,l^{-1}}$ and $5.05 \pm 0.12\,\mathrm{mg\,SiO_2\,l^{-1}}$, respectively. The lake outlet DSi concentration shows little variability, with the lowest concentration of $0.94 \pm 0.01\,\mathrm{mg\,SiO_2\,l^{-1}}$ in July and only a small increase up to $1.12 \pm 0.03\,\mathrm{mg\,SiO_2\,l^{-1}}$ towards the end of the summer season in August. In September, when the inlet streams are snow covered, the DSi concentration in the outlet stream is the same as the lake water concentration at $1.37 \pm 0.01\,\mathrm{mg\,SiO_2\,l^{-1}}$.

The stable Si isotope ratios of the lake, inlet, and outlet streams vary during the year. The heaviest lake $\delta^{30}\mathrm{Si_{lake}}$ ratio, $1.27 \pm 0.15‰$, is observed during the ice-cover period, and the lightest ratio, $0.73 \pm 0.10‰$, occurs during the snowmelt in June (Table 1). In June, the inlet has a lighter $\delta^{30}\mathrm{Si_{in}}$ of $0.02 \pm 0.10‰$, whereas in August the inlet isotopic ratio $0.78 \pm 0.15‰$ has similar values as the lake. The $\delta^{30}\mathrm{Si_{out}}$ of the outlet in June is slightly heavier ($0.89 \pm 0.10‰$) compared to the lake $\delta^{30}\mathrm{Si_{lake}}$. In July the outlet $\delta^{30}\mathrm{Si_{out}}$ is lighter than the inlet one (Table 1). During the remainder of the year, the outlet $\delta^{30}\mathrm{Si_{out}}$ is closely similar to the lake and inlet $\delta^{30}\mathrm{Si_{lake}}$.

5.2 Groundwater discharge

Surface lake Rn concentrations range between $94\,\mathrm{Bq\,m^{-3}}$ to $136\,\mathrm{Bq\,m^{-3}}$ in August and from $96\,\mathrm{Bq\,m^{-3}}$ to $126\,\mathrm{Bq\,m^{-3}}$ in September. Dissolved Ra in lake waters is assumed to be similar to those found in other lakes in the region ($1.4 \pm 0.6\,\mathrm{Bq\,m^{-3}}$). However, the measured Rn inputs (the stream inlets) due to Ra decay were below 0.5%, compared to the net excess of Rn delivered by groundwater discharge. Thus, the inlet Rn flux was neglected in the total Rn balance.

There was no significant vertical stratification of Rn concentration with Rn concentrations in deep waters (105 ± 26 and $79 \pm 24\,\mathrm{Bq\,m^{-3}}$) in August and September, respectively. Equation 1 was solved analytically to obtain the amount of groundwater discharging into the lake ($\mathrm{Q_{gw}}$) in August and September 2019. Uncertainties of individual terms were included in the estimation of the associated uncertainty (NORM, 1995; Taylor and Kuyatt, 1994).

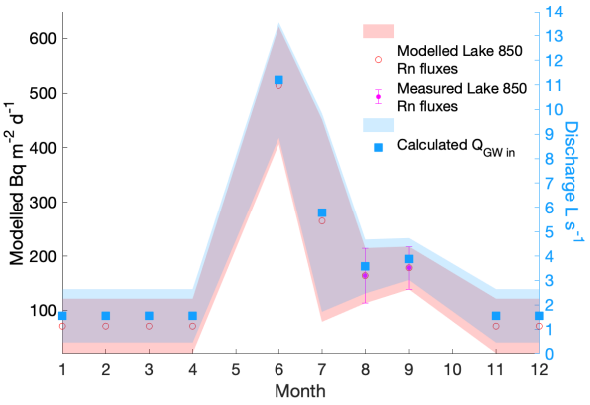


Figure 2. The modelled groundwater radon flux of Lake 850 (red circles) based on Rn fluxes in 10 other lakes in Abisko (*Olid et al., unpublished data*), the measured Rn fluxes in August and September (magenta filled points), and the calculated groundwater discharge in $\mathrm{l\,s^{-1}}$ throughout the year (blue squares). Uncertainties are shown as error bars and with shading.

Using the mean wind-speed for 48 h period prior sampling (3.1 ± 1.2 and $5.0 \pm 1.8\,\mathrm{m\,s^{-1}}$ in August and September, respectively) resulted in $\mathrm{k_{Rn}}$ estimates of 1.1 ± 0.2 and $1.2 \pm 0.4\,\mathrm{m\,s^{-1}}$. Uncertainties include the variation of wind speed and uncertainties associated with the empirical equation to estimate $\mathrm{k_{Rn}}$. Using the Rn concentration in lake waters, total losses of Rn to the atmosphere are 123 ± 32 and $138 \pm 32\,\mathrm{Bq\,m^{-2}\,d^{-1}}$ in August and September, respectively. Radon losses due to decay were 125 ± 22 and $123 \pm 15\,\mathrm{Bq\,m^{-2}\,d^{-1}}$, respectively, where uncertainties are obtained from the analytical uncertainties for Rn concentrations in lake waters. Losses of Rn through the outlet stream were 7 ± 4 and $9 \pm 4\,\mathrm{Bq\,m^{-2}\,d^{-1}}$. Among all Rn losses, atmospheric evasion (50%) and decay (47%) were the terms that have the largest contribution to the Rn mass balance. Radon losses through the outlet stream are almost negligible (3%).

Diffusive Rn flux from underlying sediments ($\mathrm{F_{diff}}$) obtained from diffusion experiments in the lab is $89 \pm 17\,\mathrm{Bq\,m^{-2}\,d^{-1}}$, and it is one of the main sources of Rn into the system. Fluxes of Rn from the sediment compensate for up to 57% of total Rn losses. Uncertainties associated with this flux are from analytical uncertainties in the slope for the regression analyses of the increase in Rn concentration through time in the sediment diffusion experiment. Due to the low concentrations of Ra in lakes from the same area ($1.4 \pm 0.6\,\mathrm{Bq\,m^{-3}}$, *C. Olid, unpublished data*), Rn inputs due to Ra decay were considered negligible in the Rn mass balance.

Rn inputs from groundwater are required to balance the Rn losses from the lake. The Rn flux into the lake through groundwater discharge is calculated to be

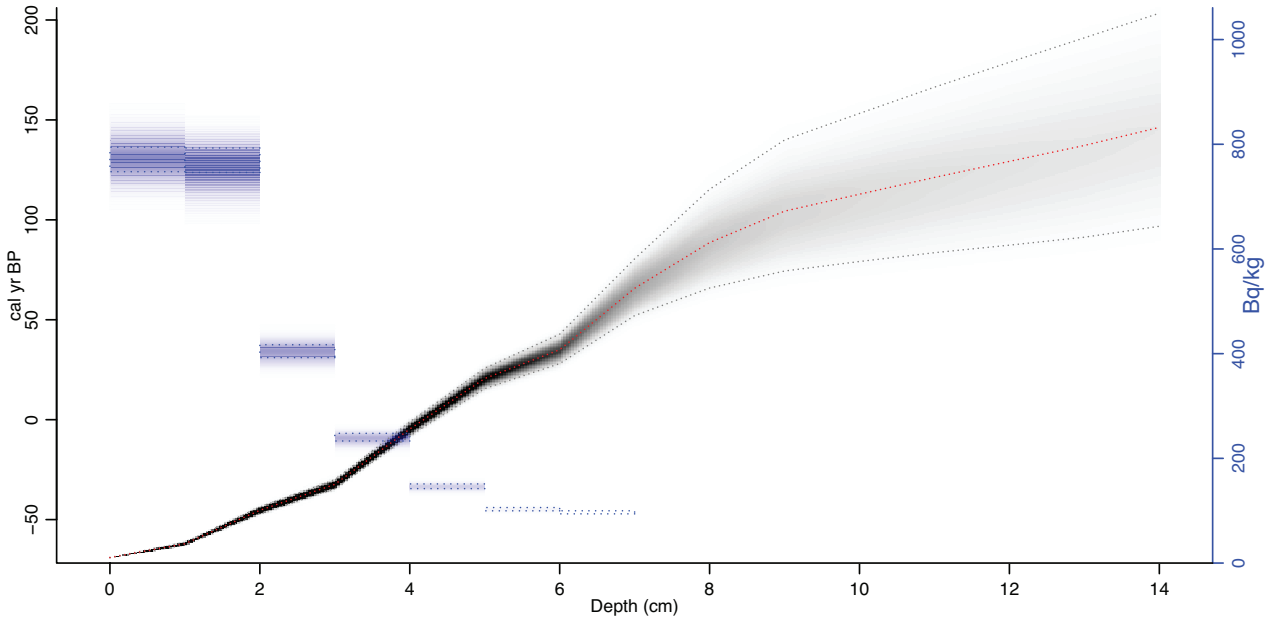


Figure 3. Age-depth model of gravity core plotted in R using package Plum (Aquino-López et al., 2018) and modified. Red line is the median probability age from all age-depth iterations. Grey shading represents age model probability and contains 95% confidence interval (dashed lines). The blue rectangles are the unsupported ^{210}Pb concentration in $\mathrm{Bq\,kg^{-1}}$ on secondary y-axis.

$166 \pm 43\,\mathrm{Bq\,m^{-2}\,d^{-1}}$ and $180 \pm 40\,\mathrm{Bq\,m^{-2}\,d^{-1}}$ in August and September, respectively. Considering the lake area of $20\,000\,\mathrm{m^2}$ and the Rn concentration in groundwater obtained from incubation experiments ($10626 \pm 1720\,\mathrm{Bq\,m^{-3}}$), groundwater fluxes are $3.56 \pm 1.25\,\mathrm{l\,s^{-1}}$ and $3.88 \pm 1.06\,\mathrm{l\,s^{-1}}$ for August and September, respectively. Note that this is a conservative estimate for groundwater fluxes, because we use the highest measured Rn concentration as the endmember.

Due to the lack of Rn measurements for the entire year, we estimated groundwater inputs for the months where no sampling was carried out using two scenarios: (i) constant groundwater inflow of $3.73 \pm 1.25\,\mathrm{l\,s^{-1}}$, calculated as the mean of the August and September data; and (ii) modelled groundwater inflow based on groundwater fluxes obtained from a lake survey in the Abisko region in 2018–2019 (*C. Olid, unpublished data*), which ranged from $1.55 \pm 1.09\,\mathrm{l\,s^{-1}}$ to $11.20 \pm 2.34\,\mathrm{l\,s^{-1}}$ (Figure 2). The annual Rn fluxes follow a pattern of a distinct peak in discharge in June and a gradual decrease towards July – October, reaching the base-flow level in November (Figure 2). The ratio between the groundwater Rn flux in September in Lake 850 and the groundwater Rn fluxes from the lake survey was used to model the missing groundwater Rn fluxes in Lake 850 (Figure 2, Appendix A1).

5.3 Age-depth model, lithology and mass accumulation rates

The age-depth model for the sediment core is shown in Figure 3. The mean sediment accumulation rate (SAR) was estimated to be $0.083 \pm 0.041\,\mathrm{cm\,yr^{-1}}$, which equals a sediment accumulation rate of $12 \pm 6\,\mathrm{yr\,cm^{-1}}$ and a mass accumulation rate (MAR) of $16.0 \pm 9.3\,\mathrm{mg\,cm^{-2}\,yr^{-1}}$. The presence of mosses in the sediment was observed during the core processing and also was described in the sediment lithology by Shemesh et al. (2001). Changes in the sediment content of aquatic or terrestrial mosses, was also supported by the C/N ratio (Figure 4), suggesting this is the cause of changes in MAR.

Lake 850 sediment is composed of carbonate-free clay gyttja with an mean TOC content of 11.4 wt%, mean TN of 1.1 wt%, and a resultant C/N ratio of 10.2 (Figure 4). Sediment porosity as high as 89.5% is found in the surface sediment, where sediment dry bulk density mean is $0.19 \pm 0.06\,\mathrm{g\,cm^{-3}}$. The BSi concentration along the sediment varies from 13.2 ± 0.28 wt% to 22.8 ± 0.24 wt%, with the highest BSi concentration in the surface of the core. The BSi concentrations reported here are lower than previous measurements. For example, BSi concentration in the surface sediment of Lake 850 was previously reported to be 40.3 wt% (Rosén et al., 2010), which is twice the value found here, demonstrating the high variability of BSi in the sediments.

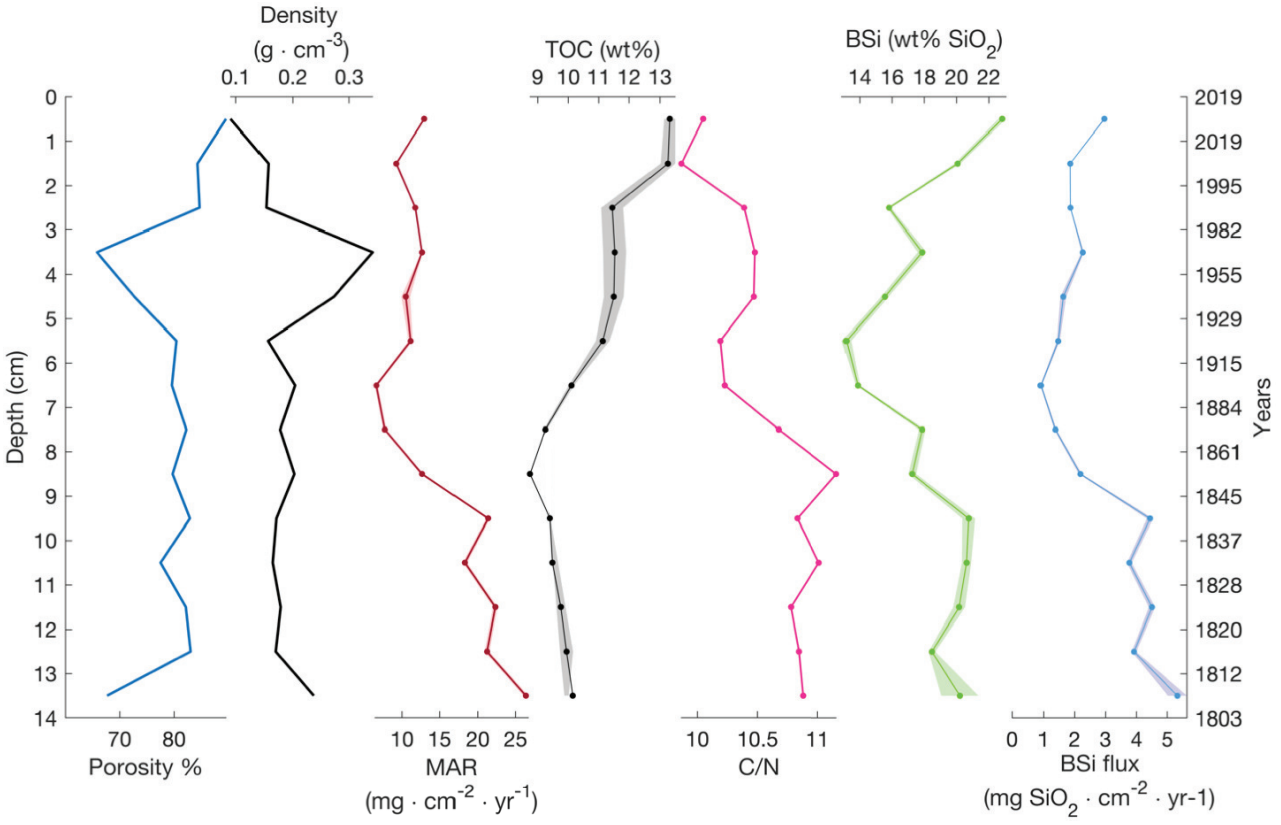


Figure 4. Gravity core sediment properties (porosity and dry bulk density), mass accumulation rate (MAR) and sediment density. Total organic carbon (TOC) and C/N showing changes in lake carbon content and sources. Biogenic silica (BSi) and BSi flux calculated from MAR and BSi concentrations. One standard deviation is shown by shading.

Using the mean MAR rate and the mean BSi wt% of 18.2 wt% we estimated the BSi accumulation rate (ϕ_{BSi}) to be $2.9 \pm 1.5\,\mathrm{mg\ SiO_2\ cm^{-2}\,yr^{-1}}$. BSi accumulation rates show stable values around $1.8\,\mathrm{mg\ SiO_2\ cm^{-2}\,yr^{-1}}$ in the upper $7\,\mathrm{cm}$ of the core, whereas an increase in BSi accumulation is observed towards the bottom $7\,\mathrm{cm}$ of the core (Figure 4) likely connected to the higher MAR. The mean diatom isotopic ratio ($\delta^{30}\mathrm{Si_{BSi}}$) measured on cleaned diatoms from the upper most $8\,\mathrm{cm}$ of sediment piston core from 1999 (Shemesh et al., 2001) is $0.07 \pm 0.43\,‰$ (n = 3).

6 Mass balance models

6.1 Water balance

Two water balance scenarios were considered where changes in the lake level were evaluated: (i) constant groundwater inflow over the annual cycle as an additional water source, and (ii) modelled groundwater discharges varying throughout an annual cycle (Figure 5 and A1). In both scenarios, lake-level increases during the ice-covered period (Figure 5, blue and green line) are a result of a potential groundwater inflow. This accumulated water is released through the outlet when the lake ice starts to melt in May-June, and the outlet discharge is thus high (Table 1). After this period, lake-level is stabilized and groundwater replenishes the lake original volume during short periods over the summer.

When groundwater discharge is assumed to be constant (Scenario i, $3.73 \pm 1.25\,\mathrm{l\,s^{-1}}$) based on our data from August and September, the lake shows annual lake-level changes up to $1.9\,\mathrm{m}$ (Figure 5 and A1, blue line). From July to December, the lake volume is restored by the groundwater inflow, and, on the annual time scale, the lake-level would increase around $2\,\mathrm{m}$ every year (Figure 5, blue line).

Using the modelled annual groundwater inflow (Scenario ii, Figure 2), limited lake-level changes were observed. The maximum lake-level decrease is $95\,\mathrm{cm}$ during summer (Figure 5 and A1, green line), but groundwater discharge restores lake-level during upcoming months. Taking into account the uncertainties, lake-level variation can be as great as $2.4\,\mathrm{m}$ or none (Figure 5 and A1, green shading). This scenario with the smallest lake-level changes is in agreement with previous results of oxygen isotopes mass balance (Shemesh et al.,

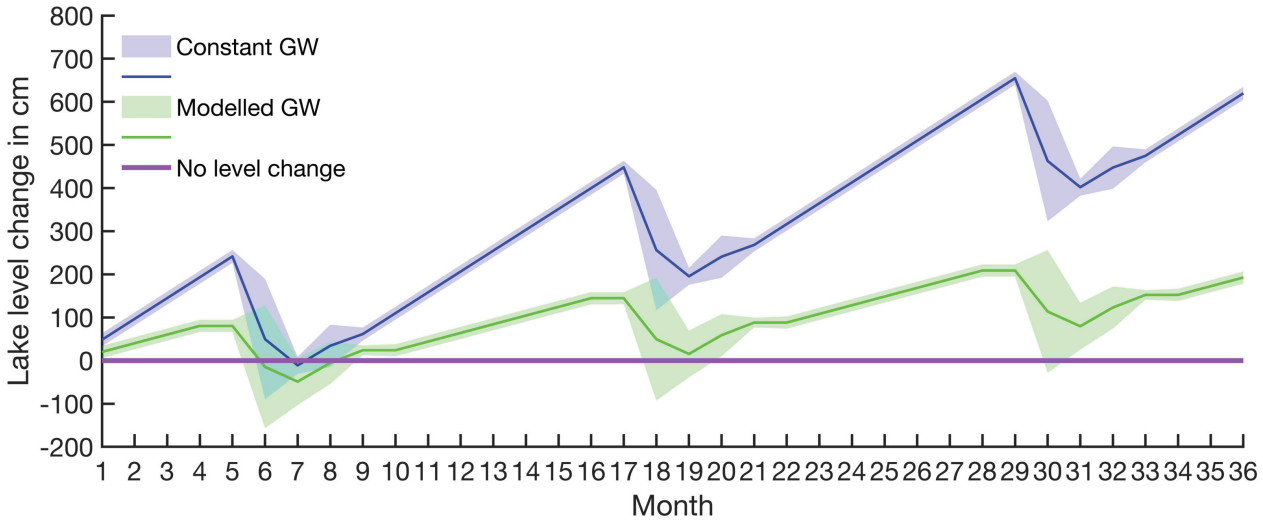


Figure 5. Long-term lake-level change calculated based on lake volume changes and water balance. The purple solid line indicates the lake-level starting point. The blue line with shading is the lake-level change with constant groundwater flow (scenario i), and the green line with shading is the lake-level change based on water balance with modelled groundwater discharges (scenario ii).

2001). Therefore, we used this water balance model further for the Si balances.

6.2 Silicon and Silicon isotope mass balance

BSi accumulation occurs in conditions when the total DSi influx is higher that the stream DSi outflux. Therefore, we construct a Si mass balance based on stream inlets and the outlet. The DSi influx through the inlet stream is not sufficient to maintain lake DSi concentration at steady-state in June (red and blue triangles, Figure 6A). In contrast, in July and August sufficient DSi enters the lake to supply the outlet DSi flux. The monthly inlet DSi flux is between 0.22 ± 0.11 to $0.62 \pm 0.31\,\mathrm{kg\ SiO_2\ day^{-1}}$, while the outlet DSi flux ranges from 0.19 ± 0.10 to $2.21 \pm 1.11\,\mathrm{kg\ SiO_2\ day^{-1}}$. However, diatom production is an additional sink of Si by creating a BSi flux into the sediment. The DSi influx is, thus, not sufficient to account for both the DSi outflux and the BSi flux into the sediment (Figure 6A). Therefore, an additional external source (i.e., groundwater discharge) must supply additional DSi to compensate for the mean BSi flux ($2.9\,\mathrm{mg\ SiO_2\ cm^{-2}\,yr^{-1}}$) into the sediment.

Groundwater discharges from scenario ii (Figure 2) were used to build a Si mass balance and a Si isotope mass balance. Here, we assume that the recent BSi flux into the sediment occurs only during the diatom growing season (from June until September) (Figure 6A; Shemesh et al., 2001). The missing DSi flux resulting from the mass balance was considered to originate from the groundwater flux, and thus, we use this flux to calculate back the groundwater DSi concentration and isotopic ratio.

During the diatom growing season, BSi flux into the sediment increases up to $1.76 \pm 0.87\,\mathrm{kg\ SiO_2\ day^{-1}}$ (magenta line, Figure 6A), which produces DSi deficiency in the lake. To balance this deficiency, groundwater discharge must supply between 1.62 ± 1.21 and $3.39 \pm 1.77\,\mathrm{kg\ SiO_2\ day^{-1}}$ during the diatom growing season (cyan line, Figure 6A). Considering the modelled groundwater discharges derived from Rn mass balance, the DSi concentration in the groundwater is estimated to range from $3.50 \pm 1.68\,\mathrm{mg\,SiO_2\,l^{-1}}$ to $5.85 \pm 2.99\,\mathrm{mg\,SiO_2\,l^{-1}}$ from diatom growth (cyan line, Figure 6B). During the ice-covered period, the diatom growth ans thus BSi flux into the sediment is considered to be negligible, while groundwater is still flowing into the lake. The winter groundwater concentration is calculated from the difference in the lake concentration from September ($1.02 \pm 0.91\,\mathrm{mg\,SiO_2\,l^{-1}}$) to March ($2.51 \pm 0.35\,\mathrm{mg\,SiO_2\,l^{-1}}$) (Appendix A2). Therefore, the groundwater discharging into the lake from late-October until mid-June is the only water inflow with a DSi concentration of $6.95 \pm 4.90\,\mathrm{mg\,SiO_2\,l^{-1}}$.

The Si isotopes mass balance using the open fractionation model (Varela et al., 2004) shows that the higher demand of DSi in the productive months (Figure 6A, B) needs to have a lighter isotopic composition in order to produce the $\delta^{30}\mathrm{Si_{BSi}}$ of $0.07 \pm 0.43‰$ measured on diatoms preserved in the sediment. The isotopically lighter source is assumed to be groundwater discharge, with calculated ranges from $-0.55 \pm 0.55‰$ in July to $0.23 \pm 0.58‰$ in September (Figure 6C). Using the modelled groundwater δ^{30}Si, the expected $\delta^{30}\mathrm{Si_{BSi}}$ in all productive months varies from $-0.49 \pm 0.49‰$ to $-0.01 \pm 0.56‰$ (not shown), values that are in agreement with the sediment BSi of $\delta^{30}\mathrm{Si_{BSi}} = 0.07 \pm 0.43‰$.

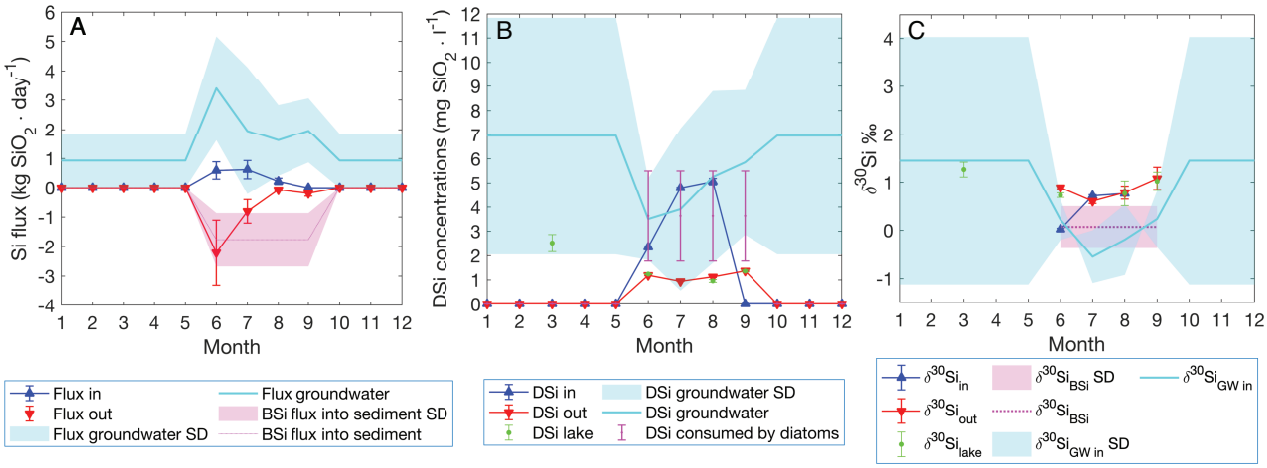


Figure 6. Si and Si isotope mass balance model of Lake 850 throughout the year. (A) Mass balance showing the stream DSi influx (blue triangles), the lake outlet DSi outflux as negative flux (red triangles), the diatom BSi flux based on a diatom bloom season lasting 4 months (magenta dotted line), also as a negative flux. The calculated groundwater DSi flux is shown as a positive flux (cyan line). (B) The monthly changes in the DSi concentration of the inlet (blue triangles), outlet (red triangles), lake (green circles), diatom DSi uptake (magenta circles), and groundwater (cyan line). (C) The stable Si mass balance showing monthly variation of the isotopic composition of all DSi sources and sinks. Shading and error bars represent uncertainties.

The production consumes 63% of the initial DSi in June, 77% in July and September, and 79% in August. During the ice-covered period from late-October until mid-June, the groundwater base flow is considered to be constant, calculated from the difference of the lake isotopic ratios from September until March (Appendix A3), and thus the $\delta^{30}\mathrm{Si}_{\mathrm{gw}} = 1.45 \pm 2.58‰$ (Figure 6C).

7 Discussion

Lake 850 is unusual in terms of both the DSi and BSi concentration in water and sediment, respectively. The maximum DSi concentration of 2.51 mg SiO_2 l^{-1} in March is among the top 10% of lakes in Northern Sweden (Bigler and Hall, 2002). The mean BSi content in the lake sediment of 40 wt% (Rosén et al., 2010) places Lake 850 in the upper 6% of lake sediments studied worldwide (Frings et al., 2014). Although several factors, including the morphology of the watershed (Jenny, 1941; Rubensdotter and Rosqvist, 2003), diatom production and low detrital input (Conger, 1942), vegetation (Struyf et al., 2010), and preservation potential (Ryves et al., 2003) are known to affect sedimentation regimes and BSi accumulation resulting in a diatom-rich sediment, we show here that groundwater input is an important factor leading to the high BSi accumulation in Lake 850.

The combined results from the water, Rn, and Si mass balances indicated the importance of an external source of DSi through groundwater discharge. Groundwater inflow was the primary water and DSi supply to the lake, with a contribution about 3 times higher than the stream inlets (Figure 6A). The Si and Si isotope mass balance models showed that groundwater DSi concentration and isotopic composition varied during the ice-free period, compared to the ice-covered period, when they were stable (Figure 6B, C).

The significance of groundwater-sourced DSi to the lake's Si cycle is also evidenced by the relatively lighter stable Si isotope ratio of diatoms from sediment, which suggests that groundwater is the primary DSi source for diatoms. Stream inputs could also be a source of DSi for diatoms, especially in early spring, when snowmelt can deliver isotopically lighter DSi by displacement of shallow groundwater into the stream inlet (Campbell et al., 1995). However, spring snowmelt water and groundwater in June are likely to have the same isotopic composition (Figure 6C) because the same factors, e.g., short residence time in the watershed are present in both types of water. Thus, only by using mass balance is the quantification of each DSi source apparent, providing evidence that groundwater supplies almost 4 times more DSi compared to streamflow in June. Our results suggest that the groundwater supply plays a crucial role in providing DSi for the production of diatoms and accumulation of BSi in Lake 850.

7.1 The role of groundwater in the water balance

The water balance coupled with the Rn mass balance indicated that groundwater discharge is an essential water source for the lake. Both models of groundwater inflow (constant and varying groundwater inputs) demonstrated changes in lake volume as a result of high-water discharge at the outlet of the lake during spring snowmelt. More pronounced

changes in lake volume were observed in scenario i, where constant groundwater inflow was assumed (Figure 5, blue line). However, because the oxygen isotope data showed negligible evaporation and precipitation effect on lake volume change (Shemesh et al., 2001), this model is not considered to be the most realistic. Scenario ii, which considered a variable groundwater flow (Figure 5, green line) seems to be more realistic. The modelled groundwater hydrograph (Figure 2) is comparable with the hydrograph of the neighbouring river Miellejokha (Figure S1) and resembles the hydrographs of groundwater discharge in studies of high-altitude lakes from other regions (Clow et al., 2003; Hood et al., 2006; Huth et al., 2004; Liu et al., 2004). The results from this model show that groundwater discharge is up to 5 times higher values than the lake water outflow through the outlet. Similarly, groundwater discharge brings from 3 to 24% of the lake volume depending on the month.

7.2 The role of groundwater in Si concentration mass balance and Si isotope mass balance

The lake Si mass balance (Figure 6A) shows that modelled groundwater concentration and flux of BSi vary through the year, which is similar to observations from Crystal Lake in Wisconsin (Hurley et al., 1985). Seasonal variations in groundwater DSi concentration related to discharges were also observed in Canadian rivers with groundwater inputs (Maavara et al., 2018). Moreover, the calculated BSi flux into the sediment is comparable (or higher) with BSi fluxes observed in some of the North American Great Lakes (Conley, 1988; Newberry and Schelske, 1986; Schelske, 1985) and lakes with diatomaceous sediment in the Arctic (McKay et al., 2008; Kaplan et al., 2002; Tallberg et al., 2015).

The model of stable Si isotopes shows little variation during the ice-covered period, as no diatom production is expected. The modelled $\delta^{30}\mathrm{Si}$ of groundwater for the ice-covered period (Figure 6C) falls into the range of measured groundwater isotopic composition worldwide, which ranges from -1.5 to $2‰$ (Frings et al., 2016). However, the modelled groundwater ratio $\delta^{30}\mathrm{Si_{gw}}$ is heavier than found in other groundwater studies (Georg et al., 2009; Opfergelt et al., 2011; Ziegler et al., 2005), which may reflect lower dissolution of primary minerals, longer groundwater residence time, and possibly some clay mineral formation in the groundwater pathway (Frings et al., 2016; Pokrovsky et al., 2013) during the ice-covered period. Further, no diatom production, and thus no associated Si isotope fractionation, is expected in winter. Therefore, the $\delta^{30}\mathrm{Si_{lake}}$ is influenced by the input of $\delta^{30}\mathrm{Si_{gw}}$ only and not by diatom production. The $\delta^{30}\mathrm{Si_{lake}}$ measured in March is slightly lighter than all modelled $\delta^{30}\mathrm{Si_{gw}}$ for the ice-covered period, which can be explained by diatom dissolution in the uppermost sediment layers. However, if the uncertainties of the modelled groundwater isotopic composition are taken into account, the lake ratio is within the same range as the groundwater ratio. Therefore, no additional processes must be present during the ice-covered period, and the groundwater isotopic ratio is reflected in the lake isotopic signal. With snowmelt, the decrease of the modelled $\delta^{30}\mathrm{Si_{gw}}$ reflects the increase in weathering of primary minerals and decrease in the groundwater residence time due to higher discharges, as also observed in Arctic rivers (Pokrovsky et al., 2013).

The greatest variation in the isotopic ratio of groundwater occurs in August, when the modelled groundwater isotopic composition is fully dependent on the changes in BSi flux into the sediment. As the yearly BSi accumulation occurs during the diatom growing season which is only 4 month, the modelled groundwater must bring additional DSi to supply diatom production. Hence, the isotopic model calculating the groundwater isotopic composition shows $\delta^{30}\mathrm{Si_{gw}}$ comparable with values for groundwater reported in the small number of other studies (Frings et al., 2016; Opfergelt et al., 2011). Further, the calculated $\delta^{30}\mathrm{Si_{BSi}}$ based on the initial mixture of the modelled groundwater and stream inlet ratio gives results within the range of the measured $\delta^{30}\mathrm{Si_{BSi}}$.

7.3 Model uncertainties

The largest sources of uncertainty in the water and silicon balance models (Figure 5, SA1 and 6) are the discharge uncertainties of the inlet and outlet and the winter groundwater discharges. The spring snowmelt is dynamically changing the inlet and outlet discharges, as has been observed on rivers in the area, such as Miellejohka (Figure S1). With only a single sample every month, there is no information on variation of the stream on a finer temporal scale. Thus, monthly stream flow and the modelled groundwater discharges might be over- or underestimated. Further, the uncertainties in isotopic model and the isotopic composition of the groundwater were propagated from the mass balance model and from the stable isotopic measurements, especially in the outlet water in August.

The water balance based on modelled groundwater inflow suggests that lake-level changes throughout the year are within a range of $0.95\,\mathrm{m}$ (Figure 5, green line), and, thus, lake area and mean depth also vary throughout the year. Therefore, the underlying assumptions of constant depth and area are likely overestimating lake-level change. For a more precise model of lake-level, lake volume variations and a detailed bathymetry of Lake 850 is needed. However, the importance of the groundwater contribution to Lake 850 supports the evidence that groundwater should be considered as an important water and DSi source for high-altitude and high-latitude lakes, with support of data on groundwater DSi in Lake O'Hara (Hood et al., 2006), Lake Myvatn (Opfergelt et al., 2011) and Crystal Lake (Hurley et al., 1985; Kenoyer and Anderson, 1989).

Another source of uncertainties in the Si and Si isotope mass balance models originates from the uncertainties on the age-depth model. The uncertainties on MAR, which are cal-

culated from the SAR and the densities are as high as 50%. It is likely due to changes in the sediment composition and increased content of mosses. Therefore, the BSi flux to the sediment carries similar or higher uncertainty. As a result of those uncertainties, the modelled groundwater concentrations and isotopic composition are ranging greatly.

Additionally, the diatom preservation efficiency, which is globally around 3% in the oceans (Treguer et al., 1995), and, in deep lakes around $1-2\%$ (Ryves et al., 2003) of the total diatom production, suggests that $97-99\%$ of diatom BSi is redissolved in the water column in those environments. However, no estimates of sediment preservation efficiency are available for small, cold lakes such as Lake 850. Therefore, the mass balance can be slightly underestimated, in case that the BSi flux into the sediment, which was calculated from the sediment record represents only a fraction of the total production. To eliminate this source of uncertainty annual monitoring of diatom production and accumulation would be needed.

Uncertainty also results from the variability among sediment cores in their BSi content. BSi concentrations in the sediment vary from 13 to 40 wt% in different cores (this study; Rosén et al., 2010). We have tested the combination of the MAR ($16.0\,\mathrm{mg\,cm^{-2}\,yr^{-1}}$) reported from this study with the highest BSi of 40.3 wt% from a companion core from Lake 850 (Rosén et al., 2010) to evaluate the impact of BSi flux on the groundwater concentrations. The yearly BSi flux would increase 2.2 times, which would result in 1.6 to 2.3 times higher groundwater DSi concentration to support the BSi flux and keep the Lake 850 at steady-state. However, the BSi content is variable within the sedimentary basin, and thus the sedimentation rate is a crucial factor for the estimate of BSi accumulation. For future model improvement a monitoring of all inlets, groundwater, pore water, and the outlet together with sediment traps to constrain the production, BSi flux and dissolution would be needed.

8 Conclusions

The diatom-rich sediment in Lake 850 is formed because of high DSi supply by groundwater during the diatom growing season coupled with low sedimentation rates, which fosters a high accumulation of diatoms in the form of BSi. Water and Si mass balance demonstrated the importance of groundwater as a source of water and DSi, with fluxes that are 3 times greater than stream input. Groundwater supplies lighter δ^{30}Si, which is reflected in the lighter diatom δ^{30}Si ratio. By quantifying the groundwater inputs, the Si and Si isotopic mass balances allowed for the estimate of the stable Si isotope ratios of groundwater throughout the year. The modelled isotopic ratio of groundwater falls into the same range as the world groundwater δ^{30}Si ratio (Frings et al., 2016; Sutton et al., 2018).

The results from our study can be applied more broadly to other lakes to evaluate factors governing the accumulation of diatom-rich sediment. BSi rich sediments are likely to be found in lakes situated on silica-rich bedrock, such as in Lake Challa, Tanzania/Kenya (Barker et al., 2013) or as shown here in lakes with sufficient DSi inputs from groundwater source that supply DSi during the diatom growing season to alleviate potential DSi limitation of diatom growth. In addition, lakes with high autochthonous carbon production and deposition combined with very low mean sedimentation rates generally found in Arctic lake sediments (Wolfe et al., 2004), as well as lakes with low-relief watershed morphology and with low stream input that yield low quantities of fine-grain clastic input, are potential systems for high BSi accumulation (Conger, 1942). These water bodies with high BSi accumulation act as important sinks of Si in the global Si cycle. Our results support the importance of groundwater in the lake silicon budget and suggest that this process should not be overlooked in future investigations on BSi in lakes and global estimates of the terrestrial lake BSi sink.

Data availability. All data, if not directly available in tables and appendices, will be available in the PANGAEA database. In the meantime data is available upon request to the authors.

Author contributions. PZ and DJC designed the research. PZ and CO carried out the fieldwork. CO performed radon measurements and radon mass balance. PZ performed the TOC, TN, BSi, DSi, stable Si isotopes analyses and performed the data processing. All authors contributed to discussion and data interpretation. PZ and CO wrote the paper with contributions and comments provided by JS, SCF, SO and DJC.

Competing interests. No competing interests are present.

Disclaimer. The authors declare that they have no conflict of interest.

Acknowledgements. This work was supported by The Royal Physiographic Society in Lund and by the Center for Geosphere Dynamics (UNCE/SCI/006) to PZ, the Swedish Research Council to DJC, and NSF EAR-1514814 to SCF. Part of this work was supported by a FORMAS (d.nr. 2018-01217) grant attributed to CO. We also thank to Aldo Shemesh for providing diatom samples, Christian Bigler, Reiner Gielser and Carl-Magnus Morth for advice and help with fieldwork design. Further we thank the organizations and the individuals who helped with the fieldwork and provided us with equipment and advice: Thomas Westin, Keith W. Larson, Erik Lundin, Svante Zachrisson, CIRC and field assistants Albin Bjärhall, Mathilde Schnuriger, Lukas Guth, Rosine Cartier, Geert Hensgens and Jan Foniok. We acknowledge Hans Schöberg and Melanie Kielman for assistance during sample preparation and

isotope data acquisition. This is Vegacenter contribution number # XXX (number will be provided upon acceptance).

References

ANS, A. S. R. S.: Meteorological data from Abisko Observatory, daily mean 1913-01-01–2019-01-01, 2020a.

ANS, A. S. R. S.: Water discharge data from Miellejohka 685 m a.s.l., 2020b.

Aquino-López, M. A., Blaauw, M., Christen, J. A., and Sanderson, N. K.: Bayesian Analysis of ^{210}Pb Dating, Journal of Agricultural, Biological and Environmental Statistics, 23, 317–333, https://doi.org/https://doi.org/10.1007/s13253-018-0328-7, 2018.

Barker, P. A., Hurrell, E. R., Leng, M. J., Plessen, B., Wolff, C., Conley, D. J., Keppens, E., Milne, I., Cumming, B. F., Laird, K. R., et al.: Carbon cycling within an East African lake revealed by the carbon isotope composition of diatom silica: a 25-ka record from Lake Challa, Mt. Kilimanjaro, Quaternary Science Reviews, 66, 55–63, https://doi.org/https://doi.org/10.1016/j.quascirev.2012.07.016, http://www.sciencedirect.com/science/article/pii/S0277379112002831, international Association of Limnogeology – Isotopes and Lakes, 2013.

Battarbee, R. W., Jones, V. J., Flower, R. J., Cameron, N. G., Bennion, H., Carvalho, L., and Juggins, S.: Diatoms, in: Tracking environmental change using lake sediments, edited by Smol, J. P., Birks, H. J. B., Last, W. M., Bradley, R. S., and Alverson, K., pp. 155–202, Springer, https://doi.org/10.1007/0-306-47668-1_8, 2002.

Bigler, C. and Hall, R. I.: Diatoms as indicators of climatic and limnological change in Swedish Lapland: a 100-lake calibration set and its validation for paleoecological reconstructions, Journal of Paleolimnology, 27, 97–115, https://doi.org/10.1023/A:1013562325326, https://doi.org/10.1023/A:1013562325326, 2002.

Brodie, C. R., Casford, J. S., Lloyd, J. M., Leng, M. J., Heaton, T. H., Kendrick, C. P., and Yongqiang, Z.: Evidence for bias in C/N, δ^{13}C and δ^{15}N values of bulk organic matter, and on environmental interpretation, from a lake sedimentary sequence by pre-analysis acid treatment methods, Quaternary Science Reviews, 30, 3076–3087, https://doi.org/10.1016/j.quascirev.2011.07.003, 2011.

Burnett, W. C. and Dulaiova, H.: Estimating the dynamics of groundwater input into the coastal zone via continuous radon-222 measurements, Journal of environmental radioactivity, 69, 21–35, https://doi.org/10.1016/s0265-931x(03)00084-5, 2003.

Campbell, D. H., Clow, D. W., Ingersoll, G. P., Mast, M. A., Spahr, N. E., and Turk, J. T.: Processes controlling the chemistry of two snowmelt-dominated streams in the Rocky Mountains, Water Resources Research, 31, 2811–2821, https://doi.org/10.1029/95wr02037, 1995.

Chanyotha, S., Kranrod, C., and Burnett, W. C.: Assessing diffusive fluxes and pore water radon activities via a single automated experiment, Journal of radioanalytical and nuclear chemistry, 301, 581–588, https://doi.org/10.1007/s10967-014-3157-3, 2014.

Clarke, J.: The occurrence and significance of biogenic opal in the regolith, Earth-Science Reviews, 60, 175–194, https://doi.org/10.1016/s0012-8252(02)00092-2, 2003.

Clow, D., Schrott, L., Webb, R., Campbell, D., Torizzo, A., and Dornblaser, M.: Ground water occurrence and contributions to streamflow in an alpine catchment, Colorado Front Range, Groundwater, 41, 937–950, https://doi.org/10.1111/j.1745-6584.2003.tb02436.x, 2003.

Conger, P. S.: Accumulation of diatomaceous deposits, Journal of Sedimentary Research, 12, 55–66, https://doi.org/10.1306/d4269143-2b26-11d7-8648000102c1865d, 1942.

Conley, D. J.: Biogenic silica as an estimate of siliceous microfossil abundance in Great Lakes sediments, Biogeochemistry, 6, 161–179, https://doi.org/10.1007/bf02182994, 1988.

Conley, D. J.: An interlaboratory comparison for the measurement of biogenic silica in sediments, Marine chemistry, 63, 39–48, https://doi.org/10.1016/s0304-4203(98)00049-8, 1998.

Conley, J. D. and Schelske, C.: Biogenic Silica, vol. 1, pp. 281–293, Springer Netherlands, Dordrecht, https://doi.org/10.1007/0-306-47668-1_14, 2001.

De La Rocha, C. L., Brzezinski, M. A., and Deniro, M. J.: Fractionation of silicon isotopes by marine diatoms during biogenic silica formation, Geochimica et Cosmochimica Acta, 61, 5051–5056, https://doi.org/10.1016/s0016-7037(97)00300-1, 1997.

Dimova, N. T. and Burnett, W. C.: Evaluation of groundwater discharge into small lakes based on the temporal distribution of radon-222, Limnology and Oceanography, 56, 486–494, https://doi.org/10.4319/lo.2011.56.2.0486, 2011.

Dimova, N. T., Burnett, W. C., Chanton, J. P., and Corbett, J. E.: Application of radon-222 to investigate groundwater discharge into small shallow lakes, Journal of Hydrology, 486, 112–122, https://doi.org/10.1016/j.jhydrol.2013.01.043, 2013.

Fortin, M.-C. and Gajewski, K.: Assessing the use of sediment organic, carbonate and biogenic silica content as indicators of environmental conditions in Arctic lakes, Polar biology, 32, 985–998, https://doi.org/10.1007/s00300-009-0598-1, 2009.

Frings, P. J., Clymans, W., Jeppesen, E., Lauridsen, T. L., Struyf, E., and Conley, D. J.: Lack of steady-state in the global biogeochemical Si cycle: emerging evidence from lake Si sequestration, Biogeochemistry, 117, 255–277, https://doi.org/10.1007/s10533-013-9944-z, https://doi.org/10.1007/s10533-013-9944-z, 2014.

Frings, P. J., Claymans, W., Fontorbe, G., Rocha, C. L. D. L., and Conley, D. J.: The continental Si cycle and its impact on the ocean Si isotope budget, Chemical Geology, 425, 12–36, https://doi.org/10.1016/j.chemgeo.2016.01.020, 2016.

Georg, R., Reynolds, B., Frank, M., and Halliday, A.: New sample preparation techniques for the determination of Si isotopic compositions using MC-ICPMS, Chemical Geology, 235, 95 – 104, https://doi.org/http://dx.doi.org/10.1016/j.chemgeo.2006.06.006, http://www.sciencedirect.com/science/article/pii/S000925410600307X, 2006.

Georg, R., West, A., Basu, A., and Halliday, A.: Silicon fluxes and isotope composition of direct groundwater discharge into the Bay of Bengal and the effect on the global ocean silicon isotope budget, Earth and Planetary Science Letters, 283, 67–74, https://doi.org/10.1016/j.epsl.2009.03.041, 2009.

Hood, J. L., Roy, J. W., and Hayashi, M.: Importance of groundwater in the water balance of an alpine headwater lake, Geophysical Research Letters, 33, https://doi.org/10.1029/2006gl026611, 2006.

Hurley, J. P., Armstrong, D. E., Kenoyer, G. J., and Bowser, C. J.: Ground water as a silica source for diatom production in a precipitation-dominated lake, Science, 227, 1576–1578, https://doi.org/10.1126/science.227.4694.1576, 1985.

Huth, A., Leydecker, A., Sickman, J., and Bales, R.: A two-component hydrograph separation for three high-elevation catchments in the Sierra Nevada, California, Hydrological Processes, 18, 1721–1733, https://doi.org/10.1002/hyp.1414, 2004.

Jenny, H.: Factors of Soil Formation: A System of quantitative Pedology, New York: McGraw-Hill., 1941.

Johnson, T. C., Brown, E. T., and Shi, J.: Biogenic silica deposition in Lake Malawi, East Africa over the past 150,000 years, Palaeogeography, Palaeoclimatology, Palaeoecology, 303, 103–109, https://doi.org/10.1016/j.palaeo.2010.01.024, 2011.

Kahle, D. and Wickham, H.: ggmap: Spatial Visualization with ggplot2, The R Journal, 5, 144–161, https://doi.org/10.32614/rj-2013-014, https://journal.r-project.org/archive/2013-1/kahle-wickham.pdf, 2013.

Kaplan, M. R., Wolfe, A. P., and Miller, G. H.: Holocene environmental variability in southern Greenland inferred from lake sediments, Quaternary Research, 58, 149–159, https://doi.org/10.1006/qres.2002.2352, 2002.

Kenoyer, G. J. and Anderson, M. P.: Groundwater's dynamic role in regulating acidity and chemistry in a precipitation-dominated lake, Journal of Hydrology, 109, 287–306, 1989.

Leng, M. J., Swann, G. E., Hodson, M. J., Tyler, J. J., Patwardhan, S. V., and Sloane, H. J.: The potential use of silicon isotope composition of biogenic silica as a proxy for environmental change, Silicon, 1, 65–77, https://doi.org/10.1007/s12633-009-9014-2, 2009.

Liu, F., Williams, M. W., and Caine, N.: Source waters and flow paths in an alpine catchment, Colorado Front Range, United States, Water Resources Research, 40, https://doi.org/10.1029/2004wr003076, 2004.

Maavara, T., Slowinski, S., Rezanezhad, F., Van Meter, K., and Van Cappellen, P.: The role of groundwater discharge fluxes on Si: P ratios in a major tributary to Lake Erie, Science of the Total Environment, 622, 814–824, https://doi.org/10.1016/j.scitotenv.2017.12.024, 2018.

MacIntyre, S., Wanninkhof, R., and Chanton, J.: Trace gas exchange across the air-water interface in freshwater and coastal marine environments, pp. 52–97, Blackwell Science Ltd, 1995.

McKay, N. P., Kaufman, D. S., and Michelutti, N.: Biogenic silica concentration as a high-resolution, quantitative temperature proxy at Hallet Lake, south-central Alaska, Geophysical Research Letters, 35, https://doi.org/10.1029/2007gl032876, 2008.

Newberry, T. L. and Schelske, C. L.: Biogenic silica record in the sediments of Little Round Lake, Ontario, Hydrobiologia, 143, 293–300, https://doi.org/10.1007/978-94-009-4047-5_37, 1986.

NORM, I.: Guide to expression of uncertainty in measurement. Corrected and Reprinted, International Organization for Standardization, Geneva, Switzerland, 1995.

Opfergelt, S. and Delmelle, P.: Silicon isotopes and continental weathering processes: Assessing controls on Si transfer to the ocen, Comptes Rendus Geoscience, 344, 723–738, https://doi.org/10.1016/j.crte.2012.09.006, 2012.

Opfergelt, S., Eiriksdottir, E. S., Burton, K. W., Einarsson, A., Siebert, C., Gislason, S. R., and Halliday, A. N.: Quantifying the impact of freshwater diatom productivity on silicon isotopes and silicon fl uxes: Lake Myvatn, Iceland, Earth and Planetary Science Letters, 305, 73–82, https://doi.org/10.1016/j.epsl.2011.02.043, http://dx.doi.org/10.1016/j.epsl.2011.02.043, 2011.

Pienitz, R., Doran, P., and Lamoureux, S.: Origin and geomorphology of lakes in the polar regions, Oxford University Press, https://doi.org/10.1093/acprof:oso/9780199213887.003.0002, https://oxford.universitypressscholarship.com/view/10.1093/acprof:oso/9780199213887.001.0001/acprof-9780199213887-chapter-2, 2008.

Plunkett, G. M., Whitehouse, N. J., Hall, V. A., Brown, D. M., and Baillie, M. G. L.: A precisely-dated lake-level rise marked by diatomite formation in northeastern Ireland, Journal of Quaternary Science, 19, 3–7, https://doi.org/10.1002/jqs.816, https://onlinelibrary.wiley.com/doi/abs/10.1002/jqs.816, 2004.

Pokrovsky, O., Reynolds, B., Prokushkin, A., Schott, J., and Viers, J.: Silicon isotope variations in Central Siberian rivers during basalt weathering in permafrost-dominated larch forests, Chemical Geology, 355, 103–116, https://doi.org/10.1016/j.chemgeo.2013.07.016, 2013.

Reynolds, B. C., Aggarwal, J., Andre, L., Baxter, D., Beucher, C., Brzezinski, M. A., Engstrom, E., Georg, R. B., Land, M., Leng, M. J., Opfergelt, S., Rodushkin, I., Sloane, H. J., van den Boorn, S. H. J. M., Vroon, P. Z., and Cardinal, D.: An inter-laboratory comparison of Si isotope reference materials, Journal of Analytical Atomic Spectrometry, 22, 561–568, https://doi.org/10.1039/b616755a, http://dx.doi.org/10.1039/B616755A, 2007.

Rosén, P., Vogel, H., Cunningham, L., Reuss, N., Conley, D. J., and Persson, P.: Fourier transform infrared spectroscopy, a new method for rapid determination of total organic and inorganic carbon and biogenic silica concentration in lake sediments, Journal of Paleolimnology, 43, 247–259, https://doi.org/10.1007/s10933-009-9329-4, 2010.

Rubensdotter, L. and Rosqvist, G.: The effect of geomorphological setting on Holocene lake sediment variability, northern Swedish Lapland, Journal of Quaternary Science, 18, 757–767, https://doi.org/10.1002/jqs.800, 2003.

Russell, J. M. and Johnson, T. C.: A high-resolution geochemical record from Lake Edward, Uganda Congo and the timing and causes of tropical African drought during the late Holocene, Quaternary Science Reviews, 24, 1375–1389, https://doi.org/10.1016/j.quascirev.2004.10.003, 2005.

Ryves, D. B., Jewson, D. H., Sturm, M., Battarbee, R. W., Flower, R. J., Mackay, A. W., and Granin, N. G.: Quantitative and qualitative relationships between planktonic diatom communities and diatom assemblages in sedimenting material and surface sediments in Lake Baikal, Siberia, Limnology and Oceanography, 48, 1643–1661, https://doi.org/10.4319/lo.2003.48.4.1643, 2003.

Schelske, C. L.: Biogeochemical silica mass balances in Lake Michigan and Lake Superior, Biogeochemistry, 1, 197–218, https://doi.org/10.1007/bf02187199, 1985.

Schubert, M., Paschke, A., Lieberman, E., and Burnett, W. C.: Air–water partitioning of ^{222}Rn and its dependence on water temperature and salinity, Environmental Science & Technology, 46, 3905–3911, https://doi.org/10.1021/es204680n, 2012.

Shemesh, A., Rosqvist, G., Rietti-Shati, M., Rubensdotter, L., Bigler, C., Yam, R., and Karlén, W.: Holocene climatic change

in Swedish Lapland inferred from an oxygen-isotope record of lacustrine biogenic silica, The Holocene, 11, 447–454, 2001.

Strickland, J. and Parsons, T.: A practical handbook of seawater analysis, second edition edn., 1972.

Struyf, E., Mörth, C.-M., Humborg, C., and Conley, D. J.: An enormous amorphous silica stock in boreal wetlands, Journal of Geophysical Research: Biogeosciences, 115, https://doi.org/10.1029/2010jg001324, 2010.

Sun, X., Andersson, P., Land, M., Humborg, C., and Mörth, C.-M.: Stable silicon isotope analysis on nanomole quantities using MC-ICP-MS with a hexapole gas-collision cell, Journal of Analytical Atomic Spectrometry, 25, 156–162, 2010.

Sutton, J. N., André, L., Cardinal, D., Conley, D. J., De Souza, G. F., Dean, J., Dodd, J., Ehlert, C., Ellwood, M. J., Frings, P. J., et al.: A review of the stable isotope bio-geochemistry of the global silicon cycle and its associated trace elements, Frontiers in Earth Science, 5, 112, https://doi.org/10.3389/feart.2017.00112, 2018.

Swann, G. E. and Mackay, A. W.: Potential limitations of biogenic silica as an indicator of abrupt climate change in Lake Baikal, Russia, Journal of Paleolimnology, 36, 81–89, https://doi.org/10.1007/s10933-006-0005-7, 2006.

Tallberg, P., Opfergelt, S., Cornelis, J.-T., Liljendahl, A., and Weckström, J.: High concentrations of amorphous, biogenic Si (BSi) in the sediment of a small high-latitude lake: implications for biogeochemical Si cycling and for the use of BSi as a paleoproxy, Aquatic Sciences, 77, 293–305, https://doi.org/10.1007/s00027-014-0387-y, 2015.

Taylor, B. N. and Kuyatt, C. E.: Guidelines for evaluating and expressing the uncertainty of NIST measurement results, https://doi.org/10.6028/nist.tn.1297-1993, 1994.

Theriot, E. C., Fritz, S. C., Whitlock, C., and Conley, D. J.: Late Quaternary rapid morphological evolution of an endemic diatom in Yellowstone Lake, Wyomin, Paleobiology, 32, 38–54, https://doi.org/10.1666/02075.1, 2006.

Treguer, P., Nelson, D. M., Van Bennekom, A. J., DeMaster, D. J., Leynaert, A., and Queguiner, B.: The silica balance in the world ocean: a reestimate, Science, 268, 375–379, https://doi.org/10.1126/science.268.5209.375, 1995.

Tréguer, P. J. and De La Rocha, C. L.: The world ocean silica cycle, Annual review of marine science, 5, 477–501, 2013.

Turnipseed, D. and Sauer, V.: Discharge measurements at gaging stations: US Geological Survey Techniques and Methods, book 3, chap, 2010.

Vachon, D. and Prairie, Y. T.: The ecosystem size and shape dependence of gas transfer velocity versus wind speed relationships in lakes, Canadian Journal of Fisheries and Aquatic Sciences, 70, 1757–1764, https://doi.org/10.1139/cjfas-2013-0241, 2013.

Varela, D. E., Pride, C. J., and Brzezinski, M. A.: Biological fractionation of silicon isotopes in Southern Ocean surface waters, Global biogeochemical cycles, 18, https://doi.org/10.1029/2003gb002140, 2004.

Wolfe, A. P., Miller, G. H., Olsen, C. A., Forman, S. L., Doran, P. T., and Holmgren, S. U.: Geochronology of high latitude lake sediments, in: Long-term environmental change in Arctic and Antarctic lakes, pp. 19–52, Springer, 2004.

Zhang, A., Zhang, J., and Liu, S.: Spatial and temporal variations of dissolved silicon isotope compositions in a large dammed river system, Chemical Geology, p. 119645, https://doi.org/10.1016/j.chemgeo.2020.119645, 2020.

Ziegler, K., Chadwick, O. A., Brzezinski, M. A., and Kelly, E. F.: Natural variations of δ^{30}Si ratios during progressive basalt weathering, Hawaiian Islands, Geochimica et Cosmochimica Acta, 69, 4597–4610, https://doi.org/10.1016/j.gca.2005.05.008, 2005.

Appendix A: Methods

A1 Modelling groundwater Rn fluxes

Radon fluxes for 10 lakes from the Abisko region were estimated using the same approach in summer and autumn 2018 and 2019 (*C.Olid, unpublished data*). The derived Rn fluxes obtained from the lake survey were used here to model groundwater fluxes through the year in Lake 850. To do this, we divided the estimated groundwater Rn flux from the Rn mass balance in Lake 850 in September ($178 \pm 39\,\mathrm{Bq\,m^{-2}\,d^{-1}}$) by the mean groundwater Rn flux obtained from the lake survey in September ($74.5 \pm 55\,\mathrm{Bq\,m^{-2}\,d^{-1}}$, *C. Olid, unpublished data*). The derived ratio (2.39) was then multiplied by the mean groundwater Rn fluxes from the lake survey to model the groundwater Rn fluxes in Lake 850 for those months were Rn measurements were not available (June, July and September). Rn fluxes through groundwater during the ice-covered period were assumed to be 40% lower than those measured in September (*C. Olid, unpublished data*; Table A1). The groundwater Rn flux from November to April was assumed to be constant and equal to April estimations.

A2 Groundwater DSi and $\delta^{30}Si$ calculations during the ice-covered period

The groundwater concentration $\mathrm{c_{gw}}$ in during the ice-covered period was calculated from the groundwater discharge, the lake volume from the water balance, and the lake DSi differences between September and March though a mixing model:

$$\mathrm{c_{gw}} = \frac{(\mathrm{c_{Mar}}(\mathrm{V_{Sept}} + \mathrm{V_{gw}})) - (\mathrm{c_{Sept}} \cdot \mathrm{V_{Sept}})}{\mathrm{V_{gw}}} \quad \text{(A1)}$$

where $\mathrm{c_{Mar}}$ is the lake concentration in March, $\mathrm{c_{Sept}}$ is the lake concentration in September, $\mathrm{V_{Sept}}$ is the lake volume in September, and $\mathrm{V_{gw}}$ in is the total volume of water brought by groundwater in 8 months. The total water volume brought by groundwater in 8 months was calculated from the modelled groundwater winter discharges (Figure 2). The lake volume in September is taken from the water balance model, where the modelled groundwater discharges were used (Figure 5 and A1, green line).

Similarly, the $\mathrm{c_{gw}}$ in during the ice-covered period in the scenario with continuous BSi flux to the sediment for period of 8 month was calculated by adding flux into the sediment into the mixing model:

$$\mathrm{c_{gw}} = \frac{(\mathrm{c_{Mar}}(\mathrm{V_{Sept}} + \mathrm{V_{gw}})) - (\mathrm{c_{Sept}} \cdot \mathrm{V_{Sept}}) + \phi_{\mathrm{BSi}}}{\mathrm{V_{gw}}} \quad \text{(A2)}$$

where the ϕ_{BSi} is the total flux of BSi to sediment in 8 months. The BSi flux into the sediment for 8 months was calculated as a sum of the continuous monthly BSi flux from September until March.

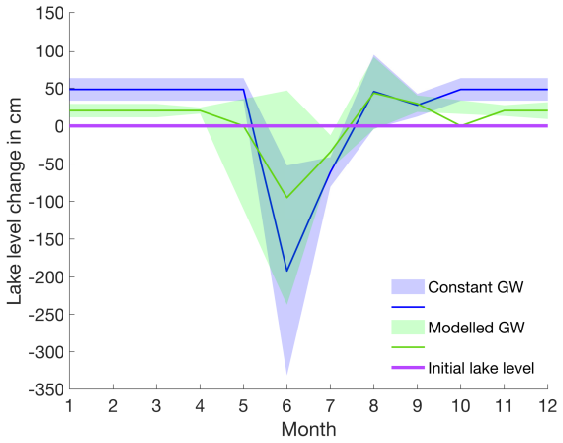


Figure A1. Estimated lake-level variation between neighbouring months throughout the year with uncertainties as shading. No lake-level change is depicted by the solid purple line. The blue line presents lake-level increase or decrease from one to another month with constant groundwater discharge (scenario i), and the green line is the rate of lake-level variation with modelled groundwater discharges (scenario ii).

The isotopic composition of the groundwater during the ice-covered period, based on measured data was calculated as:

$$\delta^{30}\mathrm{Si_{gw}} = \frac{(\delta^{30}\mathrm{Si_{Mar}}(\mathrm{c_{Sept}} \cdot \mathrm{V_{Sept}})) + (\mathrm{c_{gw}} \cdot \mathrm{V_{gw}})}{\mathrm{c_{gw}} \cdot \mathrm{V_{gw}}} - \frac{(\mathrm{c_{Sept}} \cdot \mathrm{V_{Sept}} \cdot \delta^{30}\mathrm{Si_{Sept}})}{\mathrm{c_{gw}} \cdot \mathrm{V_{gw}}} \quad \text{(A3)}$$

where $\delta^{30}\mathrm{Si_{Mar}}$ is the lake isotopic composition in March, $\delta^{30}\mathrm{Si_{Sept}}$ is the lake isotopic composition in September, $\mathrm{c_{Sept}}$ is the lake concentration in September, $\mathrm{c_{gw}}$ in is the concentration of groundwater during the ice-covered period (eq. A1 or A2, depending on model), $\mathrm{V_{gw}}$ in is the total volume of water brought by groundwater in 8 months, and $\mathrm{V_{Sept}}$ is the lake volume in September.

A3 Silicon isotope mass balance – $\delta^{30}Si_{gw}$ calculation

Due to the high groundwater input in Lake 850 proven by the Rn mass balance (see section Results: 5.2 Groundwater discharge), the inlet δ^{30}Si does not represent the initial δ^{30}Si used by diatoms. Therefore, the initial δ^{30}Si of DSi is a mixture of groundwater δ^{30}Si and inlet δ^{30}Si flux weighted. The $\delta^{30}\mathrm{Si_{initial}}$ in was calculated from $\delta^{30}\mathrm{Si_{postuptake}}$, which equals to $\delta^{30}\mathrm{Si_{lake}}$ as:

$$\delta^{30}\mathrm{Si_{initial}} = \delta^{30}\mathrm{Si_{postuptake}} + {}^{30}\varepsilon \cdot (1 - \frac{\mathrm{c_{out}}}{\mathrm{c_{initial}}}) \quad \text{(A4)}$$

Table A1. Estimated Rn fluxes in August and September with the derived water discharges through groundwater based on the Rn mass balance.

Measure data	$\mathrm{Bq\,m^{-2}\,d^{-1}}$	SD	Month	$\frac{\mathrm{Rn_{L850}}}{\mathrm{Rn_{10lakes}}}$	Q $[\mathrm{m^3\,d^{-1}}]$	SD
08/2019	164	51	8		309	108
09/2019	178	39	9	2.39	335	92

Further the groundwater $\delta^{30}\mathrm{Si_{gw}}$ which fits the measured data and keeps the steady-state, was calculated as:

$$\delta^{30}\mathrm{Si_{gw}} = \frac{\delta^{30}\mathrm{Si_{initial}} \cdot ((\mathrm{c_{in}} \cdot \mathrm{Q_{in}}) + (\mathrm{c_{gw}} \cdot \mathrm{Q_{gw}}))}{\mathrm{c_{gw}} \cdot \mathrm{Q_{gw}}} - \frac{(\mathrm{c_{in}} \cdot \mathrm{Q_{in}} \cdot \delta^{30}\mathrm{Si_{in}})}{\mathrm{c_{gw}} \cdot \mathrm{Q_{gw}}} \quad \text{(A5)}$$

Appendix B: Mass balance models: Extreme Si and Si isotope mass balances

The Si and Si isotopic mass balances models were tested for two extreme scenarios to model the highest and the lowest possible concentration of groundwater brought into the lake. Further, a scenario based on recent diatom growth season is modelled (Table B1). The DSi concentration and isotopic composition from the inlet and outlet streams are similar in all three scenarios. The groundwater DSi concentrations and isotopic composition are calculated from the groundwater fluxes influenced by the three potential BSi fluxes into the sediment, representing three possible lengths of diatom production. All scenarios are using the open system isotopic model (Varela et al., 2004) to describe the effect of diatom production on the lake water $\delta^{30}\mathrm{Si}$ ratio. The difference between the first and second scenario is the BSi flux into the sediment: (1) considers BSi flux into the sediment throughout the whole year representing lack of ice-covered period, and (2) BSi flux into sediment is present only from June until September (Shemesh et al., 2001). Scenario (3) utilizes the open system isotopic model only for June, with no diatom production the rest of the year, and thus no fractionation in the lake, which describes lake behaviour with only short ice-free period. Here we describe only scenario 1 and 3, whereas in the main text scenario 2 is presented and discussed.

B1 Scenario 1: 12 months of BSi flux into sediment

A scenario assuming a constant BSi flux to the sediment throughout the year (magenta line, Figure B1A) simulates a situation when climate is warming, and the diatom growth season is prolonged to maximum. Additionally, this scenario was characterized by the minimal groundwater fluxes and DSi concentrations. The DSi removal by diatoms is of $1.21 \pm 0.62\,\mathrm{mg\,SiO_2\,l^{-1}}$ SiO_2 monthly (magenta points, Figure B1B). Therefore, with an added BSi flux of $0.58 \pm 0.29\,\mathrm{kg}$ SiO_2 per day, the lake inlet does not supply sufficient DSi for diatoms to grow. The groundwater DSi concentration is calculated as the DSi flux needed to keep the lake balanced and sustain the diatom production. The groundwater flux of DSi varies from 0.43 ± 0.51 to $2.20 \pm 1.35\,\mathrm{kg}$ SiO_2 per day, depending on the season (cyan line, Figure B1A). The highest groundwater DSi flux occurs in June, followed by a decreasing trend towards August, when it reaches the minimum. From August until November, the groundwater DSi flux increases and is stabilized after November, and it is constant until May. From the calculated groundwater flux, the groundwater concentration is between $1.40 \pm 1.59\,\mathrm{mg\,SiO_2\,l^{-1}}$ to $2.31 \pm 1.03\,\mathrm{mg\,SiO_2\,l^{-1}}$ during the ice-free period, and, when combined with the lake DSi deficiency at the end of the season, it is $11.29 \pm 1.07\,\mathrm{mg\,SiO_2\,l^{-1}}$ (cyan line, Figure B1B) in the ice-covered period.

In scenario 1, with constant BSi flux into the sediment during the whole year of $0.58 \pm 0.29\,\mathrm{kg}$ SiO_2 per day, high superficial and groundwater discharges occur in June, with DSi concentrations of 2.34 and $2.28\,\mathrm{mg\,SiO_2\,l^{-1}}$, respectively (Figure B1B). The stream inlet has a light isotopic ratio of $\delta^{30}\mathrm{Si_{in}} = 0.02 \pm 0.10‰$. The initial DSi available for diatoms is a mixture of the groundwater and the stream inlet, with $\delta^{30}\mathrm{Si_{inital}} = 0.36 \pm 0.29‰$. The groundwater was calculated from the $\delta^{30}\mathrm{Si_{inital}}$ to have an isotopic ratio of $\delta^{30}\mathrm{Si_{gw}} = 0.46 \pm 0.51‰$ in June. Thus, the expected BSi isotopic ratio was calculated to be $-0.21 \pm 0.41‰$, which is within the range of mean measured $\delta^{30}\mathrm{Si_{BSi}} = 0.07 \pm 0.43‰$ in the top sediment layers. The diatom production consumes approximately 48% of the DSi influx in June.

Although groundwater discharge culminates in July, compared with the decreasing trend in the stream inlet, the isotopic composition of the lake in July is influenced by both the groundwater and the stream. The DSi concentration of the inlet is $4.79 \pm 0.03\,\mathrm{mg\,SiO_2\,l^{-1}}$, but with 4 times lower discharge than groundwater. The calculated groundwater DSi concentration from the steady-state model is only $1.54 \pm 1.39\,\mathrm{mg\,SiO_2\,l^{-1}}$ (Figure B1B). Further, the initial isotopic mixture for diatom growth $\delta^{30}\mathrm{Si_{initial}} = -0.02 \pm 0.10‰$ is composed of the stream $\delta^{30}\mathrm{Si_{in}} = 0.72 \pm 0.10‰$ and the groundwater $\delta^{30}\mathrm{Si_{gw}} = -0.63 \pm 0.75‰$ (Figure B1C). The expected BSi isotopic ratio is $\delta^{30}\mathrm{Si_{BSi}} = -0.49 \pm 0.41‰$, which still falls within the mean measured $\delta^{30}\mathrm{Si_{BSi}} = 0.07 \pm 0.43‰$ in the sediment. The diatom production in July consumes 57% of the DSi.

In August, the isotopic composition of the stream inlet, lake, and outlet are similar. The DSi concentration of the

Table B1. A summary of all 3 scenarios, which were examined through Si and Si isotope mass balance models

scenario	BSi flux time	daily BSi flux	range c_{gw}	range $\delta^{30}Si_{gw}$	DSi% consumed by production	range $\delta^{30}Si_{BSi}$
1	12 months	$0.58\,kg\,SiO_2\,day^{-1}$	1.40 to 11.29 $mg\,SiO_2\,l^{-1}$	-0.63 to $1.38‰$	$39-57\%$	-0.49 to $-0.01‰$
2	4 month	$1.77\,kg\,SiO_2\,day^{-1}$	3.51 to 6.95 $mg\,SiO_2\,l^{-1}$	-0.55 to $1.45‰$	$63-79\%$	-0.49 to $-0.01‰$
3	1 month	$7.08\,kg\,SiO_2\,day^{-1}$	0.37 to 8.99 $mg\,SiO_2\,l^{-1}$	-0.04 to $1.45‰$	$0-84\%$	$-0.21‰$

inlet is at its maximum, with an isotopic composition of $0.78 \pm 0.15‰$, but due to a very low inlet discharge it is not affecting the lake. The concentration and isotopic ratio of the outlet and the lake are almost identical, thus, the groundwater input is $1.40 \pm 1.59\,mg\,SiO_2\,l^{-1}$ of DSi (Figure B1B), with an isotopic ratio of $\delta^{30}Si_{gw} = 0.14 \pm 0.73‰$ (Figure B1C). The expected BSi isotopic ratio is $\delta^{30}Si_{BSi} = -0.31 \pm 0.67‰$, which is in agreement with the mean measured $\delta^{30}Si_{BSi}$ in the diatoms from sediment. The diatom production in August consumes 39% of the lake DSi.

September is the last month before the lake is ice-covered. There is no stream inlet, as the watershed is snow-covered. The groundwater input, with a concentration of $2.31 \pm 1.03\,mg\,SiO_2\,l^{-1}$, is four times higher than the removal by the lake outlet. This suggests that the lake-level is changing throughout seasons, which is not considered in any of the Si mass balance and isotopic models examined. The lake DSi of $1.37 \pm 0.04\,mg\,SiO_2\,l^{-1}$ is fully influenced by groundwater and diatom production. The groundwater isotopic ratio is $0.65 \pm 0.55‰$, and the diatom production is using 41% of the lake DSi. The expected BSi isotopic ratio is $\delta^{30}Si_{BSi} = -0.01 \pm 0.47‰$, which is in agreement with the mean measured $\delta^{30}Si_{BSi}$ in the diatoms from sediment.

This scenario assumes that the groundwater concentration during the ice-covered lake is recharging the lake DSi, while the BSi flux into the sediment is still present (Figure B1B). Applying the mixing model (equation A2 and A3), groundwater DSi concentration ($11.29 \pm 1.07\,mg\,SiO_2\,l^{-1}$), groundwater discharge, lake volume change during the ice-covered period, and the difference of the isotopic composition of the lake water between September ($1.02 \pm 0.24‰$) and March ($1.27 \pm 0.10‰$), the isotopic ratio of the groundwater is calculated to be $1.45 \pm 2.58‰$ (Figure B1C).

B2 Scenario 3: only 1 month of BSi flux into the sediment

The third scenario is based on the inlet and outlet DSi fluxes but assumes that diatom production occurs only in June. This scenario could occur if the climate would experience cooling and the diatom growth period would be extremely shortened. Additionally, this scenario demonstrated the highest groundwater concentrations during the diatom growing season. The rest of the year diatom production, and so the BSi flux into the sediment, is negligible or zero. Therefore, the yearly accumulated BSi settles into the sediment within one month, which yields a BSi flux of $7.08 \pm 3.62\,kg$ SiO_2 per day (magenta line, Figure B1G). In this scenario, groundwater input must be from $0.15 \pm 0.37\,kg$ SiO_2 to $8.70 \pm 4.59\,kg$ SiO_2 per day, and the DSi concentration ranges between $0.37 \pm 0.69\,mg\,SiO_2\,l^{-1}$ to $8.99 \pm 4.35\,mg\,SiO_2\,l^{-1}$ during the ice-free period (cyan line, Figure B1H). Similar to the second scenario (in the main text), to restore the lake DSi concentration during the ice-covered period from lake-October to mid-June, groundwater DSi concentration is around $6.95 \pm 4.90\,mg\,SiO_2\,l^{-1}$.

Scenario 3 assumes the BSi flux into the sediment occurs only in June, and the rest of the year there are no processes causing stable Si isotope fractionation. This scenario originates from data in August and September, when the $\delta^{30}Si$ of inlet, outlet and the lake are very similar. Only in June is there fractionation between the lake stream inlets and the lake, which is described by the open-system-fractionation model. Therefore, the groundwater concentration in June increases to $8.99 \pm 4.35\,mg\,SiO_2\,l^{-1}$ (Figure B1H), with an isotopic ratio of $-0.04 \pm 0.52‰$ (Figure B1I) to sustain the diatom production represented by BSi flux into the sediment. The production consumes 84% of the available DSi.

In July, August, and September the groundwater DSi concentration is low, as the lake does not have any production, thus no demand on the DSi. The isotopic composition of the groundwater is $0.23 \pm 1.41‰$, $0.75 \pm 2.83‰$, and $1.02 \pm 0.53‰$, respectively (Figure B1I). High uncertainties in the isotopic composition of the groundwater reflect the uncertainties in the stream and groundwater discharges and fluxes.

Appendix C: Discussion: Scenarios evaluation

Scenarios 1 and 3 of Si mass balance (Table B1, Figure B1A and G) are demonstrating how the groundwater concentration would change with changes of length of diatom production. It is likely that the diatom growth season would be driven by the changes in climate and thus the ice-free period length. Our models aimed to estimate the changes in the lake DSi and Si balance in those extreme changes of growing season driven by changes in climate. However, the groundwater con-

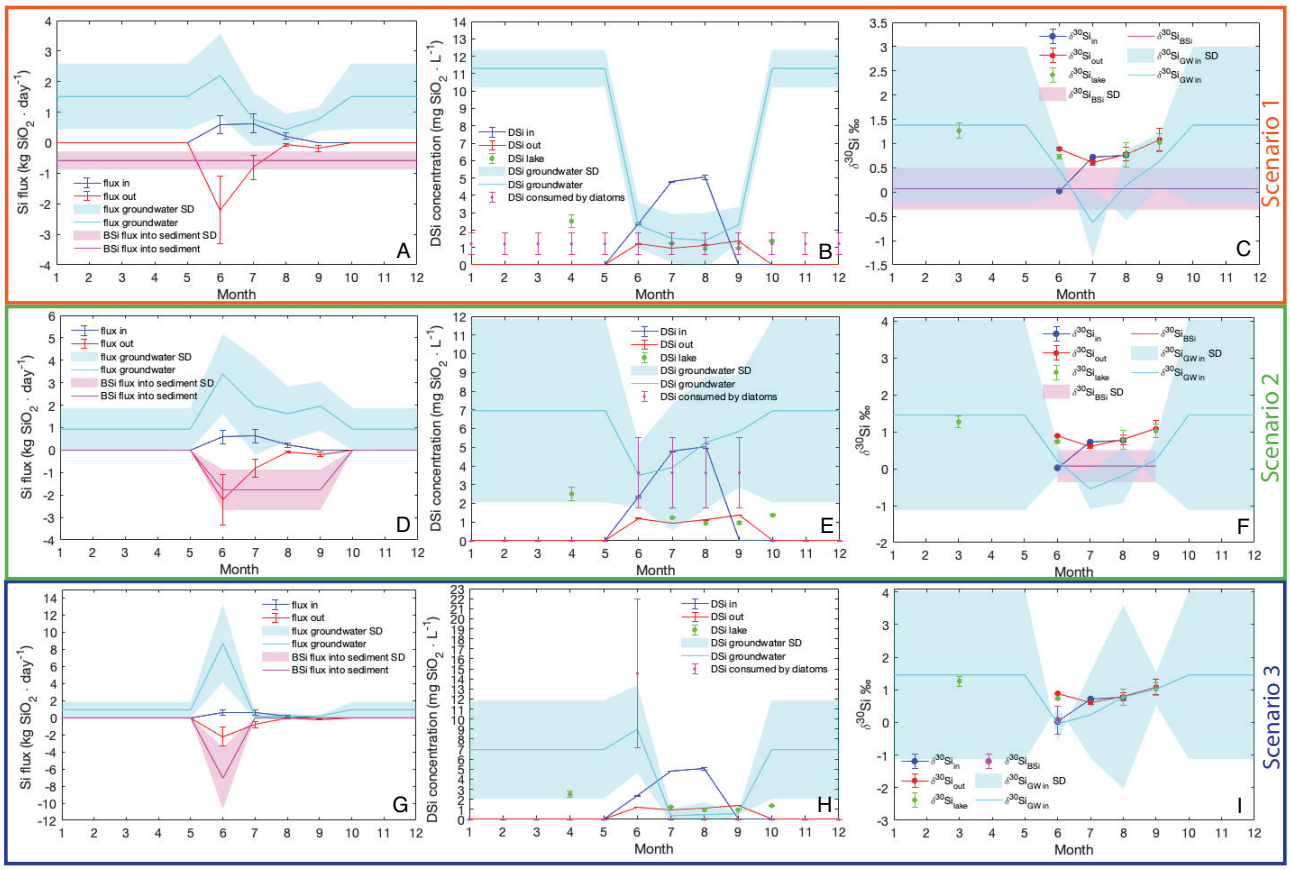


Figure B1. Inlet (blue), outlet (red), groundwater (cyan), and the BSi (magenta) fluxes, concentrations and isotopic composition. Scenario 1: A-C The constant BSi flux into sediment (A) influences the groundwater DSi concentration (B) and the silicon isotopic composition (C). Scenario 2: D-F present the effect of BSi flux adjusted to the diatom bloom season of 4 months (D) on the groundwater concentration (E) and isotopic composition (F). Scenario 3: G-I The diatom bloom represented by the BSi flux into the sediment is restricted to 1 month only. During June all BSi accumulated for 1 year is produced and the groundwater concentration (H) and the isotopic composition (I) is affected.

centrations are commonly higher than the superficial streams (Frings et al., 2016; Maavara et al., 2018; Opfergelt et al., 2011), which is not the case in scenario 1 and 3. The groundwater DSi concentrations are lower than in the stream inlet during the ice-free period in those two scenarios (Figure B1B and B1H), which suggest that those scenarios have either missing or surplus data of the inlet and outlet DSi concentration and discharges. A more complex model with variable discharges of groundwater and stream inlets and outlet depending on precipitation end evaporation changes would be needed. Therefore, those two scenarios bring only a rough estimate hinting the changes in DSi and Si isotopic mass balances connected to changes in climate.

Supplementary material

Table S1. Summary of all samplings of Lake 850

Site Description	Coordinates	Max Depth	Sampling Depth	Sampling Date	Sample Type	Sample number
Inlet 1	N 68°17′50.6″ E19°7′6.9″	5 cm		26/Jun/18 03/Jun/19	water, Q	n=2
Inlet 2	N 68°17′53.5″ E19°7′8.3″	6 cm		13/Jul/19 22/Aug/19 20/Sept/19	water, Q	n=3
Outlet	N 68°17′54.8″ E19°7′26.3″	10 cm		26/Jun/18 03/Jun/19 13/Jul/19 22/Aug/19 20/Sept/19	water, Q	n=5
Lake water	N 68°17′51.3″ E19°7′10.3″		surface	03/Jun/19	water	n=1
Water profile	N 68°17′53.5″ E19°7′15.6″	4.2-7.5 m	1 m to 7 m	22/Mar/19 22/Aug/19 20/Sept/19	water	n=14
Rn sampling 100	N 68°17′53.1″ E19°7′20.4″	0.75 m	0.5 m	22/Aug/19	water	n=1
Rn sampling 101	N 68°17′53.5″ E19°7′16.9″	7.5 m	1.5-4 m	22/Aug/19	water	n=2
Rn sampling 102	N 68°17′54.2″ E19°7′18.7″	4 m	1.5 m	22/Aug/19	water	n=1
Rn sampling 103	N 68°17′51.5″ E19°7′11.7″	2 m	1.5 m	22/Aug/19	water	n=1
Rn sampling 104	N 68°17′53.3″ E19°7′11.9″	5 m	1.5 m	22/Aug/19	water	n=1
Rn sampling 20	N 68°17′54.4″ E19°7′21.4″	0.9 m	0.5 m	20/Sept/19	water	n=1
Rn sampling 21	N 68°17′54.8″ E19°7′18.2″	5.4 m	1.5 m	20/Sept/19	water	n=1
Rn sampling 22	N 68°17′52.7″ E19°7′12.0″	4.2 m	1.5 m	20/Sept/19	water	n=1
Rn sampling 23	N 68°17′53.2″ E19°7′17.7″	6.1 m	1.5-4 m	20/Sept/19	water	n=2
Rn sampling 24	N 68°17′52.5″ E19°7′16.6″	4.2 m	1.5 m	20/Sept/19	water	n=1
HTH core 1	N 68°17′53.2″ E19°7′17.2″	7.6 m	15 cm	22/Mar/19	sediment	n=1
HTH core 2	N 68°17′52.9″ E19°7′14.1″	6.8 m	33 cm	22/Aug/19	sediment	n=1

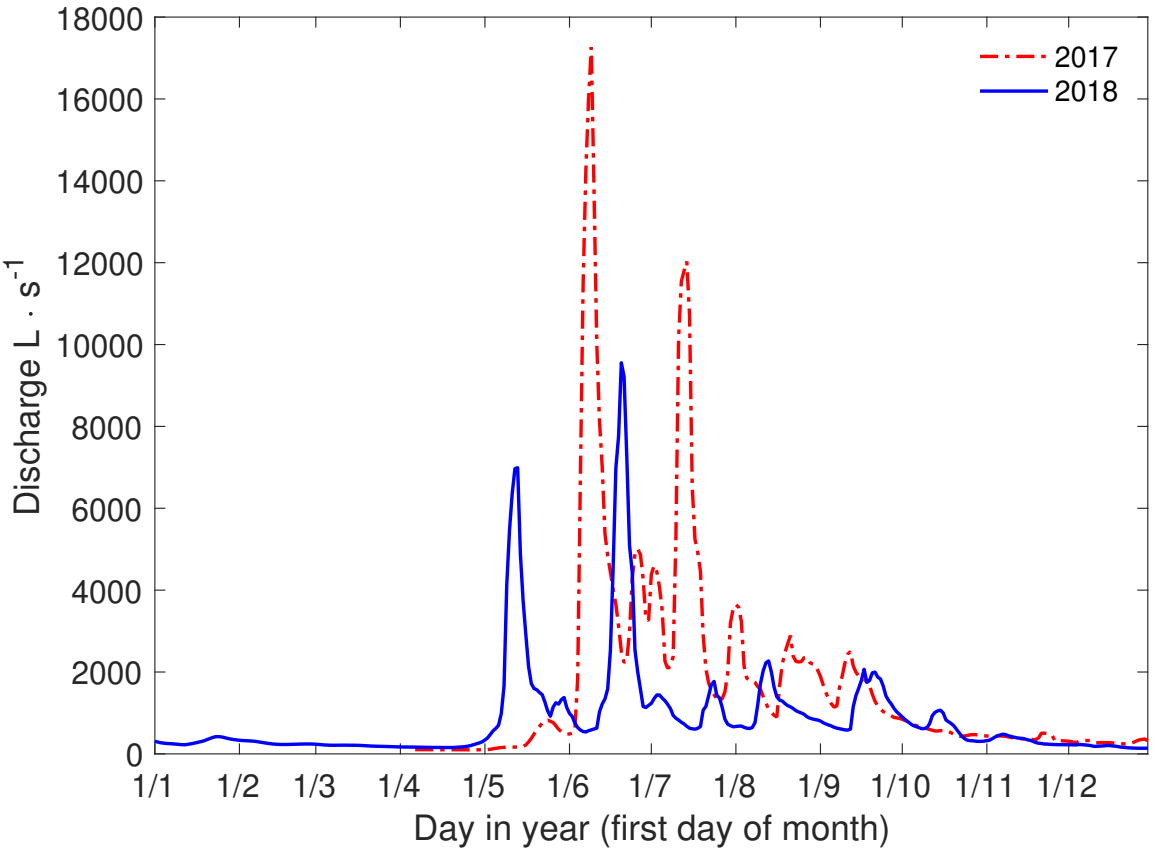


Figure S1. Daily mean discharge in $1\,s^{-1}$ of neighbouring river Miellejohka in years 2017 and 2018 (ANS, 2020b)



Paper III

"All sorts of things can happen when you're open to new ideas and playing around with things."

Stephanie Kwolek

Cover photo: Lake 850 in March 2019

Picture credits: Ethan Silvester

Impact of Holocene climate change on silicon cycling in Lake 850, Northern Sweden

The Holocene
XX(X):1–13
©The Author(s) 2021
Reprints and permission:
sagepub.co.uk/journalsPermissions.nav
DOI: 10.1177/ToBeAssigned
www.sagepub.com/
SAGE

Petra Zahajská[1,5], Rosine Cartier[1], Sherilyn C. Fritz[2], Johanna Stadmark[1], Sophie Opfergelt[3], Ruth Yam[4], Aldo Shemesh[4] and Daniel J. Conley[1]

Abstract

Diatom-rich sediment in a small subarctic lake (Lake 850) was investigated in a 9400 cal. yr BP sediment record in order to explore the impact of Holocene climate evolution on silicon cycling. Diatom stable silicon isotopes ($\delta^{30}Si_{BSi}$) and biogenic silica (BSi) indicate that high BSi accumulation throughout Holocene is associated with a lighter Si isotope source of dissolved silica (DSi), such as groundwater or freshly weathered primary minerals. Furthermore, higher BSi accumulation was favoured during the mid-Holocene by low detrital inputs and possibly a longer ice-free period allowing for more diatom production to occur. The diatom $\delta^{30}Si_{BSi}$ signature shows a link to changes in regional climate and is influenced by length of diatom growth period and hydrological fluctuations. Lighter Si isotopic values occur during the mid-Holocene, when climate is inferred to be more continental and drier, with pronounced seasonality. In contrast, a heavier Si isotopic signature is observed in the early- and late-Holocene, when oceanic influences are thought to be stronger and the climate wetter. The $\delta^{30}Si_{BSi}$ values have generally lighter signatures as compared with other studies, which supports a light DSi source.

Keywords

diatom, lake, silicon, isotope, Holocene, sediment

Introduction

In natural waters silicon is primarily present in the dissolved form as silicic acid H_4SiO_4, also called dissolved Si (DSi), which originates from the weathering of primary minerals. Rivers and lakes act as a sink for DSi in the global silicon cycle, where lakes store the DSi primarily as diatoms (Frings et al. 2014b), which are unicellular siliceous golden algae. The DSi delivered to a lake is a product of processes in the lake catchment area, such as weathering and erosion, and can be modified by vegetation and soils. Subsequently, diatom production and dissolution are partly controlled by the sensitivity of diatoms to DSi concentration (Hamm et al. 2003; Yool and Tyrrell 2003), and thus both processes – production and dissolution – influence changes in lake DSi (Panizzo et al. 2017). Fossil diatoms in lake sediment are used as an archive of environmental history and can be used for unravelling changes in silicon cycling as a result of their high preservation potential. Biogenic silica (BSi) concentrations have been used previously in Canadian Arctic lakes as an indicator of aquatic palaeoproductivity (Fortin and Gajewski 2009). In Lake Baikal the sedimentary BSi concentration recorded diatom responses to changes in summer temperatures associated with variation in summer insolation (Khursevich et al. 2001). However, BSi concentration in lake sediments is also affected by diatom preservation (Panizzo et al. 2016; Ryves et al. 2003). Additionally, low detrital input can result in high sediment BSi concentration (Conger 1942; Zahajská et al. in review).

Diatoms preferentially incorporate the lighter Si isotope, ^{28}Si, to form the diatom frustule when sufficient DSi is present (De La Rocha et al. 1997). The stable silicon isotopes from diatoms ($\delta^{30}Si_{BSi}$) can be used to record DSi utilization controlled by diatom productivity associated with changes in climate (De La Rocha et al. 1998; Hendry and Brzezinski 2014; Opfergelt and Delmelle 2012), diatom production and dissolution (Chen et al. 2012; Street-Perrott et al. 2008), vegetation impacts on the Si cycle (Frings et al. 2014a, 2016; Leng et al. 2009; Sun et al. 2011), rates of nutrient supply (Swann et al. 2010) or DSi sources (Nantke et al. 2019; Vandevenne et al. 2015). Additionally, changes in $\delta^{30}Si$ in the water column can result from seasonal diatom DSi uptake and clay mineral formation in the sediments (Ehlert et al. 2016; Frings et al. 2014c; Geilert et al. 2020; Zhang et al. 2020). Moreover, studies on Lake Baikal suggest that long-term changes in isotopic composition are complex and involve several simultaneous processes affecting the isotopic signature (Panizzo et al. 2017).

[1]Department of Geology, Lund University, Lund, Sweden
[2]Department of Earth and Atmospheric Sciences and School of Biological Sciences, University of Nebraska–Lincoln, Lincoln, Nebraska, USA
[3]Earth and Life Institute, Université catholique de Louvain, Louvain-la-Neuve, Belgium
[4]Department of Environmental Sciences and Energy Research, The Weizmann Institute of Science, Rehovot, Israel
[5]Institute of Geology and Paleontology, Faculty of Science, Charles University, Prague, Czech Republic

Corresponding author:
Petra Zahajská, Department of Geology, Lund University, Sölvegatan 12, 22632, Lund, Sweden
Email: petra.zahajska@geol.lu.se

Prepared using sagej.cls *[Version: 2017/01/17 v1.20]*

Changes in climate, recorded in lake sediments in northern Sweden spanning the last 9400 years, have been reconstructed using stable oxygen isotopes, changes in diatom communities (Bigler and Hall 2003; Rosén et al. 2001; Shemesh et al. 2001), pollen-based vegetation reconstruction (Barnekow 1999; Berglund et al. 1996; Seppä and Hammarlund 2000) and chironomids (Rosén et al. 2001). In northern Sweden, post-glacial climate and vegetation development is commonly subdivided into three periods (Barnekow 1999; Hammarlund et al. 2002; Seppä and Hammarlund 2000). Early Holocene climate was characterized as humid oceanic, with warm summer temperatures, rising treeline and a shift in vegetation from subarctic shrub and birch tundra to boreal pine-birch forest (Seppä and Hammarlund 2000). Mid-Holocene climate was more stable and continental compared with the early Holocene, with warm and dry summers and strong seasonality (Berglund et al. 1996; Rosén et al. 2001). Gradual cooling with some short-term fluctuations is suggested for the late Holocene (Barnekow 1999; Bigler et al. 2003; Rosén et al. 2001).

We examine here the impact of changes in climate on silicon cycling and BSi accumulation in Lake 850 within the framework of existing knowledge on Holocene climate changes in the Abisko area, northern Sweden (Berglund et al. 1996; Bigler and Hall 2003; Hammarlund et al. 2002; Rosén et al. 2001; Seppä and Hammarlund 2000). Pollen records in the Lake 850 area suggest that the lake has been above the pine treeline throughout the last 9400 cal. yr BP. We hypothesize that changes in DSi sources, derived from hydrological changes connected to changes in climate, are responsible for BSi concentration and $\delta^{30}Si_{BSi}$ variation. The long-term evolution of lake BSi accumulation is hypothesized to be dependent on climate-driven sedimentation rates, detrital input, and diatom production. Sediment lithology, diatom BSi concentration, and diatom stable silicon isotopes are used to reconstruct these processes.

Study area

Lake 850 is situated in northern Sweden, 14 km south-east from Abisko Research Station (388 m a.s.l.). Mean temperatures during summer and winter in the Abisko region are 9.8 °C and −10.1 °C, respectively, and the mean annual temperature (from 1913 to 2019) was −0.4 °C (ANS, Abisko Scientific Research Station 2020). The diatom growing season is from June to August (Shemesh et al. 2001). The lake, at an elevation of 850 m a.s.l. (68°15′ N, 19°7′ E), lies above treeline, which is currently at 600 m a.s.l. The catchment area is 0.35 km^2 (Rubensdotter and Rosqvist 2003), and the lake surface area is 0.02 km^2. Approximately 48 % of the lake area lies within the deep basin, with a maximum depth of 8 m, and 52 % of the lake surface area is shallow, with a depth of <4 m. The vegetation in the catchment area is comprised of Arctic species of mosses, grasses and shrubs, and the bedrock is composed of granites and syenites overlain by a thin layer of till (Shemesh et al. 2001). There are two ephemeral 1–2 cm deep inlets in the eastern part of the lake and one outlet in the western part (see Zahajská et al. in review, in review). From mid-October until late May–early June, the lake is ice-covered, and its catchment area is snow-covered from mid-September to mid-June. In August the lake is well-mixed with no thermal stratification and has a pH of 6.8. The lake is classified as oligotrophic and has a dissolved organic carbon concentration of 2.3 $mg\,l^{-1}$ (Shemesh et al. 2001; Bigler et al. 2002).

Methods

Core collection

In April 1999, a 125-cm sediment core was cored from the centre of the ice-covered Lake 850 using a modified Livingstone piston corer (Shemesh et al. 2001). The core was subsampled into 62 2-cm sections, but only the top 56 samples contained sufficient biogenic silica (Shemesh et al. 2001) and are used here for stable Si isotope analysis.

To investigate BSi accumulation, a 74 cm-long sediment core was taken using a modified Livingston piston corer in March 2019 from the ice in the deep basin (68°17′53.2″ N, 19°7′17.2″ E) at a depth of 7 m. The piston core was scanned for density, magnetic susceptibility, and X-ray fluorescence (XRF) with an ITRAX CS37 at the GLOBE Institute, Copenhagen University, Denmark. The core was correlated with the previously collected piston core (Core 3) from 1999 (Shemesh et al. 2001; Rubensdotter and Rosqvist 2003) using age-depth models and total organic carbon (TOC) (see section Chronology).

Sediment characterization

The 2019 core was halved, and one half was continuously subsampled in 1-cm sections and placed into cubic boxes with known volume. The other half of the piston core was used for XRF and magnetic susceptibility scanning and archived. All sediments were weighed before and after freeze drying for water content, to obtain porosity and wet and dry bulk densities.

Total organic carbon (TOC) and total nitrogen (TN) analyses were carried out on freeze dried samples (n = 28), where 5 mg to 10 mg of dry sediment was packed into tin capsules. Six samples throughout the core were tested for carbonate by acidifying with HCl and heating to 60 °C before total carbon (TC) measurements were conducted (Brodie et al. 2011). The measurements were done on a COSTECH ECS4010 elemental analyzer at the Department of Geology, Lund University, with the mean analytical uncertainty for TOC of 0.3 wt% based on duplicate analysis (n = 17). The carbonate content was calculated as a difference in TC between de-calcified and bulk sample. Because these analyses indicated that the sediments do not contain carbonate, the TC measurements are used as a measure of TOC. The published LOI data (Rubensdotter and Rosqvist 2003) show values above 20 %, thus an experimental conversion factor from LOI to TOC of 2 was used to recalculate LOI into TOC (Bojko and Kabała 2016).

The BSi concentration was analyzed at a resolution of 1 cm by sequential alkaline extraction (Conley and Schelske 2001). Freeze-dried homogenized samples were digested in 0.1 M Na_2CO_3 in a shaking bath at 85 °C. Subsamples were

Table 1. Samples from Lake 850 sediment core from 2019 dated by ^{14}C AMS method.

^{14}C dated piston core

Depth (cm)	Dated material	Weight (mg C)	Lab no	Radiocarbon age (BP)	Calibrated age[a] (cal. yr BP, 2σ range)
28–29	*Betula nana* leaf	1.0	LuS 15652	3405 ± 45	3562–3732
40–41	*Betula nana* leaf	0.8	LuS 15655	3965 ± 45	4287–4528
54–55	*Betula nana* leaf	1.1	LuS 15658	4525 ± 40	5047–5202
70–71	*Vaccinum sp.* leaf	1.4	LuS 15661	6300 ± 50	7156–7366
73–74	*Vaccinum sp.* leaf	1.0	LuS 15663	6370 ± 40	7247–7419

[a] ^{14}C dates were calibrated using the IntCal20 radiocarbon calibration dataset by Reimer et al. (2020).

taken at 3, 4 and 5 hours and neutralized with HCl to examine for the dissolution of minerals. There were no changes in the amount of total amorphous SiO_2 extracted during the time course of the dissolution, therefore mean values were used to estimate BSi concentration with no mineral correction applied (Conley 1988).

Chronology

Five terrestrial macrofossil samples from the piston core were dated by ^{14}C using accelerator-mass-spectrometer at the Radiocarbon Dating Laboratory, Department of Geology, Lund University (Table 1). Radiometric dates were calibrated with IntCal20 radiocarbon calibration dataset (Reimer et al. 2020). The age-depth model (Figure 1) was established based on ^{14}C dates using the software package Bacon with five age controls (Blaauw 2010). A priori assignment of mean sediment accumulation rate was set to 100 yr cm^{-1}, as suggested by Bacon. Thickness for spline calculation was set at 15.5 cm, above which the model diverged greatly from the age controls provided. The age-depth model had 100 % of the dates overlapping within the mean 95 % confidence ranges.

An updated age-depth model for the core from 1999 (Figure S1) was established based on six original ^{14}C dates from the published age-depth model (Shemesh et al. 2001) using the same approach as described above. A priori assignment of mean sediment accumulation rate was set to 100 yr cm^{-1}, and thickness for spline calculation was set at 24.5 cm. Only 86 % of the dates overlapped with the age-depth model's mean 95 % confidence ranges.

Both cores were aligned based on age-depth models. A secondary control of the alignment was done through comparison of TOC calculated from loss on ignition (LOI) on the core from 1999 and a proxy for organic carbon (incoherent/coherent scanning ratio) measured on the new piston core (Figure 2), which showed good fit. The proxy for organic content is based on the rhodium (Rh) scatter peak areas, expressed as Rh_{inc}/Rh_{coh}, where the Rh incoherent (Rh_{inc}) responds to valence of electrons and Rh coherent (Rh_{coh}) scatter peak (K-alpha) responds to bulk electrons in sample material (Burnett et al. 2001). When the number of valence electrons is large compared to the number of bulk electrons, the density of the sample is lower, which indicates high organic content. All data are plotted with age, as the ages of both cores do not correspond to similar depths.

Stable Si isotopes analysis

Clean bulk diatom material (several diatom species) from Lake 850 with 2-cm resolution was obtained from a 125-cm-long core used in a previous study (Shemesh et al. 2001) and processed for stable silicon isotopes. Cleaned diatom samples (~ 0.8 mg) were digested with 0.5 to 1 ml of 0.4 M NaOH (analytical purity) at 50 °C for at least 48 hours. When all diatoms were dissolved, samples were diluted with Milli-Q® water to prevent precipitation and fractionation of amorphous silica, then neutralized by 0.5 ml to 1 ml of 0.4 M suprapur® HCl. The solutions were measured for their silicon concentration to obtain Si recovery, which was between 90 and 100 % of the calculated concentration based on initially weighed and dissolved diatom SiO_2. Samples solutions, Si standards RM-8546 and Diatomite prepared by NaOH fusion (Georg et al. 2006) were purified for silicon analysis by ion-chromatographic separation using 1.5 ml cation-exchange DOWEX® 50W-X8 (200-400 mesh) resin following the method by Georg et al. (2006).

Stable Si isotopes were measured on a NuPlasma (II) HR multi-collector inductively conducted plasma mass spectrometry (MC-ICP-MS, Nu Instruments™) with an Apex HF desolvation nebulizer at the Vegacenter, Swedish Natural History Museum, Stockholm. The ^{28}Si signal of full procedural blanks was determined to be less than 0.35 % of the total signal, thus sample contamination was not observed. All samples were diluted to 2–3 mg l^{-1} of Si and matrix matched with standards in 0.12 M SeaStar HCl. Further, all samples and standards were doped to contain 3 mg l^{-1} of Li (IPC-MS standard) to match the matrix of Vegacenter standards prepared by $LiBO_2$ fusion (Sun et al. 2010).

Silicon isotopes data are reported as deviations of $\frac{^{30}Si}{^{28}Si}$ and $\frac{^{29}Si}{^{28}Si}$ from the RM-8546 (former NBS-28) in ‰, denoted δ^{30}Si and δ^{29}Si as follows:

$$\delta^{30}\mathrm{Si} = \left(\frac{\frac{^{30}Si}{^{28}Si\,\mathrm{sample}}}{\frac{^{30}Si}{^{28}Si\,\mathrm{NBS28}}} - 1 \right) \cdot 1000. \quad (1)$$

Each sample was measured three to six times with bracketing of NBS-28 in between. Full chemical replicates were measured on 68 % of all samples ($n = 56$). A three-isotope plot δ^{30}Si vs δ^{29}Si is used to ensure that there are no polyatomic interferences present during mass spectrometry measurements. All measured samples should fall on the expected mass-dependent fractionation line with a slope of 0.5092 (Figure S2, Reynolds et al. 2007).

Long-term (ca. 3 years) variance from the secondary reference materials is as follows: Diatomite $\delta^{30}\mathrm{Si} = 1.24 \pm 0.20$ ‰ ($2SD_{repeated}$, $n = 285$), Big-Batch $\delta^{30}\mathrm{Si} = -10.63 \pm 0.34$ ‰ ($2SD_{repeated}$, $n = 109$) and IRMM $\delta^{30}\mathrm{Si} = -1.77 \pm 0.22$ ‰ ($2SD_{repeated}$, $n = 195$). All secondary reference materials values were in good agreement with values from a

previous interlaboratory comparison (Reynolds et al. 2007). The reproducibility of all samples was < 0.2 ‰. At the Vegacenter laboratory, the long-term precision is 0.15 ‰ (expressed as 2SD).

Statistical analyses

For testing the statistical significance of proxy correlations, a Pearson correlation test was run on data in R software. A statistically significant correlation was considered to have a confidence interval of 95 % and thus, the p-value < 0.05. The correlation tests were run on the entire core record, as well as on three chosen zones. The $\delta^{30}Si_{BSi}$, BSi, LOI, TOC or OC proxy, Ti, Fe and MS were tested for correlation to identify processes connected to the $\delta^{30}Si_{BSi}$ signature and variation of BSi. The correlation results are heavily dependent on the alignment of two cores, thus a significant correlation between LOI and the OC proxy, which supports the robustness of the core alignment, was tested before any other correlation tests.

Results

Age-depth model and core alignment

The base of the 2019 piston core was dated at approximately 7400 cal. yr BP (Table 1). The mean sedimentation rate over the entire core was estimated to be $0.012\,cm\,yr^{-1}$ or $83.3\,yr\,cm^{-1}$ (Figure 1), which is in the same range as a previously published sedimentation rate from Lake 850 of $0.013\,cm\,yr^{-1}$ (Shemesh et al. 2001). Based on this sedimentation rate, the mass accumulation rate was calculated to be $1.9\,mg\,cm^{-2}\,yr^{-1}$. However, the age-depth model is not linear, especially in the top 28 cm. The increased sedimentation rate in the top of the core has a high uncertainty, as no age constraint was obtained between the surface and 28 cm. The top of the core is considered to have the age of the coring year. However, the sediment-water interface was disturbed during coring and thus, the age-depth model can suffer from the incompleteness of the record. The age-depth model of a short core from Lake 850 also shows non-linear changes in sedimentation rate in the surface of the core (Zahajská et al. in review, in review).

A new age-depth model of the published core from 1999 (Figure S1) indicates that the base of the core is approximately 9400 cal. yr BP and shows linear changes in sedimentation rate through time, which is in agreement with the previous Holocene age-depth model (Shemesh et al. 2001; Rubensdotter and Rosqvist 2003).

Lithology

The 74-cm 2019 sediment core was examined for its lithology, elemental composition using XRF, total organic carbon (TOC), total nitrogen (TN), biogenic silica (BSi) and magnetic susceptibility. The sediment is composed predominantly of carbonate-free clay gyttja, similar to the lithology of the previously published 125-cm sediment core (Shemesh et al. 2001). The sediment porosity (data not shown) is generally high, averaging 86 %, with maximum values of 90 %. The wet bulk density (data not shown) is $1.15\,g\,cm^{-3}$, and the dry bulk density is $0.162\,g\,cm^{-3}$. The magnetic susceptibility (MS) and the titanium (Ti) and iron normalized by Ti (Fe/Ti) XRF data are used as proxies for changes in grain-size and detrital/terrigenous input into the sediment, respectively (Figure 2). Titanium, iron and magnetic susceptibility show a generally increasing trend from the base to the top of the core. An increase in all three proxies is observed, especially in the last 3000 cal. yr BP. In contrast, the TOC and C/N data show elevated values from 7400 to 3500 cal. yr BP and are generally stable during the last 3500 cal. yr BP. Total organic carbon and BSi share some similarities in their trends, with increased values from 7400 to 3500 cal. yr BP, followed by lower values in last 3500 cal. yr BP. However, BSi varies greatly, whereas TOC and C/N display smaller variations. BSi concentrations and TOC together constitute from 23 to 52 wt% of the sediment. The remainder of the sediment is considered to be minerogenic.

The non-minerogenic component of the sediment is used as a proxy for changes in productivity or terrigenous input. TOC varies greatly throughout the core, from 8.4 ± 0.5 wt% to 16.4 ± 0.4 wt%, with a mean of 11 ± 1.4 wt%. One standard deviation is used as uncertainty when data are presented. Typical C/N values for autochthonous aquatic production range from 4 to 10, whereas terrestrial plants have C/N > 20 (Meyers 1994). Thus, our values, which range from 9.7 to 13.7, represent the dominance of autochthonous sources.

The BSi shows large variability, with the BSi minimum of 23.2 ± 1.3 wt% SiO_2 at 2280 cal. yr BP, maximum of 42.5 ± 1.6 wt% at 3580 cal. yr BP and the core mean of BSi is 32.3 ± 1.4 wt%. A distinct local minimum in BSi concentration occurs at 4750 cal. yr BP, with BSi of 25.7 ± 1.0 wt%. Elevated BSi concentrations above 30 wt% are observed $\sim$ 2800 cal. yr BP, 3800 cal. yr BP, 5100 cal. yr BP and 6600 cal. yr BP. The minerogenic fraction resulting from the BSi and TOC measurements varies between 48 and 77 wt%.

Biogenic silica fluxes

The Holocene BSi flux into the sediment was determined from the piston core BSi and the mass accumulation rate of $1.9\,mg\,cm^{-2}\,yr^{-1}$. The mean BSi flux into the sediment from 7300 cal. yr BP to present is $0.67\,mg\,SiO_2\,cm^{-2}\,yr^{-1}$ (Figure 2). At the bottom of the core, the BSi flux is higher, with values up to $1.31\,mg\,SiO_2\,cm^{-2}\,yr^{-1}$, and with a mean of $1.25\,mg\,SiO_2\,cm^{-2}\,yr^{-1}$ from the period 7300 to 7100 cal. yr BP. From approximately 7100 cal. yr BP to 5200 cal. yr BP, the BSi flux stabilizes at a mean of $0.48\,mg\,SiO_2\,cm^{-2}\,yr^{-1}$, excluding two intervals of increased BSi fluxes of 1.44 and $1.50\,mg\,SiO_2\,cm^{-2}\,yr^{-1}$ at 6600 cal. yr BP and 6000 cal. yr BP, respectively. An increasing trend in the BSi accumulation rate during younger ages is observed from 5200 cal. yr BP to 3700 cal. yr BP, with values varying from $0.51\,mg\,SiO_2\,cm^{-2}\,yr^{-1}$ up to $1.18\,mg\,SiO_2\,cm^{-2}\,yr^{-1}$, with a mean of $0.80\,mg\,SiO_2\,cm^{-2}\,yr^{-1}$. From 3700 cal. yr BP to present, the BSi flux is stable at $0.53\,mg\,SiO_2\,cm^{-2}\,yr^{-1}$, with some minor variation (Figure 2). Large uncertainties in the top part of the core are propagated from the age-depth model, where ages are extrapolated between the youngest ^{14}C date and the top of the core, which is considered to be recent.

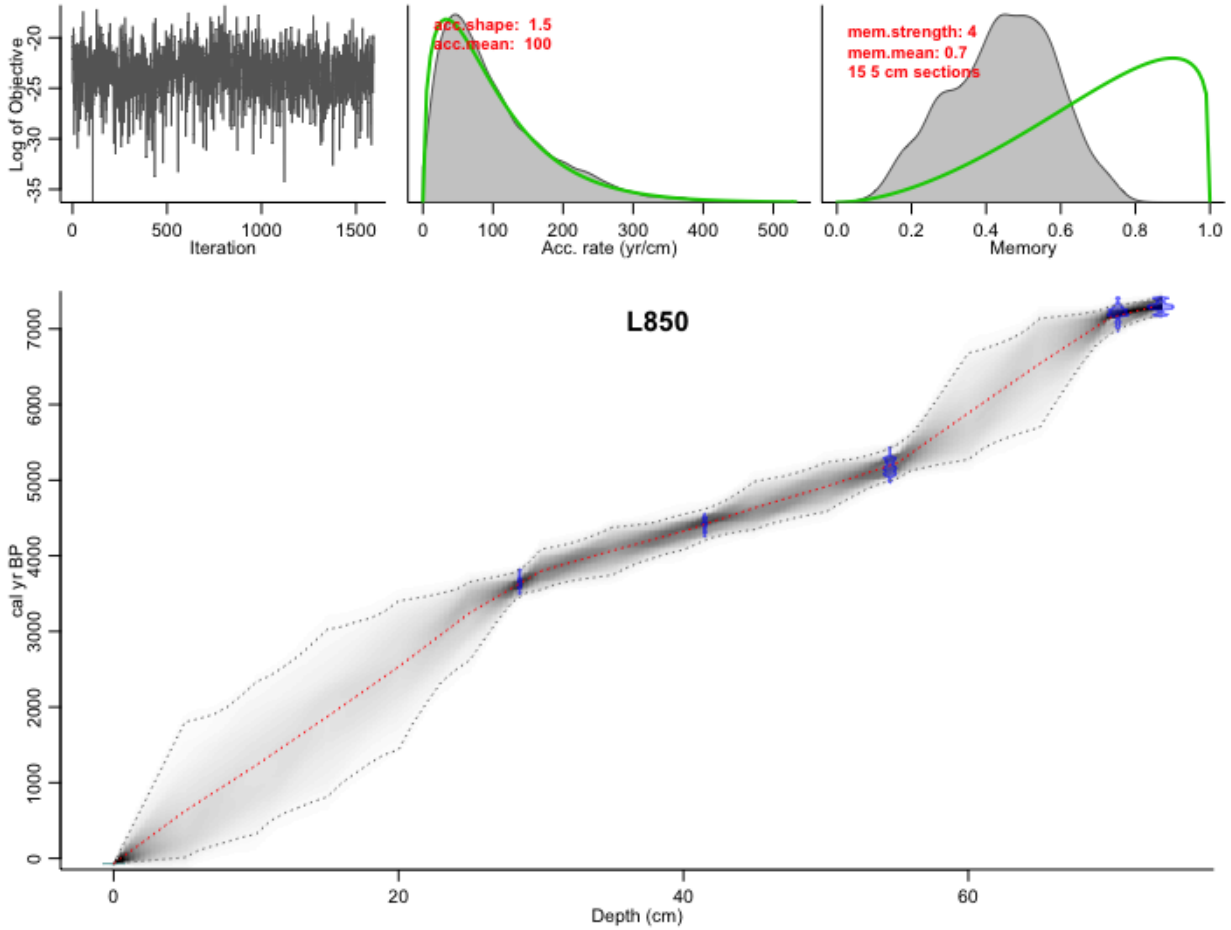


Figure 1. The age-depth model of piston core from 2019 from Lake 850 based on ^{14}C data (see Table 1) using the software package Bacon (Blaauw 2010). The red line is the median probability age from all age-depth iterations, representing the best point estimate of age for any given depth. Grey shading represents the age model probability and contains the 95 % confidence interval (dashed lines). Iteration history (left inset), prior and posterior densities of the mean accumulation rate (middle inset), and prior and posterior of the memory (right inset).

Stable Si isotope record

The stable silicon isotopes measured on cleaned bulk diatoms from the 125-cm-long core from 1999 show generally light isotopic composition of preserved diatoms with subtle variations. Three Holocene periods with different trends (Figure 2) are distinguished based on records from similar lakes in the Scandes mountain range: Sjuodjijaure (Rosén et al. 2001) and Njulla (Bigler et al. 2003). During the early Holocene ($\sim$ 9400–7300 cal. yr BP), there is a decreasing trend from heavier isotopic composition to lighter $\delta^{30}Si_{BSi}$ from the base upward, with the heaviest $\delta^{30}Si_{BSi} = 0.51 \pm 0.03$ ‰ (2SD) at the bottom of the core, a mean $\delta^{30}Si_{BSi}$ of 0.17 ± 0.16 ‰ (1SD) and shifts between two subsequent samples < 0.34 ‰ (Figure 2). The middle Holocene (7300–3900 cal. yr BP) has a light $\delta^{30}Si_{BSi}$ signal that oscillates very little (± 0.25 ‰), including the lightest signal in the entire core ($\delta^{30}Si_{BSi} = -0.49 \pm 0.31$ ‰, 2SD) and mean values of -0.27 ± 0.12 ‰ (1SD). In the late Holocene $\delta^{30}Si_{BSi}$ values are lighter and stable between 3900 cal. yr BP and 2700 cal. yr BP, ranging between -0.34 and -0.11 ‰ with a small shift between two subsequent samples of 0.18 ‰. The topmost part of the core from 2700 cal. yr BP to present shows a gradual shift towards heavier isotopic composition, with values ranging from -0.15 to 0.11 ‰ and varying by 0.18 ‰. The core $\delta^{30}Si_{BSi}$ mean is -0.19 ± 0.16 ‰ (1SD).

Statistical analysis

Pearson correlation tests conducted on the entire core record of XRF, LOI, OC, TOC, BSi and $\delta^{30}Si_{BSi}$ data showed weak or no correlation between $\delta^{30}Si_{BSi}$, BSi and the proxy for production (OC, LOI, TOC) or the proxy for detrital input (MS, Ti).

Magnetic susceptibility, reflecting changes in grain-size, is positively correlated with the detrital input proxy – Ti ($R^2 = 0.56$, p-value $< 2.2 \cdot 10^{-16}$), except at a few depths, where it may be more affected by organic matter content or sediment of autochthonous origin (Figure 2). Similarly, Fe is positively correlated with MS ($R^2 = 0.64$, p-value $< 2.2 \cdot 10^{-16}$), which suggests that MS, Fe and Ti similarly record detrital input. Mineral input is generally low, based on the low XRF counts of detrital elements and on the sedimentation rate. Further, the negative correlation between OC and density ($R^2 = 0.26$, p-value $= 5.18 \cdot 10^{-6}$) suggests that OC matter

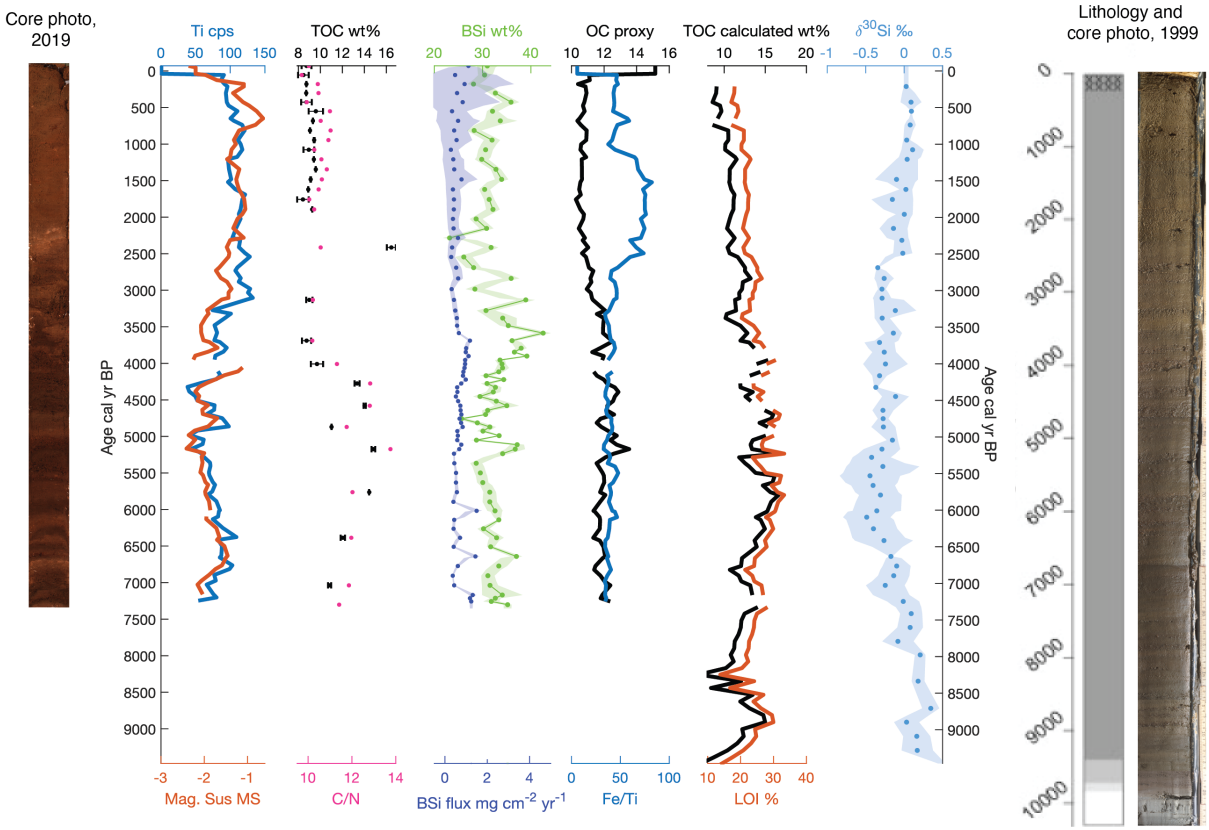


Figure 2. On the left, data for the 2019 piston core: core photo with lithology, titanium (Ti in cps) as a detrital input proxy, magnetic susceptibility (MS) as the grain size changes proxy, total organic carbon (TOC wt%) and C/N ratios for OM composition, biogenic silica (BSi) as SiO_2 weight percentage of dry sediment, BSi fluxes ($mg\,cm^{-2}\,yr^{-1}$), the (Rh_{inc}/Rh_{coh}) as an additional OC proxy and Fe/Ti as an additional detrital input proxy. On the right, data for the core from 1999: TOC (wt%) calculated from LOI and LOI% (Rubensdotter and Rosqvist 2003) are used for correlation of the two cores, stable silicon isotope record (δ^{30}Si in ‰) of cleaned bulk diatoms with shading of 1SD from duplicates, lithology and photo of the 1999 core modified from Rubensdotter and Rosqvist (2003), where dark-gray color represents gyttja, lighter gray layer is clay-gyttja, the lightest gray is gyttja-clay and the white section is clay/silt.

content may be responsible for the changes in the sediment density. Thus, 26 % of the variation in sediment density can be attributed to organic carbon variation and 25 % to detrital input represented by Ti ($R^2 = 0.25$, p-value $= 8.8 \cdot 10^{-6}$). A few pulses of detrital input, identified by elevated MS, Ti and Fe, occur during the late- and mid-Holocene periods around 4700 cal. yr BP, 3000 cal. yr BP and 1700 cal. yr BP.

The negative correlation between BSi and Fe ($R^2 = 0.07$, p-value $= 0.03$) suggests a negative relationship between those two proxies. Iron XRF counts were 10 to 100 times higher than all other identified elements (Figure 2). Lower iron content occurs during the mid-Holocene period, together with high BSi accumulation. Iron is brought by run-off, which is demonstrated by strong positive correlations between Fe, MS and Ti.

Discussion

Factors influencing the diatom accumulation and $\delta^{30}Si_{BSi}$

To explain sedimentary $\delta^{30}Si_{BSi}$, possible factors influencing the source of DSi to the system in which the diatoms grew must be considered. In DSi-limited systems, $\delta^{30}Si_{BSi}$ reflects processes in the watershed and relative changes in DSi sources (Nantke et al. 2019; Phillips 2020; Zhang et al. 2020). Factors influencing the DSi isotopic composition in a lake include riverine diatom production, vegetation, the soil Si pool and secondary mineral formation. Lake 850 is situated above the pine and birch treeline and is surrounded by bedrock with very sparse pockets of poorly developed soils. The lake is fed by small ephemeral inlets. Thus, none of those factors are likely to have had an influence on the δ^{30}Si of the source DSi, although these factors are important in environments below the treeline (Fontorbe et al. 2013; Frings et al. 2016; Nantke et al. 2019).

In DSi-unlimited systems, such as Lake 850, diatom accumulation and $\delta^{30}Si_{BSi}$ are likely reflecting several processes acting together. More specifically: 1. changes in diatom production and species composition derived from changes in summer temperatures and the length of the ice-free period, and 2. relative changes of DSi sources (groundwater vs surficial streams). The Holocene lake history suggests that a combination of low detrital input (Ti, MS) and high BSi production are governing the diatom-rich sediment formation (Figure 2). Low detrital input is not diluting the diatom accumulation, and, thus, BSi

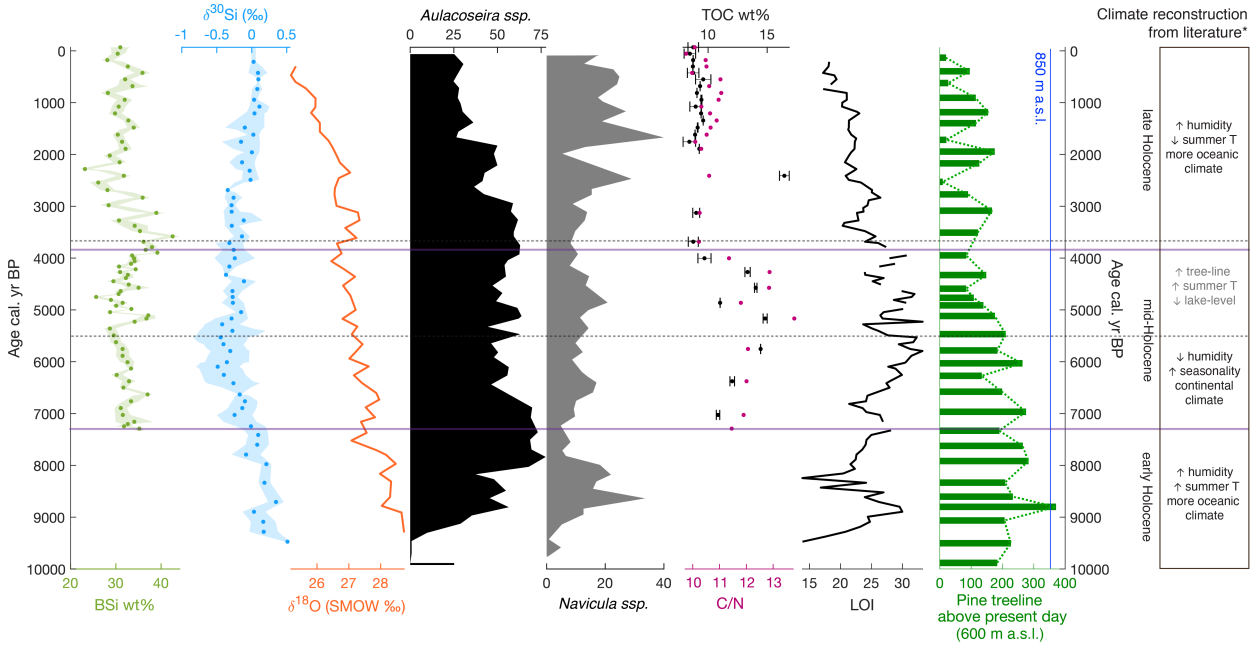


Figure 3. Summary of BSi wt%, TOC wt% and C/N ratios from the 2019 core and δ^{30}Si (‰) from the 1999 core according to ages and compared with previously published δ^{18}O (‰ VSMOW), *Aulacoseira ssp.* and *Navicula ssp.* abundances from the 1999 core (Shemesh et al. 2001). Further, pine treeline reconstruction at northern Scandinavia (Shemesh et al. 2001).

* Climate and vegetation reconstruction based on Barnekow (1999); Berglund et al. (1996); Hammarlund et al. (2002); Rosén et al. (2001); Seppä and Hammarlund (2000).

concentrations as high as 42 wt% accumulated. Additionally, many of the processes influencing $\delta^{30}Si_{BSi}$ and BSi accumulation are partially controlled by changes in climate (Figure 3).

Climate reconstructions in the Abisko area suggest a warmer and more humid early-Holocene influenced by Atlantic air masses (Berglund et al. 1996; Rosén et al. 2001), more continental climate with pronounced seasonality and increased elevation of the pine treeline during the mid-Holocene (Barnekow 1999; Berglund et al. 1996; Hammarlund et al. 2002; Rosén et al. 2001), cooling connected with decreasing insolation (Barnekow 1999) and a more oceanic climate (Berglund et al. 1996) reflected in δ^{18}O (Figure 3, Shemesh et al. 2001) in the late Holocene. Although $\delta^{30}Si_{BSi}$ data show a pattern that coincides with intervals of change in Holocene climate as described above, the δ^{18}O data from Lake 850 do not consistently follow the same patterns (Figure 3, Shemesh et al. 2001). In addition, $\delta^{30}Si_{BSi}$ does not show substantive changes coincident with fluctuations in treeline (Figure 3), which suggests that vegetation is not driving changes in $\delta^{30}Si_{BSi}$.

Diatom production and species composition

No significant correlation of BSi and $\delta^{30}Si_{BSi}$ was found throughout the Holocene, therefore, diatom production is not the only factor driving $\delta^{30}Si_{BSi}$, which is in agreement with the hypothesis that $\delta^{30}Si_{BSi}$ formed in DSi-unlimited lakes does not reflect DSi utilization. However, reported changes in diatom production and species composition (Shemesh et al. 2001) may influence variation in $\delta^{30}Si_{BSi}$ and BSi concentration, as indicated by the similarity in trends. Planktic *Aulacoseira ssp.* have lower relative abundance in the early and late Holocene, when benthic *Navicula ssp.* abundances increased (Figure 3, Shemesh et al. 2001). BSi concentrations are higher during the mid-Holocene in comparison with a decreasing trend in the late Holocene, which coincides with changes in the abundance of heavily silicified *Aulacoseira ssp.* Additionally, increased diatom production and thus the BSi accumulation during mid-Holocene was possibly triggered by a longer growing season, which is suggested by large abundance of planktic species (*Aulacoseira ssp.*, Figure 3) and lower amounts of benthic species (*Fragilaria ssp.*, see Shemesh et al. 2001) (Lotter and Bigler 2000; Smol 1988), as well as by warmer and drier climate indicated in the heavier δ^{18}O values (Figure 3, Shemesh et al. 2001). Stable $\delta^{30}Si_{BSi}$ has heavier values during the early- and late-Holocene, which may be driven by differential species-specific fractionation (Sutton et al. 2013) or heavier DSi sources, such as pore waters at the water-sediment interface (Ehlert et al. 2016; Geilert et al. 2020; Ng et al. 2020) for benthic species, whereas a lighter isotopic signature can be connected to the higher relative abundance of planktic *Aulacoseira ssp.* (Figure 3).

Relative changes in DSi sources

Changes in DSi sources have been demonstrated to influence $\delta^{30}Si_{BSi}$, however, in other studies those changes were connected to changes in watershed vegetation or soil development (Fontorbe et al. 2013; Frings et al. 2016; Nantke et al. 2019). Analysis of recent temporal dynamics in Lake 850 revealed the importance of groundwater supply as a source of DSi fuelling high diatom growth (Zahajská et al. in review). The isotopic signature of the diatoms in Lake 850 shows no significant correlation with the wt% of

BSi or BSi accumulation rate, which supports the hypothesis that the $\delta^{30}Si_{BSi}$ is not connected to production but instead is driven by changes in DSi sources (Nantke et al. 2019). Relative changes in DSi sources during the diatom growing season measured in groundwater (ranging from −0.55 to 0.24 ‰, mean −0.07 ‰) and surficial run-off (ranging from 0.02 to 0.77 ‰, mean 0.5 ‰) in the modern Lake 850 (Zahajská et al. in review) are suggested to be responsible for contemporary $\delta^{30}Si_{BSi}$ values. Moreover, the $\delta^{30}Si_{BSi}$ values are within a narrow range throughout the Holocene, therefore, a stable DSi source must be present through time. The light $\delta^{30}Si_{BSi}$ during the Holocene reflects the absence of processes that fractionate Si in the lake watershed, such as soils or vegetation.

Holocene climate reconstructions of the Abisko area suggest changes in summer temperatures (Barnekow 1999; Berglund et al. 1996; Bigler et al. 2003; Hammarlund et al. 2002; Rosén et al. 2001; Seppä and Hammarlund 2000) , which may have influenced the length of the ice-free period and in turn diatom growth. Thus, Holocene $\delta^{30}Si_{BSi}$ may reflect changes in the duration of the ice-free period and associated changes in the relative proportion of surface inputs versus groundwater as DSi sources. Changes in summer temperatures are connected with changes in vegetation cover, where shrub dominance increases during warmer periods (Myers-Smith et al. 2015). Even though the lake was shown to be above the pine treeline in last 8000 cal. yr BP (Shemesh et al. 2001), the expansion or contraction of shrub vegetation can trigger feedback processes, such as development of soils and/or localized snow patches (Myers-Smith et al. 2011), which can influence the DSi delivery to the lake.

Holocene Lake development

Early Holocene – shift in DSi sources

No BSi and XRF data are available for the early Holocene period, however, the $\delta^{30}Si_{BSi}$ record combined with LOI data and the treeline increase (Figure 3) are consistent with a warm and humid climate. Climate reconstructions from diatoms, pollen, and chironomids for the Abisko region suggest the influence of Atlantic air masses creating more humid and oceanic climate (Berglund et al. 1996; Rosén et al. 2001). The decreasing $\delta^{30}Si_{BSi}$ (Figure 3) can be associated with prolonged ice-free periods, as recorded in an increase of planktic diatom species (Figure 3) and in the $\delta^{18}O$ data reflecting changes in isotopic composition of the influx water originating from precipitation or changes in water balance (Shemesh et al. 2001). Thus, changes in the relative proportion of DSi sources from surficial-dominated DSi input relative to groundwater-dominated DSi sources, would result in the isotopic shift towards lighter $\delta^{30}Si_{BSi}$ based on recent mass balance of the lake (Zahajská et al. in review). Indeed, groundwater represents three times more water input compared to ephemeral streams today and has a modelled isotopic signature between −0.55 to 0.24 ‰ (Zahajská et al. in review). The relative proportion of DSi sources are connected to changes in summer temperature and precipitation.

Mid-Holocene – lake dominated by diatom production and groundwater

Climate reconstructions from other sites in the region suggest a reduced influence of Atlantic air masses, thus a more continental climate with lower humidity, more pronounced seasonality and colder winters (Barnekow 1999; Berglund et al. 1996; Hammarlund et al. 2002; Rosén et al. 2001). Yet, $\delta^{18}O$ data from Lake 850 suggest cooling and higher precipitation in summer (Figure 3, Shemesh et al. 2001).

High and variable TOC together with increased C/N (Figure 3) suggest more terrestrial organic carbon input, especially during the altitudinal increase of treeline in the Abisko area between 5500 and 3400 cal. yr BP (Barnekow 1999; Berglund et al. 1996; Hammarlund et al. 2002; Rosén et al. 2001; Seppä and Hammarlund 2000). This increase in treeline corresponds with an increase of summer temperature documented in nearby Lake Tibetanus (Barnekow 1999; Seppä and Hammarlund 2000) and Lake Sjuodjijaure (Rosén et al. 2001). However, the pine treeline did not reach an altitude of 850 m a.s.l. (Figure 3), and the detrital input (Ti, MS, Fe) during this period is at a minimum and negatively correlated with TOC. Together these data suggest that the total organic carbon is likely originating from the shoreline and littoral areas of the lake.

Additionally, lake-level changes evident in other lakes in Scandinavia (Seppä and Birks 2002, and references therein) suggest the possibility that lake shallowing and expanded growth of terrestrial mosses in littoral areas could account for both increased TOC and C/N but low detrital input. A slight increase in benthic *Navicula ssp.* is consistent with the hypothesis of moderate lake-level change and expanded littoral habitat. Alternatively, the low detrital input could be explained by lower run-off due to a generally drier period.

The diatom assemblage (Figure 3) does not show substantial changes, and the prolonged dominance of heavy silicified *Aulacoseira ssp.* may be responsible for the high BSi accumulation as a result of a prolonged ice-free period (Bigler et al. 2002). A prolonged ice-free period would increase the relative contribution of isotopically lighter groundwater DSi to the lake water balance (Zahajská et al. in review) and produce isotopically lighter $\delta^{30}Si_{BSi}$. Therefore, BSi accumulation is likely connected to an unlimited isotopically light DSi source for diatom uptake (reflected in $\delta^{30}Si_{BSi}$), coupled with a long ice-free period, as indicated by the dominance of *Aulacoseira ssp.* (Figure 3), associated with higher mid-Holocene summer temperatures.

Late Holocene – increased run-off and shortening of ice-free period

The oscillations of BSi concentration during the late Holocene reflect changes in sedimentation due to a slight increase in detrital input (Ti, Fe, MS, Figure 2), coincident with a C/N ratio that suggests increased autochthonous production. Thus, detrital input is likely to be of mineral composition originating from enhanced physical weathering during spring snowmelt with little organic carbon. A positive correlation was found between BSi concentration and the OC proxy ($R^2 = 0.32$, p-value $= 7 \cdot 10^{-3}$), which indicates that BSi accumulation is correlated with autochthonous algal production during this period, supported by C/N values. However, BSi and $\delta^{30}Si_{BSi}$ in this period show no significant

correlation, therefore, other processes, such as changes in DSi sources, changes in diatom production connected to relative species abundance and preservation potential are responsible for the $\delta^{30}Si_{BSi}$ signature. The decreasing trend in OC and LOI, similar to BSi, suggest changes in diatom production likely driven by a shorter ice-free period.

During the late Holocene, a gradual shift towards heavy $\delta^{30}Si_{BSi}$ shows a trend similar to that of the cooling climate reflected in $\delta^{18}O$ (Figure 3), driven by decreasing summer insolation (Barnekow 1999) and a more oceanic climate (Berglund et al. 1996). These changes in climate are responsible for a shorter ice-free period, as reflected in decreasing abundances of *Aulacoseira ssp.*, which grows during longer ice-free periods in a well-mixed water column (Figure 3). Longer winters are responsible for more meltwater, a higher contribution of spring stream water and increased erosion (Rosén et al. 2001; Snowball et al. 1999). A shorter ice-free period is connected with the input of relatively heavier groundwater $\delta^{30}Si_{BSi}$ (Zahajská et al. in review).

Additionally, during the spring snow melt a higher relative contribution of run-off and stream DSi supply is expected to influence the lake Si isotope signature. Further, if the BSi fluxes to the sediment are similar to the longer ice-free period, to accumulate the same BSi during the short ice-free period, the diatom production must be enhanced. Thus, higher DSi uptake during the shorter diatom growth can be reflected in the increased $\delta^{30}Si_{BSi}$ (Zahajská et al. in review). Alternatively, the higher relative abundance of benthic species *Navicula ssp.* can be hypothetically responsible for the trend in $\delta^{30}Si_{BSi}$.

Sparse δ^{30}Si sediment records

Approximately, 100 lakes in Northern Sweden have been investigated for BSi concentrations in surface sediments (Rosén et al. 2010), including Lake 850, but no Si stable isotope analyses have been made on any of these lakes. Lake 850 has a surface sediment BSi concentration of 40.3 wt%, which places this lake into the top 10 % of high BSi concentrations among the 100 lakes studied, and it is the only lake above current treeline with high BSi concentrations (based on data from Rosén et al. 2010). The closest lake in Lappland with a stable silicon isotopic record is Lake Kuutsjärvi, situated below the pine treeline at 341 m a.s.l. (Tallberg et al. 2015). The top 25 cm of sediment from Lake Kuutsjärvi has a stable silicon isotopic signature of sedimentary diatoms similar to the uppermost sediment of Lake 850, although unlike this study, for Lake Kuutsjärvi the $\delta^{30}Si_{BSi}$ was calculated and not measured directly on diatoms.

The mean $\delta^{30}Si_{BSi}$ in Lake 850 is at the lower end of the global marine and freshwater diatom isotopic composition range (Frings et al. 2016). The $\delta^{30}Si_{BSi}$ values throughout the core in this study are generally lighter than published lacustrine $\delta^{30}Si_{BSi}$ from the Arctic Lake El'gygytgyn, where $\delta^{30}Si_{BSi}$ ranges from 0.9 to 1.4 ‰ (Swann et al. 2010), and Lake Baikal $\delta^{30}Si_{BSi}$, where values range from 1 to 1.5 ‰ (Panizzo et al. 2016).

The isotopically light signature of fossil diatoms from Lake 850 (mean -0.19 ± 0.16 ‰) is comparable with $\delta^{30}Si_{BSi}$ in volcanic lakes (Chen et al. 2012; Street-Perrott et al. 2008). The more similar isotopic signature of diatoms from the sediments of volcanic Lake Huguangyan, where $\delta^{30}Si_{BSi}$ ranges from -0.6 ‰ to 1.1 ‰ (Chen et al. 2012), and Lake Rutundu, where values span from -1.3 ‰ to 0.5 ‰ (Street-Perrott et al. 2008), suggest that the DSi sources carry isotopically lighter signature originating from freshly weathered bedrock and lack of processes that would fractionate the DSi.

In Lake Huguangyan, the $\delta^{30}Si_{BSi}$ is driven by diatom production rather than changes in DSi supply (Chen et al. 2012), however, as it lies in a crater and has small watershed, the DSi likely carries isotopically light DSi due to weathering of basaltic bedrock. Lake Rutundu is a small maar lake at a high-altitude with an isotopically light DSi source originating in lavas and tuffs (-0.4 ‰ to -0.5 ‰, Ding et al. 1996). In Lake Rutundu, the changes in maximal $\delta^{30}Si_{BSi}$ are explained by full DSi utilization by diatom production, and the minimal $\delta^{30}Si_{BSi} \sim -1.3$ ‰ is interpreted to originate from isotopically light DSi enriched groundwater supply during low lake-level (Street-Perrott et al. 2008). Therefore, the interpretations of these two lakes are consistent with the hypothesis that the $\delta^{30}Si_{BSi}$ in Lake 850, ranging from -0.49 ‰ to 0.51 ‰, is influenced by an isotopically light DSi source originating from groundwater (Zahajská et al. in review).

Conclusions

Changes in detrital input and TOC suggest that increased run-off and changes in summer temperatures are responsible for the long-term variation in BSi concentration. Additionally, the stable Si isotopes show that the DSi source for BSi likely originates from groundwater discharge into the lake. The diatom-rich sediment in Lake 850 is then formed because of low sedimentation rates, a stable DSi source from groundwater supporting diatom growth that is not DSi-limited. The Holocene environmental changes, such as increases in treeline recorded by other proxies, are not reflected in $\delta^{30}Si_{BSi}$; however, diatom production, species composition and relative proportions of DSi sources driven by climate forcing influence the $\delta^{30}Si_{BSi}$.

The Holocene history of Lake 850 is influenced by climate-inducing changes in the relative proportions of DSi sources, as well as changes in the growing season length, and thus diatom species composition and diatom production. The lighter Si isotopic signature of the diatoms during the mid-Holocene suggests higher groundwater input bringing isotopically lighter DSi into the lake compared to the early- and late-Holocene. The late-Holocene Si isotopic composition of the diatoms is consistent with changes in climate documented in $\delta^{18}O$, driving shortening of the growing season (reflected in diatom species composition) and increased surface run-off that dilutes groundwater input, resulting in heavier Si isotopes.

Additionally, the $\delta^{30}Si_{BSi}$ signature throughout the Holocene varies within a narrow range suggesting stable environmental conditions and a continuous sufficient supply of DSi. The $\delta^{30}Si_{BSi}$ record of Holocene diatoms has a light signature (mean -0.19 ± 0.16 ‰), comparable to the diatom Si signature in volcanic lakes (ranging from -1.3 ‰ to 1.1 ‰; Chen et al. 2012; Street-Perrott et al. 2008). This

suggests that Lake 850 is fed by generally isotopically lighter DSi sources, such as water source with time-limited contact with bedrock and transported over short distance (mean of measured samples ~ 0.5 ‰; Zahajská et al. in review) and groundwater (mean of modelled $\delta^{30}Si_{BSi} \sim -0.07$ ‰; Zahajská et al. in review) compared to mean freshwater $\delta^{30}Si$ (1.26 ‰; Sutton et al. 2018) during the Holocene.

This study shows that combining BSi concentration and the $\delta^{30}Si_{BSi}$ in the sediment has the potential to identify DSi sources responsible for diatom production and accumulation. Comparing our data with other, still sparse, lacustrine sedimentary $\delta^{30}Si_{BSi}$ data reveals the importance of local factors and processes that affect the lake Si cycle. More studies on lacustrine sedimentary $\delta^{30}Si_{BSi}$ are needed to improve the estimates of the sinks and sources in aquatic ecosystems.

Data accessibility All data, if not directly available in tables and supplementary materials, will be uploaded to the PANGAEA database (upon acceptance). In the meantime data is available upon request to the authors.

Acknowledgements

This work was supported by The Royal Physiographic Society in Lund and by the Center for Geosphere Dynamics (UNCE/SCI/006) to PZ, the Swedish Research Council to DJC, and a Swedish Research Council Tage Erlander Professorship to SCF. Further we thank the organizations and the individuals who helped with the fieldwork and/or provided us with equipment and/or advice: Thomas Westin, Keith W. Larson, Erik Lundin, Svante Zachrisson, CIRC, Christian Bigler, Lena Rubensdotter, Gunhild Rosqvist, field assistants Carla Nantke and Ethan Silvester. We thank Mats Rundgren for help with ^{14}C samples evaluation and species identification. We acknowledge Hans Schöberg and Melanie Kielman for assistance during sample preparation and isotope data acquisition. This is Vegacenter contribution number # XXX (number will be provided upon acceptance).

Declaration of conflicting interests

The authors declare that they have no conflict of interest.

References

ANS, Abisko Scientific Research Station (2020) Meteorological data from Abisko Observatory, daily mean 1913-01-01–2019-01-01. Technical report, Abisko Scientific Research Station.

Barnekow L (1999) Holocene tree-line dynamics and inferred climatic changes in the Abisko area, northern Sweden, based on macrofossil and pollen records. *The Holocene* 9(3): 253–265. DOI:10.1191/095968399676322637.

Berglund BE, Barnekow L, Hammarlund D, Sandgren P and Snowball IF (1996) Holocene forest dynamics and climate changes in the Abisko Area, Northern Sweden: The Sonesson model of vegetation history reconsidered and confirmed. *Ecological Bulletins* 45: 15–30. URL http://www.jstor.org/stable/20113180.

Bigler C, Grahn E, Larocque I, Jeziorski A and Hall R (2003) Holocene environmental change at Lake Njulla (999 m asl), northern Sweden: a comparison with four small nearby lakes along an altitudinal gradient. *Journal of Paleolimnology* 29(1): 13–29. DOI:10.1023/A:1022850925937.

Bigler C and Hall RI (2003) Diatoms as quantitative indicators of July temperature: a validation attempt at century-scale with meteorological data from northern Sweden. *Palaeogeography, Palaeoclimatology, Palaeoecology* 189(3): 147–160. DOI: 10.1016/s0031-0182(02)00638-7.

Bigler C, Larocque I, Peglar SM, Birks HJB and Hall RI (2002) Quantitative multiproxy assessment of long-term patterns of Holocene environmental change from a small lake near Abisko, northern Sweden. *The Holocene* 12(4): 481–496. DOI: 10.1191/0959683602hl559rp.

Blaauw M (2010) Methods and code for 'classical' age-modelling of radiocarbon sequences. *Quaternary Geochronology* 5(5): 512–518. DOI:10.1016/j.quageo.2010.01.002.

Bojko O and Kabała C (2016) Loss-on-ignition as an estimate of total organic carbon in the mountain soils. *Polish Journal of Soil Science* 47(2): 71. DOI:10.17951/pjss.2014.47.2.71.

Brodie CR, Casford JS, Lloyd JM, Leng MJ, Heaton TH, Kendrick CP and Yongqiang Z (2011) Evidence for bias in C/N, $\delta^{13}C$ and $\delta^{15}N$ values of bulk organic matter, and on environmental interpretation, from a lake sedimentary sequence by pre-analysis acid treatment methods. *Quaternary Science Reviews* 30(21-22): 3076–3087. DOI:10.1016/j.quascirev.2011.07.003.

Burnett W, Kim G and Lane-Smith D (2001) A continuous monitor for assessment of ^{222} Rn in the coastal ocean. *Journal of Radioanalytical and Nuclear Chemistry* 249(1): 167–172. DOI:10.1023/A:1013217821419.

Chen J, Li J, Tian S, Kalugin I, Darin A and Xu S (2012) Silicon isotope composition of diatoms as a paleoenvironmental proxy in Lake Huguangyan, South China. *Journal of Asian Earth Sciences* 45: 268–274. DOI:10.1016/j.jseaes.2011.11.010.

Conger PS (1942) Accumulation of diatomaceous deposits. *Journal of Sedimentary Research* 12(2): 55–66. DOI:10.1306/d4269143-2b26-11d7-8648000102c1865d.

Conley DJ (1988) Biogenic silica as an estimate of siliceous microfossil abundance in Great Lakes sediments. *Biogeochemistry* 6(3): 161–179. DOI:10.1007/bf02182994.

Conley JD and Schelske C (2001) Biogenic Silica. In: *Tracking environmental change using lake sediments*, volume 3, chapter 14. Springer Netherlands, Dordrecht, pp. 281–293. DOI:10.1007/0-306-47668-1_14.

De La Rocha C, Brzezinski MA, DeNiro M and Shemesh A (1998) Silicon-isotope composition of diatoms as an indicator of past oceanic change. *Nature* 395(6703): 680–683. DOI:10.1038/27174.

De La Rocha CL, Brzezinski MA and Deniro MJ (1997) Fractionation of silicon isotopes by marine diatoms during biogenic silica formation. *Geochimica et Cosmochimica Acta* 61(23): 5051–5056. DOI:10.1016/s0016-7037(97)00300-1.

Ding T, Jiang S, Wan D, Li Y, Li J, Song H, Liu Z and Yao X (1996) *Silicon Isotope Geochemistry*. Geological Publishing House.

Ehlert C, Doering K, Wallmann K, Scholz F, Sommer S, Grasse P, Geilert S and Frank M (2016) Stable silicon isotope signatures of marine pore waters–Biogenic opal dissolution versus authigenic clay mineral formation. *Geochimica et Cosmochimica Acta* 191: 102–117. DOI:10.1016/j.gca.2016.07.022.

Fontorbe G, De La Rocha CL, Chapman HJ and Bickle MJ (2013) The silicon isotopic composition of the ganges and its tributaries. *Earth and Planetary Science Letters* 381: 21 – 30. DOI:10.1016/j.epsl.2013.08.026.

Fortin MC and Gajewski K (2009) Assessing the use of sediment organic, carbonate and biogenic silica content as indicators of environmental conditions in Arctic lakes. *Polar biology* 32(7): 985–998. DOI:10.1007/s00300-009-0598-1.

Frings PJ, Claymans W, Fontorbe G, Rocha CLDL and Conley DJ (2016) The continental Si cycle and its impact on the ocean Si isotope budget. *Chemical Geology* 425: 12–36. DOI: 10.1016/j.chemgeo.2016.01.020.

Frings PJ, Clymans W and Conley DJ (2014a) Amoprhous silica transport int he Ganges basin: Implications for Si delivery to the oceans. *Procedia Earth and Planetary Science* 10: 271–274. DOI:10.1016/j.proeps.2014.08.059.

Frings PJ, Clymans W, Jeppesen E, Lauridsen TL, Struyf E and Conley DJ (2014b) Lack of steady-state in the global biogeochemical Si cycle: emerging evidence from lake Si sequestration. *Biogeochemistry* 117(2): 255–277. DOI:10.1007/s10533-013-9944-z.

Frings PJ, De La Rocha C, Struyf E, van Pelt D, Schoelynck J, Hudson MM, Gondwe MJ, Wolski P, Mosimane K, Gray W et al. (2014c) Tracing silicon cycling in the Okavango Delta, a sub-tropical flood-pulse wetland using silicon isotopes. *Geochimica et Cosmochimica Acta* 142: 132–148. DOI:10.1016/j.gca.2014.07.007.

Geilert S, Grasse P, Doering K, Wallmann K, Ehlert C, Scholz F, Frank M, Schmidt M and Hensen C (2020) Impact of ambient conditions on the Si isotope fractionation in marine pore fluids during early diagenesis. *Biogeosciences* 17(7). DOI: 10.5194/bg-2019-481.

Georg R, Reynolds B, Frank M and Halliday A (2006) New sample preparation techniques for the determination of Si isotopic compositions using MC-ICPMS. *Chemical Geology* 235(1): 95 – 104. DOI:10.1016/j.chemgeo.2006.06.006.

Hamm CE, Merkel R, Springer O, Jurkojc P, Maier C, Prechtel K and Smetacek V (2003) Architecture and material properties of diatom shells provide effective mechanical protection. *Nature* 421(6925): 841–843. DOI:10.1038/nature01416.

Hammarlund D, Barnekow L, Birks HJB, Buchardt B and Edwards TW (2002) Holocene changes in atmospheric circulation recorded in the oxygen-isotope stratigraphy of lacustrine carbonates from northern Sweden. *The Holocene* 12(3): 339–351. DOI:10.1191/0959683602hl548rp.

Hendry KR and Brzezinski MA (2014) Using silicon isotopes to understand the role of the Southern Ocean in modern and ancient biogeochemistry and climate. *Quaternary Science Reviews* 89: 13–26. DOI:10.1016/j.quascirev.2014.01.019.

Khursevich GK, Karabanov EB, Prokopenko AA, Williams DF, Kuzmin MI, Fedenya SA and Gvozdkov AA (2001) Insolation regime in Siberia as a major factor controlling diatom production in Lake Baikal during the past 800,000 years. *Quaternary International* 80: 47–58. DOI:10.1016/s1040-6182(01)00018-0.

Leng MJ, Swann GE, Hodson MJ, Tyler JJ, Patwardhan SV and Sloane HJ (2009) The potential use of silicon isotope composition of biogenic silica as a proxy for environmental change. *Silicon* 1(2): 65–77. DOI:10.1007/s12633-009-9014-2.

Lotter AF and Bigler C (2000) Do diatoms in the Swiss Alps reflect the length of ice-cover? *Aquatic sciences* 62(2): 125–141. DOI: 10.1007/s000270050002.

Meyers PA (1994) Preservation of elemental and isotopic source identification of sedimentary organic matter. *Chemical Geology* 114(3-4): 289–302. DOI:10.1016/0009-2541(94)90059-0.

Myers-Smith IH, Elmendorf SC, Beck PS, Wilmking M, Hallinger M, Blok D, Tape KD, Rayback SA, Macias-Fauria M, Forbes BC et al. (2015) Climate sensitivity of shrub growth across the tundra biome. *Nature Climate Change* 5(9): 887–891. DOI: 10.1038/nclimate2697.

Myers-Smith IH, Forbes BC, Wilmking M, Hallinger M, Lantz T, Blok D, Tape KD, Macias-Fauria M, Sass-Klaassen U, Lévesque E et al. (2011) Shrub expansion in tundra ecosystems: dynamics, impacts and research priorities. *Environmental Research Letters* 6(4): 045509. DOI:10.1088/1748-9326/6/4/045509.

Nantke CK, Frings PJ, Stadmark J, Czymzik M and Conley DJ (2019) Si cycling in transition zones: a study of Si isotopes and biogenic silica accumulation in the Chesapeake Bay through the Holocene. *Biogeochemistry* 146(2): 145–170. DOI:10.1007/s10533-019-00618-w.

Ng HC, Cassarino L, Pickering RA, Woodward EMS, Hammond SJ and Hendry KR (2020) Sediment efflux of silicon on the Greenland margin and implications for the marine silicon cycle. *Earth and Planetary Science Letters* 529: 115877. DOI: 10.1016/j.epsl.2019.115877.

Opfergelt S and Delmelle P (2012) Silicon isotopes and continental weathering processes: Assessing controls on Si transfer to the ocean. *Comptes Rendus Geoscience* 344: 723–738. DOI: 10.1016/j.crte.2012.09.006.

Panizzo VN, Swann GEA, Mackay AW, Vologina E, Alleman L, André L, Pashley VH and Horstwood MSA (2017) Constraining modern-day silicon cycling in Lake Baikal. *AGU Publications* : 556–574DOI:10.1002/2016gb005518.

Panizzo VN, Swann GEA, Mackay AW, Vologina E, Sturm M, Pashley V and Horstwood MSA (2016) Insights into the transfer of silicon isotopes into the sediment record. *Biogeosciences* 13: 147–157. DOI:10.5194/bg-13-147-2016.

Phillips A (2020) *Modelling riverine dissolved silica on different spatial and temporal scales using statistical and machine learning methods*. PhD Thesis, University of Toronto. URL https://tspace.library.utoronto.ca/bitstream/1807/101210/1/Phillips_Anna_202006_PhD_thesis.pdf.

Reimer PJ, Austin WEN, Bard E, Bayliss A, Blackwell PG, Bronk Ramsey C, Butzin M, Cheng H, Edwards RL, Friedrich M and et al (2020) The IntCal20 northern hemisphere radiocarbon age calibration curve (0–55 Cal kBP). *Radiocarbon* : 1–33DOI:10.1017/RDC.2020.41.

Reynolds BC, Aggarwal J, Andre L, Baxter D, Beucher C, Brzezinski MA, Engstrom E, Georg RB, Land M, Leng MJ, Opfergelt S, Rodushkin I, Sloane HJ, van den Boorn SHJM, Vroon PZ and Cardinal D (2007) An inter-laboratory comparison of Si isotope reference materials. *Journal of Analytical Atomic Spectrometry* 22: 561–568. DOI:10.1039/b616755a.

Rosén P, Segerström U, Eriksson L, Renberg I and Birks HJB (2001) Holocene climatic change reconstructed from diatoms, chironomids, pollen and near-infrared spectroscopy at an alpine lake (Sjuodjijaure) in northern Sweden. *The Holocene* 11(5): 551–562. DOI:10.1191/095968301680223503.

Rosén P, Vogel H, Cunningham L, Reuss N, Conley DJ and Persson P (2010) Fourier transform infrared spectroscopy, a new method for rapid determination of total organic and inorganic carbon and biogenic silica concentration in lake sediments. *Journal of Paleolimnology* 43(2): 247–259. DOI: 10.1007/s10933-009-9329-4.

Rubensdotter L and Rosqvist G (2003) The effect of geomorphological setting on Holocene lake sediment variability, northern Swedish Lapland. *Journal of Quaternary Science* 18(8): 757–767. DOI:10.1002/jqs.800.

Ryves DB, Jewson DH, Sturm M, Battarbee RW, Flower RJ, Mackay AW and Granin NG (2003) Quantitative and qualitative relationships between planktonic diatom communities and diatom assemblages in sedimenting material and surface sediments in Lake Baikal, Siberia. *Limnology and Oceanography* 48(4): 1643–1661. DOI:10.4319/lo.2003.48.4.1643.

Seppä H and Hammarlund D (2000) Pollen-stratigraphical evidence of Holocene hydrological change in northern Fennoscandia supported by independent isotopic data. *Journal of Paleolimnology* 24(1): 69–79. DOI:10.1023/A:1008169800682.

Seppä H and Birks H (2002) Holocene climate reconstructions from the Fennoscandian tree-line area based on pollen data from Toskaljavri. *Quaternary Research* 57(2): 191 – 199. DOI: 10.1006/qres.2001.2313.

Shemesh A, Rosqvist G, Rietti-Shati M, Rubensdotter L, Bigler C, Yam R and Karlén W (2001) Holocene climatic change in Swedish Lapland inferred from an oxygen-isotope record of lacustrine biogenic silica. *The Holocene* 11(4): 447–454. DOI: 10.1191/095968301678302887.

Smol JP (1988) Paleoclimate proxy data from freshwater arctic diatoms. *SIL Proceedings, 1922-2010* 23(2): 837–844. DOI: 10.1080/03680770.1987.11899722.

Snowball I, Sandgren P and Petterson G (1999) The mineral magnetic properties of an annually laminated Holocene lake-sediment sequence in northern Sweden. *The Holocene* 9(3): 353–362. DOI:10.1191/095968399670520633.

Street-Perrott FA, Barker PA, Leng MJ, Sloane HJ, Wooller MJ, Ficken KJ and Swain DL (2008) Towards an understanding of late Quaternary variations in the continental biogeochemical cycle of silicon: multi-isotope and sediment-flux data for Lake Rutundu, Mt Kenya, East Africa, since 38 ka BP. *Journal of Quaternary Science: Published for the Quaternary Research Association* 23(4): 375–387. DOI:10.1002/jqs.1187.

Sun X, Andersson P, Humborg C, Gustafsson B, Conley DJ, Crill P and Mörth CM (2011) Climate dependent diatom production is preserved in biogenic Si isotope signatures. *Biogeosciences* 8(11): 3491–3499. DOI:10.5194/bg-8-3491-2011.

Sun X, Andersson P, Land M, Humborg C and Mörth CM (2010) Stable silicon isotope analysis on nanomole quantities using MC-ICP-MS with a hexapole gas-collision cell. *Journal of Analytical Atomic Spectrometry* 25(2): 156–162. DOI:10.1039/B911113A.

Sutton JN, André L, Cardinal D, Conley DJ, De Souza GF, Dean J, Dodd J, Ehlert C, Ellwood MJ, Frings PJ et al. (2018) A review of the stable isotope bio-geochemistry of the global silicon cycle and its associated trace elements. *Frontiers in Earth Science* 5: 112. DOI:10.3389/feart.2017.00112.

Sutton JN, Varela DE, Brzezinski MA and Beucher CP (2013) Species-dependent silicon isotope fractionation by marine diatoms. *Geochimica et Cosmochimica Acta* 104: 300 – 309. DOI:10.1016/j.gca.2012.10.057.

Swann GE, Leng MJ, Juschus O, Melles M, Brigham-Grette J and Sloane HJ (2010) A combined oxygen and silicon diatom isotope record of Late Quaternary change in Lake El'gygytgyn, North East Siberia. *Quaternary Science Reviews* 29(5-6): 774–786. DOI:10.1016/j.quascirev.2009.11.024.

Tallberg P, Opfergelt S, Cornelis JT, Liljendahl A and Weckström J (2015) High concentrations of amorphous, biogenic Si (BSi) in the sediment of a small high-latitude lake: implications for biogeochemical Si cycling and for the use of BSi as a paleoproxy. *Aquatic Sciences* 77: 293–305. DOI:10.1007/s00027-014-0387-y.

Vandevenne F, Barão L, Ronchi B, Govers G, Meire P, Kelly E and Struyf E (2015) Silicon pools in human impacted soils of temperate zones. *Global Biogeochemical Cycles* 29(9): 1439–1450. DOI:10.1002/2014gb005049.

Yool A and Tyrrell T (2003) Role of diatoms in regulating the ocean's silicon cycle. *Global Biogeochemical Cycles* 17(4). DOI:10.1029/2002gb002018.

Zahajská P, Olid C, Stadmark J, Fritz SC, Opfergelt S and Conley DJ (in review) Modern silicon dynamics of a small high-latitude subarctic lake. *Biogeosciences Discuss., in review* DOI:10.5194/bg-2020-441.

Zhang A, Zhang J and Liu S (2020) Spatial and temporal variations of dissolved silicon isotope compositions in a large dammed river system. *Chemical Geology* : 119645DOI:10.1016/j.chemgeo.2020.119645.

Supplemental material

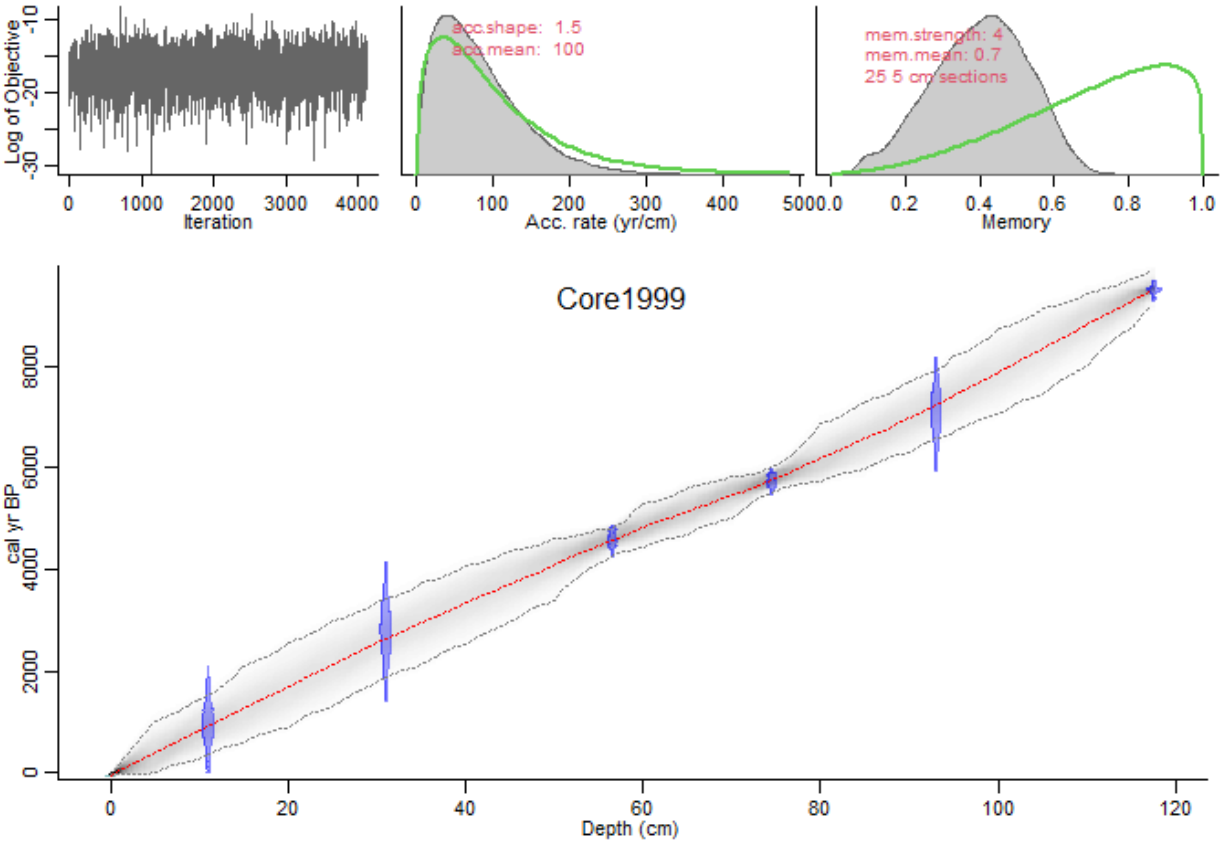


Figure S1. The age-depth model of Lake 850 based on piston core from 1999 (Shemesh et al. 2001). Red line is the median probability age from all run age-depth iterations, representing the best point estimate of age for any given depth. Grey shading represents age model probability and contains the 95% confidence interval (dashed lines). Iteration history (left inset), prior and posterior densities of the mean accumulation rate (middle inset), and prior and posterior of the memory (right inset).

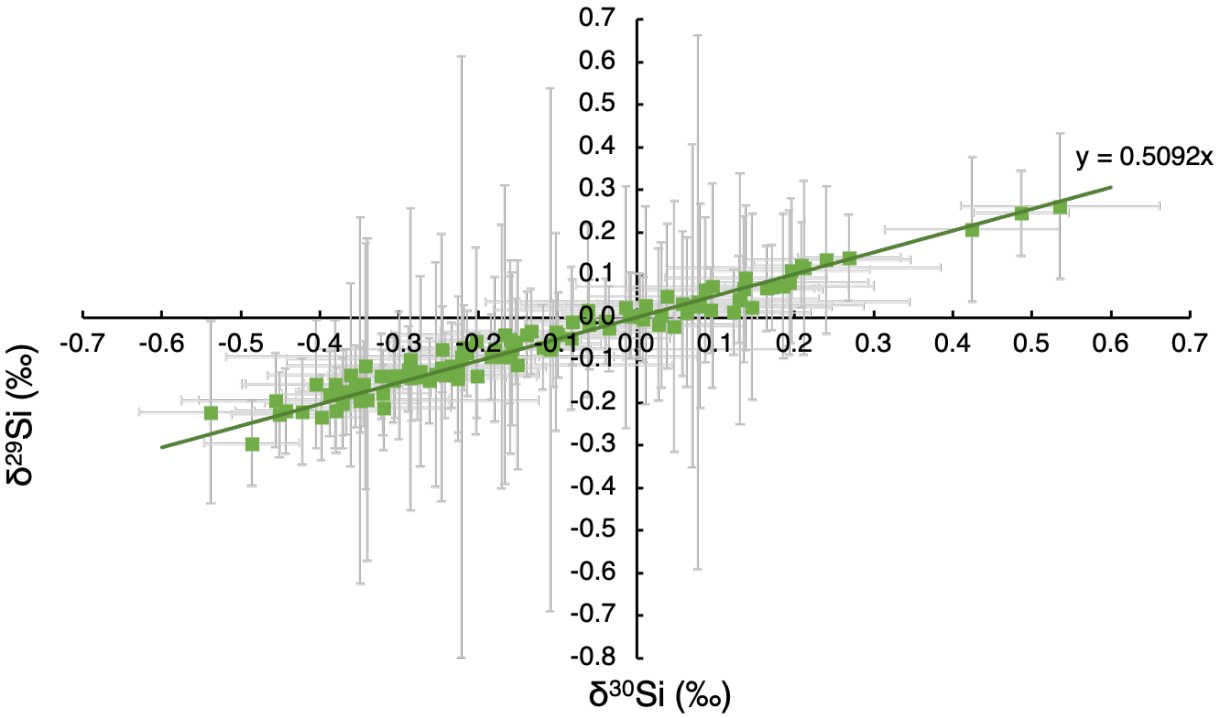


Figure S2. Three-isotopes plot of all Si isotope measurements. All data follow the expected mass-dependent fractionation line with slope 0.5092 (full green line) (Reynolds et al. 2007), $\delta^{29}\mathrm{Si} = 0.48 \cdot \delta^{30}\mathrm{Si}$, $\mathrm{R}^2 = 0.96$, $n = 104$.

Paper IV



"For a research worker the unforgotten moments of his life are those rare ones which come after years of plodding work, when the veil over nature's secret seems suddenly to lift & when what was dark & chaotic appears in a clear & beautiful light & pattern."

Gerty Cori

Cover photo: Yellowstone Lake in August 2018

Picture credits: Petra Zahajská

Impact of Holocene sub-lacustrine hydrothermal activity on the Si cycle and diatom-rich sediment accumulation in Yellowstone Lake

Petra Zahajská[1], Patrick J. Frings[2], François Gaspard[3], Sophie Opfergelt[3], Johanna Stadmark[1], Sherilyn C. Fritz[4], Rosine Cartier[1] and Daniel J. Conley[1]

[1] *Department of Geology, Lund University, Lund, Sweden*
[2] *Section 3.3 Earth Surface Geochemistry, German Research Centre for Geosciences (GFZ), Telegrafenberg, 14473 Potsdam, Germany*
[3] *Earth and Life Institute, Université catholique de Louvain, Louvain-la-Neuve, Belgium*
[4] *Department of Earth and Atmospheric Sciences and School of Biological Sciences, University of Nebraska–Lincoln, Lincoln, Nebraska, USA*

Abstract

Recent lake water, tributaries and hydrothermal vent fluids from Yellowstone Lake were analyzed for their DSi concentration, δ^{30}Si, and Ge/Si composition to aid in evaluating the sources of variability in the lake's Si cycle. In addition, elemental composition, BSi content, δ^{30}Si, and Ge/Si ratio were analyzed in sedimentary records spanning the last 9880 cal. yr BP from a hydrothermally affected area and an undisturbed deep-basin area of the lake to identify any impact on Si cycling of past hydrothermal explosions and disturbance by Mazama ash deposition.

Combinations of BSi, δ^{30}Si and Ge/Si with XRF and lithology data revealed that Yellowstone Lake has a resilient biogeochemical system on long timescales. Several of the hydrothermal explosions identified in the lithology had no identifiable impact on BSi accumulation or on the δ^{30}Si signature. Both cores show similarities that suggest a stable and homogeneous DSi source across the entire lake. Additionally, the narrow range of δ^{30}Si and Ge/Si values of a single diatom species, *Stephanodiscus yellowstonensis*, suggests that the productive layer of the lake was well mixed and biogeochemically very stable and that consistently high hydrothermal inputs of Si which occurred throughout the Holocene mask the disturbance events.

Variation in BSi concentration through time is correlated with changes in the δ^{30}Si fossil diatom record, which reflects diatom fractionation during production. An increasing trend towards heavier δ^{30}Si in both cores follows known trends in summer insolation, summer temperatures and lake water-column mixing during the Holocene. This suggests that climate forcing, which is driving diatom production, is reflected in δ^{30}Si. However, δ^{30}Si values also record changes in the relative proportion of DSi sources, diatom production or hydrothermal inputs.

keywords: diatom, Silicon, isotopes, Germanium, Yellowstone, sediment

1 Introduction

Yellowstone Lake lies in the Yellowstone volcanic caldera, which formed during the last cataclysmic eruption of the Yellowstone Plateau Volcanic Field at 0.64 Ma (Christiansen, 2001). The volcanism in Yellowstone National Park has a bimodal character, whereby both basic and acidic activity leads to the formation of andesites and rhyolites (Morzel et al., 2017). The Yellowstone Lake region includes active fault systems and has had postglacial (<15–12 ka) hydrothermal explosion events (e.g., Mary Bay and Elliott's Crater), as well as continued active hydrothermalism (Morgan et al., 2007). This hydrothermalism, driven by the interaction of meteoric water with mantle heat and volcanic gasses, influences the whole Yellowstone Caldera region (Hurwitz and Lowenstern, 2014) and occurs both within the lake and at well-known hy-

drothermal areas around the lake (Morgan et al., 2007). Thus, Yellowstone Lake is enriched in various dissolved elements (As, B, Cl, Cs, Ge, Li, Mo, Sb) that originate from hydrothermal vent fluids, and an elemental mass balance suggests that the lake is a mixture of 1 % hydrothermal source and 99 % inflowing surface water (Balistrieri et al., 2007; Gemery-Hill et al., 2007).

Lakes are considered to be sinks in the global Si cycle as they accumulate biogenic silica (BSi) mainly originating from diatom production (Frings et al., 2014). Silicon is enriched in Yellowstone Lake with an mean dissolved silicon (DSi) concentration of 12 mg SiO_2 L^{-1} (Gemery-Hill et al., 2007) compared to a global river mean of 9.5 mg SiO_2 L^{-1} (Dürr et al., 2011), a high-altitude alpine lakes range from 0 to 8.6 mg SiO_2 L^{-1} (Mosello, 1984; Psenner, 1989), a USA lake mean of 8.6 mg SiO_2 L^{-1} (Wang et al., 2016), and a global lake DSi mean of 1.18 mg SiO_2 L^{-1} (Frings et al., 2014).

Diatoms are important primary producers in Yellowstone Lake (Interlandi et al., 1999; Kilham et al., 1996), and the high DSi concentrations have two important ecological implications: diatom production is conferred a competitive advantage relative to other algal groups, and the preservation efficiency of diatom frustules in the sediment is enhanced. The result is high BSi content (up to 40 wt%) in the sediment (Conley, 1998).

Several large sublacustrine hydrothermal events have occurred in Yellowstone Lake during the Holocene and influenced the lake basin. The explosions have been localized at the northern part of the lake and are recorded in the sedimentology and trace-element geochemistry of the lake sediment (Morgan et al., in preparation). The impact of those explosions on the lake system has been studied through diatom (Brown, 2019) and pollen (Schiller, 2020) assemblages, as well as using stable oxygen isotopes of diatom silica, where all proxies show a very limited reaction to the explosions. However, as the hydrothermal vent fluids entering the lake are enriched in DSi (Balistrieri et al., 2007; Fowler et al., 2019b), hydrothermalism and the explosions may have influenced the lake Si cycling and the BSi concentration in the sediment throughout the Holocene, but this has not been investigated previously.

Silicon isotope geochemistry is a powerful tool that exploits differences in the relative abundances of the three stable Si isotopes in natural systems – ^{28}Si, ^{29}Si and ^{30}Si – to trace the Si origin. During uptake of DSi, diatoms actively discriminate against the heavier silicon isotope ^{30}Si, which results in the residual solution being enriched in heavier isotopes (De La Rocha et al., 1997). The DSi released from primary mineral weathering or hydrothermally formed DSi carries the isotopic signature of the primary minerals from the rock. The DSi transported through soils after secondary mineral formation, or DSi of lake water after diatom production will generally have an isotopically heavier signature, because the lighter isotopes are preferentially taken up by those processes (Cornelis et al., 2014; De La Rocha et al., 1997; Ziegler et al., 2005). The silicon isotope composition of rivers and oceans (Opfergelt and Delmelle, 2012) is thus almost exclusively heavier than silicate bedrock. The stable silicon isotope ratios of diatoms (expressed as $\delta^{30}Si$, the deviation in permille of the $\frac{^{30}Si}{^{28}Si}$ ratio from a reference material) can be used as paleoproxy for past Si cycling and reflects changes in DSi sources and nutrient supply into the system (Nantke et al., 2019; Swann et al., 2010). However, an outstanding problem in diatom $\delta^{30}Si$ interpretation is the extent to which diatom $\delta^{30}Si$ reflects changes of DSi sources versus diatom production and dissolution (Opfergelt et al., 2011; Panizzo et al., 2017; Street-Perrott et al., 2008).

To help constrain DSi sources, the trace element germanium (Ge), which mimics the chemical behavior of Si, is used in this study. Ge has a similar ionic radius and thus forms Ge–O with a similar covalent bond length as Si–O, permitting easy substitution in silicon tetrahedra. Additionally, Ge has identical outer electronic structures and so is often considered to behave as a heavier stable Si isotope (Froelich et al., 1992), though there are also important differences in geochemical behavior of the two elements. Dissolved Ge (DGe) originates from similar sources as DSi – the weathering of primary silicate minerals (Mortlock and Frohlich, 1987). Similar to the stable isotopes of silicon, Ge and Si are fractionated relative to each other during most chemical and biological processes, and thus Ge/Si ratios change as a result of fractionation (Froelich et al., 1989; Murnane and Stallard, 1988; Shemesh et al., 1989). Ge is a trace element in bedrock, whereas Si is a major rock-forming element. Ge/Si ratios in bedrock are around 1.5–3 µmol/mol (Mortlock et al., 1993; Rouxel et al., 2006; Tribovillard, 2013; Tribovillard et al., 2011). Because Ge is preferentially incorporated into secondary weathering products, Ge/Si ratios in river waters are typically even lower, ranging from 0.1 to 1.3 µmol/mol (Filippelli et al., 2000; Froelich et al., 1992; Hammond et al., 2004; Mort-

lock and Frohlich, 1987). However, hydrothermal fluids carry higher DGe concentration relative to DSi, because Si is preferentially precipitated in quartz during the cooling of the hydrothermal fluids, and, thus, Ge/Si ranges from 2 to 1000 µmol/mol (Arnórsson, 1984; Evans and Derry, 2002; Kurtz et al., 2002; Mortlock et al., 1993; Pokrovski and Schott, 1998). As a result, the influence of Ge-enriched hydrothermal fluids in pristine environments, such as Yellowstone Lake, can be identified through Ge/Si ratios. Furthermore, Ge/Si can be used to understand the terrestrial filter of DSi delivery into the ocean (Frings et al., 2014; Sutton et al., 2018), as waters are enriched in Ge by terrestrial processes, such as diatom production and secondary mineral formation, which fractionate the Ge/Si (Froelich et al., 1989; Murnane and Stallard, 1990). Additionally, the Ge/Si ratio can be used to estimate chemical weathering intensity, where relatively higher Ge/Si ratios in clays start to dissolve and thus, the Ge/Si in waters carries this signal and represent enhanced weathering intensity (Filippelli et al., 2000; Froelich et al., 1992; Kurtz et al., 2002; Lugolobi et al., 2010; Shemesh et al., 1989). Hydrothermal fluids can also have Ge/Si ratios similar to waters with intensive secondary mineral dissolution (Froelich et al., 1992; Kurtz et al., 2002), and, in these cases, the two cannot be distinguished. Using stable silicon isotopes and Ge/Si together can help to identify sources of DGe and DSi, as well as processes influencing Si and Ge cycling.

A handful of studies have examined uptake of DGe by diatoms (Azam et al., 1973; Froelich et al., 1989; Murnane and Stallard, 1988; Shemesh et al., 1989; Sutton et al., 2010) and have identified a discrimination by diatoms against Ge, expressed as a distribution coefficient (K_D) defined as $K_D = \frac{[Ge/Si]_{diatom}}{[Ge/Si]_{solution}}$ (Froelich et al., 1992, 1989; Murnane and Stallard, 1988; Sutton et al., 2010). The K_D ranges from 0.4 to 1.2 and Ge/Si ratios of diatoms range from 0.3 to 2.1 µmol/mol (Froelich et al., 1992; Mortlock et al., 1991; Shemesh et al., 1989; Sutton et al., 2010; Tribovillard, 2013). Furthermore, Ge uptake by diatoms was shown to be dependent on DSi concentration and the Ge/Si ratio in solution. High concentrations of both Si and Ge result in a distribution coefficient of up to 1.2 (Froelich et al., 1992), which translates to no discrimination against Ge relative to Si, or even a slight positive discrimination. To our knowledge, only one study has looked at Ge/Si ratios of fossil lake diatoms, together with measurements in lake water and bedrock in the watershed (Filippelli et al., 2000). They concluded that relative changes in the preferential weathering of different minerals (easy erodible mica vs quartz) through time in addition to clay mineral transformations, may affect Ge/Si ratio in lake paleorecords.

Here, we use a fossil diatom record to test the hypothesis that hydrothermalism in the watershed and Holocene hydrothermal explosions identified previously in Yellowstone Lake influenced lake Si cycling and BSi concentrations in the sediment, with pronounced changes in lake sediment BSi, δ^{30}Si and Ge/Si records following hydrothermal explosion events. After a hydrothermal explosion, we hypothesize there could be an excess of DSi in the lake water, which would result in higher BSi production and also lower diatom dissolution and thus a transient increase in BSi accumulation rates. We hypothesize a decrease in the δ^{30}Si signal around the hydrothermal explosion deposits, because lower δ^{30}Si DSi is brought into the lake by hydrothermal fluids. We use Ge/Si ratios of recent water and fossil diatoms to couple the changes in silicon isotopes with hydrothermal input into the lake.

2 Study site

Yellowstone Lake (YL) is located in north-western Wyoming, USA (44°29N, 110°21W) in Yellowstone National Park. The lake is at an elevation of 2358 m a.s.l. With its surface area of 344 km^2 and depth of 131 m, it is the largest high-altitude lake in North America (Morgan et al., 2003). The main lake basin is on the eastern margin of the Yellowstone Caldera, and the southern parts of the lake, shaped by the glacial scour, are located outside of the caldera (Morgan et al., 2003). The Yellowstone Caldera rim divides the lake into two different bedrock provinces. The north-western part of YL overlies rhyolitic post-caldera bedrock (Figure 1, pink), whereas the south-eastern part is characterized mainly by Quaternary detrital deposits – silt, sand, gravel and till (Figure 1, yellow), Quaternary rhyolitic ash-flow tuff (Figure 1), orange) and Pleistocene rhyolite flow and andesitic alluvial facies with volcanic breccia (Figure 1, gray).

Several large hydrothermal-explosion events have occurred in the lake in the last 15 ka, including the Mary Bay (13 ka) and Elliott's Crater (~8 ka) hydrothermal-explosions (Figure 1, Morzel et al., 2017). Those explosions were sublacustrine eruptions accompanied with rapid ejection of boiling water, steam, sediment, mud and rock fragments from source craters (Browne and Lawless, 2001; Muffler

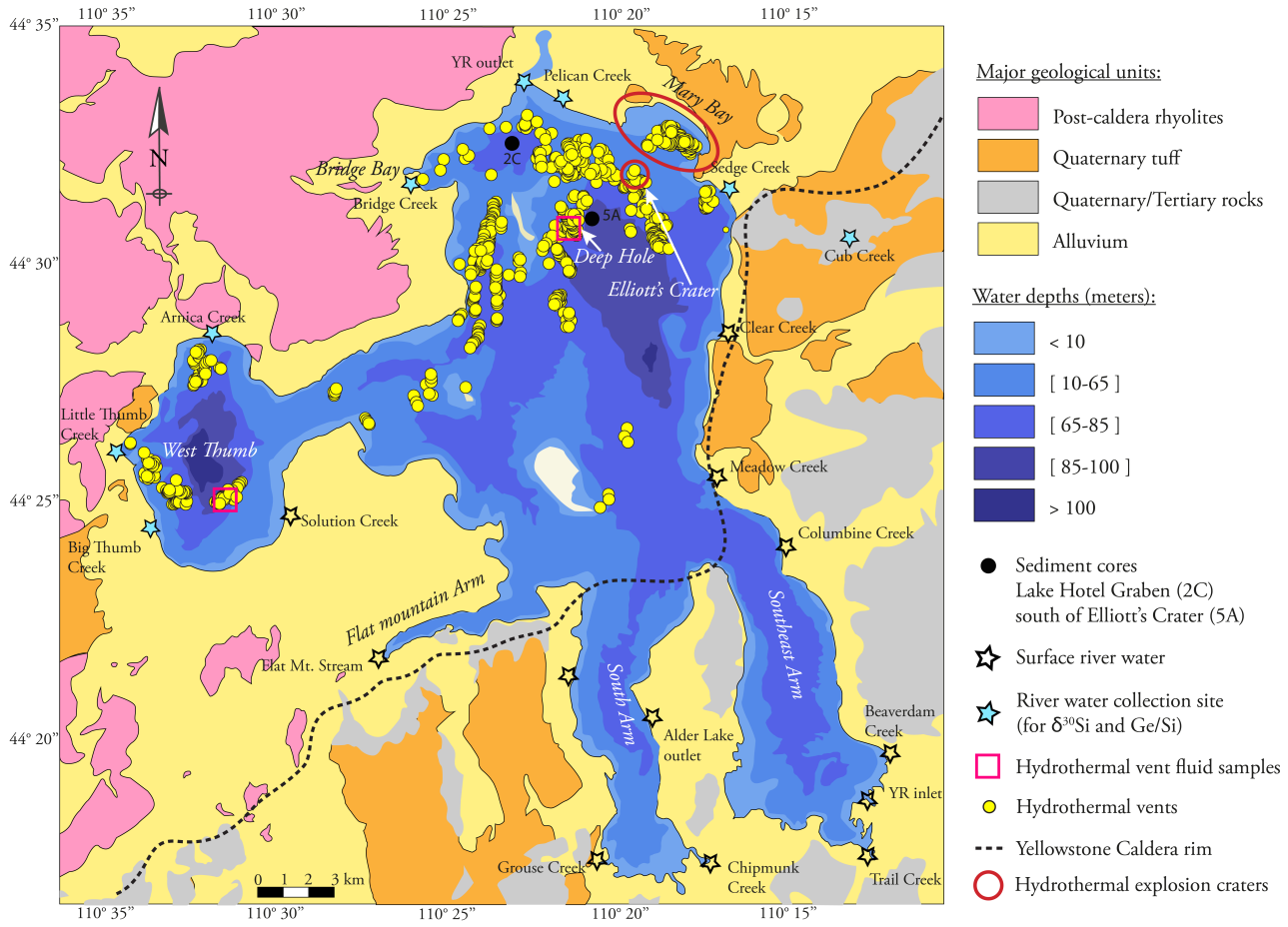


Figure 1: A simplified geological map of Yellowstone Lake with lake bathymetry (modified from Morgan et al. (2007)). Sampling sites for sediment cores are marked as solid black circles, collected river samples shown as blue-filled stars, and hydrothermal vent fluids locations are in pink squares. All major tributaries which were not sampled are added as empty stars and the hydrothermal vents present in the lake are shown as yellow circles. The dashed line is defining the Yellowstone Caldera rim, where the north-west of Yellowstone lake is in the Yellowstone Caldera.

et al., 1971). The largest hydrothermal explosions, such as Mary Bay, may have had an explosion column up to 1.9 km in height (Morgan et al., 2009). The deposits of Mary Bay explosion are distributed up to ~2.5 to 4 km from the crater rim and cover ~30 km^2, whereas the Elliot's Crater deposits extend ~0.8 km from the rim. Hydrothermal fluids carry high concentrations of DSi and other elements (Balistrieri et al., 2007; Fowler et al., 2019b), and the geochemical signature of those fluids is recognized in deposits surrounding the vents (Shanks et al., 2007).

The hydrothermal features in YL are caused by convective-meteoric hydrothermal fluid circulation, steam separation during fluid ascent, and possible CO_2 accumulation and release above an actively degassing magma chamber (Morgan et al., 2007). Two types of hydrothermal vent fields have been found within the lake. In the West Thumb area, the vents have a liquid form with distinct elemental composition, enriched in Cl, Sb or W (Fowler et al., 2019a; Shanks et al., 2007), whereas in the Deep Hole area of the central basin, the character of the fluids is gaseous, with condensation at shallow depths and mixing with the lake bottom waters (Fowler et al., 2019b).

Yellowstone Lake was glaciated until ca 14 ka. Since deglaciation, changes in summer insolation have produced variations in regional temperature and effective moisture that are reflected in diatom community shifts (Brown, 2019; Lu et al., 2017), endemic diatom species evolution (Theriot et al., 2006), fire history and vegetation shifts (Brown et al., unpublished, Huerta et al., 2009; Iglesias et al., 2018; Millspaugh

et al., 2000; Whitlock, 1993), and geochemical records (Whitlock et al., 2012). The region has a subarctic climate regime, influenced by Arctic and Pacific air masses in winter and by warm and moist Pacific air masses in summer (Despain, 1987). The watershed has been covered by coniferous forest for the last 9800 years, which has been disturbed by forest fires with an mean frequency of 2–5 fires per 1000 years (Millspaugh et al., 2000). The lake diatom community and the $\delta^{18}O$ highlighted a progressive change towards cooler and wetter conditions during the Holocene associated with changes in lake stratification and nutrient inputs driven by changes in temperature and precipitation (Brown, 2019; Brown et al., unpublished).

3 Methods

3.1 Sampling

Sediment cores YLAKE-YL16-2C-1K (hereafter '2C', taken at 61 m water depth, core length 11.62 m) and YLAKE-YL16-5A-1K ('5A', taken at 102 m water depth, core depth 11.02 m) were collected with a Kullenberg sampler (Kelts et al., 1986) in 2016. Core 2C was retrieved from the deep basin at the north of the lake, and core 5A was located in the proximity of Elliott's Crater (Figure 1). Lithologic description (Morgan et al., unpublished), subsampling, magnetic susceptibility (MS) measurements, and X-ray fluorescence core scanning (XRF) were done in the LacCore facility at the University of Minnesota. Subsampling of both cores was done at 8 cm intervals, and ~2 cm^3 of wet bulk sediment was sampled and freeze dried. MS was measured on both whole and split cores. XRF scanning was done at 0.5 cm resolution with 120 s scanning time with a Mo X-ray source at 30 kV and 15 mA to evaluate bulk sediment elemental (Al, Si, K, Ca, Ti, Fe, Rb, Sr, S, Mn, Zn, Zr, Cu, and As) composition.

Water samples from tributaries in the northern Yellowstone Lake watershed, situated within the Yellowstone Caldera and influenced by hydrothermal springs, were collected in August 2016 and June 2017 (Figure 1). Tributaries from outside of the Yellowstone Caldera are not used in this study as they are not hydrothermally affected. Sampling was conducted to constrain two different hydrological regimes – a low-flow regime at the end of the growing season and a high-flow regime during snowmelt (based on the Yellowstone River outlet hydrograph, USGS database). All water samples were filtered through 0.45 µm Sterivex-HV Durapore filters and acidified to pH 2 using HCl directly in the field. Samples of hydrothermal fluids from the Deep Hole and the West Thumb vent fields (Figure 1) were obtained 25 times diluted (see sampling details in Fowler et al. (2019b)) from collaborators from the HD-YLake project, University of Minnesota, with DSi already measured (Fowler et al., 2019b). Hydrothermal fluid samples with low DSi concentration were concentrated by MAGIC methodology following Zhang et al. (2014). All water samples were purified by cation-exchange chromatographic separation for analyses of stable silicon isotopes (Georg et al., 2006).

3.2 Biogenic silica, total organic carbon, and dissolved silicon measurements

Sediment biogenic silica concentrations were analyzed using a weak-alkaline extraction (40 ml of 0.1 M Na_2CO_3, at 85 °C) of the bulk, freeze-dried, homogenized sediment (30 mg) adapted from Conley and Schelske (2001). The original protocol is premised on the idea that the BSi dissolves within first 2 h of extraction, and so an increase in DSi concentration in subsamples at 3, 4 and 5 h or 6 h of extraction reflect the (slower) dissolution of lithogenic material. The potential non-biogenic amorphous silica dissolution during the extraction was tested by a prolonged subsampling scheme up to 24 h (Clymans et al., 2015) and resulted in no surplus amorphous SiO_2 dissolved after 3 h. Thus, the mineral dissolution correction was not applied and the estimates of BSi were simply calculated as the mean of subsamples. All samples ($n = 277$) were analyzed with two to four full chemical replicates. Previous experiments on tephra samples have shown that the possible contribution from volcanic glass to BSi concentration during the alkaline extraction ranges between 0.2 and 4 wt% SiO_2 (Clymans et al., 2015).

The total organic carbon (TOC) and total nitrogen content (TN) in the sediment were analyzed using an elemental analyzer (COSTECH ECS4010) at the Department of Geology, Lund University. Freeze-dried, homogenized samples ($n = 74$) were packed in tin capsules for TOC and TN analysis. All samples were analyzed in duplicates. Additionally, 18 % and 10 % of TOC samples throughout cores 2C and 5A, respectively, were tested for carbonate content by a decalcifying procedure prior to the TOC measurement following Brodie et al. (2011).

All water samples were analyzed for DSi concen-

trations using the automated molybdate-blue method (Strickland and Parsons, 1972) with a SmartChem 200, AMS System™ discrete analyzer. The laboratory long-term external reproducibility of DSi concentration is within 4 %, and the quantification limit is 0.017 mg L^{-1}.

3.3 Preparation of diatoms for Si and Ge analyses

Freeze-dried bulk sediment (2 cm^3 wet volume) was treated with H_2O_2 and HCl to remove organics and carbonates, respectively (Morley et al., 2004). Additionally, detrital particles were removed by high liquid density separation using sodium polytungstate (SPT) at density range of 2.05 to 2.1 g cm^{-3}. Separated fraction was sieved and rinsed on 25 µm sieve and 5 µm filer. Final cleaning from clay minerals was conducted by using 0.05 M sodium pyrophosphate for 0.5 to 24 h (with occasional shaking or sonication), and pure diatoms were obtained by another sieving at 25 µm. Sieving resulted in a single species *Stephanodiscus yellowstonensis* in the fraction >25 µm, and thus potential biases due to species specific fractionation were reduced. The sample purity was visually checked using a scanning electron microscope (Figure S1), and the absence of contamination was confirmed by energy dispersive spectroscopy (EDS) mapping, both on Tescan Mira3 at the Department of Geology, Lund University. A similar procedure was applied to hydrothermal deposits and Mazama ash layer samples resulting in a cleaned mixture of diatoms and volcanic glass, which was further cleaned for Si isotopes analysis.

Clean single species diatom samples (0.8–1.5 mg) were digested in 0.5 ml of 0.4 M NaOH (analytical purity) at 50 °C for at least 48 h. After initial dissolution, samples were diluted by Milli-Q® water to lower DSi concentrations to prevent SiO_2 precipitation, and after 24 h they were neutralized by 0.4 M Suprapur® HCl. Before further sample processing, the silicon recovery was checked. Based on the initial individual sample amount weight and the volume of solvents, the expected DSi concentrations (as Si mg L^{-1}) were calculated and then compared to DSi concentration measured in the produced solutions. The silicon recovery was 90 to 100 %.

Diatom sample solutions were purified prior to stable Si isotope and Ge/Si analyses by ion-exchange chromatographic separation using 1.5 ml cation-exchange resin DOWEX® 50W-X8 (200–400 mesh) following the method by Georg et al. (2006). International Si standard NIST reference material RM-8546 (NBS-28), secondary standard Diatomite prepared by NaOH fusion (Georg et al., 2006) and full procedural blanks were purified along the sample purification using the identical protocol.

3.4 Stable silicon isotopes and Ge/Si analyses

The stable isotopes of purified water samples and *Stephanodiscus yellowstonensis* diatom samples were measured on a NuPlasma (II) HR multi-collector inductively conducted plasma mass spectrometer (MC-ICP-MS, Nu Instruments™) with an Apex HF desolvation nebulizer at the Vegacenter, Swedish Museum of Natural History, Stockholm. Samples were checked for contamination by measuring the ^{28}Si signal of full procedural blanks that showed less than 0.35 % of the total ^{28}Si signal. Samples were diluted to 2–3 mg L^{-1} and matrix matched with standards in 0.12 M SeaStar HCl. Further, all samples and standards were doped to contain 3 mg L^{-1} of Li (IPC-MS standard) to match the matrix of the Vegacenter standards (Sun et al., 2010). Stable Si isotope data are reported as deviations of $^{30}Si/^{28}Si$ and $^{29}Si/^{28}Si$ from the NBS-28 standard in per mil (‰), denoted $\delta^{30}Si$ and $\delta^{29}Si$ as follows:

$$\delta^{x}\mathrm{Si} = \left(\frac{\left(\frac{^{x}\mathrm{Si}}{^{28}\mathrm{Si}}\right)_{\mathrm{sample}}}{\left(\frac{^{x}\mathrm{Si}}{^{28}\mathrm{Si}}\right)_{\mathrm{NBS28}}} - 1 \right) \cdot 1000, \qquad (1)$$

where x is either 30 or 29 depending on which δ we aim for. Each sample was measured three to four times in a single measurement session with a standard-sample-standard bracketing technique. Full chemical replicates were analyzed for the majority of samples ($n = 292$, total measurements = 1875). Accuracy and reproducibility over 3 years on the secondary reference materials Diatomite ($\delta^{30}Si = 1.24 \pm 0.20$ ‰, 2SD, $n = 285$), Big-Batch ($\delta^{30}Si = -10.63 \pm 0.34$ ‰, 2SD, $n = 109$) and IRMM ($\delta^{30}Si = -1.77 \pm 0.22$ ‰, 2SD, $n = 195$) were in good agreement with values from a previous interlaboratory comparison (Reynolds et al., 2007). The repeatability of all samples was < 0.2 ‰. The absence of any potential polyatomic interferences was checked in a three-isotope plot of $\delta^{29}Si$ vs $\delta^{30}Si$, where all measurements must fall onto a line that corresponds to the terrestrial mass-dependent fractionation curve (Figure S2).

Ge/Si analyses on the water samples were conducted at UCLouvain, Belgium. The Si concentra-

tions in the thermal ($n = 7$) and river ($n = 30$) waters were determined by inductively-coupled plasma-optical emission spectrometry (ICP-OES; iCAP 6500 Thermo Fisher Scientific). The accuracy was assessed using the trueness (±4 %) of the river water reference material SLRS-5 (Yeghicheyan et al., 2013) and the analytical precision (±0.5 %) for each element. The detection limit was 0.36 µmol L^{-1}. The Ge concentration in the water samples was determined by ICP-mass spectrometry (ICP-MS, ICAPQ Thermo Fisher Scientific) using the ^{74}Ge isotope. Accuracy and long-term repeatability of the Ge analysis were assessed by measuring an international riverine standard, SLRS-5 ([Ge] = 0.083 ± 0.014 nmol L^{-1}; $n = 3$) or SLRS-6 ([Ge] = 0.097 ± 0.0069 nmol L^{-1}; $n = 3$) (Yeghicheyan et al., 2013) in each analytical session. The limit of detection on Ge was 0.04 nmol, and the analytical precision ($n = 3$) was ±8 % for Ge concentrations <0.013 nmol and 4 % for Ge concentrations >0.013 nmol. The precision on the Ge/Si ratio is 10 % (1SD).

Chromatographically (cation) purified solutions of dissolved diatom samples were analyzed for their Ge/Si ratios at GFZ Potsdam, Germany using an iCAP Q quadrupole ICP-MS (Thermo Fisher). This approach exploits the recent demonstration that Ge is unfractionated relative to Si during the cation-exchange procedure used to purify Si from matrix elements for δ^{30}Si analyses (Delvigne et al., 2018). This means Si column elutants have a much cleaner matrix, which makes Ge amenable to measurement by ICP-MS without the hydride-generation and isotope-dilution protocols conventionally employed elsewhere (e.g., Kurtz et al., 2011). Samples were introduced in a 0.3 M HNO_3 matrix, via a ESI prepFast autodilutor system with the instrument operated under standard conditions. The measurement was based on 300 integrations of the isotopes of ^{74}Ge and ^{29}Si for 0.1 s, with the less abundant isotopes of Ge integrated 300 times for 0.01 s. Polyatomic interferences (e.g., ^{36}Ar, ^{38}Ar, or ^{74}Ge) were removed by a collision cell with He as reaction gas, at a flow rate of 5 L min^{-1}, yielding acid-blank counting statistics < 1 cps. Beam intensities on the minor Ge isotopes correlate strongly with that of ^{74}Ge ($R^2 > 0.95$), corroborating the successful removal of unexpected isobaric or polyatomic interferences on ^{74}Ge by the column purification protocol and the instruments collision cell. Ge/Si ratios were calculated directly from the ratio of beam intensities by reference to a set of gravimetrically prepared, matrix-matched calibration standards with matching Si concentrations but varying Ge concentrations. Thus, this approach does not directly yield Ge concentrations, because the column elutions are typically not performed gravimetrically, though these can be derived, if necessary, from pre-column Si concentration analyses. International standards BIR-1 (Ge/Si = 2.72 ± 0.05 µmol/mol; 1SD, $n = 16$) (Baronas et al., 2018; Kurtz et al., 2002; Mortlock and Froelich, 1996; Mortlock and Frohlich, 1987) and BHVO-2 (Ge/Si = 2.72±0.13 µmol/mol; 1SD, $n = 12$) (Scribner et al., 2006) were measured in each analytical session to assess the accuracy and long-term repeatability of the Ge analysis.

3.5 Chronology and accumulation rates

Chronologies were constructed from both cores based on ^{14}C dates, and sedimentation rates were calculated based on published age-depth models (Schiller et al., 2020). The BSi accumulation rate (F_{BSi}) was calculated from the sedimentation rates (SR), measured wet bulk density (ρ), porosity (Φ) and BSi weight percentages for each sample as

$$F_{BSi} = SR \cdot \rho \cdot (1 - \Phi) \cdot BSi\,wt\%. \quad (2)$$

3.6 Numerical analyses

Proxies for detrital input (Ti, Zr, MS), hydrothermal and volcanic activity (As, Cl) (Balistrieri et al., 2007; Fowler et al., 2019b; Shanks et al., 2007) and diatom production and dissolution (TOC, BSi, δ^{30}Si) were tested for correlation within both cores using Pearson correlation tests in the software R. The significance of a correlation was evaluated through the p-value, the R-square, and the correlation coefficient. A statistically significant correlation was considered to have a confidence interval of 95 % (p-value < 0.05).

4 Results

4.1 Chronology and accumulation rates of lake sediments

Diatom accumulation in the Yellowstone Lake sediment is quantified through mass accumulation rate

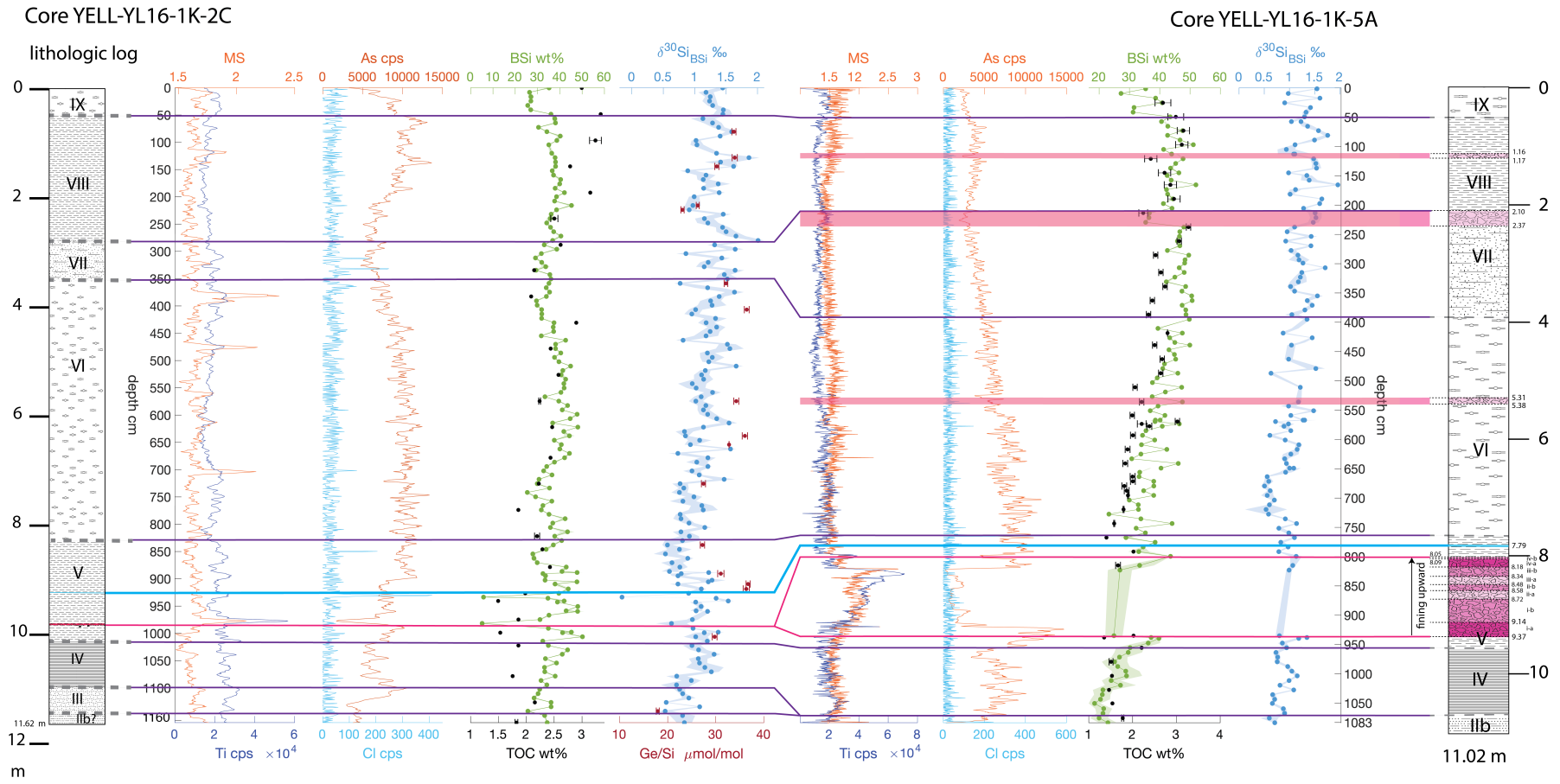


Figure 2: Aligned cores 2C and 5A showing the lithological units (Morgan et al., unpublished, in preparation), magnetic susceptibility (MS), titanium (Ti) as proxy for detrital input, arsenic (As) and chloride (Cl) count from XRF as proxy of hydrothermal activity (pink horizontal lines and zones) and tephra layers (blue horizontal line), biogenic silica (BSi) in dry weight percentages SiO_2, total organic carbon (TOC) in dry weight percentages, stable silicon isotopes of single species *Stephanodiscus yellowstonensis* (δ^{30}Si(‰)) and Ge/Si ratio of fossil single species diatom in µmol/mol.

calculations. The age-depth models of core 2C and 5A (Schiller et al., 2020) produce mean sedimentation rates of $0.12\,\mathrm{cm\,yr^{-1}}$ for the last 9800 years for core 2C, and of $0.11\,\mathrm{cm\,yr^{-1}}$ for core 5A. Thus, the mean BSi accumulation rates for the whole cores are $8.01 \pm 2.76\,\mathrm{mg\,cm^{-2}\,yr^{-1}}$ (1SD) for core 2C, and $5.68 \pm 2.97\,\mathrm{mg\,cm^{-2}\,yr^{-1}}$ (1SD) for core 5A. Mass accumulation rates in both cores show only slight variation, therefore, the variation in BSi accumulation is represented directly in BSi wt%. However, the uncertainties of both age-depth models are large, and, additionally, core 5A contains 1 m-thick hydrothermal explosion deposits, and no ^{14}C dates constrain the age below those deposits; therefore, those numbers need to be taken with caution.

4.2 Lithological, chemical, δ^{30}Si and Ge/Si composition of the sediment cores

The lithology of the two cores was described in Morgan et al., (in preparation), where several lithological units originally defined by Tiller (1995) were identified and are used for core alignment. A sequence of hydrothermal explosion deposits is found in both cores. In core 2C these events are represented in a 5 cm-thick layer at depths 977 to 984 cm, whereas in core 5A those events are recorded in over 1 m-thick deposits in depths from 805 cm to 937 cm (*L. Morgan, personal communication*). The hydrothermal deposits are dated at ~8000 cal. yr BP. Additionally, Mazama tephra is found at core depths 931.5 cm and 779 cm in core 2C and 5A, respectively. The data from XRF scanning, TOC measurements, BSi concentration, δ^{30}Si and Ge/Si are aligned with the lithology logs through distinct changes in lithology, magnetic susceptibility and elemental composition specific for tephra layer (chloride – Cl) and hydrothermal events (arsenic – As, strontium – Sr). As is an indicator of hydrothermalism in Yellowstone Lake as it is depleted in the hydrothermal fluid due to loss during steam separation, adsorption by iron or co-precipitation with calcite (Stauffer and Thompson, 1984).

4.2.1 Core 2C

Core 2C shows relatively undisturbed sedimentation recorded in MS and Ti data, which are slightly positively correlated ($R^2 = 0.02$, p-value $= 1.9 \cdot 10^{-7}$) reflecting changes in detrital input (Figure 2). The Ti is negatively correlated with As ($R^2 = 0.09$, p-value $< 2.2 \cdot 10^{-16}$), which is the hydrothermal input proxy. The distinct peak in Cl is indicative of the Mazama ash tephra at depth of 933.5 cm. Aluminum is strongly correlated with potassium (K) ($R^2 = 0.82$, p-value $< 2.2 \cdot 10^{-16}$), which may be connected with the character of detrital minerals.

The BSi concentration ranges from 25 wt% to 50 wt%, averaging 37 wt%. There is no pronounced trend in BSi concentration throughout the Holocene, although variations in BSi concentration partly follow changes in As (Figure 2), a proxy for hydrothermal activity. A negative correlation between BSi concentration and detrital input (Ti) ($R^2 = 0.43$, p-value $< 2.2 \cdot 10^{-16}$) is consistent with decreases in BSi with increased detrital input. Al and K are both negatively correlated with BSi ($R^2 = 0.18$, p-value $= 2.4 \cdot 10^{-8}$, and $R^2 = 0.28$, p-value $= 1.4 \cdot 10^{-12}$, respectively), because of the inverse relationship between BSi concentration and detrital mineral concentrations. Total organic carbon (TOC) shows no significant correlation with BSi concentration, suggesting that accumulated TOC is not a direct measure of total diatom production, but rather represents the total carbon primary production or that its variation is primarily controlled by other processes, such as organic matter inputs from the watershed.

The Si isotopic composition of the diatom species *Stephanodiscus yellowstonensis* in core 2C shows a trend toward heavier values near the top of the core, with a mean of 1.13 ± 0.29 ‰ (1SD) (Figure 2), with one standard deviation expressing the spread of data ($n = 149$). The lowest values of δ^{30}Si (0.53 ± 0.11‰, 2σ – analytical error) are in the bottom part of the core, below the hydrothermal explosion deposits, which are dated at ~8000 cal. yr BP (Schiller et al., 2020). δ^{30}Si is slightly positively correlated with changes in BSi concentration ($R^2 = 0.06$, p-value $= 2.2 \cdot 10^{-3}$). No obvious impact of the hydrothermal events on δ^{30}Si in the vicinity of the deposits is observed.

The Ge/Si data measured on the fossil diatom *Stephanodiscus yellowstonensis* show extraordinarily high values, ranging from 17.9 to $36.7 \cdot 10^{-6}$ (µmol/mol), with an mean Ge/Si ratio of $30.9 \cdot 10^{-6}$ (µmol/mol) (Figure 2). The record is only of low resolution, nevertheless, an expected increase in the Ge/Si ratios is observed above the Mazama ash tephra layer. Although, the Ge/Si ratios follow the As trends, there is a positive correlation between Ge/Si and As ($R^2 = 0.25$, p-value $= 0.04$). Additionally, the hydrothermal activity proxy (As) shows no significant correlation with the δ^{30}Si record.

4.2.2 Core 5A

Core 5A reflects its proximity to the periphery of Elliot's Crater through evidence of disturbance in sedimentation from 802 to 937 cm, which represent several hydrothermal deposits (Figure 2), and also is evident in the decreased As. MS and Ti, which are positively correlated ($R^2 = 0.46$, p-value $< 2.2 \cdot 10^{-16}$), represent changes in detrital input and both proxies increase in the hydrothermal deposits. Additionally, Ti is negatively correlated with As ($R^2 = 0.07$, p-value $< 2.2 \cdot 10^{-16}$), which also suggests increased detrital input during hydrothermal activity (low As).

BSi in core 5A ranges from 18 wt% to 52 wt%, averaging 37 wt% throughout the Holocene sequence (Figure 2). A gradual increase of BSi content is observed from the bottom of the core toward the top, with some small variation. In unit VIII, the BSi concentration stabilizes, and in the topmost lithological unit IX BSi gradually decreases. The BSi record is negatively correlated with As ($R^2 = 0.15$, p-value $= 6.9 \cdot 10^{-6}$), which suggests that BSi variation can be connected to changes in hydrothermal inputs (As). Similarly, Ti is negatively correlated with BSi ($R^2 = 0.52$, p-value $< 2.2 \cdot 10^{-16}$) with the detrital input diluting the accumulated BSi. At this site, BSi concentration is positively correlated with TOC content ($R^2 = 0.48$, p-value $= 7.9 \cdot 10^{-8}$).

The record of Si isotopes shows a long-term increase toward heavier δ^{30}Si of *Stephanodiscus yellowstonensis* near the top of the core with shift of 0.6 ‰ (Figure 2). Values range from 0.51 ± 0.06 ‰ (2σ – analytical error) to 1.96 ± 0.07 ‰ (2σ), with a mean of 1.09 ± 0.31 ‰ (1SD, $n = 126$). The δ^{30}Si is positively correlated with changes in BSi concentration ($R^2 = 0.26$, p-value $= 1.9 \cdot 10^{-9}$), which may indicate the effect of diatom production. The δ^{30}Si and the BSi concentration show no long-term changes triggered by hydrothermalism.

4.3 δ^{30}Si and Ge/Si ratios in tributaries and hydrothermal waters

All tributaries in the northern part of the lake, within the Yellowstone Caldera, show evidence of seasonality in flow (not shown), DSi concentrations, Ge/Si and δ^{30}Si (Table 1, Gaspard, 2020). The δ^{30}Si of tributaries ranges from 0.37 ± 0.05 ‰ (1σ–analytical error) in the high-flow season to 1.19 ± 0.02 ‰ (1σ) in the low-flow season, with a yearly mean of 0.65 ± 0.30 ‰ (1SD, $n = 12$) (Table 1). The Yellowstone River outlet, which we assume represents the Si isotope composition of the lake, has an annual mean δ^{30}Si of 1.94±0.28 ‰ (1SD, $n = 8$) (Table 1).

Ge/Si ratios in Yellowstone Lake tributaries situated within the caldera show differences between the two flow regimes (Table 1 Gaspard, 2020). The Ge/Si ratio ranges from 0.98 ± 0.10 µmol/mol (1σ) in the high-flow regime to 11.35 ± 0.10 µmol/mol (1σ) during the low-flow regime, with an annual mean of 4.26± 3.20 µmol/mol (1SD, $n = 12$). This seasonal behavior is also observed in the Yellowstone River outlet, where Ge/Si ranges from 13.6 ± 0.10 µmol/mol (1σ) up to 23.3 µmol/mol, with the annual mean Ge/Si ratio of 18.8 ± 4.05 µmol/mol (1SD, $n = 8$) (Table 1, Gaspard, 2020).

Water samples of hydrothermal vents reflect two different vent systems in the lake: the fluid from the West Thumb vent field has isotopically lighter δ^{30}Si signatures with an mean δ^{30}Si of −0.11 ± 0.27 ‰ (1SD, $n = 8$), whereas the Deep Hole samples are isotopically heavier averaging at 0.54±0.33 ‰ (1SD, $n = 14$), and have Ge/Si ratios as high as 25.5 µmol/mol (Table 1).

Table 1: Data on tributaries and Yellowstone River outlet together with sublacustrine hydrothermal vents. DSi is dissolved silicon expressed as mg SiO_2 L^{-1}, stable Si isotopic signature expressed as δ^{30}Si in permille. Ge/Si ratio expresses in µmol/mol. All Ge/Si data were measured at UCLouvain, Belgium. The numbers of analytical replicates for DSi and δ^{30}Si are shown in column named *n*. Abbreviated 1SD represents standard deviation of several replicates and 1σ is the analytical error.

Yellowstone Lake tributaries in high-flow regime

	DSi[c] [mg SiO_2 L^{-1}]	1SD	δ^{30}Si [‰]	1σ	*n*	Ge/Si [µmol/mol]	1σ
Arnica Creek	39.48	7.07	0.37^{L}	0.05	1	5.67	0.10
Big Thumb Creek	13.03	2.53	0.86^{L}	0.02	1	0.88	0.10
Bridge Creek	44.53	6.26	0.71^{L}	0.07	1	2.08	0.10

Little Thumb Creek	8.13	1.37	1.09^{S}	0.11	5	0.98	0.10
Pelican Creek	27.55	0.95	0.78^{L}	0.07	1	3.12	0.10
Sedge Creek	18.46	0.45	0.77^{L}	0.05	1	6.02	0.10
Yellowstone River outlet	12.50	0.28	1.73^{S}	0.08	3	18.21	0.10
			1.82^{L}	0.04	1		

Yellowstone Lake tributaries in low-flow regime

	DSi[c] [mg SiO_2 L^{-1}]	1SD	δ^{30}Si [‰]	1σ	n	Ge/Si [µmol/mol]	1σ
Arnica Creek	58.18	2.13	0.40^{L}	0.04	1	4.58	0.10
Big Thumb Creek	100.67	3.70	1.19^{L}	0.03	1	7.04	0.10
Bridge Creek	91.95	3.30	0.48^{L}	0.01	1	2.64	0.10
Little Thumb Creek	33.02	1.17	0.92^{S}	0.06	4	1.47	0.10
Pelican Creek	63.54	1.10	1.17^{L}	0.06	1	8.95	0.10
Sedge Creek	35.14	2.01	1.05^{L}	0.05	1	11.35	0.10
Yellowstone River outlet	11.71	0.15	2.05^{S}	0.06	4	20.13	0.10
			2.17^{L}	0.03	1		
	11.62	0.57	1.89^{S}	0.09	10	23.29	0.10
			2.01^{L}	0.09	2		
	12.90	1.90	1.45^{S}	0.09	4	13.60	0.10
			1.63^{L}	0.03	1		

West Thumb vent field

	DSi* [mg SiO_2 L^{-1}]	1SD	δ^{30}Si [‰]	1σ	n	Ge/Si [µmol/mol]	1σ
YL18F06	156.06	< 10 %	-0.32^{P}	0.05	3		
YL18F12	276.11	< 10 %	-0.36^{S}	0.05	3		
YL18F12			-0.32^{S}	0.05	5		
YL18F12			-0.40^{P}	0.05	3		
YL18F13	270.11	< 10 %	0.25^{P}	0.08	2		
YL18F13			0.21^{S}	0.01	3		
YL18F13			0.24^{S}	0.08	3		
YL18F14	162.06	< 10 %	-0.15^{P}	0.06	3		

Deep Hole vent field

	DSi* [mg SiO_2 L^{-1}]	1SD	δ^{30}Si [‰]	1σ	n	Ge/Si [µmol/mol]	1σ
YL16F06	32.41	< 10%	0.69^{S}	0.08	3	10.87	0.10
YL16F06			0.62^{P}	0.14	3		
YL16F07	13.81	< 10%	0.97^{P}	0.15	3	25.54	0.10
YL16F10	23.41	< 10%	0.90^{S}	0.08	3	11.20	0.10
YL16F12	27.01	< 10%	0.48^{S}	0.03	3	12.74	0.10
YL16F12			0.49^{S}	0.08	5		
YL16F14	32.41	< 10%	0.44^{S}	0.08	3	14.61	0.10
YL16F14			0.41^{P}	0.01	2		
YL17F01	25.21	< 10%	0.06^{P}	0.09	3		
YL17F02	24.61	< 10%	0.11^{P}	0.23	2		

YL17F03	25.81	< 10%	0.37^{P}	0.14	3
YL17F08	16.21	< 10%	1.10^{P}	0.09	3
YL18F02	25.21	< 10%	0.14^{P}	0.10	3
YL18F04	16.81	< 10%	0.84^{P}	0.04	3

* Concentrations measured by ICP-OES (Thermo Scientific iCAP 6500 duo) at the University of Minnesota (UMN), Department of Earth Sciences (Fowler et al., 2019b).
^{c} Concentration measured by molybdate-blue spectrophotometry AMS SmartChem 200, Lund University, Sweden.
^{S} Samples were measured by MC-ICP-MS (NuPlasma II) at Vegacenter, Swedish Museum of Natural history, Stockholm.
^{P} Samples were measured on MC-ICP-MS (Neptune) at GFZ, Potsdam, Germany.
^{L} Samples were measured by MC-ICP-MS (Neptune) at UCLouvain, Belgium.

5 Discussion

In two cores from Yellowstone Lake we observed high and relatively stable BSi concentrations and fluxes. The long-term increase in the δ^{30}Si signature of *Stephanodiscus yellowstonensis* of 0.6 ‰ in both cores from early to late-Holocene is a pattern similar in direction and magnitude to that observed in marine records, where diatom production is driven by climate and nutrient supply by upwelling (Ehlert et al., 2013). These drivers are connected to three main factors influencing the diatom δ^{30}Si signature – the fractionation factor associated with diatom Si uptake, the signature of the DSi source and the degree of DSi utilization by diatoms. We can exclude the species-specific fractionation factor, as the measurements are made on samples that contain of almost all from a single diatom species, *Stephanodiscus yellowstonensis* (Figure S1). Therefore, we test three non-exclusive hypotheses to identify the factors responsible for variation in δ^{30}Si and BSi accumulation throughout Holocene:

1. the effect of DSi utilization by diatoms;
2. the impact of changes in DSi sources:
   a. abrupt hydrothermal inputs during explosion events, or
   b. continuous hydrothermal input.

1. The effect of DSi utilization by diatoms

The isotopic shift in lake water and then in diatoms connected to DSi utilization is described by fractionation models (De La Rocha et al., 1997; Varela et al., 2004). In short, due to a diatom fractionation of −1 ‰, the more DSi is utilized by diatoms, the less of the light Si isotope (^{28}Si) is available in the solution, and thus the Si isotope ratio becomes heavier in the source solution, and accordingly it also gradually increases in the diatoms. In Yellowstone Lake, diatom-rich sediment formation is likely driven by a lake DSi concentrations of 11 mg L^{-1} (Balistrieri et al., 2007; Gemery-Hill et al., 2007) that enables high diatom production and enhances diatom preservation. In the cores, BSi concentrations are negatively correlated with Ti (Figure 2), Al and K counts (not shown), which suggests that higher BSi concentrations may be connected to lower detrital input. Therefore, limited dilution by clastic material, high diatom production and good preservation may be responsible for high BSi accumulation. Thus, the variation in BSi concentration is influenced, at least in part, by dilution by detrital input. Additionally, core 5A shows a positive correlation between the primary production proxy (TOC) and BSi concentrations, which supports the hypothesis that changes in BSi concentration also are driven by diatom production. Comparing sedimentation rates of core 2C and 5A ($n = 277$), with an assumption of similar diatom production at both sites, the higher the sedimentation rates are, the more BSi is buried. A similar phenomenon has been observed in marine sediments (Rickert et al., 2002). This is likely connected to the diatom accumulation rate, where the more diatoms settle, the more likely they are well preserved in the sediment. However, low detrital input is crucial in this case. Thus, both cores must have low detrital input and relatively higher diatom accumulation rates at the same time to accumulate sediment composed of up to 50 wt% of diatoms.

The diatom δ^{30}Si signature shows a positive, albeit weak, correlation with BSi concentration in both cores, which suggests that DSi utilization is one of the factors driving the diatom δ^{30}Si signature throughout the Holocene. Higher diatom production partly reflected in BSi concentrations results in higher DSi consumption and thus, shifts the δ^{30}Si signature towards heavier values in both cores. The similarities between cores in diatom δ^{30}Si in each lithological section of the cores (Figure 3) suggest that the productive layer

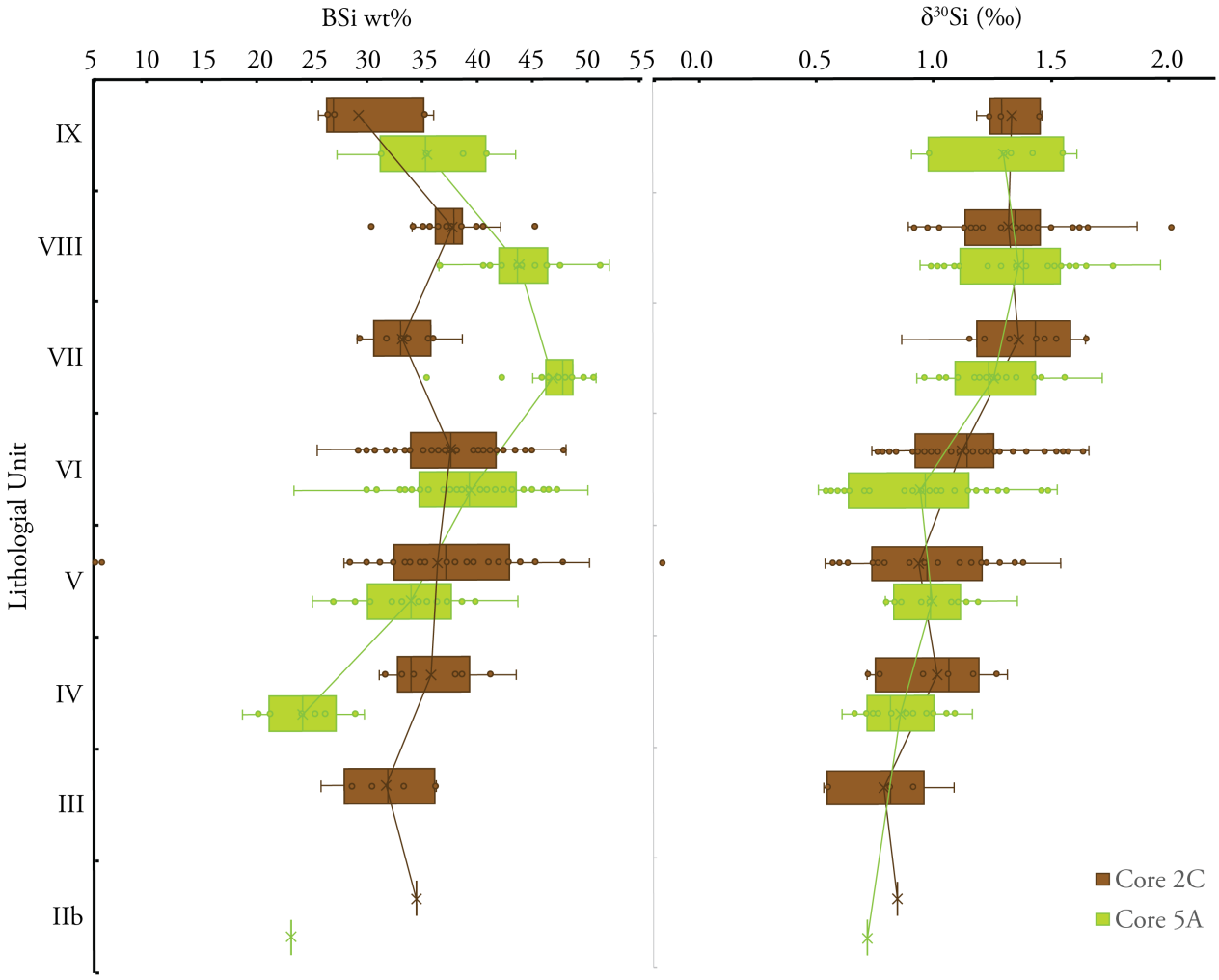


Figure 3: Comparison of mean BSi dry wt% of SiO_2 and δ^{30}Si [‰] values of separate lithological units showing core 2C in brown and core 5A at the distal part of Elliott's Crater in green.

of the water column was a homogeneous, stable and well mixed DSi reservoir (Interlandi et al., 1999), with no depletion of DSi during the growing season, resulting in a small variation in diatom δ^{30}Si. The common trend of a shift of δ^{30}Si toward more positive values is seen in both cores and is likely connected to the influence of Holocene climate change in the Greater Yellowstone Ecosystem as indicated by multiple proxies (Brown, 2019; Brown et al., unpublished; Schiller, 2020). Heavier Si isotopic values are usually connected to increased diatom production and greater relative DSi utilization (De La Rocha et al., 1997). Decreasing summer insolation triggering a long term trend towards cooler and wetter conditions at Yellowstone Lake Brown et al., using (Laskar et al., 2004) could have led to a greater abundance of heavily silicified diatom species, enhanced diatom production due to a longer period of spring water mixing (Brown et al., unpublished), and thus, higher DSi utilization, resulting in heavier δ^{30}Si.

However, DSi utilization by diatoms is not the only factor driving the δ^{30}Si, because of the weak correlation between BSi concentration and δ^{30}Si, as well as the absence of a correlation between TOC and BSi in core 2C. The weak correlation between δ^{30}Si and BSi concentration suggests that diatom production has only a small influence on δ^{30}Si and that the prevailing factor driving the δ^{30}Si is changes in DSi sources. Therefore, we hypothesize that an additional factor influencing changes in diatom δ^{30}Si and BSi accumulation in our record is the relative proportion of DSi originating from watershed bedrock weathering versus hydrothermal DSi.

Table 2: Estimated end-members based on means of all measured water samples responsible for current lake δ^{30}Si and Ge/Si composition.

Estimated end-members

	δ^{30}Si [‰]	1SD	Ge/Si [µmol/mol]	1SD
Tributaries	$0.65^{L,S}$	0.30	4.48^{L}	3.21
West Thumb	$-0.11^{S,P}$	0.27	–	–
Land springs	-0.14^{L}	0.14	160^{L}	26
Deep Hole	$0.54^{S,P}$	0.33	15^{L}	6
Lake	$1.94^{L,S}$	0.28	18.8^{L}	4.1

^{L} Samples were measured by MC-ICP-MS (Neptune) at UCLouvain, Belgium.
^{S} Samples were measured by MC-ICP-MS (NuPlasma II) at Vegacenter, Swedish Museum of Natural history, Stockholm, Sweden.
^{P} Samples were measured on MC-ICP-MS (Neptune) at GFZ, Potsdam, Germany.

2. Impact of changes in DSi sources

a. Impact of hydrothermal explosions

We test the hypothesis of an impact of changes in DSi with hydrothermal explosions by tracking the sedimentary record around the hydrothermal events. Hydrothermal explosions are accompanied by an input of boiling water, steam and mud (Browne and Lawless, 2001; Muffler et al., 1971). Hydrothermal fluid composition is enriched in many elements, including DSi (Balistrieri et al., 2007; Fowler et al., 2019b). We hypothesized an increase in BSi and decrease in δ^{30}Si as a consequence of isotopically lighter DSi enrichment originating from fluids brought by the explosion (Chen et al., 2020; De La Rocha et al., 2000; Ding et al., 1996; Douthitt, 1982; Geilert et al., 2015, 2014; Grasse et al., 2020; Opfergelt et al., 2011).

A series of hydrothermal explosion deposits occurred in core 5A, as well as, to a smaller extent, in core 2C. Core 5A, located in proximity to Elliott's Crater, has a 1m-thick hydrothermal deposit. However, no distinct increases in BSi accumulation nor a decrease in δ^{30}Si is observed in either of the cores above these deposits. Similarly, neither the BSi concentration nor the δ^{30}Si record changed directly after the explosion deposits in core 2C nor 5A. These observations suggest that the lake DSi residence time (8 to 24 years, *Zahajská and Conley, unpublished data*) is too long to record short episodic explosions, resulting in a lake that has a stable and a homogeneous source of DSi for the diatoms on long time time scales (shown in, e.g., Richter and Turekian, 1993). Consistent with the geochemical data, only very subtle changes were found in the diatom community composition or in watershed vegetation (Brown, 2019; Brown et al., unpublished; Schiller, 2020). As impacts of hydrothermal explosions could not be identified in either of the cores, the resolution of the δ^{30}Si sampling is not sufficient for identifying hydrothermal activity in a well-buffered environment with high DSi and several DSi sources carry similar isotopic signature.

Ge/Si ratios offer another tool to test the contribution from hydrothermal activity, because hydrothermal end-members can have distinct Ge/Si signatures (Table 2). Specifically, in Yellowstone, hydrothermal vent fluids often have high Ge/Si ratios, because of preferential uptake of Si into amorphous silica precipitates (Evans and Derry, 2002), which occurs due to DSi supersaturation of fluids during the contact with lake water and cooling (Fowler et al., 2019b; Shanks et al., 2007). When Si is incorporated in siliceous spires and precipitates, the residual solution is enriched in DGe and thus characterized by high Ge/Si ratios. Contrary to high-temperature DSi and DGe sources, the low-temperature process of bedrock weathering produces Si-enriched solutions, resulting in low Ge/Si ratios (Baronas et al., 2018; Kurtz et al., 2011).

The Ge/Si ratios of *Stephanodiscus yellowstonensis* are much higher than values found in the literature (Figure 4), which suggests either that the Ge/Si ratio of source water is high or, alternatively, that diatoms in Yellowstone Lake do not discriminate against Ge during uptake ($K_D \leq 1$). To our knowledge, the only evidence of this behavior has been in cultivation experiments using solutions with high Ge/Si ratios and DSi concentrations above 100 µmol L^{-1} to grow di-

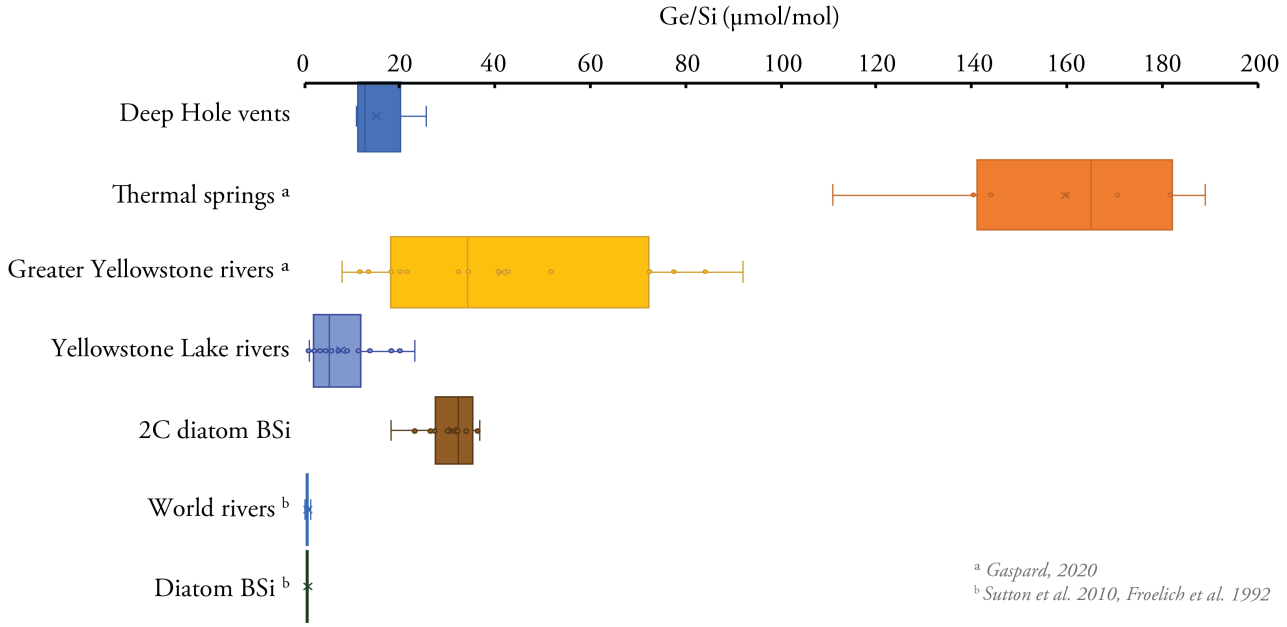


Figure 4: Ranges of Ge/Si ratios in the Deep Hole vent fluids, Yellowstone Lake tributaries and the fossil single species diatom opal from core 2C are shown. Further, the Ge/Si ratios in Greater Yellowstone rivers, Midway Geyser Basin thermal springs (Gaspard et al., 2020) and ranges of world's Ge/Si ratios in rivers and diatom opal (Froelich et al., 1992; Mortlock et al., 1991; Sutton et al., 2010) are presented.

atoms, which resulted in high Ge/Si ratios in the diatom frustules and K_D ranging from 1 to 1.2 (Froelich et al., 1992). Our observations are in agreement with those experimental results, as the DSi concentration of YL is around 200 µmol L^{-1} (12 mg SiO_2 L^{-1}), and the Ge/Si ratio is almost 30 times higher than in the ocean or worldwide rivers (Figure 4). Thus, diatoms in YL likely do not discriminate against Ge during uptake. If we assume the K_D to be constant through time and equal to 1, the Ge/Si ratios in fossil diatoms could reflect changes of Ge/Si in the lake water through time. However, recent Ge/Si ratios of YL rivers (Figure 4) are lower than the Ge/Si ratios in the fossil diatoms, which may suggest that the K_D in Yellowstone Lake is even higher than 1.2. However, the thermal springs and Greater Yellowstone rivers show high Ge/Si values, thus if these waters reach the YL, they would be great source of Ge for the fossil diatoms without need of K_D being higher than 1.2. Nevertheless, for precise K_D determination, the lake water and recent living diatom Ge/Si ratios would be needed. Enhanced knowledge of K_D and detailed mass and isotope balances constraining all DSi and DGe sources and sinks would bring more clarity into the Yellowstone Lake Si and Ge cycling.

Overall, the sedimentary record shows an isotopic shift in δ^{30}Si of 0.6‰ to heavier values toward the top of the cores and highly variable Ge/Si ratios in the fossil diatoms. Even though the Ge/Si ratios of fossil diatoms suggests some increase in Ge concentrations above the hydrothermal deposits (Figure 2), there is no direct evidence that this increase is connected to the hydrothermal event, because similar values are found higher up in the record. The consistent range of variation in Ge/Si supports the hypothesis of a consistent long-term background of high hydrothermal inputs and the buffering capacity of the lake to these disturbances. In addition to the Ge/Si ratios suggesting long-term hydrothermal background inputs, the δ^{30}Si exhibits a consistent balance of DSi sources during the last 9800 years. Our preliminary mass-balance suggests that up to 55 % of the DSi tributary inputs can be brought into the lake by hydrothermal fluids (this thesis, section 6.4). Thus, even an extensive hydrothermal explosion, such as Elliott's Crater, had no observed impact on the lake Si cycle with respect to the DSi retention time.

b. Impact of input from hydrothermal vent fluids vs. DSi river input

The hypothesis that BSi accumulation and δ^{30}Si signal is affected by variation in DSi sources is based on the absence of reaction of the lake system to abrupt

events. Therefore, the long-term trend in diatom δ^{30}Si is hypothesized to be affected by changes in the relative proportion of DSi sources.The mean δ^{30}Si signal of the tributaries situated within the Yellowstone Caldera (0.65 ± 0.30‰) is at the lower end of the world riverine δ^{30}Si range (Figure 5). The Yellowstone River outlet (1.94 ± 0.28‰), representing the lake isotopic signature, falls into the measured range of lakes globally (Frings et al., 2016) and suggests that diatom production fractionates the originally lighter tributary DSi source. However, based on the inlet, outlet and the diatom δ^{30}Si, the recent lake water δ^{30}Si should show heavier values through fractionation by diatom DSi uptake. There is great uncertainty regarding species specific fractionation by diatoms which could play a role in the δ^{30}Si of lake water (Sutton et al., 2013).

An isotopically lighter DSi source from hydrothermal vents (Figure 5), is in agreement with existing data on hydrothermal vent fluids (Chen et al., 2020; De La Rocha et al., 2000; Ding et al., 1996; Douthitt, 1982; Geilert et al., 2015, 2014; Grasse et al., 2020; Opfergelt et al., 2011) including hydrothermal vent fluids from West Thumb (Figure 5), which suggests that the vents in West Thumb can contribute to a lowering of the lake δ^{30}Si. The Deep Hole hydrothermal fluids have previously been identified to be a mixture of lake water and pore water extruded by a vapor-driven hydrothermal system underlying the area (Fowler et al., 2019a), and the isotopic composition reflects those processes and therefore is closer to the lake δ^{30}Si.

To better constrain the hydrothermal influence, the Ge/Si and δ^{30}Si data allows us to disentangle processes in the watershed, as well as sources of DSi. Recent lake Ge/Si and δ^{30}Si values suggest that Yellowstone Lake is greatly influenced by hydrothermalism, which creates high Si background concentrations (Gaspard, 2020, Figure 4). The mean Ge/Si ratios of the world rivers ranges from 0.4 to 1.2 µmol/mol (Baronas et al., 2018; Filippelli et al., 2000; Froelich et al., 1992; Hammond et al., 2004; Mortlock and Frohlich, 1987), whereas marine hydrothermal fluids show higher Ge/Si values within a range of 8 µmol/mol to 14 µmol/mol (Froelich et al., 1992; Sutton et al., 2010). The tributaries of Yellowstone Lake are mostly above the riverine mean, and some show values are similar to marine hydrothermal fluids and higher. The Deep Hole hydrothermal fluids, which may contain recycled Ge from the sediments or from diatom frustules, show even higher Ge/Si ratios than the tributaries. Additionally, data from other rivers in the Greater Yellowstone area suggest that the whole Yellowstone area is highly enriched in Ge (Figure 4 Gaspard, 2020). Also, similarly elevated Ge/Si ratios have been observed in rivers of the Eastern Tibetan Plateau that have hydrothermal input (Evans and Derry, 2002; Han et al., 2015).

With knowledge of the Ge/Si and δ^{30}Si of the hydrothermal fluids, a relative change in hydrothermal DSi and riverine DSi sources can be one explanation for variation in BSi accumulation and the δ^{30}Si signature. The long-term increase toward heavier δ^{30}Si could be a response to a long-term decline of hydrothermal inputs relative to DSi brought in by tributaries, which carry heavier δ^{30}Si. Consistently, the multiproxy study on core 2C including both geochemical data and biotic proxies has shown a long-term trend towards cooler and wetter conditions during the Holocene (Brown et al., unpublished). Particularly, late-Holocene was interpreted as a period with lower lake water evaporation and possibly increased run-off from snowmelt, which could increase the delivery of relatively heavier δ^{30}Si DSi from the watershed soils, where processes fractionating Si occur. However, the diatom Ge/Si data and the arsenic (As) data, both indicators of hydrothermal activity (Figure 2), do not support a decline in hydrothermal activity. Therefore, an increasing contribution of water inputs from snowmelt with a continuous proportion of hydrothermal water input could explain the trend in δ^{30}Si associated with a slight increase in DSi utilization by diatom production.

Another explanation is that although the proportion of DSi brought by tributaries and hydrothermal fluids is stable though the Holocene, the riverine endmember has shifted towards heavier isotopic signatures. Changes in δ^{30}Si towards heavier values can be caused by fractionation processes before and during the delivery into the lake. Processes, such as neoformation of secondary minerals, formation of Fe- and Al-oxides or plant uptake could result in a gradual increase in the delivered DSi δ^{30}Si (Cornelis et al., 2011, 2014; Nantke et al., 2019; Struyf et al., 2010). The wetter late-Holocene climate at YL with increased runoff could bring more soil DSi from the lake watershed, which would carry heavier δ^{30}Si. Yet, the vegetation in the YL watershed has not changed substantively over this period (Schiller, 2020) with only slight changes in vegetation from a more open vegetation to more forested landscape. Thus, the isotopically heavier DSi from the soils has likely not been delivered in higher amounts compared to early-Holocene supported by the stable vegetation with persistence of Pi-

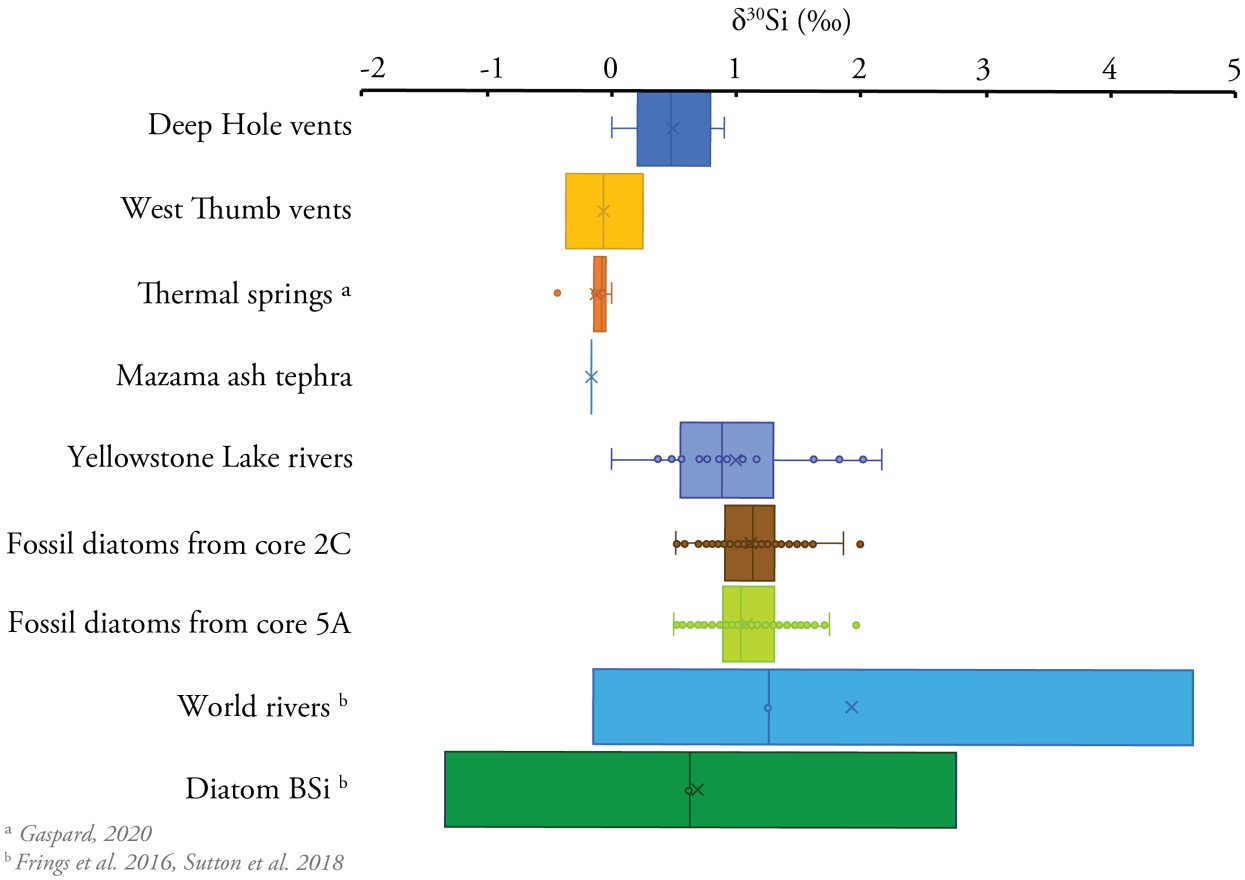


Figure 5: Ranges of stable silicon isotopes (δ^{30}Si) of Yellowstone Lake hydrothermal vent fluids and Yellowstone Lake tributaries, from thermal springs in Midway Geyser Basin (Gaspard, 2020) and the range of δ^{30}Si found in the world's rivers (Frings et al., 2016; Sutton et al., 2018). In addition, the isotopic signature δ^{30}Si of the Mazama ash layer, the ranges of fossil diatoms from core 2C and 5A and the world's marine and freshwater diatom δ^{30}Si range (Frings et al., 2016; Sutton et al., 2018, and references therein) are presented.

nus and Artemisia as dominant species (Schiller, 2020, in preparation). The trend towards heavier river δ^{30}Si could be rather explained by a net change in weathering reaction – i.e., the formation of relatively less depleted clays (e.g., smectites) towards the later Holocene, with more kaolinite/allophane type clays in the early Holocene. However, this hypothesis remains for future investigations.

In short, the most likely explanation for the isotopic shift of 0.6‰ in the δ^{30}Si signature of *Stephanodiscus yellowstonensis* in both cores throughout the Holocene is a combination of changes in the relative proportion of the DSi sources, e.g., bedrock weathering and hydrothermal input, together with possible changes in diatom production connected to changes in water column mixing and the length of the ice-free season (Brown et al., unpublished).

The fossil diatom δ^{30}Si in Yellowstone Lake is in the range of diatom δ^{30}Si observed worldwide(Frings et al., 2016; Opfergelt and Delmelle, 2012; Sutton et al., 2018). However, the mean diatom δ^{30}Si of both cores is below the world diatom δ^{30}Si mean (Figure 5). Comparable δ^{30}Si values of diatoms are reported from Lake El'gygytgyn (Swann et al., 2010), Lake Baikal (Panizzo et al., 2016) and Lake Edward (Cockerton et al., 2015), none of which are hydrothermally influenced, which suggest that the non-hydrothermally influenced lakes have either light isotopic sources comparable with volcanic areas or that YL is either not strongly hydrothermally affected or the isotopic signature of hydrothermalism is masked by other processes.

Lake water δ^{30}Si in Yellowstone Lake with a mean of 1.94‰ is higher than expected considering the δ^{30}Si signature of inputs from vents (ranging from $0 - 1$‰) likely due to other processes masking the direct hydrothermal input isotopic signature. One of the ex-

planations for the limited influence of inputs from hydrothermalism may be the large size and volume of the lake, which is also true for the other lakes mentioned above. This suggests that large lakes have the ability to buffer external perturbations that are shorter than the lake's residence time. Thus, the chemistry of these lakes reflects several processes operating simultaneously at longer time scales, such as changes in climate, vegetation, or DSi sources. However, for Yellowstone The Ge/Si ratios of fossil diatoms in YL provided convincing evidence of the long-term hydrothermal contribution.

6 Conclusions

The combination of recent water measurements and Holocene sedimentary data revealed that Yellowstone Lake has a stable water biogeochemistry over the long-term, highly influenced by hydrothermal background. An increase of 0.6‰ in δ^{30}Si in both cores studied over the Holocene, following changes in δ^{30}Si and diatom assemblages from a previous multiproxy study at one of the site (Brown et al., unpublished), suggest an influence of climate on the δ^{30}Si records through a change in the relative contribution of river and hydrothermal inputs to the lake. Considering a constant influence of hydrothermal inputs, increasing river inputs from snowmelt during late-Holocene associated with a slight increase in DSi utilization by diatoms due to a longer period of spring water mixing could explained the trend in δ^{30}Si.

Extreme hydrothermal events during the Holocene, such as occurred during the formation of Elliott's Crater (Morzel et al., 2017), did not dramatically disrupted the lake system. The influence of hydrothermalism on the lake was observed in recent water Ge/Si ratios. Continuous, long-term sublacustrine and terrestrial hydrothermal inputs drive the lake Ge and Si composition, which is reflected in extremely high Ge/Si ratios in fossil diatoms. However, the evidence of a hydrothermal contribution following explosions events is not observed in the diatom δ^{30}Si, likely because of the large size of the lake with well mixed waters, the potential of other processes masking the hydrothermal signature, or the DSi sources that share similar δ^{30}Si signatures.

The absence of evidence of increased BSi, as an indicator of DSi, after the hydrothermal explosion deposits leads to the conclusion that either the hydrothermal explosion was vapor-driven and disrupted sedimentation by clastics but did not contribute hydrothermal liquids or, alternatively the impact of the explosion is buffered by the long lake residence time. The Ge/Si ratios in fossils diatom do not add clarity into the interpretation, because they are consistently high throughout the core, showing only the long-term hydrothermal influence.

The Ge/Si ratios of the fossil diatoms compared to the recent lake tributaries and the recent lake water Ge/Si ratios suggest that *Stephanodiscus yellowstonensis* does not discriminate against Ge and thus can potentially be used for tracking changes in Ge/Si ratios of lake water during the Holocene. However, the Ge/Si ratio of recent diatoms and water need to be measured to verify this statement. Future work focused on Si and Ge budgets in lakes can contribute to a better understanding of the Si and Ge lacustrine sinks in volcanic systems.

Acknowledgments

This work was supported by The Royal Physiographic Society in Lund to PZ, RC, the Swedish Research Council to DJC, and NSF Grant No. 1515377 to SCF. The research was conducted under Yellowstone National Park research permits YELL-2016-SCI-7018, YELL-2016-SCI-5054, YELL-2018-SCI-5054 and YELL-2018-SCI-7084. Yellowstone Lake coring was aided by M. Baker, C. Linder, R. O'Grady, M. Shapley, R. Sohn, and Yellowstone National Park rangers. LacCore provided coring infrastructure, laboratory space for core splitting, subsampling, and analyses including magnetic susceptibility. We also thank to Lisa Morgan and Pat Shanks for assistance and help with core descriptions and lithological logs. Further we thank participants of fieldworks Christopher Schiller, Jessica A. Eggers, Jacob Queen, Trisha Spanbauer and YNP rangers for their help. We acknowledge Hans Schöberg and Melanie Kielman for assistance during sample preparation and isotope data acquisition. This is Vegacenter contribution number # XXX (number will be provided upon acceptance).

References

Arnórsson, S. (1984) Germanium in Icelandic geothermal systems. *Geochimica et Cosmochimica Acta* 48(12), 2489–2502. doi:10.1016/0016-7037(84)90300-4.

Azam, F., Hemmingsen, B.B., and Volcani, B.E. (1973) Germanium incorporation into the silica of diatom cell walls. *Archiv für Mikrobiologie* 92(1), 11–20. doi: 10.1007/bf00409507.

Balistrieri, L.S., Shanks, W.C., Cuhel, R.L., Aguilar, C., and Klump, J.V. (2007) The influence of sublacustrine hydrothermal vent fluids on the geochemistry of Yellowstone Lake. *Publications of the US Geological Survey* (66), 1–30. URL `https://digitalcommons.unl.edu/usgspubs/66`.

Baronas, J.J., Torres, M.A., West, A.J., Rouxel, O., Georg, B., Bouchez, J., Gaillardet, J., and Hammond, D.E. (2018) Ge and si isotope signatures in rivers: A quantitative multi-proxy approach. *Earth and Planetary Science Letters* 503, 194 – 215. doi:10.1016/j.epsl.2018.09.022.

Brodie, C.R., Casford, J.S., Lloyd, J.M., Leng, M.J., Heaton, T.H., Kendrick, C.P., and Yongqiang, Z. (2011) Evidence for bias in C/N, δ^{13}C and δ^{15}N values of bulk organic matter, and on environmental interpretation, from a lake sedimentary sequence by pre-analysis acid treatment methods. *Quaternary Science Reviews* 30(21-22), 3076–3087. doi:10.1016/j.quascirev.2011.07.003.

Brown, S. (2019) *Diatom-inferred records of paleolimnological variability and continental hydrothermal activity in Yellowstone National Park, USA*. PhD thesis. URL `https://digitalcommons.unl.edu/geoscidiss/122`.

Brown, S.R., Cartier, R., Schiller, C.M., Zahajská, P., Fritz, S.C., Morgan, L.A., Whitlock, C., Conley, D., Lacey, J.H., Leng, M.J., and Shanks, W.I.C. (unpublished) A multi-proxy record of Holocene paleoenvironmental conditions from Yellowstone Lake, Wyoming, USA. In preparation.

Browne, P. and Lawless, J. (2001) Characteristics of hydrothermal eruptions, with examples from New Zealand and elsewhere. *Earth-Science Reviews* 52(4), 299–331. doi:10.1016/s0012-8252(00)00030-1.

Chen, X.Y., Chafetz, H.S., and Lapen, T.J. (2020) Silicon isotope variations in hydrothermal systems at Yellowstone National Park, Wyoming, USA. *Geochimica et Cosmochimica Acta* 283, 184–200. doi:10.1016/j.gca.2020.06.004.

Christiansen, R.L. (2001) The Quaternary and Pliocene Yellowstone plateau volcanic field of Wyoming, Idaho, and Montana. Tech. rep. URL `https://pubs.er.usgs.gov/publication/pp729G`.

Clymans, W., Barão, L .and Van der Putten, N., Wastegård, S., Gísladóttir, G .and Björck, S., Moine, B., Struyf, E., and Conley, D. (2015) The contribution of tephra constituents during biogenic silica determination: implications for soil and paleoecological studies. *Biogeosciences Discussions* 12(12), 3789–3804. doi:10.5194/bgd-12-3505-2015.

Cockerton, H.E., Street-Perrott, F.A., Barker, P.A., Leng, M.J., Sloane, H.J., and Ficken, K.J. (2015) Orbital forcing of glacial/interglacial variations in chemical weathering and silicon cycling within the upper White Nile basin, East Africa: stable-isotope and biomarker evidence from Lakes Victoria and Edward. *Quaternary science reviews* 130, 57–71. doi:10.1016/j.quascirev.2015.07.028.

Conley, D.J. (1998) An interlaboratory comparison for the measurement of biogenic silica in sediments. *Marine chemistry* 63(1-2), 39–48. doi:10.1016/s0304-4203(98)00049-8.

Conley, J.D. and Schelske, C. (2001) Biogenic Silica. In *Tracking environmental change using lake sediments*, vol. 3, chap. 14, 281–293. Springer Netherlands, Dordrecht. doi:10.1007/0-306-47668-1_14.

Cornelis, J.T., Titeux, H., Ranger, J., and Delvaux, B. (2011) Identification and distribution of the readily soluble silicon pool in a temperate forest soil below three distinct tree species. *Plant and Soil* 342(1-2), 369–378. doi:10.1007/s11104-010-0702-x.

Cornelis, J.T., Weis, D., Lavkulich, L., Vermeire, M.L., Delvaux, B., and Barling, J. (2014) Silicon isotopes record dissolution and re-precipitation of pedogenic clay minerals in a podzolic soil chronosequence. *Geoderma* 235, 19–29. doi:10.1016/j.geoderma.2014.06.023.

De La Rocha, C., Brzezinski, M.A., and DeNiro, M.J. (2000) A first look at the distribution of the stable isotopes of silicon in natural waters. *Geochimica et Cosmochimica Acta* 64(14), 2467–2477. doi:10.1016/s0016-7037(00)00373-2.

De La Rocha, C.L., Brzezinski, M.A., and Deniro, M.J. (1997) Fractionation of silicon isotopes by marine diatoms during biogenic silica formation. *Geochimica et Cosmochimica Acta* 61(23), 5051–5056. doi:10.1016/s0016-7037(97)00300-1.

Delvigne, C., Angeletti, B., Guihou, A., Basile-Doelsch, I., and Meunier, J.D. (2018) Reliable Determination of Ge in Solid Environmental Samples Using a Chemical Preparation Procedure Developed for Si Isotopes and ICP-MS Analysis. *Geostandards and Geoanalytical Research* 42(1), 139–149. doi:10.1111/ggr.12197.

Despain, D.G. (1987) The two climates of Yellowstone National Park. In *Proceedings of the Montana Academy of Science*, vol. 47, 11–20.

Ding, T., Jiang, S., Wan, D., Li, Y., Li, J., Song, H., Liu, Z., and Yao, X. (1996) *Silicon Isotope Geochemistry*.

Douthitt, C.B. (1982) The geochemistry of the stable isotopes of silicon. *Geochimica et Cosmochimica Acta* 46, 1449–1458. doi:10.1016/0016-7037(82)90278-2.

Dürr, H., Meybeck, M., Hartmann, J., Laruelle, G.G., and Roubeix, V. (2011) Global spatial distribution of natural riverine silica inputs to the coastal zone. *Biogeosciences* 8(3), 597–620. doi:10.5194/bg-8-597-2011.

Ehlert, C., Grasse, P., and Frank, M. (2013) Changes in silicate utilisation and upwelling intensity off Peru since the Last Glacial Maximum–insights from silicon and neodymium isotopes. *Quaternary Science Reviews* 72, 18–35. doi:10.1016/j.quascirev.2013.04.013.

Evans, M.J. and Derry, L.A. (2002) Quartz control of high germanium/silicon ratios in geothermal waters. *Geology* 30(11), 1019–1022. doi:10.1130/0091-7613(2002)030<1019:qcohgs>2.0.co;2.

Filippelli, G.M., Carnahan, J.W., Derry, L.A., and Kurtz, A. (2000) Terrestrial paleorecords of Ge/Si cycling derived from lake diatoms. *Chemical Geology* 168(1-2), 9–26. doi:10.1016/s0009-2541(00)00185-6.

Fowler, A.P., Tan, C., Cino, C., Scheuermann, P., Volk, M.W., Shanks, W.P., and Seyfried, W.E. (2019a) Vapor-driven sublacustrine vents in Yellowstone Lake, Wyoming, USA. *Geology* 47(3), 223–226. doi:10.1130/g45577.1.

Fowler, A.P., Tan, C., Luttrell, K., Tudor, A., Scheuermann, P., Shanks III, W.P., and Seyfried Jr., W.E. (2019b) Geochemical heterogeneity of sublacustrine hydrothermal vents in Yellowstone Lake, Wyoming. *Journal of Volcanology and Geothermal Research* 386, 106677. doi:10.1016/j.jvolgeores.2019.106677.

Frings, P.J., Claymans, W., Fontorbe, G., Rocha, C.L.D.L., and Conley, D.J. (2016) The continental Si cycle and its impact on the ocean Si isotope budget. *Chemical Geology* 425, 12–36. doi:10.1016/j.chemgeo.2016.01.020.

Frings, P.J., Clymans, W., Jeppesen, E., Lauridsen, T.L., Struyf, E., and Conley, D.J. (2014) Lack of steady-state in the global biogeochemical Si cycle: emerging evidence from lake Si sequestration. *Biogeochemistry* 117(2), 255–277. doi:10.1007/s10533-013-9944-z.

Froelich, P., Blanc, V., Mortlock, R., Chillrud, S., Dunstan, W., Udomkit, A., and Peng, T.H. (1992) River fluxes of dissolved silica to the ocean were higher during glacials: Ge/Si in diatoms, rivers, and oceans. *Paleoceanography* 7(6), 739–767. doi:10.1029/92pa02090.

Froelich, P., Mortlock, R., and Shemesh, A. (1989) Inorganic germanium and silica in the Indian ocean: biological fractionation during (Ge/Si) opal formation. *Global biogeochemical cycles* 3(1), 79–88. doi:10.1029/gb003i001p00079.

Gaspard, F. (2020) *Controls on weathering fluxes from hydrothermally-active volcanic regions: a Ge/Si ratio and Si isotopes perspective*. PhD thesis.

Gaspard, F., Opfergelt, S., Dessert, C., Robert, V., Ameijeras-Marino, Y., and Demelle, P. (2020) Imprint of chemical weathering and hydrothermal on the Ge/Si ratio and Si isotopic composition of rivers in a volcatinc tropical island, Basse-Terre, Guadeloupe (French West Indies). *Chemical Geology* Submitted.

Geilert, S., Vroon, P.Z., Keller, N.S., Gudbrandsson, S., Stefánsson, A., and van Bergen, M.J. (2015) Silicon isotope fractionation during silica precipitation from hot-spring waters: evidence from the Geysir geothermal field, Iceland. *Geochimica et Cosmochimica Acta* 164, 403–427. doi:10.1016/j.gca.2015.05.043.

Geilert, S., Vroon, P.Z., Roerdink, D.L., Van Cappellen, P., and van Bergen, M.J. (2014) Silicon isotope fractionation during abiotic silica precipitation at low temperatures: Inferences from flow-through experiments. *Geochimica et Cosmochimica Acta* 142, 95–114. doi:10.1016/j.gca.2014.07.003.

Gemery-Hill, P.A., Shanks, W.C., Balistrieri, L.S., and Lee, G.K. (2007) Geochemical data for selected rivers, lake waters, hydrothermal vents, and subaerial geysers in Yellowstone National Park, Wyoming and vicinity, 1996–2004. *Publications of the US Geological Survey* (71). URL `https://digitalcommons.unl.edu/usgspubs/71`.

Georg, R., Reynolds, B., Frank, M., and Halliday, A. (2006) New sample preparation techniques for the determination of Si isotopic compositions using MC-ICPMS. *Chemical Geology* 235(1), 95 – 104. doi:10.1016/j.chemgeo.2006.06.006.

Grasse, P., Closset, I., Jones, J., Geilert, S., and Brzezinski, M. (2020) Controls on dissolved silicon isotopes along the US GEOTRACES Eastern Pacific Zonal Transect (GP16). *Global Biogeochemical Cycles* 34(9), e2020GB006538. doi:10.1029/2020gb006538.

Hammond, D.E., McManus, J., and Berelson, W.M. (2004) Oceanic germanium/silicon ratios: Evaluation of the potential overprint of temperature on weathering signals. *Paleoceanography* 19(2), PA2016. doi:10.1029/2003pa000940.

Han, Y., Huh, Y., and Derry, L. (2015) Ge/Si ratios indicating hydrothermal and sulfide weathering input to rivers of the Eastern Tibetan Plateau and Mt. Baekdu. *Chemical Geology* 410, 40 – 52. doi:10.1016/j.chemgeo.2015.06.001.

Huerta, M.A., Whitlock, C., and Yale, J. (2009) Holocene vegetation–fire–climate linkages in northern Yellowstone National Park, USA. *Palaeogeography, Palaeoclimatology, Palaeoecology* 271(1-2), 170–181. doi:10.1016/j.palaeo.2008.10.015.

Hurwitz, S. and Lowenstern, J.B. (2014) Dynamics of the Yellowstone hydrothermal system. *Reviews of Geophysics* 52, 375–411. doi:10.1002/2014rg000452.

Iglesias, V., Whitlock, C., Krause, T.R., and Baker, R.G. (2018) Past vegetation dynamics in the Yellowstone region highlight the vulnerability of mountain systems to climate change. *Journal of Biogeography* 45(8), 1768–1780. doi:10.1111/jbi.13364.

Interlandi, S.J., Kilham, S.S., and Theriot, E.C. (1999) Responses of phytoplankton to varied resource availability in large lakes of the Greater Yellowstone Ecosystem. *Limnology and oceanography* 44(3), 668–682. doi:10.4319/lo.1999.44.3.0668.

Kelts, K., Briegel, U., Ghilardi, K., and Hsu, K. (1986) The limnogeology-ETH coring system. *Swiss journal of hydrology* 48(1), 104–115. doi:10.1007/bf02544119.

Kilham, S.S., Theriot, E.C., and Fritz, S.C. (1996) Linking planktonic diatoms and climate change in the large lakes of the Yellowstone ecosystem using resource theory. *Limnology and Oceanography* 41(5), 1052–1062. doi:10.4319/lo.1996.41.5.1052.

Kurtz, A.C., Derry, L.A., and Chadwick, O.A. (2002) Germanium-silicon fractionation in the weathering environment. *Geochimica et Cosmochimica Acta* 66(9), 1525–1537. doi:10.1016/s0016-7037(01)00869-9.

Kurtz, A.C., Lugolobi, F., and Salvucci, G. (2011) Germanium-silicon as a flow path tracer: Application to the Rio Icacos watershed. *Water Resources Research* 47(6), W06516. doi:10.1029/2010wr009853.

Laskar, J., Robutel, P., Joutel, F., Gastineau, M., Correia, A., and Levrard, B. (2004) A long-term numerical solution for the insolation quantities of the earth. *Astronomy & Astrophysics* 428(1), 261–285. doi:10.1051/0004-6361:20041335.

Lu, Y., Stone, J., Fritz, S.C., and Westover, K. (2017) Major climatic influences on Yellowstone-region lake ecosystems suggested by synchronous transitions in Late-Glacial and early-Holocene diatom assemblages. *Palaeogeography, Palaeoclimatology, Palaeoecology* 485, 178 – 188. doi:10.1016/j.palaeo.2017.06.011.

Lugolobi, F., Kurtz, A.C., and Derry, L.A. (2010) Germanium–silicon fractionation in a tropical, granitic weathering environment. *Geochimica et Cosmochimica Acta* 74(4), 1294–1308. doi:10.1016/j.gca.2009.11.027.

Millspaugh, S.H., Whitlock, C., and Bartlein, P.J. (2000) Variations in fire frequency and climate over the past 17 000 yr in central Yellowstone National Park. *Geology* 28(3), 211–214. doi:10.1130/0091-7613(2000)28<211:viffac>2.0.co;2.

Morgan, L., Shanks, W., Lee, G., and Webring, M. (2007) Bathymetry and geology of the floor of Yellowstone Lake, Yellowstone National Park, Wyoming, Idaho, and Montana. Tech. rep., USGS. doi:10.3133/sim2973.

Morgan, L., Shanks, W.C., Lovalvo, D., Johnson, S., Stephenson, W., Pierce, K., Harlan, S., Finn, C., Lee, G., Webring, M. et al. (2003) Exploration and discovery in Yellowstone Lake: results from high-resolution sonar imaging, seismic reflection profiling, and submersible studies. *Journal of Volcanology and Geothermal Research* 122(3), 221–242. doi:10.1016/s0377-0273(02)00503-6.

Morgan, L.A., Shanks, W.P., Iverson2, N., Schiller, C., Brown, S.R., Whitlock, C., Fritz, S., Cartier, R., Zahajska, P., Cash, R., and Best, J. (unpublished) THE DYNAMIC FLOOR OF YELLOWSTONE LAKE: The past-14-ka geologic record of hydrothermal explosions, doming, landslides, and faulting. In preparation.

Morgan, L.A., Shanks, W.P., and Pierce, K.L. (2009) *Hydrothermal processes above the Yellowstone magam chamber: Large hydrothermal systems and large hydrothermal explosions*, vol. 459. Geological Society of America. ISBN 9780813724591. doi:10.1130/2009.2459(01).

Morley, D.W., Leng, M.J., Mackay, A.W., Sloane, H.J., Rioual, P., and Battarbee, R.W. (2004) Cleaning of lake sediment samples for diatom oxygen isotope analysis. *Journal of Paleolimnology* 31, 391–401. doi:10.1023/B:JOPL.0000021854.70714.6b.

Mortlock, R., Charles, C., Froelich, P., Zibello, M., Saltzman, J., Hays, J., and Burckle, L. (1991) Evidence for lower productivity in the Antarctic Ocean during the last glaciation. *Nature* 351(6323), 220–223. doi:10.1038/351220a0.

Mortlock, R.A. and Froelich, P. (1996) Determination of germanium by isotope dilution-hydride generation inductively coupled plasma mass spectrometry. *Analytica Chimica Acta* 332(2), 277 – 284. doi:10.1016/0003-2670(96)00230-9.

Mortlock, R.A., Froelich, P.N., Feely, R.A., Massoth, G.J., Butterfield, D.A., and Lupton, J.E. (1993) Silica and germanium in Pacific Ocean hydrothermal vents and plumes. *Earth and Planetary Science Letters* 119(3), 365–378. doi:10.1016/0012-821x(93)90144-x.

Mortlock, R.A. and Frohlich, P.N. (1987) Continental weathering of germanium: Ge/Si in the global river discharge. *Geochimica et Cosmochimica Acta* 51(8), 2075–2082. doi:10.1016/0016-7037(87)90257-2.

Morzel, L.A.M., Shanks, W.P., Lowenstern, J.B., Farrell, J.M., and Robinson, J.E. (2017) Geologic field-trip guide to the volcanic and hydrothermal landscape of the Yellowstone Plateau. Tech. rep., US Geological Survey. doi:10.3133/sir20175022p.

Mosello, R. (1984) Hydrochemistry of high altitude alpine lakes. *Schweizerische Zeitschrift für Hydrologie* 46(1), 86–99. doi:10.1007/bf02538100.

Muffler, L.P., White, D., and Truesdell, A. (1971) Hydrothermal explosion craters in yellowstone National Park. *Geological Society of America Bulletin* 82(3), 723–740. doi:10.1130/0016-7606(1971)82[723:heciyn]2.0.co;2.

Murnane, R. and Stallard, R. (1988) Germanium/silicon fractionation during biogenic opal formation. *Paleoceanography* 3(4), 461–469. doi:10.1029/pa003i004p00461.

Murnane, R.J. and Stallard, R.F. (1990) Germanium and silicon in rivers of the Orinoco drainage basin. *Nature* 344(6268), 749–752. doi:10.1038/344749a0.

Nantke, C.K., Frings, P.J., Stadmark, J., Czymzik, M., and Conley, D.J. (2019) Si cycling in transition zones: a study of Si isotopes and biogenic silica accumulation in the Chesapeake Bay through the Holocene. *Biogeochemistry* 146(2), 145–170. doi:10.1007/s10533-019-00618-w.

Opfergelt, S. and Delmelle, P. (2012) Silicon isotopes and continental weathering processes: Assessing controls on Si transfer to the ocean. *Comptes Rendus Geoscience* 344, 723–738. doi:10.1016/j.crte.2012.09.006.

Opfergelt, S., Eiriksdottir, E.S., Burton, K.W., Einarsson, A., Siebert, C., Gislason, S.R., and Halliday, A.N. (2011) Quantifying the impact of freshwater diatom productivity on silicon isotopes and silicon fluxes: Lake Myvatn, Iceland. *Earth and Planetary Science Letters* 305(1-2), 73–82. doi:10.1016/j.epsl.2011.02.043.

Panizzo, V.N., Swann, G.E.A., Mackay, A.W., Vologina, E., Alleman, L., André, L., Pashley, V.H., and Horstwood, M.S.A. (2017) Constraining modern-day silicon cycling in Lake Baikal. *AGU Publications* 556–574. doi:10.1002/2016gb005518.

Panizzo, V.N., Swann, G.E.A., Mackay, A.W., Vologina, E., Sturm, M., Pashley, V., and Horstwood, M.S.A. (2016) Insights into the transfer of silicon isotopes into the sediment record. *Biogeosciences* 13, 147–157. doi:10.5194/bg-13-147-2016.

Pokrovski, G.S. and Schott, J. (1998) Thermodynamic properties of aqueous Ge (IV) hydroxide complexes from 25 to 350 C: implications for the behavior of germanium and the Ge/Si ratio in hydrothermal fluids. *Geochimica et Cosmochimica Acta* 62(9), 1631–1642. doi:10.1016/s0016-7037(98)00081-7.

Psenner, R. (1989) Chemistry of high mountain lakes in siliceous chatchments of the Central Eastern Alps. *Aquatic Sciences* 51(2), 108–128. doi:10.1007/bf00879298.

Reynolds, B.C., Aggarwal, J., Andre, L., Baxter, D., Beucher, C., Brzezinski, M.A., Engstrom, E., Georg, R.B., Land, M., Leng, M.J., Opfergelt, S., Rodushkin, I., Sloane, H.J., van den Boorn, S.H.J.M., Vroon, P.Z., and Cardinal, D. (2007) An inter-laboratory comparison of Si isotope reference materials. *Journal of Analytical Atomic Spectrometry* 22, 561–568. doi:10.1039/b616755a.

Richter, F.M. and Turekian, K.K. (1993) Simple models for the geochemical response of the ocean to climatic and tectonic forcing. *Earth and Planetary Science Letters* 119(1-2), 121–131. doi:10.1016/0012-821x(93)90010-7.

Rickert, D., Schlüter, M., and Wallmann, K. (2002) Dissolution kinetics of biogenic silica from the water column to the sediments. *Geochimica et Cosmochimica Acta* 66(3), 439–455. doi:10.1016/s0016-7037(01)00757-8.

Rouxel, O., Galy, A., and Elderfield, H. (2006) Germanium isotopic variations in igneous rocks and marine sediments. *Geochimica et Cosmochimica Acta* 70(13), 3387–3400. doi:10.1016/j.gca.2006.04.025.

Schiller, C.M. (2020) *Hydrothermal Influences on the Holocene Environmental History of Central Yellowstone National Park*. PhD thesis. URL `https://scholarworks.montana.edu/xmlui/bitstream/handle/1/16052/schiller-hydrothermal-2020.pdf?sequence=1`.

Schiller, C.M., Whitlock, C., Elder, K.L., Iverson, N.A., and Abbott, M.B. (2020) Erroneously old radiocarbon ages from terrestrial pollen concentrates in Yellowstone Lake, Wyoming, USA. *Radiocarbon* 1–22. doi:10.1017/rdc.2020.118.

Scribner, A.M., Kurtz, A.C., and Chadwick, O.A. (2006) Germanium sequestration by soil: Targeting the roles of secondary clays and fe-oxyhydroxides. *Earth and Planetary Science Letters* 243(3), 760 – 770. doi:10.1016/j.epsl.2006.01.051.

Shanks, W.C., Alt, J.C., and Morgan, L.A. (2007) Geochemistry of sublacustrine hydrothermal deposits in Yellowstone Lake - Hydrothermal reactions, stable-isotope systematics, sinter deposition, and spire formation. *Publications of the US Geological Survey* (85). URL `https://digitalcommons.unl.edu/usgspubs/85`.

Shemesh, A., Mortlock, R., and Froelich, P. (1989) Late Cenozoic Ge/Si record of marine biogenic opal: Implications for variations of riverine fluxes to the ocean. *Paleoceanography* 4(3), 221–234. doi:10.1029/pa004i003p00221.

Stauffer, R.E. and Thompson, J.M. (1984) Arsenic and antimony in geothermal waters of Yellowstone National Park, Wyoming, USA. *Geochimica et Cosmochimica Acta* 48(12), 2547 – 2561. doi:10.1016/0016-7037(84)90305-3.

Street-Perrott, F.A., Barker, P.A., Leng, M.J., Sloane, H.J., Wooller, M.J., Ficken, K.J., and Swain, D.L. (2008) Towards an understanding of late Quaternary variations in the continental biogeochemical cycle of silicon: multi-isotope and sediment-flux data for Lake Rutundu, Mt Kenya, East Africa, since 38 ka BP. *Journal of Quaternary Science: Published for the Quaternary Research Association* 23(4), 375–387. doi:10.1002/jqs.1187.

Strickland, J. and Parsons, T. (1972) *A practical handbook of seawater analysis*, vol. Bulletin 167. Journal of the Fisheries Research Board of Canada, 2nd edn. URL `https://epic.awi.de/id/eprint/39262/1/Strickland-Parsons_1972.pdf`. The Alger Press Ltd.

Struyf, E., Mörth, C.M., Humborg, C., and Conley, D.J. (2010) An enormous amorphous silica stock in boreal wetlands. *Journal of Geophysical Research: Biogeosciences* 115(G4), G04008. doi:10.1029/2010jg001324.

Sun, X., Andersson, P., Land, M., Humborg, C., and Mörth, C.M. (2010) Stable silicon isotope analysis on nanomole quantities using MC-ICP-MS with a hexapole gas-collision cell. *Journal of Analytical Atomic Spectrometry* 25(2), 156–162. doi:10.1039/B911113A.

Sutton, J., Ellwood, M.J., and Maher, William A .and Croot, P.L. (2010) Oceanic distribution of inorganic germanium relative to silicon: Germanium discrimination by diatoms. *Global Biogeochemical Cycles* 24(2), GB2017. doi:10.1029/2009gb003689.

Sutton, J.N., André, L., Cardinal, D., Conley, D.J., De Souza, G.F., Dean, J., Dodd, J., Ehlert, C., Ellwood, M.J., Frings, P.J. et al. (2018) A review of the stable isotope bio-geochemistry of the global silicon cycle and its associated trace elements. *Frontiers in Earth Science* 5(112). doi:10.3389/feart.2017.00112.

Sutton, J.N., Varela, D.E., Brzezinski, M.A., and Beucher, C.P. (2013) Species-dependent silicon isotope fractionation by marine diatoms. *Geochimica et Cosmochimica Acta* 104, 300 – 309. doi:10.1016/j.gca.2012.10.057.

Swann, G.E., Leng, M.J., Juschus, O., Melles, M., Brigham-Grette, J., and Sloane, H.J. (2010) A combined oxygen and silicon diatom isotope record of Late Quaternary change in Lake El'gygytgyn, North East Siberia. *Quaternary Science Reviews* 29(5-6), 774–786. doi:10.1016/j.quascirev.2009.11.024.

Theriot, E.C., Fritz, S.C., Whitlock, C., and Conley, D.J. (2006) Late Quaternary rapid morphological evolution of an endemic diatom in Yellowstone Lake, Wyomin. *Paleobiology* 32(1), 38–54. doi:10.1666/02075.1.

Tiller, C.C. (1995) *Postglacial sediment stratigraphy of large lakes in Greater Yellowstone: Scenarios of tectonic and climatic forcing*. Master's thesis, University of Minnesota.

Tribovillard, N. (2013) The Ge/Si ratio as a tool to recognize biogenic silica in chert. *Comptes Rendus Geoscience* 345(3), 160–165. doi:10.1016/j.crte.2013.02.005.

Tribovillard, N., Bout-Roumazeilles, V., Riboulleau, A., Baudin, F., Danelian, T., and Riquier, L. (2011) Transfer of germanium to marine sediments: Insights from its accumulation in radiolarites and authigenic capture under reducing conditions. Some examples through geological ages. *Chemical Geology* 282(3-4), 120–130. doi:10.1016/j.chemgeo.2011.01.015.

Varela, D.E., Pride, C.J., and Brzezinski, M.A. (2004) Biological fractionation of silicon isotopes in Southern Ocean surface waters. *Global biogeochemical cycles* 18(1), GB1047. doi:10.1029/2003gb002140.

Wang, B., Liu, C.Q., Maberly, S.C., Wang, F., and Hartmann, J. (2016) Coupling of carbon and silicon geochemical cycles in rivers and lakes. *Scientific reports* 6, 35832. doi:10.1038/srep35832.

Whitlock, C. (1993) Postglacial vegetation and climate of Grand Teton and southern Yellowstone National Parks. *Ecological Monographs* 63(2), 173–198. doi:10.2307/2937179.

Whitlock, C., Dean, W.E., Fritz, S.C., Stevens, L.R., Stone, J.R., Power, M.J., Rosenbaum, J.R., Pierce, K.L., and Bracht-Flyr, B.B. (2012) Holocene seasonal variability inferred from multiple proxy records from Crevice Lake, Yellowstone National Park, USA. *Palaeogeography, Palaeoclimatology, Palaeoecology* 331, 90–103. doi:10.1016/j.palaeo.2012.03.001.

Yeghicheyan, D., Bossy, C., Bouhnik Le Coz, M., Douchet, C., Granier, G., Heimburger, A., Lacan, F., Lanzanova, A., Rousseau, T.C., Seidel, J.L., and othersers (2013) A compilation of silicon, rare earth element and twenty-one other trace element concentrations in the natural river water reference material SLRS-5 (NRC-CNRC). *Geostandards and Geoanalytical Research* 37(4), 449–467. doi:10.1111/j.1751-908x.2013.00232.x.

Zhang, A., Zhang, J., Zhang, R., and Xue, Y. (2014) Modified enrichment and purification protocol for dissolved silicon-isotope determination in natural waters. *Journal of Analytical Atomic Spectrometry* 29(12), 2414–2418. doi:10.1039/C4JA00122B.

Ziegler, K., Chadwick, O.A., Brzezinski, M.A., and Kelly, E.F. (2005) Natural variations of δ^{30}Si ratios during progressive basalt weathering, Hawaiian Islands. *Geochimica et Cosmochimica Acta* 69(19), 4597–4610. doi:10.1016/j.gca.2005.05.008.

Supplementary Materials

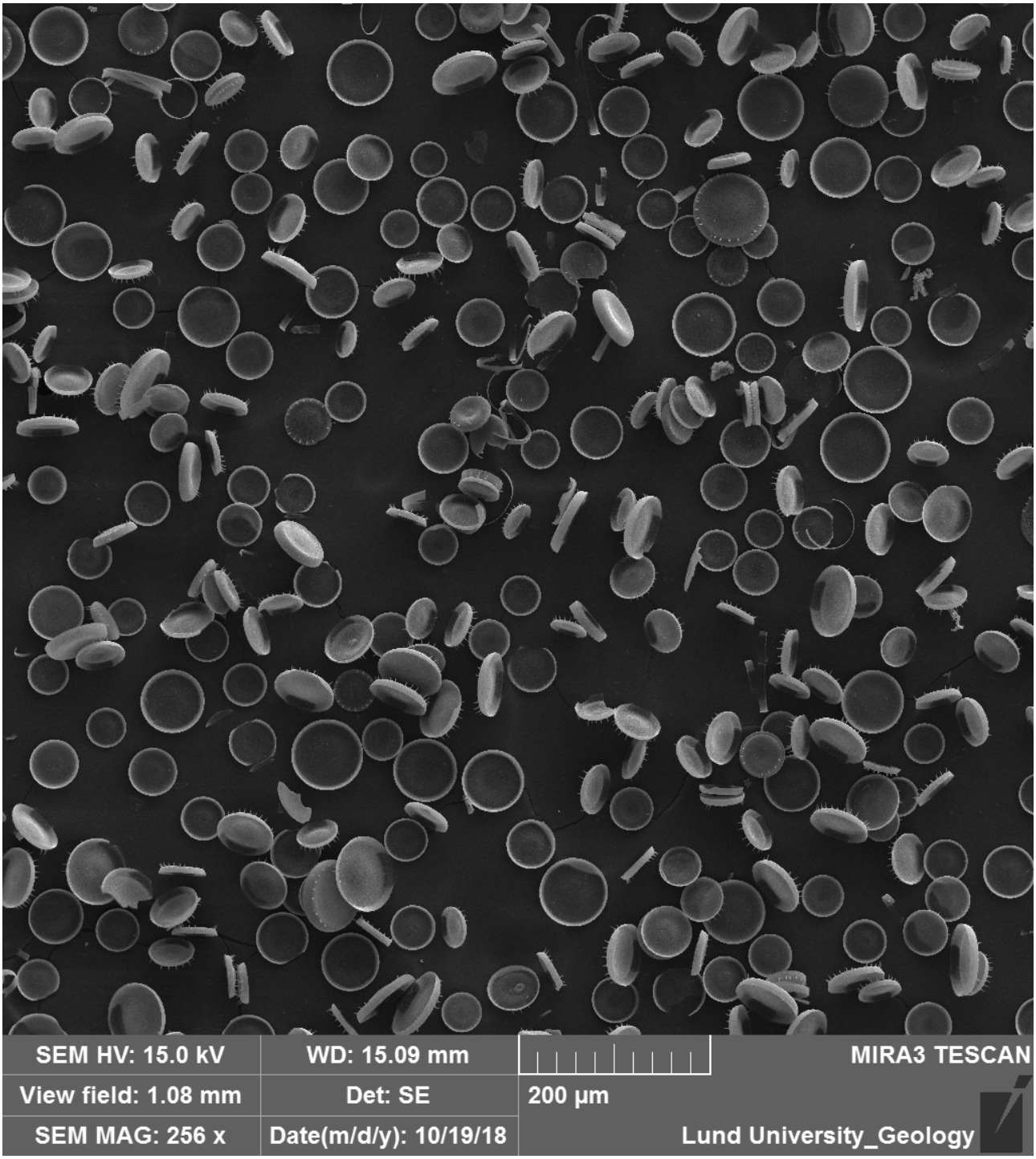


Figure S1: SEM photo of a cleaned diatom sample used for Si isotope and Ge/Si analyses from core YL-2C, depth 731 cm, showing the purity of the diatom samples.

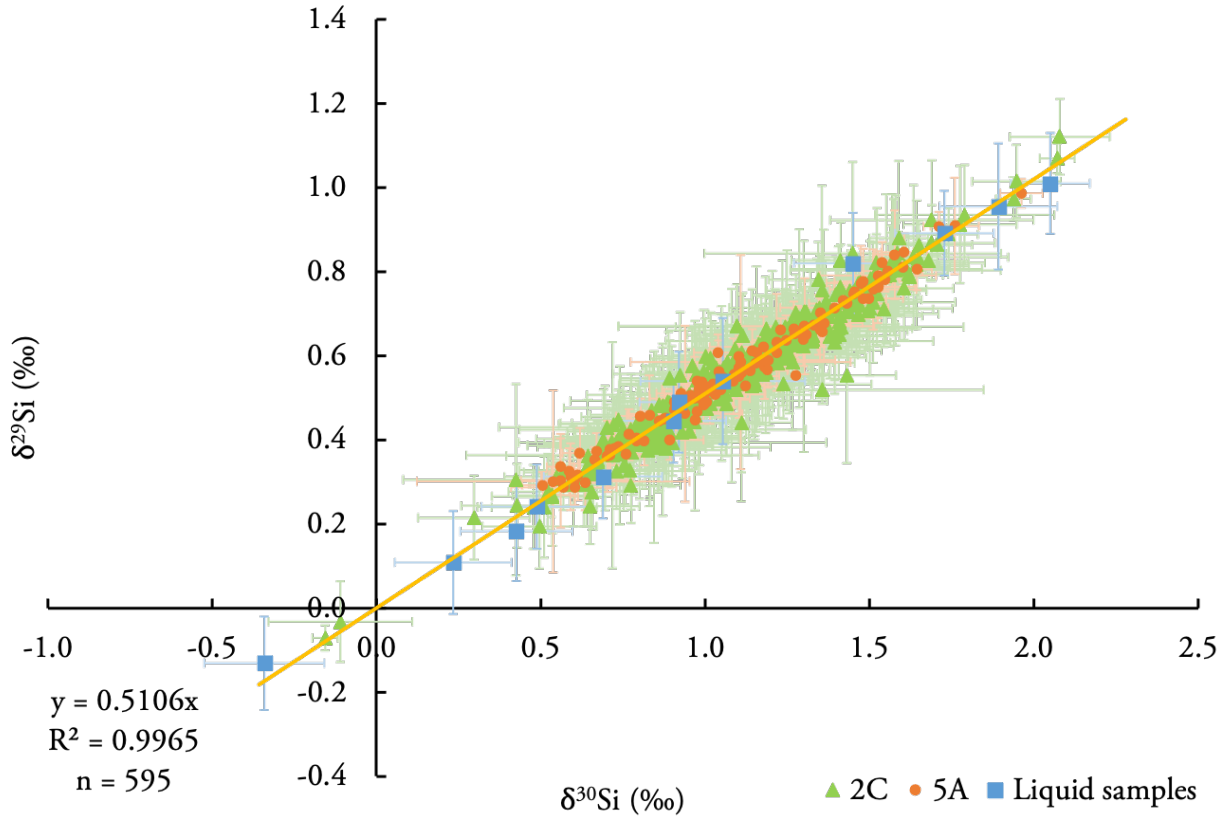


Figure S2: The three isotope plot showing all diatom samples presented in this study and constraining any potential polyatomic interferences. All measurements fall onto a line that corresponds to a mass-dependent fractionation curve.

LUNDQUA publications

At the Department of Geology, Quaternary Sciences, Lund University, three series are published, named “Thesis”, “Report” and “Uppdrag”. The “Thesis” series contains doctor dissertations; the “Report” series primary material, often of a monographic character, which cannot be published in extenso in ordinary scientific journals; the “Uppdrag” series contains selected examples of expert reports, generally in Swedish, which may be of some general interest.

The “Thesis” and the “Report” series cover different aspects of Quaternary stratigraphy and environment - methods, lithostratigraphy, biostratigraphy, chronology, as well as their applications within technical geology, resource geology, nature conservancy, archaeology etc. Complete lists of publications may be ordered from the Department of Geology, Quaternary Sciences, Sölvegatan 12, SE-223 62 Lund, Sweden.

1. Nilsson, K. 1973: Glacialgeologiska problem i Sydvästskåne (English summary: Problems of glacial geology in south-western Scania.

2. Bjelm, L. 1976: Deglaciationen av Småländska höglandet, speciellt med avseende på deglaciationsdynamik, ismäktighet och tidsställning. (Deglaciation of the Småland Highland, with special reference to deglaciation dynamics, ice thickness and chronology).

3. Göransson, H. 1977: The Flandrian Vegetational History of Southern Östergötland.

4. Miller, U. 1977: Pleistocene deposits of the Alnarp Valley, southern Sweden Microfossils and their stratigraphic application.

5. Lagerlund, E. 1977: Förutsättningar för moränstratigrafiska undersökningar på Kullen i Nordvästskåne - teoriutveckling och neotektonik (Till stratigraphical studies in the Kullen area, NW Skåne, South Sweden: basic theory and neotectonics.

6. Hilldén, A. 1979: Deglaciationsförloppet i trakten av Berghemsmoränen, öster om Göteborg (English summary: The deglaciation in the vicinity of the Berghem moraine, east of Göteborg).

7. Björck, S. 1979: Late Weichselian stratigraphy of Blekinge, SE Sweden, and water level changes in the Baltic Ice Lake.

8. Andersson, O.H. 1981: Borrning och dokumentation. Borrningsteknik jämte metodik för geologisk datainsamling under borrningsgång (Drilling and documentation).

9. Hjort, C. 1981: Studies of the Quaternary in Northeast Greenland.

10. Hjelmroos Ericson, M. 1981: Holocene development of Lake Wielkie Gacno area, northwestern Poland.

11. Liljegren, R. 1982: Paleoekologi och strandförskjutning i en Littorinavik vid Spjälkö i mellersta Blekinge (English summary: Palaeoecology and shore displacement in a Littorina bay at Spjälkö, Blekinge).

12. Norddahl, H. 1983: Late Quaternary stratigraphy of Fnjóskadalur central North Iceland, a study of sediments, ice lake strandlines, glacial isostasy and ice free areas.

13. Robison, J.M. 1983: Glaciofluvial sedimentation: A key to the deglaciation of the Laholm area, southern Sweden.

14. Sandgren, P. 1983: The deglaciation of the Klippan area, southern Sweden, a study of glaciofluvial and glaciomarine sediments.

15. Åmark, M. 1984: The deglaciation of the eastern part of Skåne, southern Sweden. A study of till and stratified drift.

16. Adrielsson, L. 1984: Weichselian lithostratigraphy and glacial environments in the Ven Glumslöv area, southern Sweden.

17. Waldemarson, D. 1986: Weichselian lithostratigraphy, depositional processes and deglaciation pattern in the southern Vättern basin, south Sweden.

18. Hallsdottir, M. 1987: Pollen analytical studies of human influence on vegetation in relation to the Landnam tephra layer in southwest Iceland.

19. Ingolfsson, O. 1987: Investigation of the Late Weichselian glacial history of the lower Borgarfjördur region, western Iceland.

20. Möller, P. 1987: Moraine morphology, till genesis, and deglaciation pattern in the Åsnen area, south central Småland, Sweden.

21. Harrison, S. 1988: Reconstructing climate from lake level changes.

22. Lemdahl, G. 1988: Palaeoclimatic and palaeoecological studies based on subfossil insects from Late Weichselian sediments in southern Sweden.

23. Malmberg Persson, K. 1988: Lithostratigraphic and sedimentological investigations around the eastern boundary of the Baltic deposits in central Scania.

24. Liedberg Jönsson, B. 1988: The Late Weichselian macrofossil flora in western Skåne, southern Sweden.

25. Svensson, N.O. 1989: Late Weichselian and early Holocene shore displacement in the central Baltic, based on stratigraphical and morphological records from eastern Småland and Gotland, Sweden.

26. Thelaus, M. 1989: Late Quaternary vegetation history and palaeohydrology of the Sandsjön-Årshult area, southwestern Sweden.

27. Regnéll, J. 1989: Vegetation and land use during 6000 years. Palaeoecology of the cultural landscape at two lake sites in southern Skåne, Sweden.

28. Olsson, S. 1991: Geochemistry, mineralogy and pore water composition in uplifted, Late Weichselian -Early Holocene clays from southern Sweden.

29. Ekström, J. 1993: The Late Quaternary History of the Urus (*Bos primigenius* Bojanus 1827) in Sweden.

30. Almquist Jacobson, H. 1994: Interaction of the Holocene climate, water balance, vegetation, fire, and the cultural land use in the Swedish Borderland.

31. Hammarlund, D. 1994: Stable carbon and oxygen isotope studies of Late Weichselian lake sediments in southern Sweden and northern Poland, with palaeoclimatic implications.

32. Eggertsson, Ò. 1994: Origin of the Arctic driftwood a dendrochronological study.

33. Sæmundsson, T. 1995: Deglaciation and shoreline displacement in Vopnafjördur, northeastern Iceland.

34. Snowball, I.F. 1995: Mineral magnetic and geochemical properties of Holocene sediments and soils in the Abisko region of northern Sweden.

35. Berglund, M. 1995: The Late Weichselian deglaciation, vegetational development and shore displacement in Halland, southwestern Sweden.

36. Lagerås, P. 1996: Vegetation and land use in the Småland Uplands, southern Sweden, during the last 6000 years.

37. Yu, G. 1996: Lake level records and palaeoclimates of northern Eurasia.

38. Jiang, H. 1996: Palaeoclimate and palaeoceanography of the Skagerrak-Kattegat since the Late Weichselian based on diatom records.

39. Björkman, L. 1996: The Late Holocene history of beech *Fagus sylvatica* and Norway spruce *Picea abies* at stand scale in southern Sweden.

40. Rundgren, M. 1997: Late Weichselian and early Holocene changes of vegetation, climate and sea level on the Skagi peninsula, northern Iceland.

41. Vassiljev, J. 1997: Simulating the paleorecord of northern European lakes using a coupled lake catchment model.

42. Andersson, G. 1997: Deglaciation pattern and dynamics in the Bolmen area, southwestern Sweden.

43. Barnekow, L. 1999: Holocene vegetation dynamics and climate changes in the Torneträsk area, northern Sweden.

44. Ising, J. 2001: Pollen analysis, chronology and palaeomagnetism of three Late Weichselian sites in southern Sweden.

45. Gedda, B. 2001: Environmental and climatic aspects of the early to mid Holocene calcareous tufa and land mollusc fauna in southern Sweden.

46. Broström, A. 2002: Estimating source area of pollen and pollen productivity in the cultural landscapes of southern Sweden - developing a palynological tool for quantifying past plant cover.

47. Pettersson, G. 2002: Weichselian glaciations in the middle Notec River region, northwest Poland.

48. Alexanderson, H. 2002: Glacial geology and palaeo-ice dynamics of two ice-sheet margins, Taymyr Peninsula, Siberia and Jameson Land, East Greenland.

49. Sander, M. 2003: Climate signals and frequencies in the Swedish Time Scale, River Ångermanälven, Central Sweden.

50. Zillén, L. 2003: Setting the Holocene clock using varved lake sediments in Sweden.

51. Yu, S.-Y. 2003: The Littorina transgression in southeastern Sweden and its relation to mid-Holocene climate variability.

52. Albrecht, J. 2004: Marginal behaviour of the last Scandinavian Ice Sheet during its final termination and deglaciation over Northeastern Germany.

53. Bergman, J. 2005: Tree-limit ecotonal response to Holocene climatic change in the Scandes Mountains of west-central Sweden.

54. Lindén, M. 2006: Glaciodynamics, deglacial landforms and isostatic uplift during the deglaciation of Norrbotten, Sweden.

55. Jessen, C. A. 2006: The ups and downs of the Holocene: exploring relationships between global CO_2 and climate variability in the North Atlantic region.

56. Sparrenbom, C.J. 2006: Constraining the southern part of the Greenland Ice Sheet since the Last Glacial Maximum from relative sea-level changes, cosmogenic dates and glacial-isotatic adjustment models.

57. Kortekaas, M. 2007: Post-glacial history of sea-level and environmental change in the southern Baltic Sea.

58. De Jong, R. 2007: Stormy records from peat bogs in south-west Sweden - implications for regional climatic variability and vegetation changes during the past 6500 years.

59. Schomacker, A. 2007: Dead-ice under different climate conditions: processes, landforms, sediments and melt rates in Iceland and Svalbard.

60. Ljung, K. 2007: Holocene climate and environmental dynamics on the Tristan da Cunha island group, South Atlantic.

61. Håkansson, L. 2008: Glacial history of Northeast Greenland: cosmogenic nuclide constraints on chronology and ice dynamics.

62. Kokfelt, U. 2009: Subarctic ecosystem responses to climate, catchment and permafrost dynamics in the Holocene.

63. Stanton, T. 2011: High temporal resolution reconstructions of Holocene palaeomagnetic directions and intensity: an assessment of geochronology, feature reliability and environmental bias.

64. Nilsson, A. 2011: Assessing Holocene and late Pleistocene geomagnetic dipole field variability.

65. Striberger, J. 2011: Holocene development of Lake Lögurinn and Eyjabakkajökull in eastern Iceland – a multi-proxy approach.

66. Fredh, D. 2012: The impact of past land-use change on floristic diversity in southern Sweden – a quantitative approach based on high-resolution pollen data.

67. Anjar, J. 2012: The Weichselian in southern Sweden and southwestern Baltic Sea: glacial stratigraphy, palaeo-environments and deglaciation chronology.

68. Edvardsson, J. 2013: Holocene climate change and peatland dynamics in southern Sweden based on tree-ring analysis of subfossil wood from peat deposits.

69. Lougheed, B. 2013: Testing palaeomagnetic and ^{14}C based geochronological methods in the Baltic Sea.

70. Randsalu-Wendrup, L. 2013: The palaeolimnological record of regime shifts in lakes in response to climate change.

71. Bragée, P. 2013: A palaeolimnological study of the anthropogenic impact on dissolved organic carbon in South Swedish lakes.

72. Reinholdsson, M. 2014: Magnetic properties of magnetosomal greigite and factors influencing its occurrence and preservation in Baltic Sea Littorina sediments.

73. Mellström, A. 2014: Investigations of temporal changes in climate and the geomagnetic field via high-resolution radiocarbon dating.

74. Åkesson, M. 2014: On the scope of pesticides in ground-water in Skåne, Sweden.

75. Frings, P. 2014: Integrating fluvial processes into the global Si cycle.

76. Adolphi, F. 2014: Solar activity changes at the end of the last ice age – influences on climate and applications for dating.

77. McKay, C. 2015: Benthic environmental responses to climatic changes during the late Quaternary – a micropalaeonto-logical and geochemical approach.

78. Lenz, C. 2015: Manganese cycling in the Baltic Sea over the past ~8000 years - the influence of redox conditions on mineral formation and burial.

79. Alfredsson, H. 2015: Terrestrial Si dynamics in the Arctic - a study on biotic and abiotic controls.

80. Dowling, T.P.F. 2016: The drumlin problem - stream-lined bedforms in southern Sweden.

81. Ning, W. 2016: Tracking environmental changes in the Baltic Sea coastal zone since the mid-Holocene.

82. Fontorbe, G. 2016: Marine silicon cycle through the Cenozoic.

83. Le, T. 2016 : Causal links of past climate change in Coupled Model Intercomparison Project Phase 5 climate models.

84. Bernhardson, M. 2018: Aeolian dunes of central Sweden.

85. Hansson, A. 2018: Submerged landscapes in the Hanö Bay – early Holocene shoreline displacement and human environments in the southern Baltic Basin.

86. Mekhaldi, F. 2018: Cosmogenic radionuclides in environ-mental archives – a paleo-perspective on space climate and a synchronizing tool for climate record.

87. Sigfusdottir, T. 2019: Past dynamics of a marine-terminating glacier in lower Borgarfjörður, west Iceland – analyses of glaciotectonic sediments and landforms.

88. Zheng, M. 2020: Disentangling the production and climate signals from high-resolution Beryllium records: implications for solar and geomagnetic reconstructions.

89. Nantke, C. 2020: Reconstructing Si cycling in transition zones during the Holocene using terrestrial and aquatic records.

90. Yang, B. 2021: Implications of land use on the carbon cycle: Impacts of long-term human activities on terrestrial organic matter input to aquatic ecosystems in southern Sweden.

91. Zahajská, P. 2021: Diatom-rich sediment formation in lakes.